CHARACTERISATION AND TOPOLOGICAL ANALYSIS OF NOVEL METAL-ORGANIC FRAMEWORKS

KATE DAVIES

Thesis presented for the degree of

DOCTOR OF PHILOSOPHY

in the Department of Chemistry

UNIVERSITY OF CAPE TOWN

November 2011

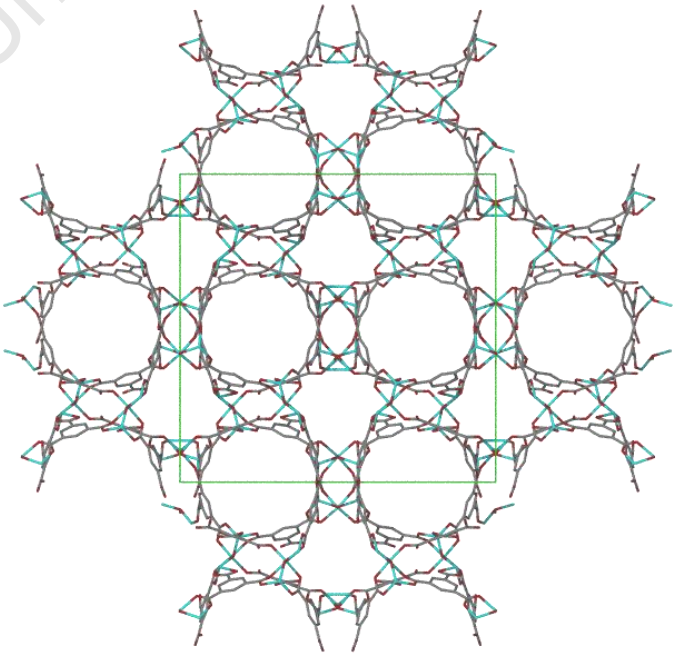

ACKNOWLEDGEMENTS

- Professor Susan A. Bourne and Dr Clive L. Oliver for their supervision, direction and support during this project as well as the multitude of opportunities they afforded me.

- Professors Luigi R. Nassimbeni and Mino R. Caira for their suggestions and help whenever I needed it

- Dr Hong Su for her assistance on the single crystal X-ray diffractometers.

- All the members of the Centre for Supramolecular Chemistry Research. To those who were here while I worked as an undergraduate student thank you for inspiring me to do my PhD. To those who I have studied with as a post-graduate student thank you many times over for all the support, forbearance and friendship you have given me. I truly appreciate it.

- Professor Lars Öhrström at the Department of Chemical and Biological Engineering at Chalmers University of Technology in Göteborg, Sweden for his help and supervision with all the work relating to topological analysis and for welcoming me to his city.

- The National Research Foundation, the Equity Development Program (UCT Chemistry Department) and the University of Cape Town for financial support.

- All my family and friends for putting up with me during this degree, and especially during the past year. Your support and help has been invaluable.

- Finally, to Jarryd. I dedicate this thesis to you. I know it was time well spent but I'm glad I have more time to spend with you now. I could not have worked as hard as I needed to without you. You made this all bearable, even enjoyable. Thank you my love.

PUBLICATIONS AND CONFERENCES

Parts of this thesis have been presented at the following conferences and seminars:

- Poster presentation: *Topological Studies of Metal-Organic Frameworks*, K .Davies, S. A. Bourne, C. L. Oliver, L. Öhrström, 22nd Congress and General Assembly of the International Union of Crystallography (IUCr), Madrid, Spain, 22-30 Aug, **2011**. (*Poster Prize*)
- Oral presentation: *Supramolecular Coordination Chemistry: Towards Functional Materials*, S. A. Bourne, 40th National Convention of the South African Chemical Institute (SACI) conference, Johannesburg, South Africa, 15-21 Jan, **2011**.
- Poster presentation: *Metal-Organic Frameworks from Common Starting Materials*, K. Davies, S. A. Bourne, C. L. Oliver, 40th SACI conference, Johannesburg, South Africa, 15-21 Jan, **2011**.
- Oral presentation at a seminar: *Metal-Organic Networks for Guest Storage and Gas Sorption*, Susan A. Bourne, Chalmers University of Technology, Gothenburg, Sweden, 18 Nov **2010**.
- Oral presentation at a seminar: *Metal-Organic Networks for Guest Storage and Gas Sorption*, Susan A. Bourne, University of Parma, Italy, 9 Sept, **2010**.
- Poster presentation:*Three Zinc-Trimesic Acid Metal-Organic Networks*, K. Davies, S. A. Bourne, C. L. Oliver, Gordon Conference on Crystal Engineering, Waterville Valley Resort, New Hampshire, USA, 6-11 June, **2010**.
- Poster presentation: *Two Anionic Zinc-Trimesic Acid Metal-Organic Networks*, K. Davies, S. A. Bourne, C. L. Oliver, Indaba 6, Kruger National Park, 30 Aug-4 Sept, **2009**.
- Poster presentation: *Chalmers – University of Cape Town Metal-Organic Framework Collaboration*, C. Borel, K. Davies, S. A. Bourne, L. Öhrström, C. L. Oliver, the Chalmers University of Technology conference, Lökeberg, Sweden, 28-29 May, **2009**.
- Poster presentation: *The Effect of Concentration on MOF Formation*, K. Davies, S. A. Bourne, C. L. Oliver, 12th International Seminar on Inclusion Compounds (ISIC), Stellenbosch, 4-9 April, **2009**.
- Poster presentation: *Metal-Organic Networks*, K. Davies, S. A. Bourne, C. L. Oliver, 39th SACI conference, Stellenbosch, South Africa, 30 Nov-5 Dec, **2008**.

Part of this thesis has been published:

- K. Davies, S. A. Bourne, L. Öhrström, C. L. Oliver, Anionic zinc-trimesic acid MOFs with unusual topologies: Reversible hydration studies, *Dalton Trans.*, **2010**, 39, 2869

ABSTRACT

KATE DAVIES *NOVEMBER 2011*

CHARACTERISATION AND TOPOLOGICAL ANALYSIS OF NOVEL METAL-ORGANIC FRAMEWORKS

The investigation of complexes in the solid state has developed exponentially over the past few decades in terms of both crystal engineering and supramolecular chemistry. The preparation of new metal-organic frameworks and coordination polymers has been of particular interest due to the large variety of structural topologies as well as the varying functionalities they offer. A study of the preparation of new metal-organic frameworks from common starting materials was undertaken to increase the understanding of the preparative methods for these compounds. The starting materials used were 1,3,5-benzenetricarboxylic acid (H_3BTRI), 5-nitroisophthalic acid (H_2NIA), zinc(II) sulphate heptahydrate and gadolinium(III) nitrate hexahydrate. Seven new metal-organic frameworks were obtained. The names of these frameworks are: $[Zn_6(\mu_3\text{-}OH)_2(BTRI)_4(DMF)_{2.5}(H_2O)_2]\cdot[Zn(H_2O)_3(DMF)_3]\cdot 2.96H_2O$ (**1**), $[Zn(HCOO)(BTRI)_{0.3}(DMF)]$ (**2**), $[Zn_2(\mu_2\text{-}OH_2)(HBTRI)(BTRI)(H_2O)_2]\cdot DMA\cdot 3H_2O$ (**3**), $[Gd(BTRI)(H_2O)_6]$ (**4**), $[Gd(NIA)_{1.5}(DMF)_2]\cdot DMF$ (**5**), $[Gd_2(NIA)_3(DMF)_4]\cdot 2.67H_2O$ (**6**), and $[Gd_4(NIA)_6(DMF)_{5.5}(H_2O)_3]\cdot 4DMF\cdot H_2O$ (**7**).

Complexes were prepared through a variety of methods including high temperature crystallisation, slow cooling and slow evaporation. The complexes formed were characterised using thermogravimetry (TG), differential scanning calorimetry (DSC) and hot stage microscopy (HSM). Single crystal X-ray analysis was used to elucidate the structure whereas powder X-ray diffraction (PXRD) was used to confirm that the single crystals selected were representative of the bulk material. PXRD was also used to follow the transformation of the structure with heating and in other experiments that had resulted in a loss of single crystal quality.

Full topological analysis was performed on compounds **1**, **2**, **3**, **5**, **6** and **7**. Three of the compounds (**1**, **3** and **7**) had new topological nets and these were fully analysed. The topological nets of **1** and **3** were submitted to the Reticular Chemistry Structure Resource (RCSR). Compound **1** was given the name **sab** and has the short symbol $(4.6^2)_2(4^2.6^{10}.8^3)$. Compound **3** was given the name **kdd** and has the short symbol $(6^3)(6^9.8)$. Compound **7** will shortly be submitted to the RCSR and has the short symbol $(4^4.6^2)(4^6.6^4)_2(4^8.6^6.8)$. Compounds **2**, **5**, and **6** were found to display the well-known **kgd**, **pcu**, and **pts** topological nets, respectively. The **kgd** net is a 2-dimensional network.

Compound **3** displayed “self-healing” properties. The cracks that form upon dehydration close when the crystal is rehydrated. This was studied using multiple techniques including scanning electron microscopy (SEM). SEM was performed on the original sample, the dehydrated sample, and the rehydrated sample.

This study illustrates the wide range of compounds that can be prepared from even the simplest of starting materials. For example there are many reported structures with 1,3,5-benzenetricarboxylic acid and zinc metal ions but very few using the zinc(II) sulphate metal salt, as in this study. The data acquired in this study increase the knowledge database for metal-organic frameworks and coordination polymers and highlight that the slightest of changes in preparative conditions can result in significantly different coordination polymers.

TABLE OF CONTENTS

Chapter 1

Introduction

Important topics associated with metal-organic frameworks and coordination polymers such as supramolecular chemistry, crystal engineering and interpenetration are discussed in this chapter. The important issue of nomenclature and the debate around the correct nomenclature for these types of compounds is explored. The definition of certain terms used in topological analysis as well as the usefulness, and the process of determining topology is discussed. The materials used and the aims and objectives of this project are stated at the end.

1.1 SUPRAMOLECULAR CHEMISTRY

"a true "paradigm shift": from one focused on atoms and bonds between atoms to one focused upon molecules and bonds between molecules." [1]

"Supermolecules are to molecules and the intermolecular bond what molecules are to atoms and the covalent bond" [2]

Supramolecular chemistry is "chemistry beyond the molecule" [2] and while molecular chemistry deals exclusively with covalent bonds between atoms, supramolecular chemistry encompasses molecular assemblies and intermolecular bonds, non-covalent interactions between molecules.[2-4] These non-covalent bonds and supramolecular interactions include coordination, coulombic interactions, van der Waals interactions and hydrogen bonds among others.[1] As such coordination polymers and metal-organic frameworks (MOFs) are good examples of supramolecular chemistry. Supramolecular chemistry also spans different fields of chemistry including organic, inorganic, organometallic and biological.[1,3] It focuses on the bulk properties of molecules caused by the ordered assembly of those molecules and on the relationship between the properties of the bulk material and those of the molecules themselves.[1] The formal definition of supramolecular chemistry does not include coordination chemistry due to coordinate bonds being short and strong rather than weak and long.[5,6] Coordination polymers and MOFs contain both the properties of their building blocks as well as those given by the periodical distribution and interactions between these building blocks and shall be considered as "supermolecules" in this thesis.[1]

Coordination polymers are a supramolecular form of coordination chemistry with a change in focus from convergent ligands to divergent ones, thereby changing the outcome from a coordination compound to a coordination network. The processes that coordination polymers and MOFs undergo during gas storage and sensing are supramolecular ones.[1] Non-covalent interactions between the host and guest molecules are formed and broken. The application of supramolecular chemistry principles to choose appropriate building blocks for MOF preparation can be called crystal engineering.[1]

1.1.1 SUPRAMOLECULAR ISOMERISM

Polymorphism is the ability of a chemical entity to have more than one crystal structure. Different polymorphs can have widely differing properties and therefore understanding the various polymorphs of a substance is essential to understanding the substance itself. Supramolecular isomerism is directly connected to the topic of polymorphism. Supramolecular isomerism deals with different superstructures or frameworks formed from the same starting materials or building blocks.[7] In fact, polymorphism may be viewed as a subset of supramolecular isomerism. However, supramolecular isomers are not necessarily polymorphs, due to the presence of the guest solvent molecules within these superstructures.[7]

A famous quotation from McCrone states that the more time and money put into discovering polymorphs the more that will probably be found.[8] This applies just as well to supramolecular isomers. However, Moulton *et al*[7] add one injunction based on work by Desiraju:[9] that the larger the number of degrees of freedom (flexibility, ability to hydrogen-bond, etc) in the basic building blocks the more polymorphs or supramolecular isomers are probable. Some examples of supramolecular isomers are given in Figure 1.1.

Supramolecular isomers can be divided into four subcategories.[7]

1. Conformational
2. Optical
3. Catenane
4. Structural

Conformational supramolecular isomers[10,11] are formed by changes in the conformation of flexible ligands during the self-assembly process. It is improbable that an isomer of this type would be observed within this project as the organic linker molecules chosen (see Section 1.5 – Organic Linkers) are not particularly flexible. Although the starting materials are not chiral, optical supramolecular isomers[12-14] are possible as achiral molecules may form chiral crystals.[7] Catenane supramolecular isomers[15-18] depend on interpenetration (see Section 1.2 – Crystal Engineering). The interpenetration or non-interpenetration of frameworks can result in a large discrepancy in the bulk properties of the materials. Structural supramolecular isomers[19,20] are built from the same basic constituents and have the same empirical formula and chemical

components. A different overall structure is present in the different isomers however. Structural supramolecular isomers are evidenced throughout the literature by the range of different network structures found from even the simplest of building blocks.[7] It is essential to have a good understanding of the formation of supramolecular isomers before attempting to "engineer" a structure.[7]

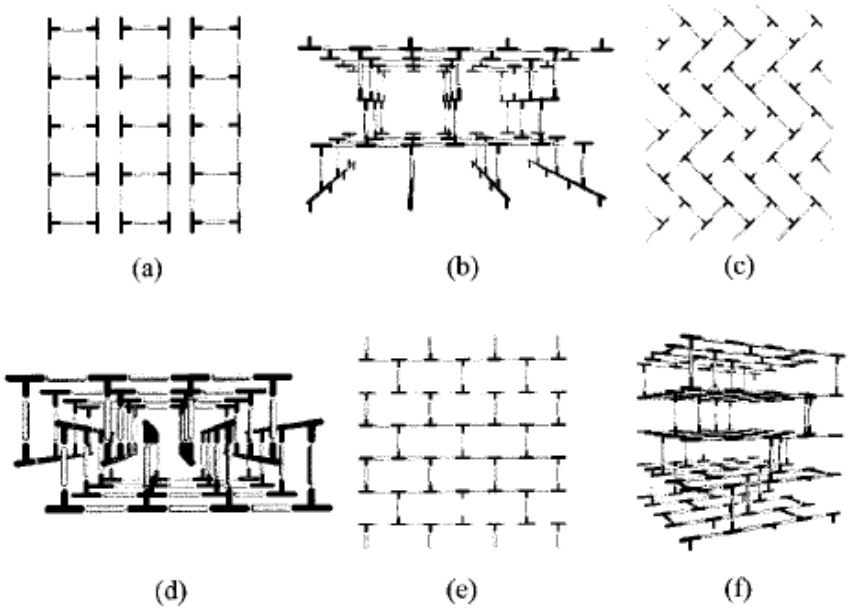

Figure 1.1: A schematic illustration given by Moulton *et al*[7] of the six supramolecular isomers reported for T-shaped nodes linked by linear bifunctional exodentate ligands. **a)** 1D ladder, **b)** 3D Lincoln logs, **c)** 2D herringbone, **d)** 2D bilayer, **e)** 2D brick wall and **f)** 3D frame

1.2 CRYSTAL ENGINEERING

"What would the properties of materials be if we could really arrange the atoms the way we want them?" [21]

Crystal engineering does not truly place atoms in the manner described above, however the idea put forward by Feynman must be the driving force behind the concept. The first use of the term "crystal engineering" is generally accredited to G. Schmidt (1971).[22] However, the phrase was first presented by R. Pepinsky at an American Physical Society Meeting in August 1955.[23] The term as used in 1955 did not have the scope that modern crystal engineering has but it shows that the idea of designing crystals has been around since at least the mid-1950s.[1,5] "Modern crystal engineering" only really emerged during the 1990s and has flourished due to

many factors. These include an increase in single crystal data collection speed, a decrease in the size and cost of computers, and the ability to manipulate molecular images in an easier manner. Perhaps the desire of crystallographers for new challenges has increased due to small molecule crystallography becoming increasingly accessible to non-specialists.[1] This modern form of the term connotes the chemistry of periodical supermolecules and it has grown particularly well in the area of coordination polymers and MOF chemistry. Crystal engineering is effectively the "bottom-up construction of functional materials from molecular or ionic building blocks".[1]

Although some people consider the word "design" to be inaccurate when applied to MOF preparation it is felt by many to be acceptable.[7,24,25] This is largely due to the difference between "design" and "structure prediction" as emphasized by Moulton *et al*. The former deals broadly with building blocks that are predisposed to form a certain network; the latter with space group determination.[7] Crystal engineering is effectively *making crystals by design*[1] and the aim is to assemble the desired solid-state structures and thereby confer new properties through this ordered structure as shown in Figure 1.2.[1,5] It has been said that the ability to control the solid state assembly of molecules is one of the most important issues when synthesising functional materials.[26]

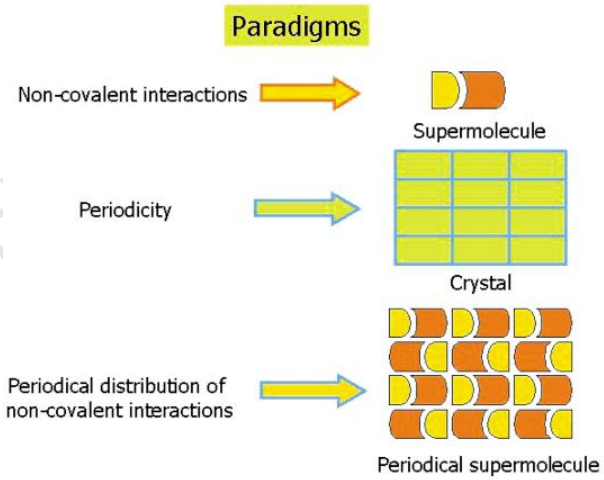

Figure 1.2: A Figure given by Braga[1] showing the transition from a molecule to a periodical supermolecule. The collective properties of a molecular crystal result from the convolution of the properties of the individual molecular/ionic building blocks with the periodical distribution of intermolecular non-covalent bonding of the crystal

Crystal engineering is hampered by supramolecular isomerism (see Section 1.1.1 – Supramolecular Isomerism), which has an influence on the crystal structure and bulk properties

of the compound. There are a large number of frameworks possible even from simple starting materials and this impedes design. Coordination polymers and MOFs have great potential for crystal engineering. This is because they are based on at least two building blocks which can be pre-selected for self-assembly, and they have possibilities in inclusion chemistry. Not only the building blocks, but also the solvent system can have a large effect on the final framework produced. The ratio of metal to ligand and the nature of the coordination of terminal ligands play important roles in determining the topology of a network.[7]

All of these criteria make design difficult but, with careful choice, a large scope of materials are available making it a worthy area to investigate. The aim of crystal engineering is to control these factors by assembling the molecular building blocks into the desired framework through control of the supramolecular interactions. It is therefore important to be careful when choosing those building blocks.[1] This means that the "design" of these complexes is the same in essentials as in classical chemistry. The classical process must necessarily be performed twice however: once for the building block preparation; once to arrange them in the desired supramolecular manner. To truly engineer a new compound one needs to understand the factors of interpenetration and design robust structures that can withstand solvent/guest exchange.[1] For example, tetrahedral nodes are more likely to form diamondoid networks whereas octahedral nodes form simple cubic, octahedral networks.[7,27] For a given size of the linker molecule tetrahedral nodes will offer frameworks with larger pores and access windows than those with octahedral nodes.[27]

Crystals have been prepared with a purpose in mind for a long time. The difference in modern crystal engineering is that there is a language to explain that design and there has been a change in perspective from viewing crystals as separate to molecules to viewing them as supermolecules.[1] Even modern crystal engineering has been around for a number of years. In the early 1990s Robson and coworkers planned the construction of coordination polymers with a targeted structure and expected the field to grow.[28] Major challenges to prediction remain: the lack of knowledge of the space group of the crystal, the size of the single crystals or even whether the solid will be crystalline. For even a miniscule single crystal it is necessary for billions of molecules to self-arrange.[1] This makes the design process difficult. However, if one can put appropriate building blocks with the desired connectivity and functionality together into solution then the result should be the preparation of the desired network.[29]

1.2.1 RETICULAR SYNTHESIS

"Crystalline materials could be made by design: we called that process reticular chemistry" [30]

The design of coordination polymers and MOFs involves the planned preparation of three-dimensional nets and is a subset of crystal engineering. This subgroup has been given the term reticular synthesis.[5] A reticular structure has the form of a net and structures which contain the same topological net are called isoreticular.[24,31] This area is especially relevant to coordination polymers and MOFs as they make up the largest portion of engineered crystal structures.[1] These compounds are formed from building blocks and knowing how these building blocks work is essential for knowing which ones are desired for a target structure. One must have a good knowledge of the desired network and be able to identify those building blocks necessary to form it.[24] This knowledge is one of the ways that topological analysis can be used in the reticular synthesis of MOFs. Of course there are difficulties as a given metal centre can adopt different coordination numbers with different geometries.[27,31] Other factors such as the ability of organic linkers to hydrogen bond can also play a vital role in the structure formed. The final outcome is often determined by a fine balance of subtle effects.[29] Isoreticular nets are a particularly good example of reticular synthesis; a range of compounds with the same basic topology but systematically varying properties and pore size are prepared from differing organic linker backbones.[32]

It is doubtful that the term "reticular synthesis" is truly necessary as it is included in the concept of crystal engineering. The definition given by Yaghi *et al* in a 2003 paper[24] was that the essential process for reticular synthesis is to:

1. Choose a target network.
2. Deconstruct the network into the component geometric parts.
3. Choose building blocks with those specified geometries.
4. Assemble these building blocks into a MOF with the targeted topology.

In a paper published in 1994 in the same journal[33] a way of approaching crystal engineering was offered:

1. Choose a geometrical or topological model of a simple 3D net.
2. Choose molecular building blocks with functionality and stereochemistry applicable for the net desired.
3. Devise ways of chemically linking these building blocks together.

As implied by Robson in 2008[28] these two methods are markedly similar in that a desired network is chosen, it is deconstructed into appropriate building blocks, which are then combined. However, the definition presented in 2003 was reported as being a new method applicable specifically to MOFs – reticular synthesis.

1.2.2 SECONDARY-BUILDING UNITS

MOFs and coordination polymers are formed from building blocks. These building blocks are metal ions and organic linker molecules. The organic linker molecules, if they have three or more points of extension, act as good directional building blocks. The metal ions often have more than one coordination mode and it is not easy to predict which one will be adopted.[27,31] Supramolecular synthons describe the bonds that are likely to form between building blocks.[5] Therefore by knowing the probable supramolecular synthons formed by particular building blocks one can determine the most probable secondary-building units (SBUs) that will form. Secondary-building units are generally formed *in situ* through a self-assembly process.[25,31] SBUs generally consist of metal ions brought together by organic linkers to form clusters. For example carboxylates would form M-O-C clusters (M = metal, O = oxygen, C = carbon).[24,34,35] These clusters act as connection points and have their own geometry and connectivity. Although SBUs are not discrete molecular bodies added to the reaction vessel[25,31] they are generally rigid and one can reproduce the formation of SBUs under specific reaction conditions.[24,31] This leads to control of the overall framework.

The paddle-wheel motif (Figure 1.3a) is found in hundreds of different binuclear metal-carboxylates. This SBU is formed by four carboxylate moieties each bridging the same two metal ions.[36] The metal ions often adopt a square pyramidal geometry with the axial position occupied by a labile ligand or guest molecule.[37] It is also possible for another ligand to coordinate in this

position. Dissociation of the axial ligands results in binding between the open metal site and a Lewis base atom on a nearby unit. This leads to cluster dimers or extended chain structures.[37] This has been useful in joining two-dimensional carboxylate sheets into three-dimensional frameworks through diamine or diimine type linkers.[38] However, it is possible for a chelating carboxylate to coordinate in this position (Figure 1.3b). This can extend the network in another dimension and leads to an octahedral geometry for the SBU. Another common SBU is the OZn_4^{6+} clusters coordinated to six carboxylate anions (Figure 1.3c). Each carboxylate is a point of extension in the SBU and this leads to an octahedral node.[25]

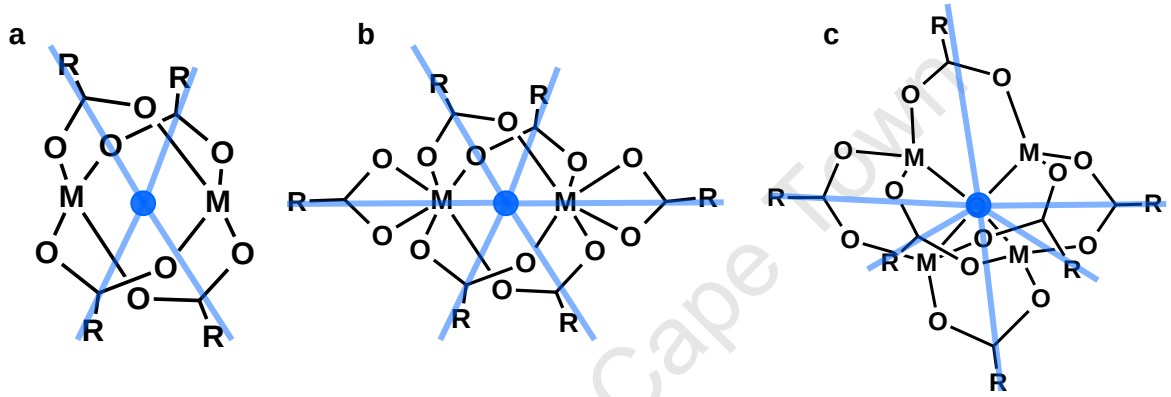

Figure 1.3: Some common bonding motifs. **a)** The paddle-wheel motif, **b)** the paddle-wheel motif with chelating carboxylates in the axial positions, and **c)** the OZn_4-carboxylate SBU.

1.3 INTERPENETRATION

Metal-organic frameworks have the potential for large void spaces. There has been much research in recent years around preparing substances with larger pore volumes. The general trend is the larger the pore volume the greater the possibility of entangled structures forming. This is because voids are generally occupied by either solvent molecules[39-42] and/or the networks "self-fill" through interpenetration.[32,42-46] Interpenetration implies that the voids of one structure are filled by other independent frameworks and that these frameworks can only be disentangled from each other by the breaking of bonds.[29] In the strictest sense of the word "interpenetration" is when the frameworks are at a maximum displacement from one another, whereas interweaving is a special case where the frameworks are located at a minimum distance and demonstrate close contacts.[31] In this thesis the term interpenetration will be used to refer to both cases.

Interpenetration can lead to exceedingly hard structures[47] as well as to compounds with electrical conductivity[48] and magnetic materials.[49,50] Homocatenation is the interpenetration of identical networks, while heterocatenation is the interpenetration of different networks.[7] A compound which forms both interpenetrated and non-interpenetrated forms may be considered as being catenate and non-catenane supramolecular isomers of one another[7] (See Section 1.1.1 – Supramolecular Isomerism). Although interpenetration reduces the pore size of a framework[51] the structure can still possess useful properties such as increased stability leading to enhanced gas uptake.[44] Interpenetration can also be a design target in order to transform two-dimensional networks into three-dimensional ones.[7]

1.4 MOFs AND COORDINATION POLYMERS

Coordination polymers and metal-organic frameworks are both common topics in modern chemistry. This thesis deals with the preparation of novel MOFs and coordination polymers. There is much debate over what exactly constitutes each of these types of compounds. The nomenclature debate, as well as the many varied uses of these compounds, is discussed in detail in this section.

1.4.1 NOMENCLATURE

There has been much debate over the nomenclature of compounds containing metal ions coordinated to organic molecules. The definition of coordination polymers and metal-organic frameworks (MOFs) varies with the author and the article. In one of the earliest references to a MOF (1995) Yaghi *et al* described the hydrothermal synthesis of a "metal-organic framework containing large rectangular channels"[46] (Figure 1.4a). Three 4,4'-bipyridine (bipy) organic linkers were coordinated to individual copper ions to form a three-dimensional, interpenetrating cationic framework. Another MOF reported by Yaghi *et al* (1995)[52] as well as MacGillivray *et al* (1994)[53] contained bipy organic linkers coordinated in a tetrahedral fashion to individual copper ions (Figure 1.4b). A cationic, interpenetrated framework was formed.

There are very few bipy frameworks reported by Yaghi after this point. However, bipy structures are still referred to as metal-organic frameworks in 2000.[25] It was found that the M-N bonds obtained in these compounds led to structures with low stability and high flexibility. As a result of

the search for stable frameworks the focus changed to carboxylate organic linkers. These led to more robust, rigid frameworks as shown in multiple papers by Yaghi and coworkers between 1996 and 2001.[26,34,37,41,45,54-58] These successes undoubtedly directed the future MOF work of these authors. In their 2001 paper in *JACS* there was only a passing mention of MOFs prepared from bipy although the definition given of a MOF remained the same.[56]

In 2003 cyanide and triazole were reported as possible organic linkers for MOFs and both "carboxylate MOFs" and "MOFs based on M-N linkages where the vertex is a single atom" were mentioned.[24] In 2004 Rowsell and Yaghi[31] defined coordination polymers as an "extended connection of metal and ligand monomers through coordination bonds". They mention that MOFs should be robust, with organic molecules that can be modified post-synthesis and have well-defined geometries.[31] These definitions clearly imply that MOFs are a special subset of coordination polymers, but appear to exclude bipy structures. Later in the same paper however, they refer to pyridyl-based MOFs and carboxylate MOFs as two distinct groups but still both MOFs.[31]

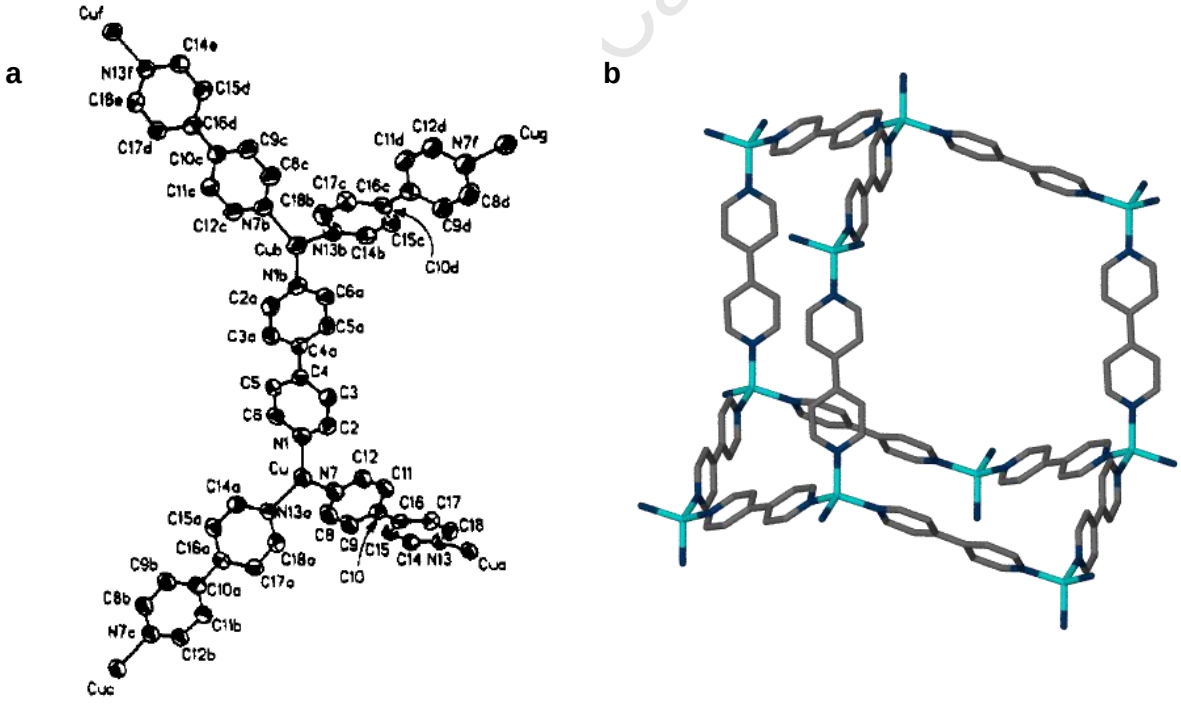

Figure 1.4: a) Figure 1 from Yaghi *et al*[46] of the $Cu(4,4'\text{-bpy})_{1.5}\cdot NO_3(H_2O)_{1.5}$ metal-organic framework and **b)** the cationic adamantoid framework formed by the copper-bipyridine framework of MacGillivray *et al*[53]

The 2003 paper mentioned that MOFs with single metal ions and M-N linkages were not as robust and had less directional control than carboxylate MOFs.[24] The poor stability of pyridyl

based MOFs and the lack of geometrical control of those with single metal ions as connectors, coupled with further triumphs in the field of carboxylate MOFs[32,35,59-61] probably caused the dramatic change in the definition of a MOF as given by Yaghi and co-workers. This change is reported in a 2009 paper in *Chemical Society Reviews*.[36] Table 1.1 summarises this definition of MOFs. M-N bonds, where the metal is a transition metal and the nitrogen belongs to bipyridine have zero formal bond valence and low bond energy. The term "coordination polymer" was assigned to materials containing this sort of bond. The term metal-organic framework was reserved for compounds containing M-O bonds with formal valence of 1/2. To be named "MOF" the compound framework must also be neutral, a feature not found in early MOFs. A high formal valence is found for M-N bonds in imidazole containing frameworks but these are placed in a class of their own, namely zeolitic imidazole frameworks (ZIFs).[36] Carboxylate groups are able to cluster metal ions into secondary-building units (SBUs) *in situ* (see Section 1.2.2 – Secondary-Building Units).[24,34,35] This was probably the reason for another change in viewpoint from "MOFs contain metal ions"[46] to "MOFs contain metal ion clusters".[36] Table 1.1 is taken from the 2009 *Chemical Society Reviews* paper[36] and lists the key differences between coordination polymers and MOFs as viewed by that group in 2009.

Table 1.1: Some distinctions between a typical MOF (MOF-5) and a typical coordination polymer $[Zn(L)_2(ClO_4)_2]$[24,41,62] as presented by Tranchemontagne *et al*.[36]

Property	MOF-5	$Zn(L)_2(ClO_4)_2$[a]
Joint (SBU)	Polyatomic (OZn_4)	Monatomic (Zn)
Framework	Neutral	Charged
Pores	Can be empty	Must contain counterions
Formal bond valence (Zn-O or Zn-N)	1/2	0
Estimated link energy (2Zn-O or Zn-N)/kJ mol^{-1}	363	100–150
Zn-X bond to break to excise SBU	12	4
Estimated energy to excise SBU/kJ mol^{-1}	2200	400–600

[a] L = *N*,*N*'-Bis(4-pyridyl)urea.

Michael O'Keeffe has written over 100 papers with Yaghi and further urges their 2009 view of MOFs in his paper in the same issue of Chemical Society Reviews.[30] O'Keeffe wrote that MOFs are not coordination polymers as the latter contain "generally weaker bonds and [have] lower stability". He also asserted that MOFs must be formed from polyatomic clusters of metal ions

(SBUs) connected by covalent bonds to one another (the organic linkers). A comparison between the MOFs presented in 1995 by Yaghi *et al*[46,52] and the definition given in 2009[36] is presented in Table 1.2.

Table 1.2: A comparison between a MOFs presented in 1995[46, 52] and the definition of MOF given by the same author in 2009[36]

Property	1994/1995 MOF	1995 MOF	2009 Definition
Joint (SBU)	Monatomic	Monatomic	Polyatomic
Framework	Charged	Charged	Neutral
Bond Type	M-N	M-N	M-O
Formal bond valence	0	0	1/2

As previously stated one of the first mentions of a MOF was of a cationic framework made of 4,4'-bipyridine coordinated to single metal ions. Each metal was coordinated to the nitrogen atoms of three separate bipy molecules. Fourteen years later the same group published a definition that excludes that structure from the term MOF. MOFs, by the new definition, must be neutral. They must contain strong M-O bonds with a formal valence of 1/2. They must contain polyatomic metal clusters and one must be able to empty the pores. It is easy to see that Yaghi's 1995 "MOF" would be classified as a coordination polymer and not a MOF by this current definition.[36] Perhaps it is relevant at this point to note two things. Firstly, a statement from a News Feature in *Nature* magazine that "Omar Yaghi was the first to design a metal-organic framework".[63] Secondly, R. Robson's opinion on that statement considering Yaghi was the first person to use the term: "given the origin of the term metal-organic framework, [this] is not (in a strictly legalistic sense) incorrect".[28]

A large amount of weight should be given to the definition put forward by those who first employed the term "metal-organic framework". However, if the opinions of this one group of authors can change so significantly over time it is unsurprising that the definitions given in the literature by different authors vary widely as well. There are authors who use the words coordination polymer and metal-organic frameworks interchangeably.[42,64-68] Others class MOFs as a special subgroup of coordination polymers based on varying properties, often mainly that they extend in three-dimensions.[69] The three-dimensional requirement is found regardless of whether they are seen as a subset of coordination polymers or not.[5,69-72] Rowsell *et al* allude to this debate in their 2004 paper[31] but appear to feel that if a structure displays sorption properties or helps with design strategies it can be referred to as a MOF regardless of dimensionality.

Borel[73] even states that ZMOF, ZIRMOF, IRMOF, MIL, ZIF, CPL, MOROF, JAST, HKUST, SPC and PCP (see footnote for definitions) are all just different ways of writing "MOF" and Kanoo *et al* use the terms PCP and MOF interchangeably.[74]

A graphic by Perry *et al*[69] shows their perspective of MOFs and coordination polymers and is given in Figure 1.5. They assert that coordination polymers can be 1D, 2D or 3D but not 0D and that MOFs are a 3D subset of coordination polymers.

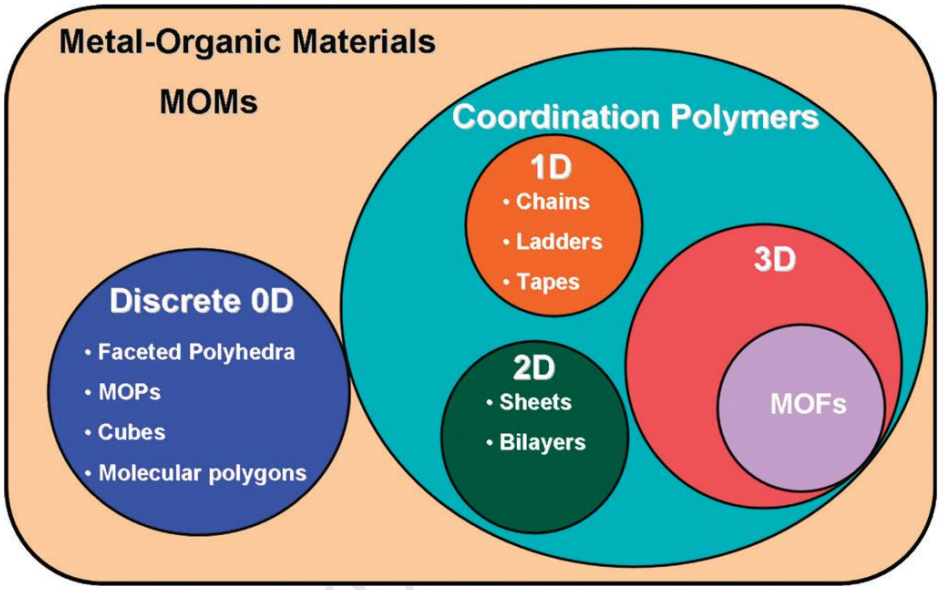

Figure 1.5: A schematic presented by Perry *et al*[69] on the relationship between various metal-organic materials (MOMs)

While Perry *et al* state that MOFs must be three-dimensional others maintain that MOFs can be either one, two or three-dimensional or report MOFs with dimensionality lower than three.[64,75-77] More generally however the author's definition of "what makes a MOF" is not explicitly stated. Yaghi and coworkers make no mention of dimensionality (see Table 1.1). Several authors state that a compound should be highly robust[71,78] and permanently porous[65,74,79] to be called a MOF whereas permanent porosity is implied but not specifically stated as a requirement in others.[31,78,80,81] Different definitions of porosity are given by various authors. It is stated by Barbour[82] that for a structure to be termed porous gas sorption experiments must have been performed. He goes on to state one must be careful not to overuse the term for fear of "diminishing [the] impact" of this "very special phenomenon". There are examples in the literature of materials that are called MOFs but lose single crystallinity and give

*Zeolite-like Metal-Organic Frameworks (ZMOF); Isoreticular Metal-Organic Framework (IRMOF); Material Institut Lavoiser (MIL); Zeolite Imidazole Framework (ZIF); Co-ordination Pillar Layer (CPL); Metal-Organic Radical Open Framework (MOROF); Jungle Gym Analog Structure (JAST); Soft Porous Crystal (SPC); Surface-Mounted Metal-Organic Frameworks (SURMOF); Porous Coordination Polymer (PCP)

a different powder X-ray diffraction (PXRD) pattern as a result of guest solvent removal. This change can include a dramatic decrease in the number of diffraction peaks as well as their positions (the structure has changed upon desolvation). In some instances exposure to solvent after desolvation did not result in the original structure being regained. This structure is therefore not permanently porous but is still referred to as a MOF.[54,83] Despite some assertion that MOFs must be neutral there are anionic and cationic frameworks reported that are reported as being MOFs.[83-85] Sometimes authors insist that MOFs contain carboxylates,[86] but more often MOFs are presented that either contain pyridyls only or a mixture of pyridyls and carboxylates.[42,75,87-89] More often than not MOFs are defined as containing either single metal ions or clusters.[75,86,90]

A recent definition of MOFs was given by D. Proserpio in a seminar presented at the 2011 IUCr conference:[91]

1. A MOF must contain a metal cation, generally in secondary-building unit clusters.
2. A MOF must contain organic linker molecules.
3. The framework must be neutral.
4. The framework must be robust and highly porous.

This definition is similar to that presented by Tranchemontagne[36] although Proserpio was not specific about whether the metal ions must form clusters or not. This definition also offers no viewpoint on dimensionality. This implies that one-dimensional chains formed into supramolecular frameworks through hydrogen bonds could potentially be considered as MOFs.

Thus, the definitions of MOFs are almost as varied as the MOFs themselves. In fact, the only thing almost all authors agree on is that MOFs and coordination polymers must be self-assembled from metal ions linked by organic ligands in some manner. This linkage must extend solely through coordination bonds in at least one-dimension.[5]

One author was even insistent that the term MOF should not be used at all. Robson stated in his 2008 paper in *Dalton Transactions*[28] that as deliberate design of these frameworks is only possible due to the large amount of information available from coordination chemistry it is only natural to call them coordination polymers. He states that the term MOF is unnecessary as it rules out so many complexes simply because they are not polymeric or contain inorganic

ligands. “The MOF terminology is unnecessarily restrictive” he asserts “why should we … relegate networks formed from perfectly respectable “inorganic” bridging species to some limbo”.

Regardless of these arguments the term MOF is in wide use with Long and Yaghi[78] reporting the existence of almost 4000 MOF structures in the Cambridge Structural Database (CSD).[92] The debate over MOF and coordination polymer nomenclature is important enough that an International Union of Pure and Applied Chemistry (IUPAC) Project on coordination polymer and MOF nomenclature was started in 2009. This project was founded to determine nomenclature and terminology guidelines, to ensure acceptance of these guidelines, and to have them implemented. This project is chaired by Professor Lars Öhrström, has many experts on MOF and coordination chemistry on the committee[93] and is still on-going. Correct nomenclature is important to prevent confusion[5] and to facilitate the search for all literature related to a specific area.[73] However, too much terminology for one area can hinder literature searches. It is important not to become “lost in endless battles of definition” without really adding anything useful to our understanding.[5]

1.4.2 DEFINTION OF MOFS IN THIS THESIS

“to assert that MOFs are not coordination polymers and constitute a new and special class ignores the unquestionable fact that they are simply polymeric systems held together by coordinate bonds.” [28]

“the language we use is a very personal thing, and up to ourselves to judge” [5]

Even the strictest of definitions given in the literature[36] allows for “intermediate materials”, which have some characteristics of both coordination polymers and metal-organic frameworks. It is into this area, if one adheres to that definition, that the compounds presented in this thesis would fall. However, the following definitions of coordination polymers and MOFs will be used in this thesis:

1. MOFs are a special subset of coordination polymers.
2. A MOF can be 1, 2 or 3-dimensional but not 0-dimensional (ie a discrete chemical entity).
3. Metal ions or secondary-building units must be connected through covalent bonds in an organic linker molecule to be termed a MOF.
4. The framework can be neutral or charged.
5. The framework should be robust and stable in air.

1.4.3 USES

It is possible to obtain a wide range of structures from very simple starting materials with both coordination polymers and MOFs.[7] This allows for uses in many diverse areas. MOFs have many similarities in design to zeolites but have the potential for larger cavities and better access to these cavities.[27] There are many examples in the literature of frameworks with high apparent surface areas,[32,37,41,45] which are stable with guest removal[32,34,37,41,55,57,58,94,95] and are porous.[32,34,37,41,55,56,94,95] It is also possible to design MOFs with a greater concentration of active sites by using building blocks containing desired moieties[27] or to modify the organic linker post-synthetically.[96,97] A good choice of building block is essential when preparing MOFs for specific functions.[98] These choices affect pore size and shape as well as the probability of interpenetration. MOFs offer varied opportunities as they contain aspects of coordination, organic and main group chemistry.[29]

The potential of coordination polymers has been noted since the early '90s with Hoskins *et al* predicting that these "scaffolding-like materials" might be useful as molecular sieves; have the potential for large void spaces; and may be chemically functionalised for catalysis.[27] These predictions have come true in many ways and lend credence to the idea of MOF crystal engineering (see Section1.2 – Crystal Engineering).

Among the useful properties displayed by coordination polymers and MOFs are chemical separation,[99-104] catalysis,[101,105,106] nonlinear optics,[85,107] gas storage/sorption,[39,61,68,108-115] magnetics,[116-120] sensing,[121-124] molecular sieves,[125,126] and luminescence.[116-118,127-130] Enantioselective separation and catalysis are particularly important for the chemical and pharmaceutical industries.[101] Separation is demonstrated by the zinc containing metal-organic supramolecular isomers reported by Kishan *et al*.[102] $[Zn_2(C_{33}O_{12}H_{24})(DMF)]\cdot DMF$ and $[Zn(C_{33}O_{12}H_{24})]$ ($C_{33}O_{12}H_{24}$ = 4-carboxylatophenoxymethyl)methane) from Kishan's paper absorb CO_2 in preference to CH_4 (Figure 1.6a), N_2, and H_2. A recent report details the inclusion of a polyoxometalate (a catalyst) into a MOF increasing the stability of both, and the catalytic turnover rate of the polyoxometalate.[131] Horike *et al*[106] report a thermally stable microporous MOF with exposed Mn(II) sites as shown in Figure 1.6b. This MOF is able to "catalyse the cyanosilylation of aromatic aldehydes and the Mukaiyama-aldol reaction in a size-selective fashion".

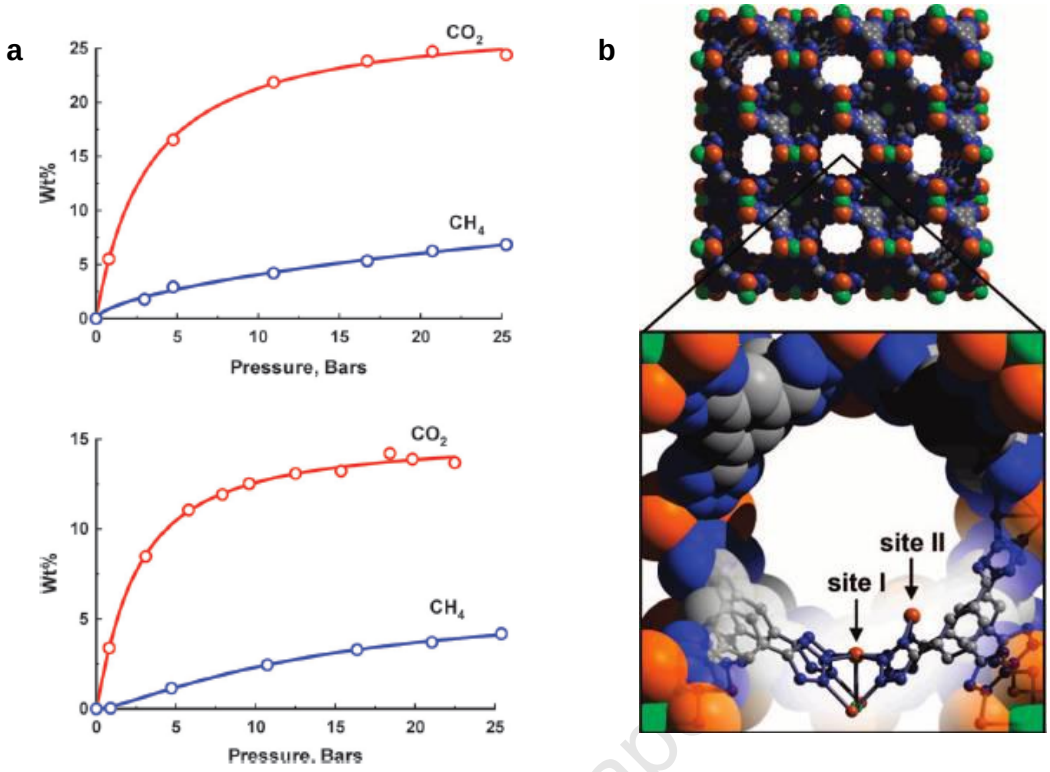

Figure 1.6: a) A figure taken from Kishan *et al*[102] showing the sorption isotherms of compounds $[Zn_2(C_{33}O_{12}H_{24})(DMF)]\cdot DMF$ (top) and $[Zn(C_{33}O_{12}H_{24})]$ (bottom). CO_2 is absorbed selectively over CH_4 in both instances. **b)** A portion of the crystal structure of $Mn_3[(Mn_4Cl)_3(BTT)_8(CH_3OH)_{10}]_2$ (H_3BTT = 1,3,5-benzenetristetrazol-5-yl) as depicted by Horike *et al*[106] showing the two types of exposed Mn(II) sites within the 10 Å wide channels. Orange, green, gray, and blue spheres represent Mn, Cl, C, and N atoms, respectively

Two compounds reported by Zhang *et al*[107] dramatically increase the emission of isophthalic acid in the visible spectrum (Figure 1.7a). The zinc network displays moderately strong second harmonic generation, is transparent in the 400 – 1100 nm range and is stable to approximately 500 °C making it a good potential candidate for nonlinear optics. Gas sorption properties are demonstrated by MOF-505[61] which displays H_2 sorption of 2.47 wt% at 77 K and 750 Torr after evacuation and complete dehydration of the MOF at 120 °C (Figure 1.7b). MOF-505 also displays reversible type-I isotherms with N_2 gas at 77 K.

$[Ni_3(\mu_3\text{-}OH)_2(\mu_4\text{-}cis\text{-}1,4\text{-}chdc)_2(H_2O)_4]\cdot 2H_2O$ (1,4-chdc = cyclohexanedicarboxylic acid) is reported by Kurmoo *et al*[120] to display isothermal magnetisation at 2 K. When in its original, virgin form it displays long-range ordering to a ferrimagnetic ground state. This is reversibly transformed to a ferromagnet at low temperatures with partial dehydration and rehydration (Figure 1.8).

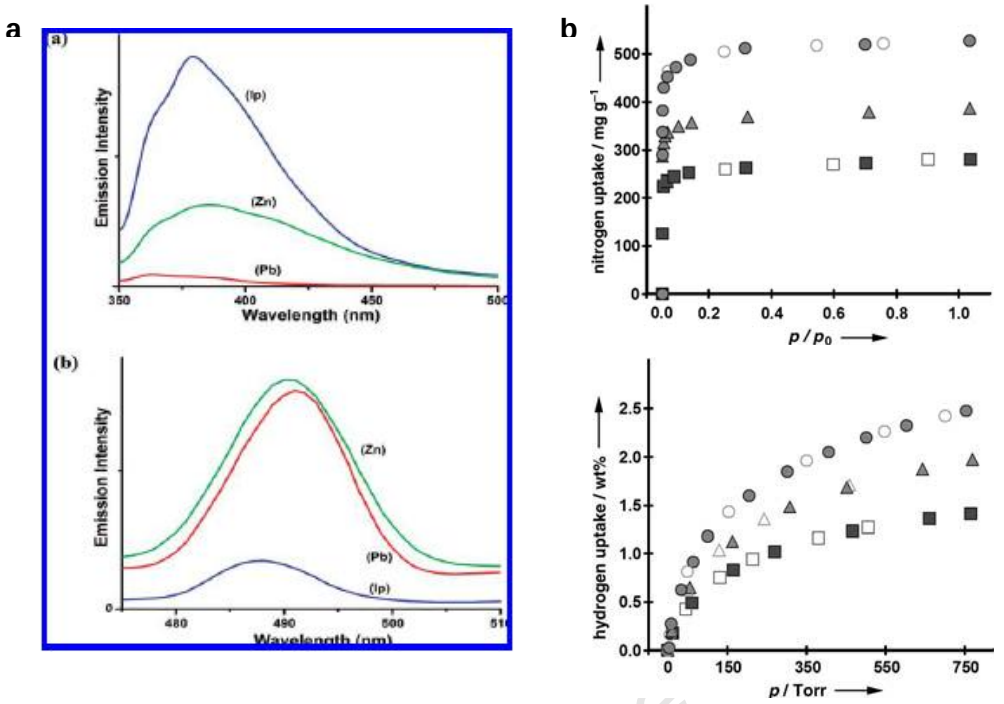

Figure 1.7: a) The solid-state emission spectra of $[Zn(ip)]_n$ and $[Pb_4(\mu_4\text{-}O)(ip)_3(H_2O)]_n$ and isophthalic acid (H_2ip) in the UV area (top) and the visible area (bottom) as reported by Zhang *et al*.[107] **b)** The N_2 (top) and H_2 (bottom) sorption isotherms of MOF-505[61] at 77 K after activation at 25 °C (squares), 70 °C (triangles) and 120 °C (circles). Filled shapes are for adsorption and open shapes for desorption data points.

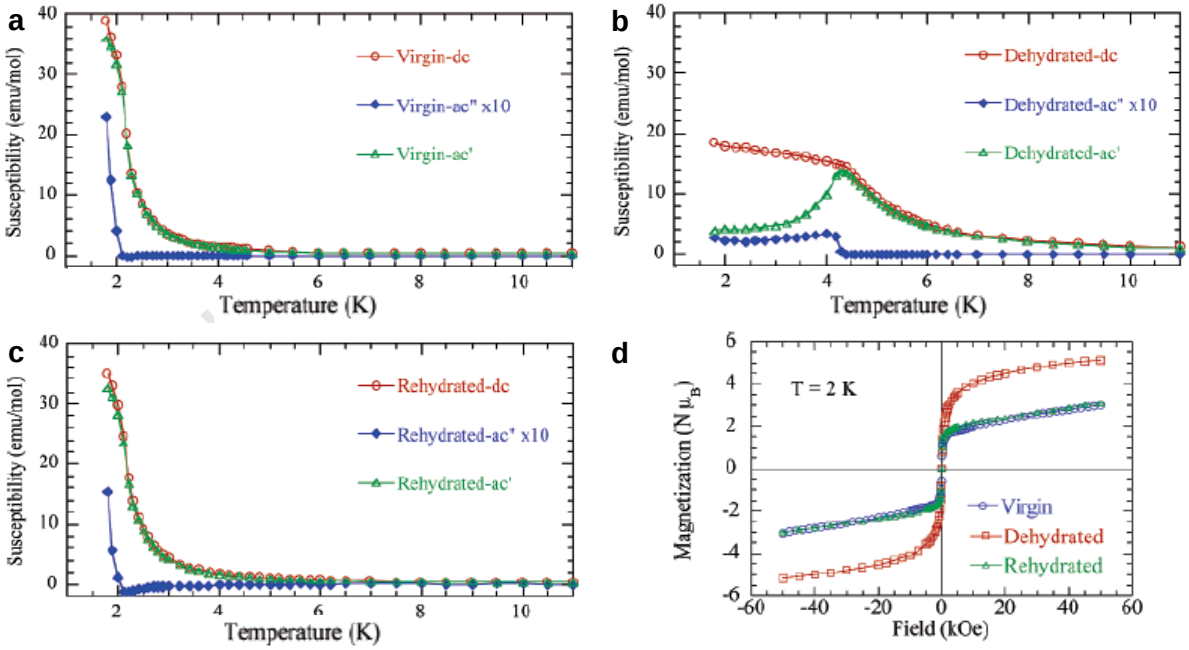

Figure 1.8: Figures taken from Kurmoo *et al*[120] showing the temperature dependence of dc (red) and ac (blue, green) magnetisations measured in an applied field of 1 Oe for **a)** the virgin form, **b)** the partially dehydrated form and **c)** the rehydrated form of $[Ni_3(\mu_3\text{-}OH)_2(\mu_4\text{-}cis\text{-}1,4\text{-}chdc)_2(H_2O)_4]\cdot 2H_2O$ (**1**) **d)** The isothermal magnetisation of **1** at 2 K in its virgin (blue circles), partially dehydrated (red squares), and rehydrated (green triangles) forms

Furman *et al*[128] report a "new approach to the development of solid state lighting phosphors" presenting two dense inorganic-organic frameworks – $Ca(FDC)(H_2O)_2$ (**1**) and $Sr(FDC)(H_2O)_5 \cdot 2H_2O$ (**2**) (H_2FDC = 9-fluorenone-2,7-dicarboxylic acid). These compounds absorb strongly between 380 and 460 nm and emit strongly at 503 and 526 nm, respectively. The temperature dependent emission spectra and excitation spectra of H_2FDC, **1** and **2** are given in Figure 1.9

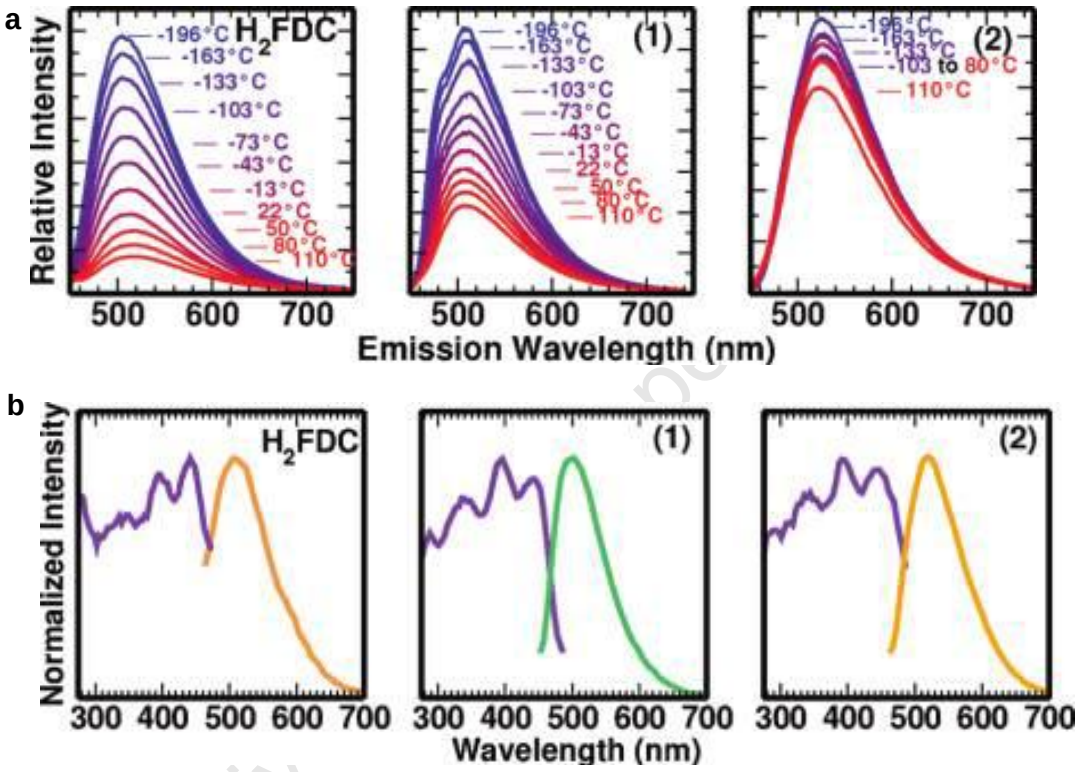

Figure 1.9: Figures taken from a paper by Furman *et al.*[128] **a)** The temperature dependent emission spectra (λ_{ex} = 405 nm) and **b)** emission and excitation spectra at λ_{ex} = 440 nm and λ_{em} = 500 nm of H_2FDC, **1**, and **2**, respectively where **1** is $Ca(FDC)(H_2O)_2$ and **2** is $Sr(FDC)(H_2O)_5 \cdot 2H_2O$

MOF 1a reported by Guo *et al*[122] is a solvent free framework with open Yb^{3+} sites able to be used in small molecule recognition. The photoluminescence (PL) spectrum of MOF 1a is dependent on the solvent molecules (Figure 1.10a). These solvent-dependent luminescence properties enable the sensing of certain solvent molecules. Chang *et al*[125] report the design of MOF-based (ZIF-8) molecular sieves for solid-phase microextraction and high-resolution gas chromatographic separation. A schematic of this process is given in Figure 1.10b.

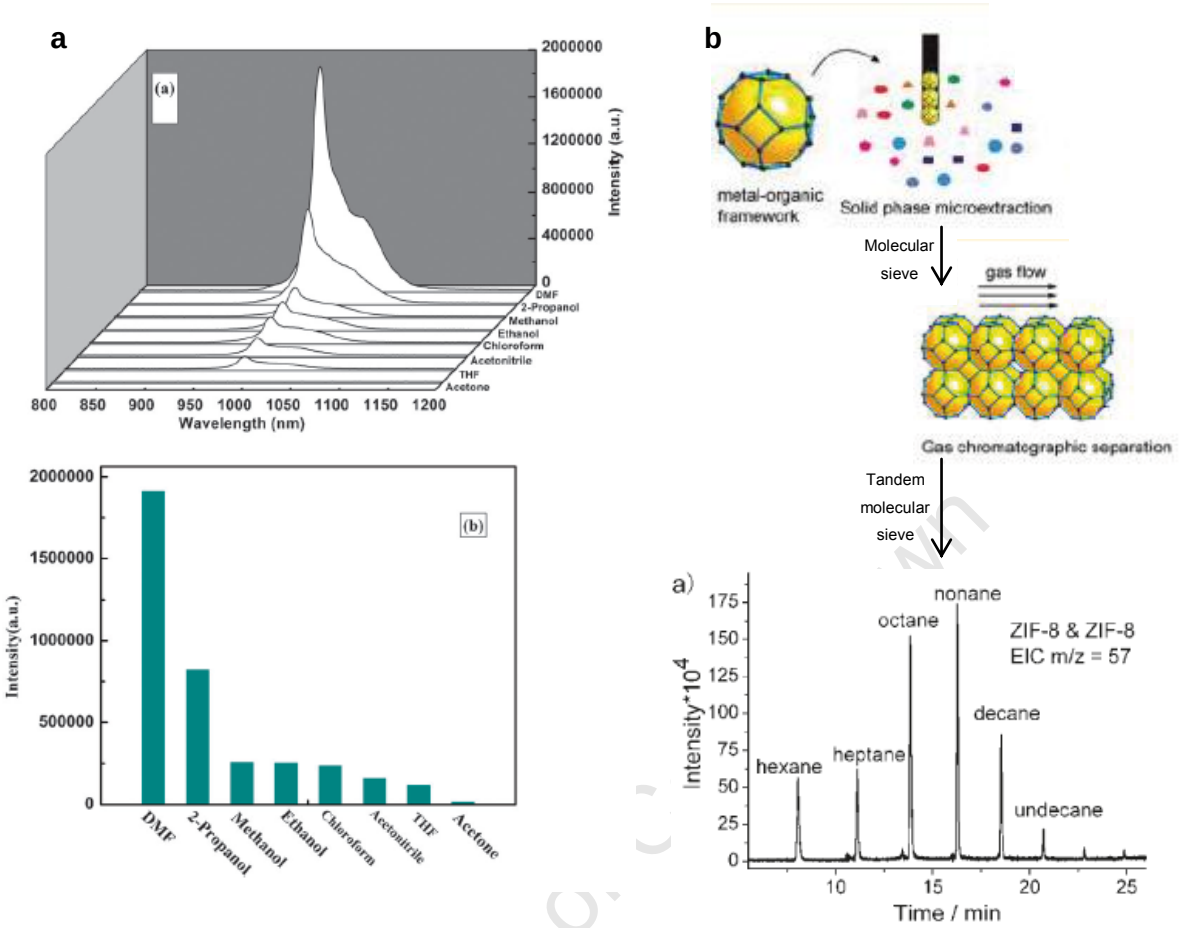

Figure 1.10: a) The photoluminescence (PL) spectra (top) and $^2F_{5/2} \rightarrow {}^2F_{7/2}$ transition intensities (bottom) of MOF **1a** introduced into various pure solvent systmes and excited at 304 nm as reported by Guo *et al*.[122] **b)** A schematic showing a MOF (ZIF-8) being used in solid phase microextraction to separate small molecules, adapted from the schematic given by Chang *et al*[125]

1.5 ORGANIC LINKERS

Two organic linkers were used in this project: 1,3,5-benzenetricarboxylic acid (H_3BTRI) and 5-nitroisophthalic acid (H_2NIA). The properties of carboxylate moieties in organic molecules, and specifically H_3BTRI, and H_2NIA, as well as their application to MOF chemistry is discussed in this section.

1.5.1 CARBOXYLATES

Carboxylate groups form particularly strong coordinate bonds with metal ions making them well suited to create robust structures. There are many well-known MOFs based on polycarboxylate ligands due to the high thermal robustness of these SBUs, which leads to thermally robust frameworks.[98] They are able to chelate to metal centres adding to the strength of the overall structure.[27] The carboxylic acid dimer is one of the most well-known supramolecular synthons.[7] Carboxylate moieties can bridge metal centres and thereby help to form SBUs. Many studies have been performed where the length of the organic backbone has been varied to change pore size, but the basic carboxylate connectors have been maintained.[32] This is through control of the synthesis conditions.[32]

Carboxylates have been found to be essential in some structures. These are used as fluorescent probes for small molecule detection.[57] Aromatic carboxylates are particularly able to aggregate metal ions into M-O-C clusters, thereby forming SBUs *in situ*[132] (see Section 1.2.2 – Secondary-Building Units). These secondary building units are known to lead to more rigid and robust frameworks. The metal clusters can contain different numbers of metal ions and therefore act as a variety of different connectors. This increases the range of possible structures. Benzoic multicarboxylate ligands specifically have been shown to work well as building blocks in metal-organic materials.[133] It is also possible to functionalise those backbones without affecting the carboxylate coordination.[32]

1.5.2 1,3,5-BENZENTRICARBOXYLIC ACID

1,3,5-benzenetricarboxylic acid (H_3BTRI) is a commonly used starting material and has been used to prepare many novel coordination polymers and interesting MOFs.[51,88,130,134-137] H_3BTRI consists of a rigid benzene ring and three regularly distributed carboxylate moieties with potentially varied coordination modes.[134,137,138] The carboxylate moieties can bridge metal centres, chelate to the same metal centre or singly coordinate to only one metal centre (Figure 1.11). Different coordination modes can be found for each carboxylate within one fully deprotonated $BTRI^{3-}$ anion. This has led to it being used a great deal to form porous frameworks.[135]

H_3BTRI has the ability to increase the thermal stability of frameworks compared to those containing only metal-nitrogen bonds.[42] The size and shape of H_3BTRI as well as its ability to coordinate through three carboxylate moieties means the rigidity of the framework can be enhanced. This in turn allows access to the metal centres of the structure.[51] $BTRI^{3-}$ can bind through all three carboxylate moieties in a multidentate fashion. This allows desirable three-dimensional structures to be formed.[51] $BTRI^{3-}$ is often used as a co-ligand[42,88,137,139,140] with other interesting organic molecules and can give rise to multidimensional MOFs.[42,51,134,135]

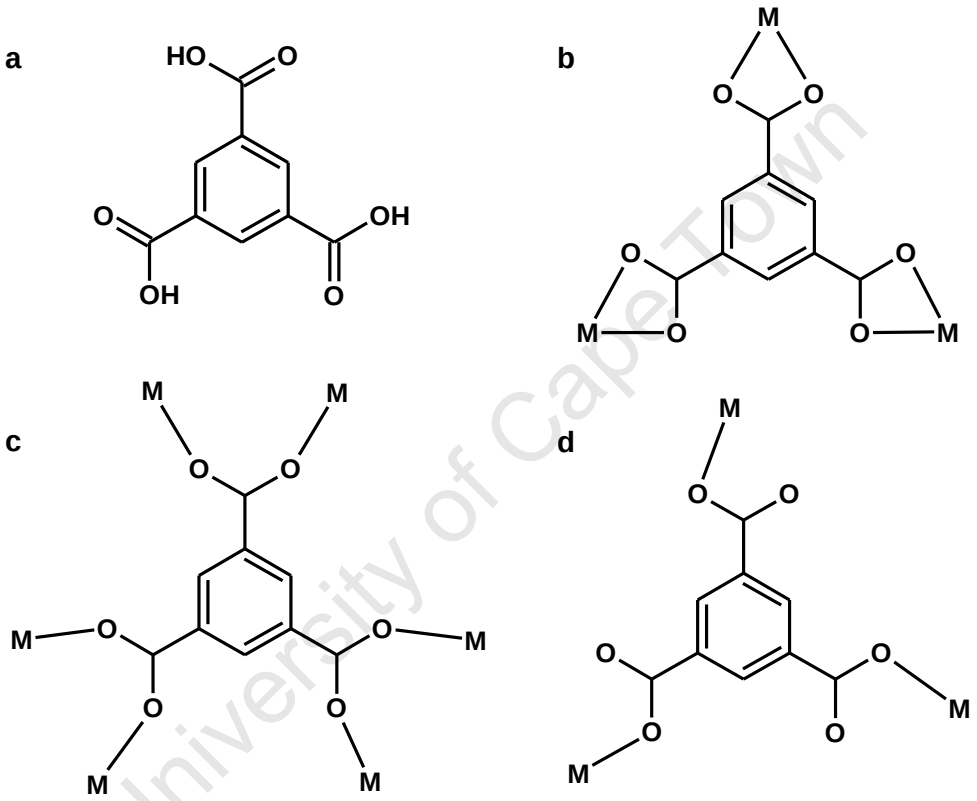

Figure 1.11: a) The structure 1,3,5-benzenetricarboxylic acid (H_3BTRI). Some binding modes of the fully deprotonated $BTRI^{3-}$ **b)** chelated through both oxygen atoms of each carboxylate to a single metal ion, **c)** bridging two metal centres with each carboxylate and **d)** coordinated through only one oxygen atom of each carboxylate to a metal ion

1.5.3 5-NITROISOPHTHALIC ACID

H_2NIA (Figure 1.12) possesses rich coordination modes. These coordination modes are similar to those seen in Figure 1.11 for $BTRI^{3-}$. Each carboxylate within a H_2NIA unit can coordinate in a different manner. NIA^{2-} anions can coordinate particularly well with lanthanide metal ions, forming SBUs of lanthanide metal clusters.[132] These structures have additional strength from

hydrogen bonds formed, with the nitro group acting as a hydrogen bond acceptor. They have also been found to possess good chemical and thermal stability.[132] Valiyaveettil *et al* studied the effect of varying the substituent on the C5-position of isophthalic acid. Their study focused on the length of the alkyl chain, hydrogen bonding opportunities and acid dimer formation.[141] Li *et al* also studied the effect of varying the C5 substituent. Their study focused on changing from no substituent (R = H), to an electron withdrawing group (R = NO_2) to an electron donating group (R = OH).[142] The nitro group can act as a hydrogen bond acceptor but is not generally found to coordinate.[142,143] This electron withdrawing group influences the electron density of the molecule as a whole, which can lead to different structures.[142] Isophthalic acid has been found to form structures with interesting properties, including fluorescence and non-linear optics.[107] The carboxylic acid moieties are at an angle of 120° to one another, which can lead to an angular "connector"[7] (see Section 1.7 - Topology). There are a number of reported coordination polymers and MOFs with NIA^{2-}.[142,144-149] Relatively few of these are with lanthanides.[132,143,150,151]

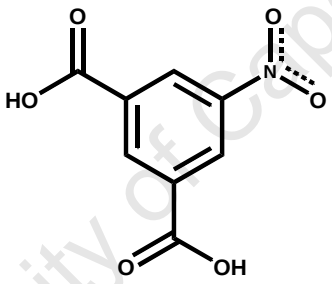

Figure 1.12: The structure of 5-nitroisophthalic acid (H_2NIA)

1.6 METAL IONS

The metal centre chosen for a particular MOF has a large impact on the properties present in the framework. The metal ion can play a major role in molecular recognition processes as well as molecular transformation, transport and storage. Open metal sites are reactive and the structure surrounding them is often not very rigid. This can lead to aggregation and the local features being distorted to block off the open metal site.[37] The two metal salts used in this project were zinc(II) sulphate heptahydrate and gadolinium(III) nitrate hexahydrate, which are described in greater detail in this section.

1.6.1 TRANSITION METALS AND ZINC

Transition metals are used in many compounds with useful properties.[42,61,80,89,100-102,104,106,110,113-115,120,124,129,130,152-154] Hydrogen molecules can coordinate onto the metal centres in transition metal complexes without breaking the H-H bond,[155] which is particularly useful for gas sorption applications. Only the very early transition metals and actinides have thus far not been observed to form stable H_2 complexes.[155] Another useful property of transition metal ions is that they form SBU clusters with carboxylate moieties and this is particularly useful in MOF synthesis.[32,34] Transition metal centres can cooperate with one another when in close proximity. This phenomenon is well known in compounds such as metallobiosites.[153] Zinc is commonly used in the preparation of coordination polymers and MOFs. A search of Chemical Abstracts[156] in October 2011 yielded 1200 papers published with "zinc" and "metal-organic frameworks" and 2700 with "zinc" and "coordination polymers". These zinc containing compounds have been found to have many useful properties.[80,89,101,102,104,114,115,124,130,152-154] MOF-508 ([Zn(BDC)(4,4'-Bipy)$_{0.5}$] where BDC is 1,4-benzenedicarboxylic acid and 4,4'-Bipy is 4,4'bipyridine) is reported to exhibit a reversible open-dense framework solid-state transformation and to be useful in the gas chromatograph separation of alkanes as shown in Figure 1.13.[104]

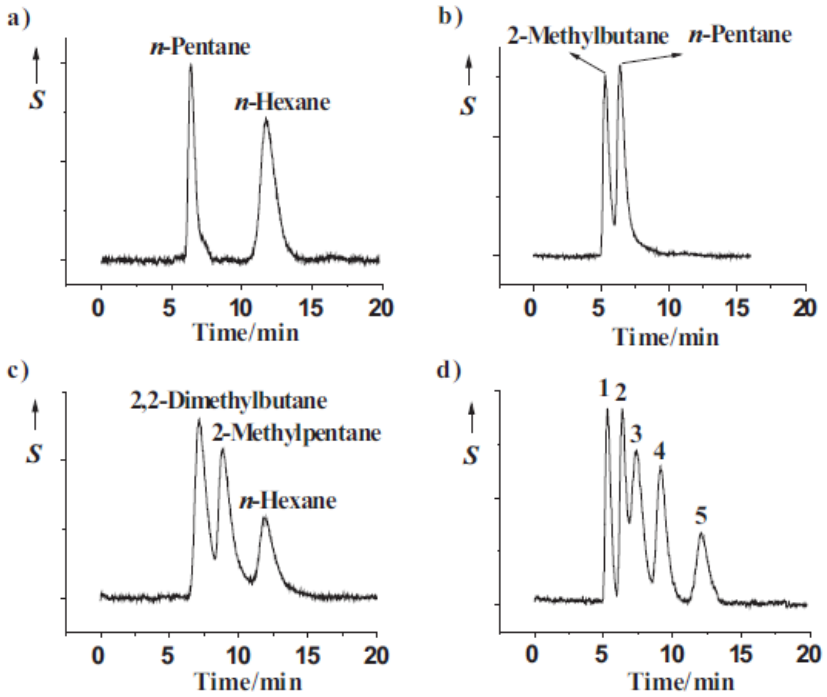

Figure 1.13: A figure from Chen *et al*[104] of chromatographs of small molecule alkane mixtures separated on a MOF-508 column

$\{[Zn(bpdc)(H_2O)_2]\}_n$ and $\{[Cd(bpdc)(H_2O)_3]\cdot 2H_2O\}_n$ (H_2bpdc = 2,2'-bipyridine-3,3'-dicarboxylic acid) are reported to display photoluminescence as shown in Figure 1.14.[89]

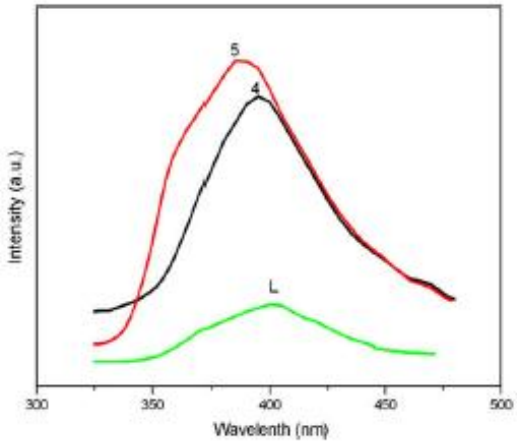

Figure 1.14: A figure presented by Chen *et al*[89] showing the emission spectra of 2,2'-bipyridine-3,3'-dicarboxylic acid, $\{Zn(bpdc)(H_2O)_2]\}_n$, and $\{[Cd(bpdc)(H_2O)_3]\cdot 2H_2O\}_n$ in the solid state and at room temperature.

1.6.2 LANTHANIDES AND GADOLINIUM

Lanthanide ions have large radii and high, variable coordination numbers.[132,143] They also have variable geometries as the 4f valence orbitals have little preference for bond direction.[157] This means that structures containing single metal lanthanide ions would be difficult to predict making lanthanides appear undesirable as building blocks. Design of lanthanide complexes with specific properties is very challenging.[132,133,143] However, lanthanides present interesting coordination geometries leading to interesting and special properties. This makes lanthanide structures desirable to study.[122,151] There is therefore a reasonable amount of interest in making coordination polymers and MOFs with lanthanides.[116,118,122,123,127,129,132,143,150,151] Lanthanides have a high affinity for the hard oxygen donor atoms of carboxylate moieties[132,133,158-160] and should therefore bond well to organic molecules such as H_3BTRI and H_2NIA.

Gadolinium MOF and coordination polymer structures are not as common as structures containing zinc with only 73 papers regarding "gadolinium" and "metal-organic frameworks" and 272 papers regarding "gadolinium" and "coordination polymers" found in a search of Chemical Abstracts.[156] In fact, only 249 metal-organic framework papers and 815 coordination polymer papers were found for lanthanide metal atoms in general. This is less than those found for zinc alone. Gadoliniuim structures have been prepared with useful properties.[116,118,127,129] The understanding of these metal centres and structures will only be improved through the

preparation of novel compounds. $\{[Gd(NIA)(HNIA)](bpyo)_{0.5}\cdot 2H_2O\}_n$ (H_2NIA = 5-nitroisophthalic acid; bpyo = 4,4'-bipyridine-N,N'-dioxide) is reported to exhibit high photocatalytic activity for dye degradation under UV light and has a good stability towards photocatalysis[129] as shown with compound "X3B" in Figure 1.15.

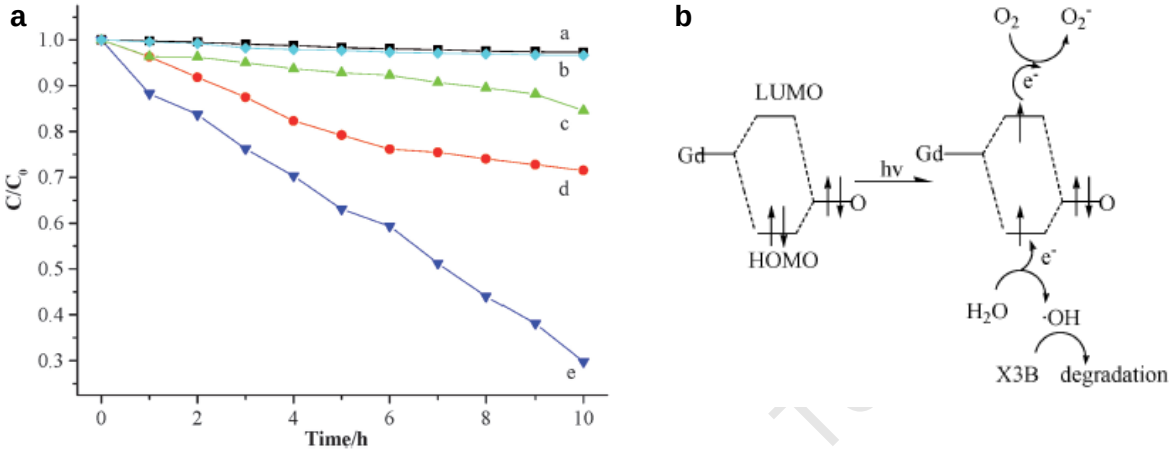

Figure 1.15: Figures presented by Wang *et al*.[129] **a)** Control experiments of the photodegradation of "X3B" X3B/**3**/dark (blue squares), X3B/UV light (blue diamonds), X3B/**3**/visible light (green triangles), X3B/3/*tert*-butyl alcohol/UV light (red circles), X3B/**3**/UV light (blue triangles). **b)** A schematic of the photocatalytic reaction mechanism of X3B on catalyst **3** (**3** = $\{[Gd(NIA)(HNIA)](bpyo)_{0.5}\cdot 2H_2O\}_n$)

$[Gd_2(N\text{-}BDC)_3(DMF)_4]_\infty$ is reported to display antiferromagnetic behaviour through magnetic susceptibility data as shown in Figure 1.16.[118]

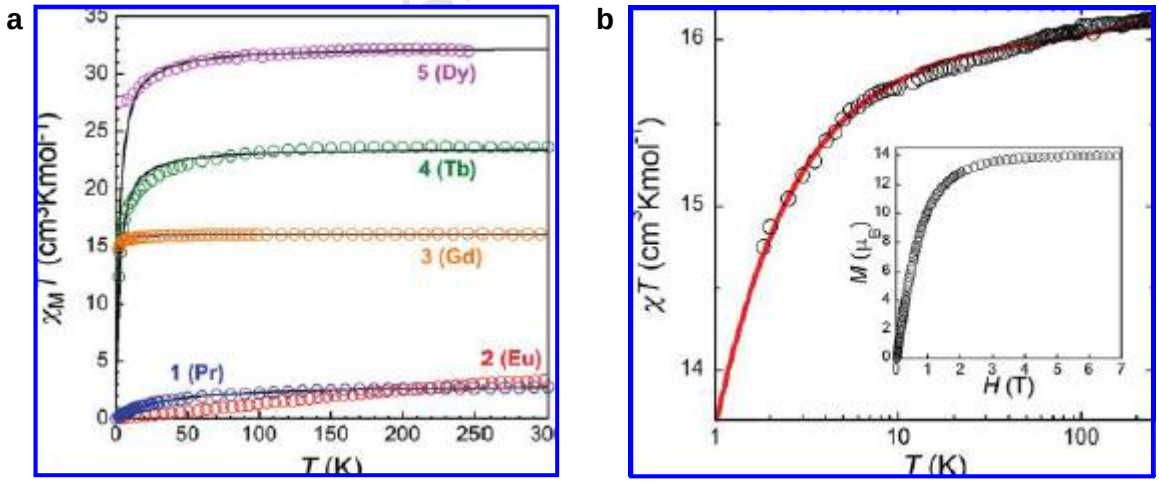

Figure 1.16: Figures presented by Black *et al*.[118] **a)** x_MT vs T plot for $[Gd_2(N\text{-}BDC)_3(DMF)_4]_\infty$ and the Dy, Tb, Eu and Pr analogues. Data is shown per Ln_2 and only half the data points are shown for clarity. Solid lines are the best-fit to a Curie-Weiss law. **b)** Semilog xT vs T plot of $[Gd_2(N\text{-}BDC)_3(DMF)_4]_\infty$ at an applied field of 0.1 T (1000 Oe). Solid line is best-fit to a simple exchange coupled dinuclear Gd(III) model. The inset is an M vs H plot measured at 1.83 K

1.7 TOPOLOGY

Topological analysis is the study of the underlying network of a structure: the connectivity of the building blocks and SBUs. There are many reasons for studying topology but three main ones are described in a 2005 monograph on the subject.[5] Network analysis offers:

1. A mental image of the three-dimensional arrangement of the structure.
2. A better understanding of why certain building blocks form specific structures.
3. The ability to "engineer" future structures through a better knowledge of connectivity.

Therefore, with a knowledge of topology it becomes easier to judiciously choose building blocks. It is possible to "design experiments to produce materials of predetermined topology and pore size and functionality".[30]

1.7.1 NODE CHOICE

"The dimensionality [of a coordination polymer or MOF] is often determined directly by the node."[7]

The idea of topological studies is to define crystal structures using nodes with specific geometry that are connected to other nodes (the same or different) via spacers.[7,161] Topology has been very useful in producing desired network architectures simply by this "node and spacer" approach.[7] By studying the topology found in various MOFs it is possible to pick specific nodes and spacers with a reasonable assumption that they will self-assemble into desired topologies.[7] Supramolecular isomerism implies that this will not always occur however as the same basic nodes and spacers can form widely different structures with varying topologies and properties. It will definitely not occur if nodes are not sensibly chosen.

Topological analysis is becoming more widely used. Network analysis allows a complex structure to be reduced to nodes and this enables one to look at the connectivity of the net.

The nodes are generally placed in one of three areas:

- The metal centre
- In the centre of a metal ion cluster (secondary-building unit)
- At the centre of the organic ligand

Therefore by looking at the net connectivity one can determine what sort of starting blocks have the potential to form a similar net. It is essential that the net not be over-simplified. Although net classification would become "easier" through simplification, information will undoubtedly be lost. If one looks at a topological net and cannot tell the basic building unit geometries that were used to create it then the net is no longer useful. The nodes chosen and the network obtained have to represent the connections that are crucial for the formation and the stability of the structure.[5] For example, 1,3,5-benzenetricarboxylate, if coordinated through all carboxylate moieties, will act as a three-connected node and in general this node should be included in the network. As much as it is not useful to over simplify a net by skipping potential node points it is also not useful to place a node at a ligand that does not add to the net in three dimensions. These nodes would not enhance understanding of the overall connectivity of the net. They only serve to add an unnecessary level of complexity. For example, it is improbable that 5-nitroisophthalic acid will coordinate through the nitro group resulting in it being a two-connected "node". It would therefore not be useful to place a node at the centre of this ligand.

One can look at a net with a three- and a four-connected node with useful types of pores and design the net with larger or smaller pores. A larger three-connected ligand could be combined with a metal known to form six-connected secondary building units in a one-pot synthesis. In theory a MOF with the same connectivity and larger pores could be made. As elegantly expressed by O'Keeffe[30] in his 2009 paper "there are a limited number of *default* structures for linking simple geometrical structures together". This means that design of structures based on simple topological building blocks is possible.

1.7.2 NOMENCLATURE

Alexander F. Wells developed nomenclature to describe the organisation of atoms or molecules in three-dimensions.[161] This nomenclature was based on viewing the atoms or molecules as nodes and the connectivity of the different components of the crystal as a network. Wells'

nomenclature is based on the number of topologically unique nodes in a network and the connectivity of the shortest ring. For example with a uninodal net the name would be (n,p). “n” denotes the number of nodes in the shortest ring in the network and “p” is the connectivity of that node. There are limitations to this nomenclature however as there may be many different nets that can have the same “n” and “p” values. The (10,3)-net is a good example of this as there are 11 possible (10,3)-nets. This means that the name does not imply the three-dimensional structure.[5, 73]

There are other more precise nomenclature systems. These include in the Schläfli symbol which will be used for all topological analysis in this thesis. The Schläfli symbol is in the form $A^{x1}.B^{x2}.C^{x3}$ where A, B and C are the smallest circuits connecting two node links for a particular node. These should be ordered with A < B < C. The connectivity of the node “p” is not explicitly stated but can be deduced in the general case from the sum of the superscripts as shown in equations (1) and (2). x_i is the superscript of the smallest circuits mentioned above and is the number of link pairs that display this smallest circuit (see example in Figure 1.17). This nomenclature system is also known as “short notation”.[5]

$$\Sigma x_i = \frac{p(p-1)}{2} \quad (1)$$

$$p = ½ + \sqrt{¼ + 2\Sigma x_i} \quad (2)$$

For example a four-connected node is shown in Figure 1.17. It would have four links: a (green), b (red), c (blue), and d (purple). These would result in six link pairs: ab, ac, ad, bc, bd, cd.

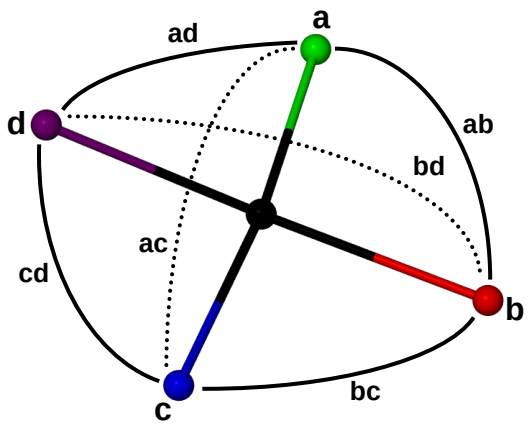

Figure 1.17: A four-connected node (shown in black) with the four links a (green), b (red), c blue) and d (purple) shown. The link pairs ab, ac, ad, bc, bd and cd are also given using solid or dashed lines

Complications can occur due to the shortest path between two links going through a third. This path can be divided into two smaller rings and is not essential. Therefore the following distinction is made. The smallest ring will always be fundamental and cannot include shortcuts. The shortest path is called a circuit. Circuits can contain shortcuts and may include rings. In "long notation" the ring for each node link is written out explicity so that A^4 in short notation may be written as $A_{y1}{\cdot}A_{y2}{\cdot}A_{y3}{\cdot}A_{y4}$ in long notation. "y" denotes the number of ways that the shortest ring can be formed. Circuits that are not rings are written as "*" in long notation.[5]

Three letter codes have also been adopted for networks and are often combined with Schläfli notation. These codes are similar to those found in zeolite research but lower case letters are used to avoid confusion. A database of these codes and the relevant short and long notations symbols can be found in the Reticular Chemistry Structure Resource (RCSR) online.[162, 163]

Some of the most common three-dimensional nets that coordination polymers and MOFs form are the (10^3)-**srs**, (10^3)-**ths**, (6^6)-**dia**, $(6^4.8^2)$-**nbo**, $(6^5.8)$-**cds**, $(4^2.8^4)$-**pts**, $(4^2.8^4)$-**bnn** and $(4^{12}.6^3)$-**pcu**.[5] Many of the three-letter names are based on well-known compounds or types of compounds that display that topology. For example the **srs**, **dia**, **cds**, **pts,** and **pcu** nets are also commonly known as the $SrSi_2$, diamond, $CdSO_4$, PtS, and α-polonium (or primitive cubic packing) nets, respectively.

$[Eu_2(NIA)_3(DMF)_4]{\cdot}(DMF)_2$, $[Pr_2(NIA)_3(DMF)_4]{\cdot}(DMF)_2$ and $[Sm_2(NIA)_3(DMF)_4]{\cdot}(DMF)_2$ all demonstrate the $(4^{12}.6^3)$-**pcu** network topology as shown in Figure 1.18a for the Europium compound.[164] The usefulness of long topological notation in addition to the Schläfli short symbol is highlighted in a paper by Li *et al*.[165] The $\{[Zn(bime)(NIA)]{\cdot}H_2O\}_n$ compound (bime = 1,2-bis(imidazole-1'-yl)ethane) has the $(6^5.8)$ short symbol in common with the **cds** net. The network topology of this compound (Figure 1.18b) is not that of the **cds** net however, having a long symbol of $6.6.6.6.6_2.8_3$ while the **cds** net long symbol is $6.6.6.6.6_2.*$. The star shows that the last circuit is not a ring as it includes a shortcut.

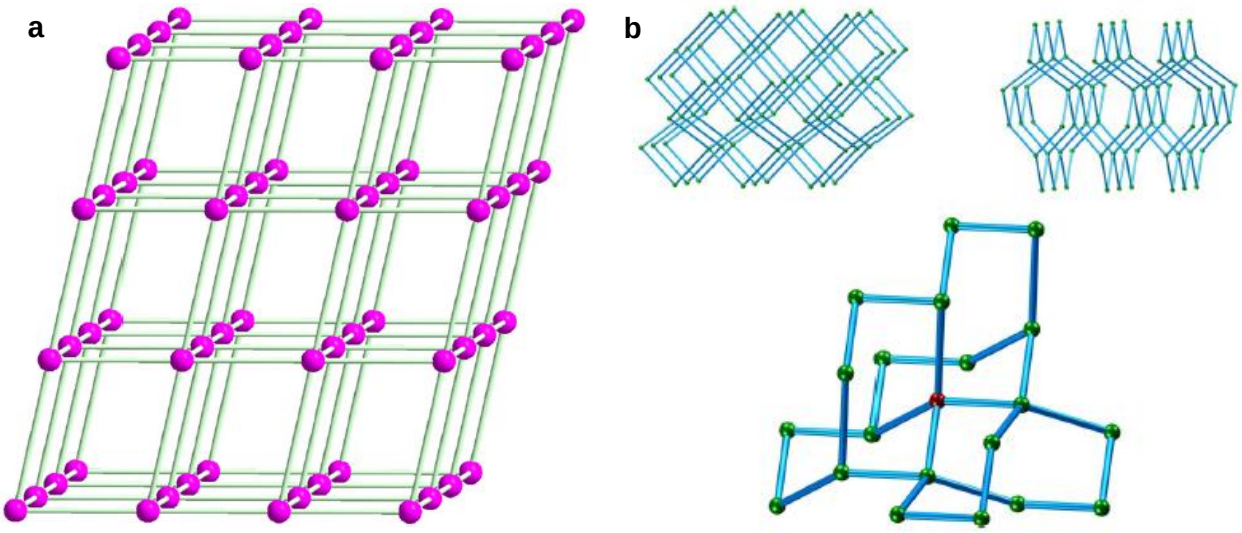

Figure 1.18: a) The 3D **pcu**-net of $[Eu_2(NIA)_3(DMF)_4]\cdot(DMF)_2$ as shown in a paper by Wang *et al*.[164] **b)** The $(6^5.8)$ net of $\{[Zn(bime)(NIA)]\cdot H_2O\}_n$ as given in a paper by Li *et al*[165]

The $[Zn(ip)]_n$ compound (H_2ip = isophthalic acid) of Zhang *et al*[107] demonstrates a $(4^2.8^4)$-**pts** network topology (Figure 1.19). Although the **pts** net is a common three-dimensional topology for MOFs and coordination polymers it is interesting to note that there are only a relatively small number of chiral frameworks with **pts**-type topology.

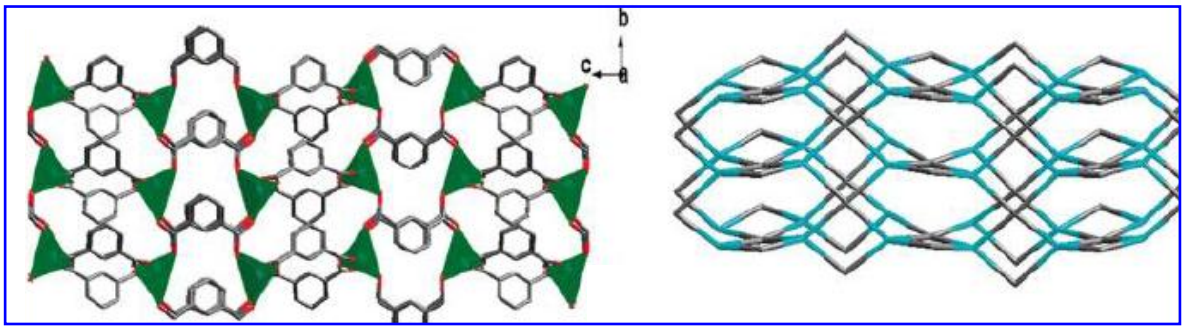

Figure 1.19: A figure from Zhang *et al*[107] showing the **a)** 3D framework and **b) pts**-net of $[Zn(ip)]_n$

1.8 MOTIVATION AND OBJECTIVES

1.8.1 MOTIVATION

Two simple organic molecules were chosen for this project. 1,3,5-benzenetricarboxylic acid (H_3BTRI) and 5-nitroisophthalic acid (H_2NIA) both contain carboxylic acid moieties. The benefits of using carboxylate containing organic linker molecules have been discussed in Section 1.5.1 - Carboxylates. It is highly desirable for the network formed to be robust so that the structure is retained with heating and upon guest molecule removal. The $BTRI^{3-}$ ligand would probably act as a three-connector in the manner described in Section 1.7.1 – Node Choice. A search of the CSD[92] revealed no structures where coordination to a metal ion through the nitro group of an H_2NIA ligand had occurred. As a result NIA^{2-} would only be a two-connector. It would serve as a way to connect the metal centres but not as an extender of the network itself. For both ligands the carboxylate moieties are related to each other by the same angle (120°). This angle is thought to be favourable to form rhombic channels in three-dimensional frameworks.[132] The carboxylate moieties in both H_3BTRI and H_2NIA have a range of different coordination modes they can adopt – unidentate, chelated, bridging – and multiple modes can occur within the same compound.[166] The NIA^{2-} ligand is also known to coordinate particularly well to lanthanide metal centres. The uncoordinated nitro group is able to act as an H-bond acceptor to further strengthen structures through supramolecular interactions.[132]

The two metal ions used in this study were zinc(II) and gadolinium(III). These metal ions have a large difference in molecular mass and coordination number and so quite different structures were expected. There are reported examples of zinc-isophthalate coordination polymers with tetrahedral coordination, and topological, geometry.[107] It was of interest to see the difference the nitro substituent would make. The geometry around the gadolinium centre is hard to predict. However, there should be strong affinity between the gadolinium metal centre and the carboxylate moieties.[132] Carboxylate moieties tend to form SBUs with metal centres and therefore it could be assumed that gadolinium clusters would be formed. These clusters were expected to have more predictable geometry (see Section 1.2.2 – Secondary-Building Units).

This study focused on the changes in the structure resulting from varying the number of carboxylate groups with a similar benzene backbone as well as the effect of changing the

C5-substituent from a carboxylate to a nitro group. The two metal centres have widely differing coordination modes and the effect of this was also studied.

1.8.2 OBJECTIVES

The primary objectives of the project presented in this thesis were:

1. To prepare novel metal-organic frameworks and coordination polymers from the carboxylate moiety containing organic molecules and common metal ions detailed in Section 1.8.1 – Motivation.
2. To fully characterise those compounds through X-ray diffraction and thermal analysis techniques.
3. To analyse the topological networks present in these compounds and to fully describe any new topological nets found.
4. To examine any compounds of particular interest with SEM, kinetics of resolvation, and gas sorption studies.
5. To explore the synthetic space with respect to temperature, metal to ligand ratio, cooling rate, and crystal growth environment.

1.9 REFERENCES

1. D. Braga, *Chem. Commun.,* 2003, 2751.

2. J. -M. Lehn, *Angew. Chem. Int. Ed.,* 1988, **27**, 89.

3. J. -M. Lehn, *Science,* 1993, **260**, 1762.

4. J. -M. Lehn, *Pure Appl. Chem.,* 1978, **50**, 871.

5. L. Öhrström and K. Larsson, ***Molecule-based materials the structural network approach (1st ed.).***, Elsevier, Amsterdam, The Netherlands, 2005.

6. I. Dance, *New J. Chem.,* 2003, **27**, 1.

7. B. Moulton and M. J. Zaworotko, *Chem. Rev.,* 2001, **101**, 1629.

8. W. C. McCrone, in ***Physics and Chemistry of the Organic Solid State***, eds. D. Fox, M. M. Labes and A. Weisemberg, Interscience, New York, 1965, pp.726.

9. J. A. R. P. Sarma and G. R. Desiraju, in ***Crystal Engineering: The Design and Application of Functional Solids.,*** eds. M. J. Zaworotko and K. R. Seddon, Kluwer, Dordrecht, 1999, pp.325.

10. T. L. Hennigar, D. C. MacQuarrie, P. Losier, R. D. Rogers and M. J. Zaworotko, *Angew. Chem. Int. Ed.,* 1997, **36**, 972.

11. T. A. Makal, A. A. Yakovenko and H. -C. Zhou, *J. Phys. Chem. Lett.,* 2011, **27**, 1682.

12. M. Lahav and L. Leiserowitz, *Angew. Chem. Int. Ed.,* 1999, **38**, 2533.

13. I. D. Cunningham, S. J. Coles and M. B. Hursthouse, *Chem. Commun.,* 2000, 61.

14. R. G. Kostyanovsky, A. P. Avdeenko, S. A. Konovalova, G. K. Kadorkina and A. V. Prosyanik, *Mendeleev Commun.,* 2000, **10**, 16.

15. S. -Z. Zhan, M. Li, X. -P. Zhou, J. Ni, X. -C. Huang and D. Li, *Inorg. Chem.,* 2011, **50**, 8879.

16. S. Ma, J. Eckert, P. M. Forster, J. W. Yoon, Y. K. Hwang, J. -S. Chang, C. D. Collier, J. B. Parise and H. -C. Zhou, *J. Am. Chem. Soc.,* 2008, **130**, 15896.

17. L. Ma and W. Lin, *J. Am. Chem. Soc.,* 2008, **130**, 13834.

18. S. Ma, D. Sun, M. Ambrogio, J. A. Fillinger, S. Parkin and H. -C. Zhou, *J. Am. Chem. Soc.,* 2007, **129**, 1858.

19. T. Panda, P. Pachfule and R. Banerjee, *Chem. Commun.,* 2011, **47**, 7674.

20. P. Pachfule, Y. Chen, S. C. Sahoo, J. Jiang and R. Banerjee, *Chem. Mater.,* 2011, **23**, 2908.

21. R. P. Feynman, *Eng. Sci.,* 1960, 22.

22. G. M. J. Schmidt, *Pure Appl. Chem.,* 1971, **27**, 647.

23. R. Pepinsky, *Phys. Rev.,* 1955, **100**, 971.

24. O. M. Yaghi, M. O'Keeffe, N. W. Ockwig, H. K. Chae, M. Eddaoudi and J. Kim, *Nature,* 2003, **423**, 705.

25. M. O'Keeffe, M. Eddaoudi, H. Li, T. Reineke and O. M. Yaghi, *J. Solid State Chem.,* 2000, **152**, 3.

26. O. M. Yaghi, H. Li and T. L. Groy, *J. Am. Chem. Soc.,* 1996, **118**, 9096.

27. B. F. Hoskins and R. Robson, *J. Am. Chem. Soc.,* 1990, **112**, 1546.

28. R. Robson, *Dalton Trans.,* 2008, 5113.

29. S. R. Batten and R. Robson, *Angew. Chem. Int. Ed,* 1998, **37**, 1460.

30. M. O'Keeffe, *Chem. Soc. Rev.,* 2009, **38**, 1215.

31. J. L. C. Rowsell and O. M. Yaghi, *Micropor. Mesopor. Mat.,* 2004, **73**, 3.

32. M. Eddaoudi, J. Kim, N. Rosi, D. Vodak, J. Wachter, M. O'Keeffe and O. M. Yaghi, *Science,* 2002, **295**, 469.

33. B. F. Abrahams, B. F. Hoskins, D. M. Michail and R. Robson, *Nature,* 1994, **369**, 727.

34. M. Eddaoudi, D. B. Moler, H. Li, B. Chen, T. M. Reineke, M. O'Keeffe and O. M. Yaghi, *Acc. Chem. Res.,* 2001, **34**, 319.

35. N. L. Rosi, M. Eddaoudi, J. Kim, M. O'Keeffe and O. M. Yaghi, *CrystEngComm,* 2002, **4**, 401.

36. D. J. Tranchemontagne, J. L. Mendoza-Cortés and M. O'Keeffe, *Chem. Soc. Rev.,* 2009, **38**, 1257.

37. B. Chen, M. Eddaoudi, T. M. Reineke, J. W. Kampf, M. O'Keeffe and O. M. Yaghi, *J. Am. Chem. Soc.,* 2000, **122**, 11559.

38. A. Pichon, C. M. Fierro, M. Nieuwenhuyzen and S. L. James, *CrystEngComm,* 2007, **9**, 449.

39. J. Chen, Z. Chen, T. Yu, L. Weng, B. Tu and D. Zhao, *Microporous and Mesoporous Materials,* 2007, **98**, 16.

40. E. Y. Lee and M. P. Suh, *Angew. Chem. Int. Ed,* 2004, **43**, 2798.

41. H. Li, M. Eddaoudi, M. O'Keefe and O. M. Yaghi, *Nature,* 1999, **402**, 276.

42. F. Luo, J. M. Zheng and S. R. Batten, *Chem. Commun.,* 2007, 3744.

43. Q. X. Yao, Z. F. Ju, W. Li, W. Wu, S. T. Zheng and J. Zhang, *CrystEngComm,* 2008, **10**, 1299.

44. M. Dincă, A. Dailly, C. Tsay and J. R. Long, *Inorg. Chem.,* 2008, **47**, 11.

45. T. M. Reineke, M. Eddaoudi, D. Moler, M. O'Keeffe and O. M. Yaghi, *J. Am. Chem. Soc.,* 2000, **122**, 4843.

46. O. M. Yaghi and H. Li, *J. Am. Chem. Soc.,* 1995, **117**, 10401.

47. D. M. Proserpio, R. Hoffmann and P. Preuss, *J. Am. Chem. Soc.,* 1994, **116**, 9634.

48. K. Sinzger, S. Hünig, M. Jopp, D. Bauer, W. Bietsch, J. U. von Schütz, H. C. Wolf, R. K. Kremer, T. Metzenthin, R. Bau, S. I. Kahn, A. Lindbaum, C. L. Lengauer and E. Tillmanns, *J. Am. Chem. Soc.,* 1993, **115**, 7696.

49. H. O. Stumpf, L. Ouahab, Y. Pei, P. Bergerat and O. Kahn, *J. Am. Chem. Soc.,* 1994, **116**, 3866.

50. D. Grandjean, O. Kahn, L. Ouahab, Y. Pei and H. O. Stumpf, *Science,* 1993, **261**, 447.

51. O. M. Yaghi, C. E. Davis, G. Li and H. Li, *J. Am. Chem. Soc.,* 1997, **119**, 2861.

52. O. M. Yaghi, D. Richardson, G. Li, C. E. Davis and T. L. Groy, *Mater. Res. Soc. Symp. Proc.,* 1995, **371**, 15.

53. L. R. MacGillivray, S. Subramanian and M. J. Zaworotko, *J. Chem. Soc., Chem. Commun.,* 1994, 1325.

54. H. Li, M. Eddaoudi, T. L. Groy and O. M. Yaghi, *J. Am. Chem. Soc.,* 1998, **120**, 8571.

55. M. Eddaoudi, H. Li and O. M. Yaghi, *J. Am. Chem. Soc.,* 2000, **122**, 1391.

56. J. Kim, B. Chen, T. M. Reineke, H. Li, M. Eddaoudi, D. B. Moler, M. O'Keeffe and O. M. Yaghi, *J. Am. Chem. Soc.,* 2001, **123**, 8239.

57. T. M. Reineke, M. Eddaoudi, M. Fehr, D. Kelley and O. M. Yaghi, *J. Am. Chem. Soc.,* 1999, **121**, 1651.

58. T. M. Reineke, M. Eddaoudi, M. O'Keeffe and O. M. Yaghi, *Angew. Chem. Int. Ed.,* 1999, **38**, 2590.

59. S. S. Kaye, A. Dailly, O. M. Yaghi and J. R. Long, *J. Am. Chem. Soc.,* 2007, **129**, 14176.

60. A. C. Sudik, A. P. Côé and O. M. Yaghi, *Inorg. Chem.,* 2005, **44**, 2998.

61. B. Chen, N. W. Ockwig, A. R. Millward, D. S. Contreras and O. M. Yaghi, *Angew. Chem. Int. Ed.,* 2005, **44**, 4745.

62. D. K. Kumar, D. A. Jose, A. Das and P. Dastidar, *Inorg. Chem. Commun.,* 2005, **44**, 6933.

63. K. Sanderson, *Nature,* 2007, **448**, 746.

64. C. Janiak, *Dalton Trans.,* 2003, **2003**, 2781.

65. A. Corma, H. García and F. X. Llabrés I Xamena, *Chem. Rev.,* 2010, **110**, 4606.

66. A. K. Cheetham, C. N. R. Rao and R. K. Feller, *Chem. Commun.,* 2006, 4780.

67. V. A. Blatov, L. Carlucci, G. Ciani and D. M. Proserpio, *CrystEngComm,* 2004, **6**, 377.

68. B. Arstad, H. Fjellvåg, K. O. Kongshaug, O. Swang and R. Blom, *Adsorption,* 2008, **14**, 755.

69. J. J. Perry IV, J. A. Perman and M. J. Zaworotko, *Chem. Soc. Rev.,* 2009, **38**, 1400.

70. P. W. Atkins, T. L. Overton, J. P. Rourke, M. T. Weller and F. A. Armstrong, ***Shrivers and Atkins' Inorganic Chemistry***, Oxford University Press, Oxford, England, 2010, pp668.

71. W. Steed and J. L. Atwood, ***Supramolecular Chemistry.***, John Wiley & Sons, Ltd, West Sussex, England, 2009, pp586.

72. P. A. Wright, ***Microporous Framework Solids.***, The Royal Society of Chemistry, Cambridge, England, 2008, pp46.

73. C. Borel, Doctor of Philosophy Thesis, Department of Chemical and Biological Engineering, Chalmers University of Technology, 2009.

74. P. Kanoo, K. L. Gurunatha and T. K. Maji, *J. Mater. Chem.,* 2010, **20**, 1322.

75. D. K. Kumar, A. Das and P. Dastidar, *CrystEngComm,* 2006, **8**, 805.

76. P. Pachfule, T. Panda, C. Dey and R. Banerjee, *CrystEngComm,* 2010, **12**, 2381.

77. J. R. Gispert, ***Coordination Chemistry.***, Wiley-VCH, Weinheim, Germany, 2008, pp521.

78. J. R. Long and O. M. Yaghi, *Chem. Soc. Rev.,* 2009, **38**, 1213.

79. C. -M. Lu, J. Liu, K. Xiao and A. T. Harris, *Chem. Eng. J.,* 2010, **156**, 465.

80. M. Fuentes-Cabrera, D. M. Nicholson and B. G. Sumpter, *J. Chem. Phys.,* 2005, **123**, 124713.

81. A. Burrows and A. Parsons, ***Chemistry^3: Introducing Inorganic, Organic and Physical Chemistry.***, Oxford University Press, Oxford, England, 2009, pp1266.

82. L. J. Barbour, *Chem. Commun.,* 2006, 1163.

83. K. Davies, S. A. Bourne, L. Öhrström and C. L. Oliver, *Dalton Trans.,* 2010, **39**, 2869.

84. A. Thirumurugan and A. K. Cheetham, *J. Inorg. Chem.,* 2010, **24**, 3823.

85. Y. Liu, G. Li, X. Li and Y. Cui, *Angew. Chem. Int. Ed,* 2007, **46**, 6301.

86. J. Y. Choi, J. Kim, S. H. Jhung, H. -K. Kim, J. -S. Chang and H. K. Chae, *B. Kor. Chem. Soc.,* 2006, **27**, 1523.

87. A. J. Fletcher, E. J. Cussen, T. J. Prior, M. J. Rosseinsky, C. J. Kepert and K. M. Thomas, *J. Am. Chem. Soc.,* 2001, **123**, 10001.

88. S. W. Liang, M. X. Li, M. Shao and H. J. Liu, *Inorg. Chem. Commun.,* 2007, **10**, 1347.

89. X. -L. Chen, Y. -J. Yao, H. -M. Hu, S. -H. Chen, F. Fu, Z. -X. Han, T. Qin, M. -L. Yang and G. -L. Xue, *Inorg. Chim. Acta,* 2009, **362**, 2686.

90. L. -M. Yang, P. Vajeeston, P. Ravindran, H. Fjellvåg and M. Tilset, *Phys. Chem. Chem. Phys.,* 2011, **13**, 10191.

91. D. Proserpio (University of Milan, Italy), XXII Congress and General Assembly of the International Union of Crystallography, 22-30 August 2011, Madrid, Spain.

92. Cambridge Structural Database and Cambridge Structural Database System, Version 5.32, Cambridge Crystallographic Data Centre, University Chemical Laboratory, Cambridge, England, February 2011.

93. L. Öhrström, S. Batten, N. Champness, X. -L. Chen, J. García-Martínez, S. Kitagawa, M. O'Keeffe, J. Reedijk and M. P. Suh, 2011, http://www.iupac.org/web/ins/2009-012-2-200, accessed 19th October.

94. B. Rather and M. J. Zaworotko, *Chem. Commun.,* 2003, 830.

95. B. Chen, M. Eddaoudi, S. T. Hyde, M. O'Keeffe and O. M. Yaghi, *Science,* 2001, **291**, 1021.

96. J. G. Nguyen, K. K. Tanabe and S. M. Cohen, *CrystEngComm,* 2010, **12**, 2335.

97. Z. Wang, K. K. Tanabe and S. M. Cohen, *Chem. Eur. J.,* 2010, **16**, 212.

98. F. Luo, S. R. Batten, Y. Che and J. M. Zheng, *Chem. Eur. J.,* 2007, **13**, 4948.

99. R. Custelcean, T. J. Haverlock and B. A. Moyer, *Inorg. Chem.,* 2006, **45**, 6446.

100. R. Custelcean, V. Sellin and B. A. Moyer, *Chem. Commun.,* 2007, 1541.

101. J. S. Seo, D. Whang, H. Lee, S. Im Jun, J. Oh, Y. J. Jeon and K. Kim, *Nature,* 2000, **404**, 982.

102. M. R. Kishan, J. Tian, P. K. Thallapally, C. A. Fernandez, S. J. Dalgarno, J. E. Warren, B. P. McGrail and J. L. Atwood, *Chem. Commun.,* 2010, **46**, 538.

103. J. R. Li, R. J. Kuppler and H. C. Zhou, *Chem. Soc. Rev.,* 2009, **38**, 1477.

104. B. Chen, C. Liang, J. Yang, D. S. Contreras, Y. L. Clancy, E. B. Lobkovsky, O. M. Yaghi and S. Dai, *Angew. Chem. Int. Ed.,* 2006, **45**, 1390.

105. L. Ma, C. Abney and W. Lin, *Chem. Soc. Rev.,* 2009, **38**, 1248.

106. S. Horike, M. Dincă, K. Tamaki and J. R. Long, *J. Am. Chem. Soc.,* 2008, **130**, 5854.

107. L. Zhang, Y. -Y. Qin, Z. -J. Li, Q. -P. Lin, J. -K. Cheng, J. Zhang and Y. -G. Yao, *Inorg. Chem.,* 2008, **47**, 8286.

108. T. Sagara, J. Ortony and E. Ganz, *J. Chem. Phys.,* 2005, **123**, 214707.

109. S. Ma and H. C. Zhou, *Chem. Commun.,* 2010, **46**, 44.

110. M. Dincă, A. Dailly, Y. Liu, C. M. Brown, D. A. Neumann and J. R. Long, *J. Am. Chem. Soc.,* 2006, **128**, 16876.

111. L. J. Murray, M. Dincă and J. R. Long, *Chem. Soc. Rev.,* 2009, **38**, 1294.

112. M. Dincă and J. R. Long, *Angew. Chem. Int. Ed.,* 2008, **47**, 6766.

113. H. J. Choi, M. Dincă and J. R. Long, *J. Am. Chem. Soc.,* 2008, **130**, 7848.

114. H. J. Park and M. P. Suh, *Chem. Commun.,* 2010, **46**, 610.

115. H. J. Park and M. P. Suh, *Chem. Eur. J.,* 2008, **14**, 8812.

116. Y. -F. Han, X. -H. Zhou, Y. -X. Zheng, Z. Shen, Y. Song and X. -Z. You, *CrystEngComm,* 2008, **10**, 1237.

117. R. -B. Zhang, J. Zhang, Z. -J. Li, J. -K. Cheng, Y. -Y. Qin and Y. -G. Yao, *Cryst. Growth & Des.,* 2008, **8**, 3735.

118. C. A. Black, J. S. Costa, W. T. Fu, C. Massera, O. Roubeau, S. J. Teat, G. Aromí, P. Gamez and J. Reedijk, *Inorg. Chem.,* 2009, **48**, 1062.

119. M. Kurmoo, *Chem. Soc. Rev.,* 2009, **38**, 1353.

120. M. Kurmoo, H. Kumagai, M. Akita-Tanaka, K. Inoue and S. Takagi, *Inorg. Chem.,* 2006, **45**, 1627.

121. O. Hallale, S. A. Bourne and K. R. Koch, *New J. Chem.,* 2005, **29**, 1416.

122. Z. Guo, H. Xu, S. Su, J. Cai, S. Dang, X. Shengchang, G. Qian, H. Zhang, M. O'Keeffe and B. Chen, *Chem. Commun.,* 2011, **47**, 5551.

123. H. Xu, F. Liu, Y. Cui, B. Chen and G. Qian, *Chem. Commun.,* 2011, **47**, 3153.

124. Z. Zhang, S. Xiang, X. Rao, Q. Zheng, F. R. Fronczek, G. Qian and B. Chen, *Chem. Commun.,* 2010, **46**, 7205.

125. N. Chang, Z. -Y. Gu, H. -F. Wang and X. -P. Yan, *Anal. Chem.,* 2011, **83**, 7094.

126. M. Shmilovits, Y. Diskin-Posner, M. Vinodu and I. Goldberg, *Cryst. Growth & Des.,* 2003, **3**, 855.

127. L. Yan, Q. Yue, Q. -X. Jia, G. Lemercier and E. -Q. Gao, *Cryst. Growth & Des.,* 2009, **9**, 2984.

128. J. D. Furman, A. Y. Warner, S. J. Teat, A. A. Mikhailovsky and A. K. Cheetham, *Chem. Mater.,* 2010, **22**, 2255.

129. D. -E. Wang, K. -J. Deng, K. -L. Lv, C. -G. Wang, L. -L. Wen and D. -F. Li, *CrystEngComm,* 2009, **11**, 1442.

130. G. B. Che, C. B. Liu, B. Liu, Q. W. Wang and Z. L. Xu, *CrystEngComm,* 2008, **10**, 184.

131. J. Song, Z. Luo, D. Britt, H. Furukawa, O. M. Yaghi, K. I. Hardcastle and C. L. Hill, *J. Am. Chem. Soc.,* 2011, **133**, 16839.

132. S. -P. Chen, Y. -X. Ren, W. -T. Wang and S. -L. Gao, *Dalton Trans.,* 2010, **39**, 1552.

133. Y. -H. Wen, J. -K. Cheng, Y. -L. Feng, J. Zhang, Z. -J. Li and Y. -G. Yao, *Chinese J. Struct. Chem.,* 2005, **24**, 1440.

134. S. Noro, T. Akutagawa and T. Nakamura, *Crystal Growth Des.,* 2007, **7**, 1205.

135. L. J. Murray, M. Dincă, J. Yano, S. Chavan, S. Bordiga, C. M. Brown and J. R. Long, *J. Am. Chem. Soc.,* 2010, **132**, 7856.

136. H. A. Habib, J. Sanchiz and C. Janiak, *Dalton Trans.,* 2008, **2008**, 1734.

137. Y. Y. Liu, J. F. Ma, J. Yang and Z. M. Su, *Inorg. Chem.,* 2007, **46**, 3027.

138. Y. Zhou, B. Wu, L. Han and M. Hong, *Acta Cryst. E,* 2005, **61**, m160.

139. J. Marek and Z. Trávníček, *Acta Cryst. E,* 2008, **64**, m384.

140. H. Xie, Z. Li and Y. Zheng, *Acta Cryst. C,* 2007, **63**, m30.

141. S. Valiyaveettil and K. Müllen, *New J. Chem.,* 1998, 89.

142. X. Li, R. Cao, W. Bi, Y. Wang, Y. Wang, X. Li and Z. Guo, *Cryst. Growth Des.,* 2005, **5**, 1651.

143. Y. Ren, S. Chen, G. Xie, S. Gao and Q. Shi, *Inorg. Chim. Acta,* 2006, **359**, 2047.

144. J. Tao, X. Yin, Y. -B. Jiang, L. -F. Yang, R. -B. Huang and L. -S. Zheng, *Eur. J. Inorg. Chem.,* 2003, 2678.

145. J. Luo, M. Hong, R. Wang, R. Cao, L. Han, D. Yuan, Z. Lin and Y. Zhou, *Inorg. Chem.,* 2003, **42**, 4486.

146. M. K. Bhunia, S. K. Das, M. M. Seikh, K. V. Domasevitch and A. Bhaumik, *Polyhedron,* 2011, **30**, 2218.

147. Q. Chen, E. -C. Yang, R. -W. Zhang, X. -G. Wang and X. -J. Zhao, *J. Coord. Chem.,* 2008, **61**, 1951.

148. J. Ye, J. Wang, Y. Wu, L. Ye and P. Zhang, *J. Mol. Struct.,* 2008, **873**, 35.

149. J. Wang, X. Qian, Y. -F. Cui, B. -L. Li and H. -Y. Li, *J. Coord. Chem.,* 2011, **64**, 2878.

150. Y. Ren, S. Chen and S. Gao, *J. Coord. Chem.,* 2006, **59**, 2135.

151. Y. Huang, B. Yan and M. Shao, *J. Solid State Chem.,* 2009, **182**, 657.

152. R. Custelcean, B. A. Moyer, V. S. Bryantsev and B. P. Hay, *Crystal Growth & Design,* 2006, **6**, 555.

153. M. Fondo, A. M. García-Deibe, N. Ocampo, J. Sanmartín, M. R. Bermejo, E. Oliveira and C. Lodeiro, *New J. Chem.,* 2008, **32**, 247.

154. A. Kuc, A. Enyashin and G. Seifert, *J. Phys. Chem. B,* 2007, **111**, 8179.

155. G. J. Kubas, *Chem. Rev.,* 2007, **107**, 4152.

156. http://www.cas.org/products/sfacad/index.html, accessed 3 October 2011.

157. D. G. Karraker, *J. Chem. Ed.,* 1970, **47**, 424.

158. D. -L. Long, R. J. Hill, A. J. Blake, N. R. Champness, P. Hubberstey, D. M. Proserpio, C. Wilson and M. Schröder, *Angew. Chem. Int. Ed.,* 2004, **43**, 1851.

159. Y. -P. Ren, L. -S. Long, B. -W. Mao, Y. -Z. Yuan, R. -B. Huang and L. -S. Zheng, *Angew. Chem. Int. Ed.,* 2003, **42**, 532.

160. W. Liu, T. Jiao, Y. Li, Q. Liu, M. Tan, H. Wang and L. Wang, *J. Am. Chem. Soc.,* 2004, **126**, 2280.

161. A. F. Wells, ***Structural Inorganic Chemistry.***, Oxford University Press, London, 1975.

162. M. O'Keeffe, O. M. Yaghi and S. Ramsden, 2009, Australian National University Supercomputer Facility, Reticular Chemistry Structure Resource, http://rcsr.anu.edu.ac/.

163. M. O'Keeffe, M. A. Peskov, S. Ramsden and O. M. Yaghi, *Acc. Chem. Res.,* 2008, **41**, 1782.

164. G. Wang, T. Song, Y. Fan, W. Wan, J. Xu and L. Wang, *Inorg. Chem. Commun.,* 2010, **13**, 935.

165. X. Li, R. Cao, Z. Guo, W. Bi and D. Yuan, *Inorg. Chem. Commun.,* 2006, **9**, 551.

166. C. Daiguebonne, O. Guilloa, Y. Gérault, A. Lecerf and K. Boubekeur, *Inorg. Chim. Acta,* 1999, **284**, 139.

Chapter 2

Experimental

The organic linker molecules and metal salts used in this project are identified in this chapter. The techniques and procedures used to analyse and fully characterise the metal-organic frameworks and coordination polymers prepared in this thesis are also discussed.

2.1 STARTING MATERIALS

1,3,5-benzenetricarboxylic acid (H_3BTRI) and *N',N*-dimethylformamide (DMF), with purities of 95% and 99.8% or greater respectively, were purchased from Sigma-Aldrich (Germany). 5-nitroisophthalic acid (NIA) was obtained from EGA-Chemie (Germany) and had a purity of greater than 98%. Gadolinium(III) nitrate hexahydrate was purchased from Sigma Aldrich (Germany) at a purity of 99.9%. Zinc(II) sulphate heptahydrate with a purity greater than 99.5% was purchased from Hopkin and Williams Ltd (United Kingdom). All starting materials were used without further purification.

2.2 GENERAL SYNTHETIC PROCEDURE

There were multiple approaches taken when synthesizing the compounds presented in this thesis. As such the specific synthetic procedures used for each class of compounds will be discussed at the beginning of the relevant chapter. In all syntheses a solution of the organic ligand (H_3BTRI or H_2NIA, Figure 2.1) was added to a solution of the metal salt (zinc(II) sulphate heptahydrate or gadolinium(III) nitrate hexahydrate) using various metal to ligand molar ratios. A solvent system of either pure *N,N*'-dimethylformamide (DMF) or 1:1, v/v DMF/H_2O was used. Full details for the compounds used in this study are given in Table 2.1.

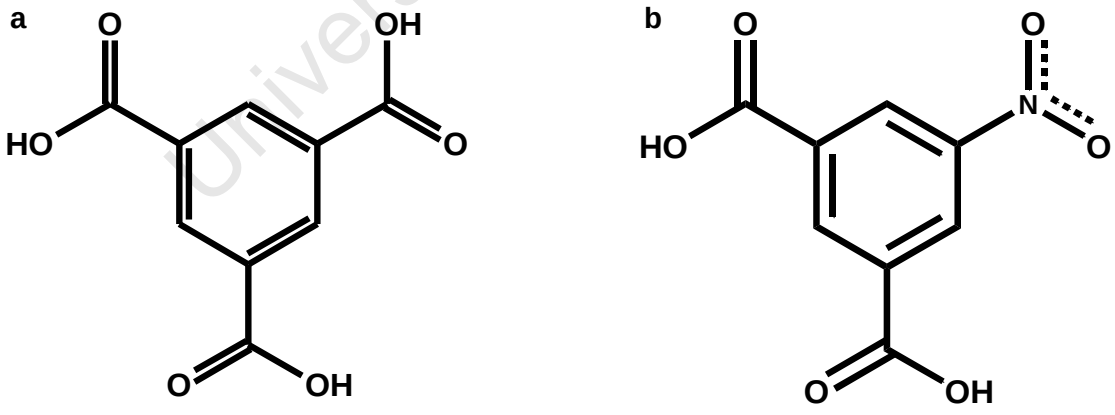

Figure 2.1: The chemical structure of **a)** 1,3,5-benzenetricarboxylic acid and **b)** 5-nitroisophthalic acid

Table 2.1: The chemical characteristics of materials used

Compound	Molecular Formula	M_r (g.mol^{-1})	mp (°C)	bp (°C)	Density (g.cm^{-3})
Ligands					
1,3,5-benzenetricarboxylic acid	$C_9H_6O_6$	210.141	375	-	-
5-nitroisophthalic acid	$C_8H_5NO_6$	211.129	260	-	-
Metal Salts					
Zinc(II) sulphate heptahydrate	$ZnSO_4 \cdot 7H_2O$	287.545	100	-	1.957
Gadolinium(III) nitrate hexahydrate	$Gd(NO_3)_3 \cdot 6H_2O$	451.352	91	-	2.406
Solvents					
***N,N*'-dimethylformamide**	C_3H_7NO	73.095	-61	153	0.944
***N,N*'-diethylformamide**	$C_5H_{11}NO$	101.149	-	176	0.908

2.3 THERMAL ANALYSIS

Three thermal analysis techniques were used. These are thermogravimetry (TG), differential scanning calorimetry (DSC) and hot stage microscopy (HSM). For all three techniques the change in the physical properties of the sample as a function of temperature was measured.

2.3.1 THERMOGRAVIMETRIC ANALYSIS (TG)

Thermogravimetric (TG) studies were used to corroborate the number and type of guest molecules and to determine the onset temperature of decomposition. Before TG experiments were performed samples were removed from the mother liquor with a spatula and placed on filter paper. The crystals were thoroughly surface-dried. They were then carefully transferred to an open alumina or aluminium crucible. Samples ranged in weight between 3 and 20 mg for all runs. A heating rate of 2, 10 or 20 °C.min^{-1} was used in order to obtain the best resolution. The temperature range of the experiment varied depending on the nature of the compound.

TG experiments were performed on one of two machines. A Mettler Toledo TGA/SDTA851^e was used with STAR^e software (Version 6.10). Dry nitrogen was used as the purging gas with a flow rate of 30 mL.min^{-1}. The instrument was calibrated using indium (m.p. = 156.6 °C) or aluminium (m.p. = 660.3 °C) in an automated process. A TA-Q500 Thermogravimetric Analyser from TA instruments was also used with the Universal Analysis 2000 software and a 50 ml.min^{-1} dry

nitrogen purge gas flow rate. The two instruments are significantly different as the furnace is horizontal in the Mettler Toledo TG and is vertical in the TA-Q500 machine.

2.3.2 DIFFERENTIAL SCANNING CALORIMETRY (DSC)

Differential Scanning Calorimetry (DSC) measures the difference in heat flow between the sample and a reference as a function of temperature while they undergo controlled heating. The enthalpy of various thermal events as well as the melting point of the compound can be determined in this way. Crystals were removed from the mother liquor and carefully surface-dried on filter paper before DSC experiments. The sample was then transferred to a closed, vented aluminium pan. For all runs samples ranged between 0.6 and 1.5 mg. Samples were heated at 2, 10 or 20 °C.min^{-1} in order to obtain the best resolution. Endothermic and exothermic reactions are depicted in the DSC traces by upward and downward peaks respectively. The temperature range studied varied depending on the nature of the compound.

DSC experiments were performed on two different machines. A Perkin Elmer PC7-Series System was used. This instrument was calibrated using standard materials including Indium (ΔH = 28.5 J/g, m.p. = 156.6 °C) and zinc (ΔH = 102.1 J/g, m.p. = 419.5 °C). Samples in this machine were placed in crimped, vented aluminium pans with lids. The apparatus was operated with a dry nitrogen purge gas flowing at a rate of 30 mL.min^{-1}. A TA instruments DSC-Q200 machine was also used and the instrument was calibrated using standard materials. Samples in this machine were placed in Tzero™ aluminium pans with lids. Two small holes were created in the lid to allow for venting. The machine operated with a dry nitrogen purge gas flowing at a rate of 50 mL.min^{-1}. Data was interpreted using the Universal Analysis 2000 program from TA Instruments.

2.3.3 HOT-STAGE MICROSCOPY (HSM)

Hot-stage microscopy (HSM) is used to correlate the thermal events seen in the TG and DSC analyses with physical processes occurring in the crystal. HSM is also used to observe visual changes which may not be indicated by DSC or TG. These processes can include solvent loss, recrystallisation, polymorphic transitions, loss of crystallinity and melting points. HSM was also used to study the thermal decomposition of the metal-organic compounds and to confirm

processes observed in TG and DSC analyses. In order to observe solvent loss single crystals were directly submerged in silicone oil and placed on a glass slide. The loss of solvent can then be seen as bubbles in the silicone oil. In this thesis HSM was primarily used to correlate solvent loss and decomposition temperatures. It was also used to determine at what temperature a sample lost single-crystallinity when heated. The temperature at which events were observed in the HSM was often minimally different to those observed with DSC or TG. This is probably due to the difference in particle size as well as the lack of purging gas in the HSM experiments.

All samples were viewed on a Nikon SMZ-10 stereoscopic microscope fitted with a Sony Digital Hyper HAD colour video camera. This was connected to a Linkam THMS600 hot stage and a Linkam TP92 temperature controlling unit. All samples were heated at 10 °C.min^{-1}. Thermal events were monitored and captured in real-time and viewed using the Soft Imaging System program, analySIS.[1]

2.4 ELEMENTAL ANALYSIS

Elemental analysis was performed on a Fisons EA1108 CHNS-O Elemental Analyser. It was used to determine the percentage of carbon, hydrogen and nitrogen present in each sample. This was used to compare with compound compositions determined from single crystal X-ray diffraction. All experimental C, H and N percentages were compared to the percentages calculated for each compound from the single crystal structure.

2.5 X-RAY DIFFRACTION

2.5.1 SINGLE CRYSTAL X-RAY DIFFRACTION

For single crystal X-ray diffraction a single crystal of suitable size was removed from the mother liquor. Some compounds produced large single crystals or clusters of crystals and where necessary the crystal was cut to obtain an appropriate size or to isolate a monocrystalline fragment. The crystal was immediately covered in paratone N oil[2] and placed on a nylon loop attached to a rigid mounting. The nylon loop was then mounted on the goniometer head under a cold stream of nitrogen.

Data collections were performed on one of two machines. A Nonius Kappa CCD (Charge Coupled Device) single crystal X-ray diffractometer was used with graphite-monochromated MoKα radiation (λ = 0.71069 Å). The X-rays were produced at 54 kV and 23 mA using a Nonius FR590 generator. A Bruker KAPPA APEX II DUO single crystal X-ray diffractometer utilising MoKα radiation (λ = 0.71069 Å) was also used. The X-rays were produced at 50 kV and 30 mA using a Bruker K780 generator.[3]

All data collections were performed at 173(2) K. Cooling was achieved using a constant stream of nitrogen gas produced by a Cryostream cooler (Oxford Cryosystems, UK) at a flow rate of 20 $mL.min^{-1}$. Unit cell refinement and data reduction for collections performed on the Nonius Kappa CCD apparatus were performed with the DENZO-SMN and SCALEPACK[4] programs. For the Bruker Apex II apparatus unit cell refinement and data reduction was performed using the program SAINT.[5] All intensity data were corrected for Lorentz-polarisation effects. All compounds reported in this thesis contain heavy atoms. The Bruker apparatus automatically applies a multi-scan absorption correction. For the Nonius apparatus it was necessary to correct for absorption separately. The SADABS[6] program is used in both cases.

The systematic absences found in the X-ray data were studied and used to determine the space group through comparison with known space groups. This space group was then confirmed using the XPREP[7] program. XPREP prepares SHELXS-97[8, 9] input files, which are then used in structure solution. As all structures presented in this thesis are relatively small the program SHELXS-97 was used to locate all non-hydrogen atoms. SHELXS-97 was used with direct methods to solve structures. The atoms were placed and refined using the full-matrix least-squares on F^2 method in SHELXL-97.[10] Metal ions were refined first, which then allowed the position of other atoms to be selected in the difference electron density map. When all non-hydrogen atoms had well-behaved isotropic temperature factors they were refined anisotropically. Reflections with low Miller indices and with observed intensities significantly lower than the calculated value were omitted due to potential interference from the beam-stop. DFIX restraints were used to help achieve ideal bond lengths (± 0.005 Å) for non-hydrogen atoms. In some cases this was due to poor crystal quality, but more often it was due to disorder in the solvent molecules. The methods of hydrogen atom placement and refinement are discussed in detail in the relevant chapters. SHELXS-97 and SHELXL-97 were accessed via the X-SEED[11] interface. The data file extensions for each program and the appendices this data can be found in are given in Table 2.2 (see Section 2.11 – Appendices).

2.5.2 POWDER X-RAY DIFFRACTION

For each compound the single crystal X-ray data (unit cell parameters, space group symmetry, atomic co-ordinates, and thermal parameters) were input in the program LAZY PULVERIX[12]. This program then generates idealised Powder X-ray Diffraction (PXRD) patterns using the same X-ray source as that used experimentally (λ = 1.5406 Å) and the formula $I(hkl) = mLp|F(hkl)|^2$. I(*hkl*) is the intensity of the reflections with diffraction indices *hkl*, *m* is the reflection multiplicity, L is the Lorentz factor, *p* is the polarisation factor, and *F(hkl)* is the structure factor. This generated pattern is compared to the experimentally obtained pattern to determine whether or not the single crystal is representative of the bulk material. PXRD is also used to determine whether the desired compound has been obtained in subsequent experiments.

All PXRD samples were crushed and thoroughly dried. They were either placed in Lindemann glass capillaries and mounted vertically in a capillary holder or applied to a MYLAR® polyester film (Thin-Film Sample supports, West Chester, Pennsylvania, USA) with a thin layer of Paratone N oil.[2] The MYLAR® was suspended on a flat sample holder. The samples were mounted on a Huber D-83253 Imaging Plate appliance fitted with a Guinier Camera 670, a Huber MC 9300 power supply unit and a Philips PW1120/00 X-ray generator. The generator was fitted with a Huber long, fine-focus tube PW2273/20 and a Huber Guinier Monochromator Series 611/15. The sample was exposed to $CuK\alpha_1$ radiation (λ=1.5406 Å) produced at 20 mA and 40 kV. Samples were exposed to radiation for 20 – 120 minutes depending on the quantity and quality of the sample and the imaging plate was scanned 10 times. A 2θ range of 4 - 100° was used with a 0.005° 2θ step size. A Huber High-Temperature Controller HTC 9634 unit was used with the capillary holder in order to obtain variable-temperature data. For the 5-nitroisophthalate-gadolinium compounds no peaks were observed in the PXRD diffraction pattern when the samples were analysed in a capillary holder. As a result this apparatus was not used for these compounds. Samples were instead heated to the desired temperature on a TG apparatus and then a thin layer was placed on the flat mount for PXRD anaylsis. The data was manipulated using Microsoft Excel and was truncated to 0 – 40° 2θ.

2.6 GAS SORPTION STUDIES

Gas sorption experiments were performed to determine the capabilities of compound **3** (see Chapter 3.5). Hydrogen, nitrogen and carbon dioxide gas were tested with pressures

ranging from 0 to 20 bar and temperatures of 0 and 20 °C. The apparatus available at the University of Cape Town (UCT) requires gram quantities of the sample for experiments. These amounts were impractical with compound **3** and so samples were sent to the Central Analytical Facility at Stellenbosch University (SUN). The quantity of sample required by the SUN apparatus is much smaller (50 – 80 mg). However the apparatus broke before the experiments could be completed. The machine had not been repaired before the completion of this thesis. As a result the gas sorption studies with compound **3** are not extensive, however initial results are reported. The results that were obtained are discussed fully in Chapter 3.5.6 – Gas Sorption Studies.

The apparatus used was an Intelligent Gravimetric Analyser (IGA-002). Ultra-high purity gasses supplied by Hiden Analytical Ltd, Warrington, UK were utilised for all experiments. The IGA-002 allows for a high level of pressure and temperature control (± 0.05 °C) as well as accurate mass change measurements. Temperature was controlled with a Grant refrigerated recirculating bath. Gas pressures of 0 – 20 bar were applied and monitored with a pressure transducer. Buoyancy effects were automatically corrected for by the software. The density of compound **3** was calculated from single crystal data and used in the buoyancy corrections.

Experiments on the IGA-002 were controlled by the Real-Time Processing software.[13-18] Samples of compound **3** were heated to 160 °C and held at this temperature on TG apparatus until all included water was removed. The dehydrated sample was also outgassed on the IGA equipment prior to runs to ensure complete dehydration. A new dehydrated sample was used for each experiment with one experiment consisting of an increase in pressure from 0 to 20 bar followed by a decrease back to 0 bar again. Each experiment was performed at a set temperature. More details are given in Chapter 3.5.6 – Gas Sorption Studies.

2.7 SCANNING ELECTRON MICROSCOPY (SEM)

Scanning Electron Microscopy (SEM) studies were performed at the University of Cape Town Electron Microscope Unit by Dr Miranda Waldron. Single crystals were placed into a FEI Nova NanoSEM 230 under vacuum. The crystal surface was then studied at varying magnifications ranging from 50x to 2000x.

2.8 KINETICS

Kinetics studies were performed to analyse the uptake of water and ethanol vapour by dehydrated solid samples of compound **4** (Chapter 3.6.4 – Kinetic Studies) sieved to a particle size of 38 – 45 μm. Experiments were performed at 25 or 30 °C and were accomplished using a balance placed in an oven (Figure 2.2a). The balance is connected to a computer, which tracks the experiment, and the temperature is kept constant within the oven throughout the experiment.

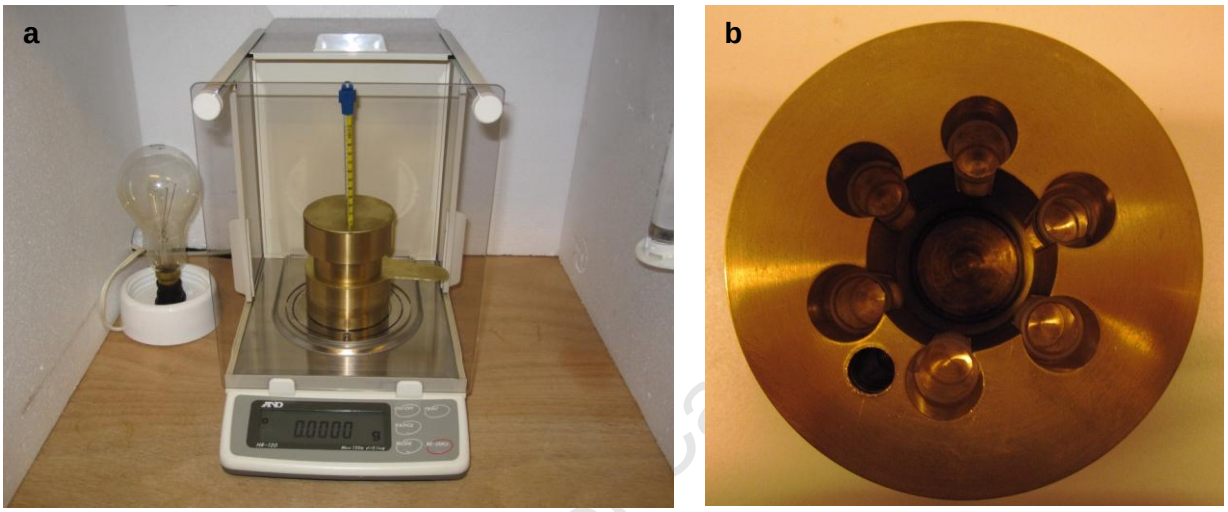

Figure 2.2: The apparatus used for kinetics experiments, **a)** The scale located in a temperature controlled oven and connected to a monitoring computer. **b)** The hollow brass container with five solvent chambers

A sample holder is placed onto the scale within the brass container. The solvent used for each of the compounds is discussed in the relevant chapters. This solvent is placed in five chambers within the hollow brass container (Figure 2.2b). The brass container fits over the sample on the balance and the top of the container is covered. The vapour pressure is then allowed to equilibrate for a minimum of one hour. The scale is zeroed, the monitoring computer program (PB303S.exe)[19] is started and the sample is added. The reported data takes into account the amount of starting material but, depending on the speed of absorption, the balance is not rezeroed to ensure all absorption is recorded. The increase in mass with respect to time is recorded. Once no more solvent is being absorbed by the compound the experiment is terminated. The data is then put through the program alphatime.exe[19] to analyse the extent of the reaction (α). α is based on the mass of water absorbed by the compound and is defined as shown in equation (1). In some cases the compound also absorbs solvent on the surface and this does not fit with the rest of the data. In these cases the reported data has been truncated.

$$\alpha = \frac{m_o - m_t}{m_o - m_\infty} \qquad (1)$$

The α versus time curve is then evaluated using a range of mathematical expressions. The expressions are derived from the suggested mechanisms of many different solid-state processes.[20] The expression which gives the best correlation coefficient when applied to our data is determined and this expression is then used to calculate the rate constant, k.

A dehydration and rehydration study was performed on compound **3** using a similar method to the kinetics experiments. The comprehensive method details are given in Chapter 3.5.5 – Dehydration and Rehydration.

2.9 TOPOLOGICAL ANALYSIS

Topological analyses were performed by eye and confirmed using the computer programs SYSTRE,[21] OLEX[22] and TOPOS.[23, 24] These are checked against the Reticular Chemistry Structural Resource (RCSR)[25, 26] and EPINET[27] databases. If the topological networks obtained did not match any known networks the complete long and short symbols for the nets were calculated with TOPOS and SYSTRE and submitted to the RCSR.

2.10 ADDITIONAL COMPUTER PACKAGES

The Cambridge Structural Database[28] (CSD) was used to find structures comparable to those presented in this thesis. The CSD was also employed to obtain bond distances and angles for compounds with similar structural motifs to the structures reported in this thesis. X-SEED[11] was used as a graphical interface for LAYER,[29] POV-RAY,[30] LAZY PULVERIX[12] and SECTION.[31]. The LAYER program was used to investigate and identify the systematic absences from the intensity data collected for space group symmetry determination. The molecular structures and crystal packing diagrams were drawn using POV-RAY. The program SECTION was used to assist in investigating the three-dimensional shapes of channels or cavities. The analysis of molecular parameter and geometrical data were calculated using PLATON.[32, 33]

2.11 APPENDICES

Table 2.2: File types found in the appendices

File Extensions	Contents	Appendix
.hkl	Reflection data	A
.res	SHELX coordinate data	A
.cif	Crystallographic information file	A
.fcf	Structure factor tables	A
.lis	Platon output	A
.xl	SHELX output file	A
.sup	Tabulated supplementary data	A
.pdf	CheckCif Report	A
.cgd	SYSTRE data file	B
.txt	OLEX output file	B
.txt	TOPOS output file	B

2.12 REFERENCES

1. Soft Imaging System GmbH: Digital Solutions for Imaging and Microscopy, Version 3.1 for Windows, © **1987 - 2000**.

2. Paratone N oil, (Exxon Chemical Co., Tx, USA).

3. APEX2, Version 1.0-27, Bruker AXS Inc., Madison, Wisconsin, USA.

4. Z. Otwinowski and W. Minor, Processing of X-ray Diffraction Data in Oscillation Mode, in *Methods in Enzymology,* eds. C. W. Carter and R. M. Sweet, Academic Press, New York, 1996, pp.307-326.

5. Program SAINT, Version 7.60a, Bruker AXS Inc., Madison, WI, USA, 2006.

6. G. M. Sheldrick, SADABS, Version 2.05, University of Göttingen, Germany, 2007.

7. XPREP, *Data Preparation and Reciprocal Space Exploration*, Version 5.1, © Bruker Analytical X-ray Systems, 1997.

8. G. M. Sheldrick, *Acta Cryst. A,* 1990, **A46**, 467.

9. G. M. Sheldrick, SHELXS-97, Program for Crystal Structure Solution, University of Göttingen, Germany, 1997.

10. G. M. Sheldrick, SHELXL-97, Program for Crystal Structure Solution, University of Göttingen, Germany, 1997.

11. L. J. Barbour, *J. Supramol. Chem.,* 2001, **1**, 189.

12. K. Yvon, W. Jeitschko and E. Parthé, *J. Appl. Cryst.,* 1977, **10**, 73.

13. A. J. Fletcher and K. M. Thomas, *Langmuir,* 2000, **16**, 6253.

14. A. J. Fletcher and K. M. Thomas, *Langmuir,* 1999, **15**, 6908.

15. N. J. Foley, K. M. Thomas, P. L. Forshaw, D. Stanton and P. R. Norman, *Langmuir,* 1997, **13**, 2083.

16. A. W. Harding, N. J. Foley, P. R. Norman, D. C. Francis and K. M. Thomas, *Langmuir,* 1998, **14**, 3858.

17. I. P. O'koye, M. Benham and K. M. Thomas, *Langmuir,* 1997, **13**, 4054.

18. C. R. Reid, I. P. O'koye and K. M. Thomas, *Langmuir,* 1998, **14**, 2415.

19. L. J. Barbour, *Private Communication*.

20. S. R. Byrn, R. R. Pfeiffer and J. G. Stowell, in *Solid-State Chemistry of Drugs,* SSCI, Inc., Indiana, USA, 1999, pp.443.

21. O. D. Friedrichs, Program SYSTRE 1.14 beta http://gavrog.sourceforge.net/, 2007.

22. O. V. Dolomanov, A. J. Blake, N. R. Champness and M. Shröder, *J. Appl. Cryst.,* 2003, **36**, 1283.

23 V. A. Blatov, Program TOPOS 4.0, http://www.topos.ssu.samara.ru/, accessed May 2009.

24. V. A. Blatov and M. V. Peskov, *Acta Cryst.,* 2006, **62**, 457.

25. M. O'Keeffe, O. M. Yaghi and S. Ramsden, Australian National University Supercomputer Facility, Reticular Chemistry Structure Resource, http://rcsr.anu.edu.ac/, 2009

26. M. O'Keeffe, M. A. Peskov, S. Ramsden and O. M. Yaghi, *Acc. Chem. Res.,* 2008, **41**, 1782.

27. S. J. Ramsden, V. Robins, S. Hungerford and S. T. Hyde, EPINET, http://epinet.anu.adu.au, 2009.

28. Cambridge Structural Database and Cambridge Structural Database System, Version 5.32, Cambridge Crystallographic Data Centre, University Chemical Laboratory, Cambridge, England, February 2011.

29. L. J. Barbour, *J. Appl. Cryst.,* 1999, **32**, 351.

30. POV-Ray for Windows, Version 3.6, The Persistence of Vision Development Team, © 1991 - 2003.

31. L. J. Barbour, *J. Appl. Cryst.,* 1999, **32**, 353.

32. A. L. Spek, Program PLATON, A Multipurpose Crystallographic Tool, Version 10500, © 1980 - 2000, Utrecht University, The Netherlands.

33. A. L. Spek, *J. Appl. Cryst.,* 2003, **36**, 7.

Chapter 3

1,3,5-Benzenetricarboxylate Compounds

Four compounds prepared from 1,3,5-benzenetricarboxylic acid are discussed in this chapter. Three of these were prepared with zinc(II) sulphate heptahydrate while one was prepared with gadolinium(III) nitrate hexahydrate. The sections are divided by compound and the full characterisation using single crystal and powder X-ray diffraction, thermal analysis and any additional techniques is given in the section relevant to each compound.

Four novel compounds were prepared using 1,3,5-benzenetricarboxylic acid (H_3BTRI). $[Zn_6(\mu_3\text{-}OH)_2(BTRI)_4(DMF)_{2.5}(H_2O)_2]\cdot[Zn(H_2O)_3(DMF)_3]\cdot 2.96H_2O$ (**1**), $[Zn(HCOO)(BTRI)_{0.3}(DMF)]$ (**2**) and $[Zn_2(\mu_2\text{-}OH_2)(HBTRI)(BTRI)(H_2O)_2]\cdot DMA\cdot 3H_2O$ (**3**) were prepared with zinc(II) sulphate heptahydrate. $[Gd(BTRI)(H_2O)_6]$ (**4**) was prepared from gadolinium(III) nitrate hexahydrate. A previously reported *N,N'*-dimethylformamide (DMF) solvate of H_3BTRI[1] (**DMFBTRI**) was obtained at high concentrations of the ligand during the preparation of **1** – **3**. The powder X-ray diffraction (PXRD) patterns calculated from single crystal data for each of these compounds are shown in Figure 3.1.

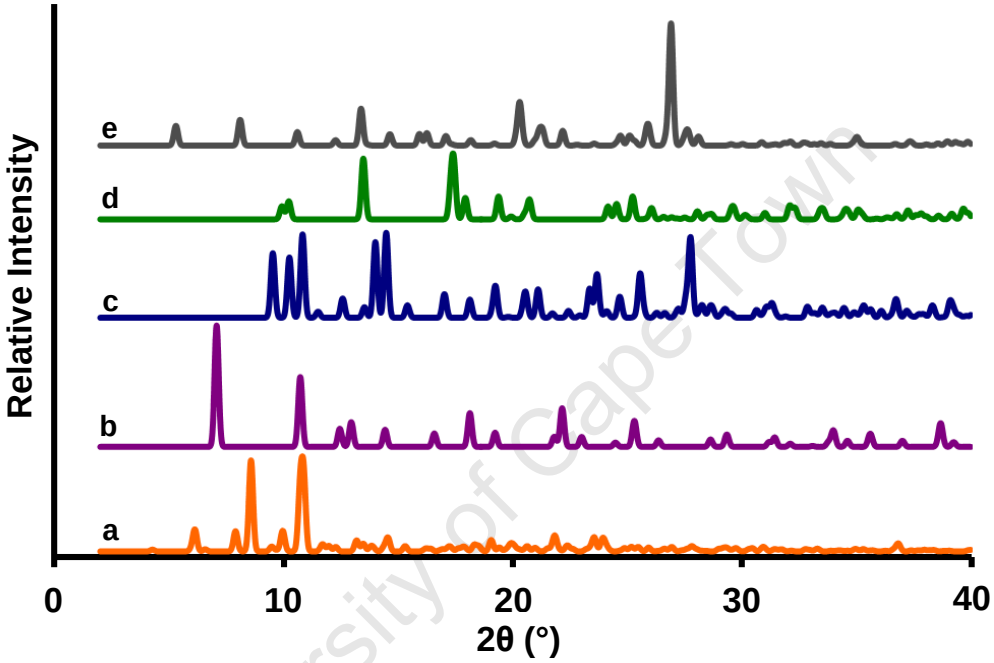

Figure 3.1: The PXRD patterns calculated from single crystal data for **a) 1** – orange, **b) 2** – purple, **c) 3** – blue, **d) 4** – green and **e) DMFBTRI** – grey

Regardless of the concentration, metal to ligand ratio, solvent system or method used compound **4** was the only product produced from gadolinium(III) nitrate and 1,3,5-benzenetricarboxylic acid. When *N,N'*-dimethylformamide (DMF) was used as the solvent a fine, crystalline powder was formed. When *N,N'*-diethylformamide (DEF) was used as the solvent it was possible to obtain single crystals.

3.1 PREPARATION OF ZINC(II) AND 1,3,5-BENZENETRICARBOXYLATE COMPOUNDS

There were multiple methods employed in the preparation of **1**, **2** and **3**. For all methods the zinc(II) sulphate was dissolved in a given amount of distilled water at 60 °C with stirring. An equimolar amount of 1,3,5-benzenetricarboxylic acid was dissolved in an equal volume of DMF also at 60 °C and with stirring. The two solutions were then filtered into the same vial.

Method 1:

1. The vial was closed and sealed with parafilm
2. Placed in an oil bath and held at 60 °C for 24 hours
3. Cooled to room temperature over 48 hours (0.83 °C/hour)

Method 2:

1. The vial was left partially open to the atmosphere for slow evaporation
2. Placed in an oven at 30 °C
3. Left at 30 °C until crystals formed

Method 3:

1. The vial was closed and sealed with parafilm
2. Allowed to cool to room temperature
3. Heated to 60 °C over a period of 24 hours (1.67 °C/hour)
4. Held at 60 °C for 24 hours
5. Cooled to room temperature again over 48 hours (0.83 °C/hour)

Method 4:

1. The vial was closed and sealed with parafilm
2. Placed in an oil bath at 60 °C and held at that temperature for 24 hours
3. Cooled to room temperature over 10 hours (4 °C/hour)

Method 5:

1. The vial was closed and sealed with parafilm
2. Placed in a Dewar containing water at a temperature of 70 °C
3. The Dewar was sealed and allowed to cool slowly to room temperature

For all methods, aside from method 2, the vial was partially opened to the atmosphere once at room temperature. This was to allow for slow evaporation when crystals did not form during cooling.

In methods 2, 3, and 4 the amount of each solvent was varied from 0.5 – 3 ml in increments of 0.5 ml. A 1:1 metal to ligand ratio of the starting materials and a 1:1 v/v ratio of the H_2O/DMF solvent system was used. For method 5 the amount of solvent was varied from 0.5 ml to 2.5 ml. For method 1 the 1:1 ratio was maintained but the amount of solvent was varied from 0.25 ml to 3 ml with an increment of 0.25 ml. In cases where the concentration was high or the rate of cooling fast **DMFBTRI** was often formed. This is discussed in greater detail later in this section.

An example of the products obtained through variation of the amount of starting material and the volume of solvent used is given in Table 3.1. The product obtained in each experiment was determined with PXRD analysis. All ligand to metal ratios are 1:1 and the molar amount of the starting materials is given in the top row. The amount of solvent used is shown in the left column. In Tables 3.1, 3.2 and 3.3 the fact that more than one compound was obtained for a particular experiment is shown. The relative number of experiments that produced a specific compound is not given in the tables.

Table 3.1: The Zn-BTRI compounds obtained through the variation of amount of starting material vs volume of solvent for method 1

L/M (mmol) → ↓ DMF/H_2O (mL)	0.095/ 0.094	0.190/ 0.188	0.286/ 0.282	0.381/ 0.376	0.476/ 0.469	0.657/ 0.666	0.952/ 0.939
0.25/0.25	3	3	DMFBTRI	3	DMFBTRI	3	DMFBTRI
0.50/0.50	1	3	2/3	2/3	3	3	DMFBTRI
0.75/0.75	1	3	3	3	3	1/3	1
1.00/1.00	3	1	3	1/3	2	3	DMFBTRI
1.25/1.25	1	3	1/3	3	1/3	3	2/3
1.50/1.50	1	1	1/2/3	3	2/3	3	3
1.75/1.75	1	1	1	3	1	3	3
2.00/2.00	3	1	1	3	1	3	2
2.25/2.25	1	1	1	1	3	3	1
2.50/2.50	2/3	1	1	1/3	1	1/3	3
2.75/2.75	1	1	1	1	1	3	3
3.00/3.00	1	1	3	1	3	3	1/2/3

* "/" indicates a mixture of compounds were obtained. No attempt to determine relative amounts was made

Concentration increases from left to right and decreases from top to bottom in Table 3.1. As shown in the table the lower the concentration – bottom left of the table – the more likely it is for compound **1** to form. The higher the concentration – top right of the table – the more likely it is for compound **3** to form. Compound **2** appears to grow at higher concentrations but is less predictable than compounds **1** or **3**.

The concentrations obtained by varying the conditions are given in Table 3.2. Table 3.2 contains the results of experiments not listed explicitly in Table 3.1. The number of experiments that produced each compound for a specific concentration is shown in Figure 3.2 in the following section. It is possible to see the trend that compound **1** forms at lower concentrations while compound **3** forms at higher concentrations. The concentration referred to is that of the combined starting materials (H_3BTRI and the zinc salt) in the final solution.

Table 3.2: Concentrations and results for the Zinc-BTRI compounds using method 1

Concentration ($mol.dm^{-3}$)	Result	Concentration ($mol.dm^{-3}$)	Result	Concentration ($mol.dm^{-3}$)	Result
0.032±2	1	0.158±2	3	0.504±9	3
0.034±1	1	0.170±5	1	0.53±1	3
0.038±2	2/3	0.19±1	1/2/3	0.57±1	2/3
0.042±2	1	0.22±1	1/3	0.63±1	3
0.047±2	3	0.238±6	1/3	0.662±9	3
0.054±3	1	0.252±7	1/3	0.76±1	2/3
0.063±3	1	0.268±6	1/3	0.88±1	1/3
0.069±2	1	0.284±6	3	0.95±1	3/DMFBTRI
0.076±4	1	0.294±4	3	1.13±2	DMFBTRI
0.084±2	1	0.303±5	3	1.26±1	1
0.095±5	1/3	0.315±5	1/2/3	1.32±2	3
0.103±2	1	0.331±4	3	1.51±3	3
0.108±3	1	0.344±4	3	1.89±3	DMFBTRI
0.113±2	1	0.38±2	1/2/3	2.65±3	3
0.126±6	1	0.420±5	1	3.78±4	DMFBTRI
0.140±5	1	0.441±6	3		
0.151±4	1/3	0.473±7	2		

* "/" indicates a mixture of compounds were obtained.
No attempt to determine relative amounts was made

As previously mentioned the amount of solvent was varied by 0.5 ml increments for methods 2 – 5. This led to a different concentration range than that obtained for method 1. The results for methods 2 – 5 as well as the relevant method 1 results are given in Table 3.3.

For methods 1, 3 and 4 we obtain compound **1** at lower concentrations while at higher concentrations we obtain compound **3** more often. For methods 2 and 5 compound **1** is formed at lower concentrations but it is more likely for **DMFBTRI** to form at higher concentrations than compound **3**. Compound **2** appears to form at higher concentrations for methods 1, 2, 3 and 4 but again is not as predictable as compounds **1** and **3**. For method 3 there is a large concentration range where both compounds **1** and **3** are commonly formed. The trends for each method will be discussed in greater detail in the relevant sections.

Table 3.3: Concentrations and results for the Zinc-BTRI compounds using methods 1 – 5

Concentration ($mol.dm^{-3}$)	Method 1	Method 2	Method 3	Method 4	Method 5
0.032±2	1	1	1	-	1
0.038±2	2/3	1	1	1	1
0.047±2	3	3	1	1	1
0.063±3	1	1	1/3	1	1
0.076±2	1	1	1	1	1
0.095±5	1/3	1/2/3	1	1	1
0.113±2	1	1	1	1	1
0.126±4	1	1	1/3	1	1
0.142±3	1	3	1	1	1
0.151±3	1/3	1	1	1	-
0.158±2	3	1	3	1	1
0.19±1	1/2/3	1/2/3	1/3	1/3	1/3
0.221±3	3	1	1/3	1	1
0.227±3	1/3	1	1/3	1/3	1
0.236±4	1	1	1/3	1	1
0.252±4	1/3	1/2	1/3	1/3	1
0.265±3	1/3	1/3	1/3	-	1
0.284±6	3	1	1/3	1	1/3
0.303±4	3	2	1/3	-	-
0.315±5	1/2/3	1/3	1/2/3	1/3	1
0.331±4	3	2	1/3	-	1
0.340±4	2	2	1/3	-	-
0.38±1	1/2/3	1/2/3	2/3	2/3	1/3
0.441±6	3	1	3	3	1
0.473±7	2	1/DMFBTRI	2/3	2	DMFBTRI
0.504±6	3	2	3	3	-
0.57±1	2/3	2/DMFBTRI	1	3	3/DMFBTRI
0.63±1	3	DMFBTRI	2	3	-
0.662±9	3	DMFBTRI	2	2/3	-
0.76±1	2/3	3/DMFBTRI	3	3	DMFBTRI
0.95±1	3/DMFBTRI	DMFBTRI	3/DMFBTRI	3/DMFBTRI	DMFBTRI
1.13±2	DMFBTRI	DMFBTRI	3	DMFBTRI	DMFBTRI
1.32±2	3	DMFBTRI	2/3	2/DMFBTRI	DMFBTRI
1.89±2	DMFBTRI	DMFBTRI	DMFBTRI	-	DMFBTRI

* "/" indicates a mixture of compounds were obtained.
No attempt to determine relative amounts was made

The following sections contain figures showing the compounds generated for each method and at varying concentrations. The size of the circle at a particular point is relative to the number of experiments that produced that compound at a given concentration.

Figures 3.2 – 3.6 in the following sections show the number of experiments that produce a specific compound at a set concentration. Where more than one type of compound is formed in the same vial, all compounds found are reflected in the figures. Studies were performed using PXRD analysis.

3.1.1 METHOD 1

As the concentration of starting materials is increased the prevalence of each compound is affected. This trend is depicted in Figure 3.2. At low concentrations it is more likely for **1** to form. The majority of experiments with concentrations of less than 0.25 mol.dm^{-3} produced **1**. As the concentration is increased more of compound **3** is produced. Between 0.25 and 0.8 mol.dm^{-3} especially the majority of experiments result in compound **3**. Over 0.8 mol.dm^{-3} compounds **1** and **3** are still formed occasionally. Compound **2** occurs sporadically and unpredictably between 0.03 – 0.8 mol.dm^{-3}. Above 0.8 mol.dm^{-3} approximately half the experiments produce **DMFBTRI**.

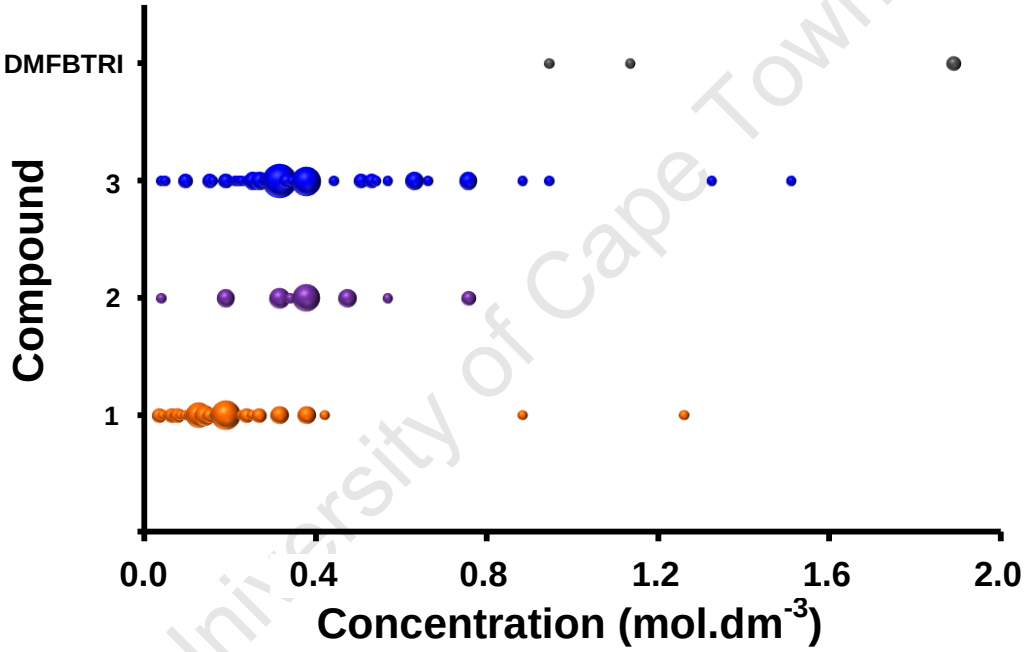

Figure 3.2: The compounds formed with method 1 between 0.03 and 2.00 mol.dm^{-3} concentrations

3.1.2 METHOD 2

Method 2 has no visible trends with regards to the preparation of compounds **1**, **2** and **3**. This is depicted in Figure 3.3. Below a concentration of 0.45 mol.dm^{-3} compounds **1**, **2** and **3** all form and compound **1** is the predominant product. Above 0.45 mol.dm^{-3} there is very little occurrence of compounds **1**, **2** or **3** and the majority product is **DMFBTRI**.

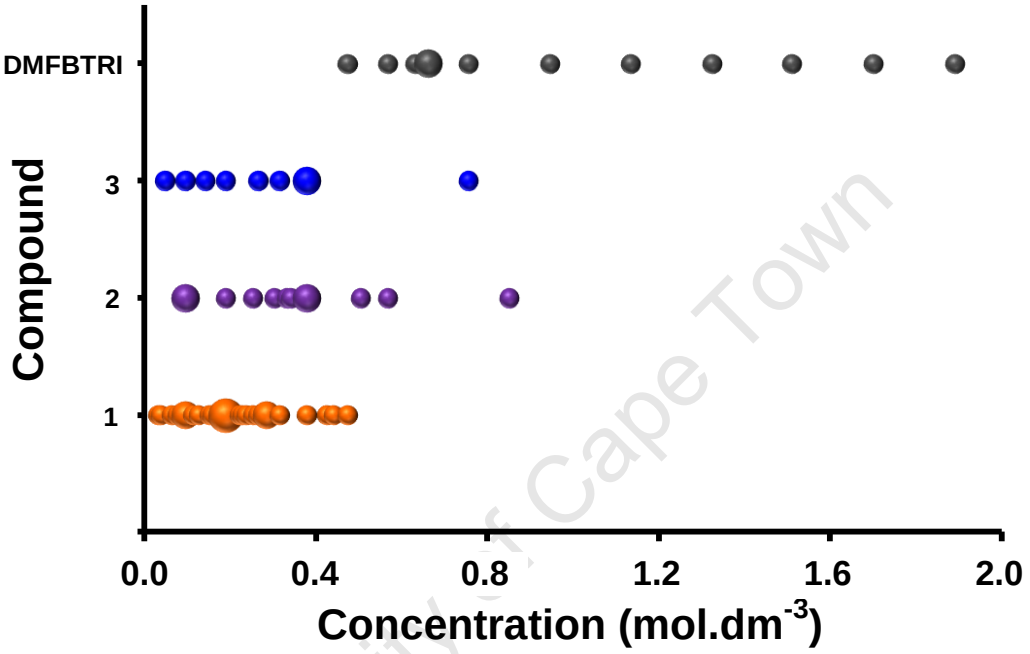

Figure 3.3: The compounds formed with method 2 between 0.03 and 2.00 mol.dm^{-3} concentrations

For all five methods the **DMFBTRI** solvate is formed when the concentration of the ligand is sufficiently high. At these higher concentrations there is insufficient time for complexation with the metal to occur thus **DMFBTRI** is a kinetically favoured product. For methods 1, 3 and 4 the concentration is always above 0.8 mol.dm^{-3} when **DMFBTRI** is produced. For methods 2 and 5 the solvate is formed at lower concentrations. With method 2 the starting materials are dissolved at 60 °C and the vial is placed in an oven at 30 °C. This results in rapid cooling from 60 °C to 30 °C allowing the kinetic product to form. With method 5 the vials are placed in a Dewar and allowed to start cooling immediately to room temperature. With the other methods the vials are held at 60 °C for longer and cooled slowly allowing more time for complexation to occur in solution and for a more thermodynamically favoured product to form.

3.1.3 METHOD 3

The product formation trends for method 3 are shown in Figure 3.4. For method 3 the majority of product formed at concentrations lower than 0.15 mol.dm^{-3} is compound **1**. Between 0.15 mol.dm^{-3} and 0.40 mol.dm^{-3} compounds **1** and **3** were produced in approximately equal amounts. Above a concentration of 0.40 mol.dm^{-3} compounds **3** was formed in half the experiments with only one experiment producing compound **1**.Compound **2** formed in only a few experiments and there are only two cases where **DMFBTRI** was formed, both at concentrations higher than 0.9 mol.dm^{-3}. The vials are cooled quickly to room temperature in method 3 but are then heated to 60 °C again and cooled slowly after that. This indicates that any **DMFBTRI** that may have formed during the faster cooling process redissolves allowing the more thermodynamically favoured compounds to form.

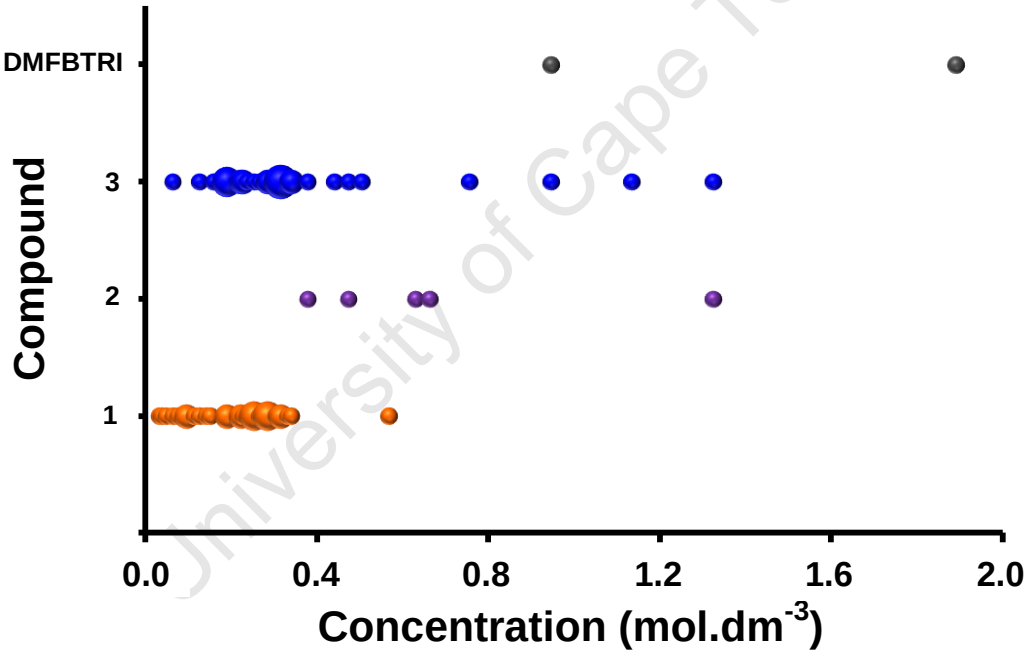

Figure 3.4: The compounds formed with method 3 between 0.03 and 2.00 mol.dm^{-3} concentrations

3.1.4 METHOD 4

Method 4 results in compound **1** exclusively below a concentration of 0.18 mol.dm^{-3} as shown in Figure 3.5. The majority of product formed in the range 0.18 – 0.32 mol.dm^{-3} was compound **1** with some of compound **3** also being produced. None of compound **1** was formed at concentrations higher than 0.32 mol.dm^{-3}. Above 0.32 mol.dm^{-3} the majority of experiments produced compound **3** and there is a small occurrence of **DMFBTRI** being formed at the higher concentrations. Compound **2** again forms sporadically and only occasionally over a large concentration range.

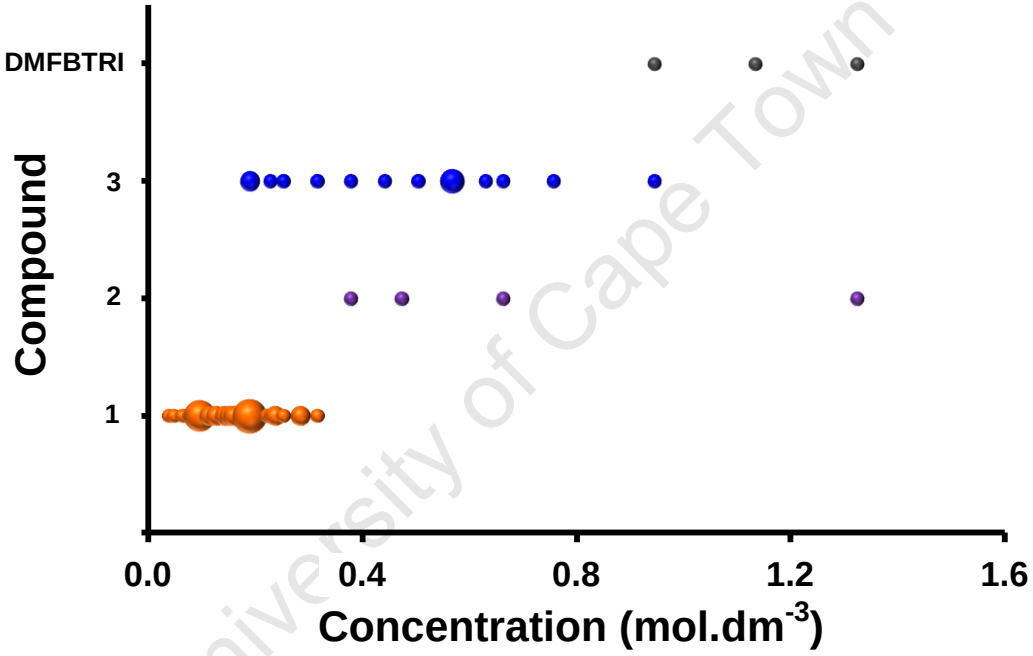

Figure 3.5: The compounds formed with method 4 between 0.03 and 1.60 mol.dm^{-3} concentrations

3.1.5 METHOD 5

Method 5 produces mainly compound **1** as shown in Figure 3.6. Below a concentration of 0.45 mol.dm^{-3} the large majority of product yielded was compound **1**. At concentrations higher than 0.45 mol.dm^{-3} **DMFBTRI** has a higher prevalence and above concentrations of 0.6 mol.dm^{-3} only **DMFBTRI** was formed. Compound **3** is formed only sporadically between 0.18 – 0.57 mol.dm^{-3}. Compound **2** was not formed at any concentration used in method 5.

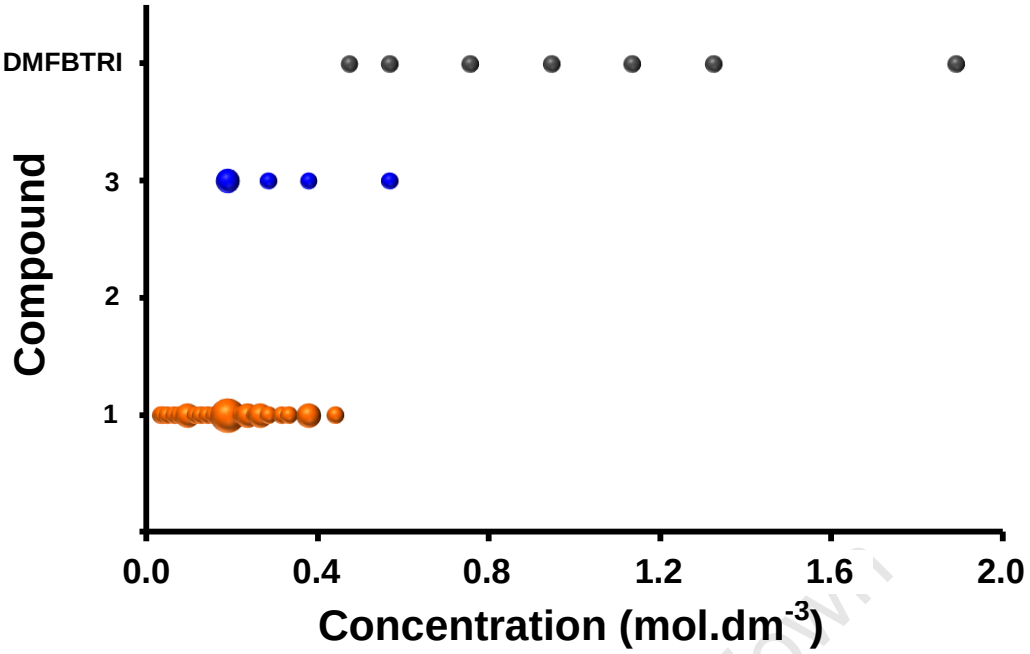

Figure 3.6: The compounds formed with method 5 between 0.03 and 2.00 mol.dm^{-3} concentrations

3.1.6 SUMMARY

Changes in concentration of the starting materials as well as the method used led to different trends in the likelihood of obtaining compounds **1** – **3**. Methods 1 and 3 both display a tendency to form **1** at lower concentrations and **3** at higher concentrations. However, method 4 shows a better selectivity for the preparation of compounds **1** and **3** and method 5 shows an exclusive preparation of compound **1** at lower concentrations. Method 2 was the best approach for the preparation of compound **2** although this compound was difficult to prepare selectively. It is necessary to use concentrations lower than 0.4 mol.dm^{-3} to form **2** with method 2 as at high concentrations the DMF solvate is exclusively formed.

3.2 DATA COLLECTION PROCEDURE FOR 1,3,5-BENZENETRICARBOXYLATE COMPOUNDS

Compounds **1** and **2** form large single crystals and these were cut to a suitable size for data collection. For all of compounds **1**, **2**, **3** and **4** the crystals were removed from the mother liquor and immediately covered in Paratone N oil[2]. Compounds **1** and **2** contain guest solvent molecules and compound **4** loses single crystallinity upon exposure to air. The Paratone N oil helps to prevent crystal degradation and the loss of solvent molecules. The crystal was placed on a nylon loop, which provides a rigid mounting for low-temperature data collection. For all four compounds single crystal X-ray diffraction data collection was performed at 173(2) K using MoKα radiation on a Nonius Kappa CCD diffractometer. Full data collection parameters are provided in Chapter 2.5.1 – Single Crystal X-ray Diffraction. The pertinent details for each compound are mentioned in the relevant sections of this chapter.

3.3 $[Zn_6(\mu_3\text{-}OH)_2(BTRI)_4(DMF)_{2.5}(H_2O)_2]\cdot[Zn(H_2O)_3(DMF)_3]\cdot 2.96H_2O$ (1)

3.3.1 SINGLE CRYSTAL X-RAY DIFFRACTION ANALYSIS

The hydrogen atoms located on the framework were placed in idealised positions in a riding model. All hydrogen atoms were refined isotropically and assigned temperature factors that relate to the atom they are attached to. The temperature factors are 1.2 times the parent atom for phenyl hydrogen atoms and 1.5 times the parent atom for methyl hydrogen atoms. The hydrogen atoms on the guest and coordinated water molecules were not modelled.

The compound crystallises in the orthorhombic crystal system, in the space group $Cmc2_1$. **1** is an anionic metal-organic framework with a charge of 2- and the counter cation is $[Zn(DMF)_3(H_2O)_3]^{2+}$. Further crystallographic data and refinement details are given in Table 3.4.

Table 3.4: Crystal data and refinement parameters of **1**

Empirical Formula	$C_{52.5}H_{68.4}N_{5.5}O_{39.5}Zn_7$
Formula Weight (g.mol^{-1})	1865.50
Temperature (K)	173(2)
Wavelength (Å)	0.71073
Crystal System	Orthorhombic
Space Group	$Cmc2_1$
a (Å)	29.555(6)
b (Å)	28.856(6)
c (Å)	17.719(4)
α (°)	90
β (°)	90
γ (°)	90
Volume (Å^3)	15111(5)
Z	8
Calculated Density (g.cm^{-3})	1.640
***μ* (mm^{-1})**	2.279
***F* (*000*)**	7581
Crystal Size (mm)	0.50 x 0.40 x 0.40
***Θ* Range Scanned (°)**	2.76 – 25.35
Index Range	-35 < h < 35, -34 < k < 34, -21 < l < 21
No. Reflections Collected	125027
No. Unique Reflections	14068
R_{int}	0.0576
Data Completeness to θ_{max} (%)	99.7
Refinement Method	Full-matrix least-squares on F^2
Data/Restraints/Parameters	14068/43/976
Goodness-of-fit on F^2	1.049
Final *R* Indices [*I>2σ(I)*]	R_1 = 0.0573, wR_2 = 0.1629
***R* Indices (all data)**	R_1 = 0.0630, wR_2 = 0.1691
Largest Diff. Peak and Hole (*e.Å*$^{-3}$)	2.542, -1.519

Figure 3.7a displays the asymmetric unit of the framework of **1** with DMF, guest water molecules and the counter cation omitted. The asymmetric unit consists of three trimeric $[Zn_3(OH)(BTRI)_6]$ secondary-building units (SBUs). SBU **X** consists of Zn1, Zn2, Zn3, SBU **Y** of Zn4, Zn5, Zn5^{i} and SBU **Z** of Zn6, Zn7, Zn8. Zn4 in SBU **Y** has half site occupancy as it is located on a mirror plane. Zn6 and Zn7 in SBU **Z** are at half site occupancy as SBU **Z** is located on a mirror plane with Zn6 and Zn7 disordered about the plane. Each SBU contains a common μ_3-OH anion (O1, O5, O7 respectively). O5 in SBU **Y** and O7 in SBU **Z** each have half site occupancy. The SBUs are bridged by fully deprotonated 1,3,5-benzenetricarboxylate (BTRI) units. Each metal centre has an oxidation state of 2+ and Zn4, Zn6, Zn7 and Zn8 have half site occupancy. The network therefore has an overall charge of 2-. This is balanced by the Zn^{2+} counter ion of Zn9 coordinated to three water molecules and three DMF molecules (Figure 3.7b).

Related by symmetry: ^{i}1-x, y, z; ^{ii}-1/2+x, 1/2+y, z; ^{iii}3/2-x, 1/2+y, z; ^{iv}x, 2-y, 1/2+z; ^{v}2-x, 2-y, 1/2+z; ^{vi}2-x, y, z; ^{vii}2-x, y, 1+z; ^{viii}3/2-x, 3/2-y, 1/2+z; ^{ix}3/2-x, 3/2-y, -1/2+z; ^{x}-1/2+x, 3/2-y, -1/2+z; ^{xi}2-x, y, -1+z; ^{xii}x, y, -1+z

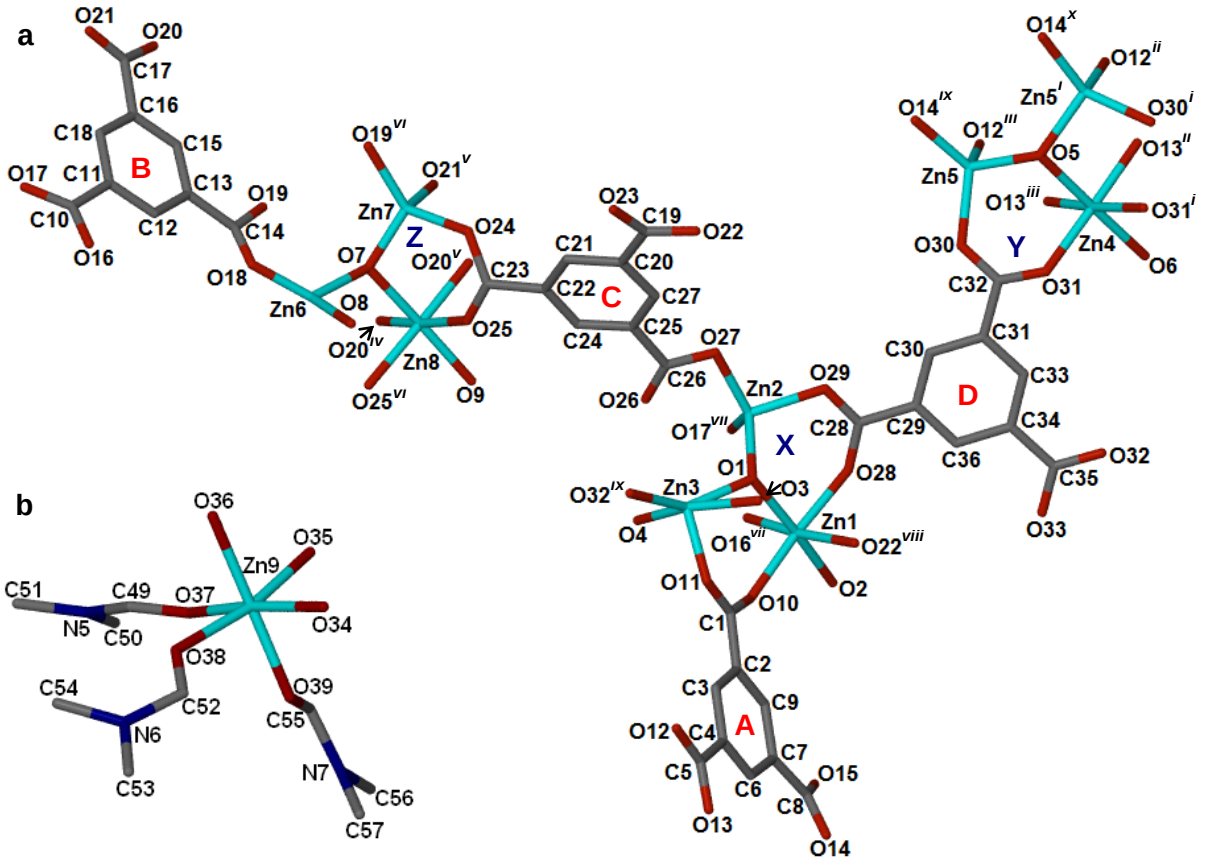

Figure 3.7: a) Asymmetric unit of the framework of **1** with DMF, guest water molecules and counter ion omitted, the oxygen atoms of the DMF molecules as shown and **b)** the counter ion of **1**

Zn1, Zn4 and Zn8 are coordinated through a distorted octahedron to four BTRI bridging units, the oxygen atom of the μ_3-OH anion and the oxygen atom of a DMF molecule (see Figure 3.7a). Zn1 has axial angles of 175.1(2) and 172.0(2)° for O10-Zn1-O28 and O16-Zn1-O22 respectively. The other, axial-equatorial and equatorial-equatorial O-Zn1-O angles range from 85.0(2) to 94.3(2)°. The exceptions are the bonds involving the disordered DMF molecules (O2A and O2B).

Zn4 lies on the (*1/2, y, z*) mirror plane and possesses half site occupancy. The minor deformation of the axial angles of O13^{ii}-Zn4-O31 and O13^{iii}-Zn4-O31^{i} (173.6(2)° for both) leads to an angle of 97.3(3)° for O31-Zn4-O31^{i}. O5-Zn4-O6 is linear (177.6(3)°) and the other O-Zn4-O bonds range from 85.3(2) to 93.0(2)°.

Zn8 lies on the (*0, y, z*) mirror plane. The slight distortion of the axial angles of O20^{iv}-Zn8-O25 and O20^{v}-Zn8-O25^{vi} (173.3(2)° for both) leads to an angle of 83.8(4)° for O20^{iv}-Zn8-O20^{v} and an angle of 96.8(3)° for O25-Zn8-O25^{vi}. O7-Zn8-O9 is linear (176.7(3)°) and the other O-Zn8-O bonds range from 88.7(2) to 92.7(2)°.

Related by symmetry: ^{i}1-x, y, z; ^{ii}-1/2+x, 1/2+y, z; ^{iii}3/2-x, 1/2+y, z; ^{iv}x, 2-y, 1/2+z; ^{v}2-x, 2-y, 1/2+z; ^{vi}2-x, y, z; ^{vii}2-x, y, 1+z; ^{viii}3/2-x, 3/2-y, 1/2+z; ^{ix}3/2-x, 3/2-y, -1/2+z; ^{x}-1/2+x, 3/2-y, -1/2+z; ^{xi}2-x, y, -1+z; ^{xii}x, y, -1+z

Zn2, Zn5, Zn5^{i} and Zn7 are coordinated in a distorted tetrahedral fashion to three BTRI bridging units and the oxygen atom of the μ_3-OH anion. The O-Zn2-O angles range from 100.9(2) to 120.5(2)°. The O-Zn5-O angles range from 104.1(2) to 122.1(2)°. Zn5 has full site-occupancy and is related to Zn5^{i} through the (*1/2, y, z*) mirror plane. The O-Zn7-O angles range from 100.8(3) to 119.8(4)°. The carboxylate oxygen atoms O19^{vi} and O24 coordinate to Zn7 and are both disordered over two positions. Zn7 has half site-occupancy and is disordered over two positions. Zn7 can be either a 3- or 4-coordinate metal ion in the structure. Zn7 and Zn7^{vi} are related by the (*0, y, z*) mirror plane. The O-Zn-O angles for 4-coordinated zinc metal centres are approximately 110 ± 9° in a search of the Cambridge Structural Database[3] (CSD).

Zn3 (SBU **X**) is five-coordinate with an irregular geometry. Zn3 bonds to two BTRI bridging units, O1 of the μ_3-OH anion and two terminal water molecules. The O-Zn3-O angles vary widely from 64.4(2) to 162.6(4)°. Zn6 (SBU **Z**) is triply coordinated to one BTRI bridging unit, O7 of the μ_3-OH anion and the oxygen atom of a DMF molecule (O8) in a trigonal pyramidal fashion. The O-Zn6-O angles range from 105.2(5) to 127.9(3)°. Zn6 has half site-occupancy and is disordered over two positions. Zn6 and Zn6^{vi} are related by the (*0, y, z*) mirror plane.

A list of Zn-O bond lengths is given in Table 3.5. A full list of angles and bond lengths can be found in the supplementary material. A paper by Orpen *et al*[4] details average bond lengths for many metal-ligand bonds determined from a thorough search of the literature. Where possible the Zn-O values obtained were compared with those literature values as well as average values obtained from a search of the CSD. The Zn-μ_3-OH bond lengths from the octahedral Zn metal centres (Zn1, Zn4, Zn8) compare well with those reported in Orpen *et al*. The marginally long length of 2.127(7) Å for Zn4-O5 helps to preserve the octahedral geometry around Zn4. Zn6-O18 and Zn7-O7 are shorter than expected (1.791(7) and 1.835(3) Å respectively) due to the high disorder around the Zn6 and Zn7 atoms.

The Zn1-O28 bond is longer than usual for terminal carboxylate oxygen atoms (2.161(5) Å) in order to maintain an octahedral geometry. The same is true of the Zn8-O terminal carboxylate bond lengths which are slightly longer than expected.

In SBU **Z** O7-Zn8-O9 is located on the (*0, y, z*) mirror plane. O7 is coordinated to Zn6, Zn7 and Zn8 in a μ_3-OH arrangement. Zn6 and Zn7 are both disordered over two positions, see Figure 3.8a. The distance between Zn7 and O19A^{vi} is too long for a bond to form while Zn7-O19B^{vi} is a typical length for a terminal carboxylate bond to zinc.

Related by symmetry: ^{i}1-x, y, z; ^{ii}-1/2+x, 1/2+y, z; ^{iii}3/2-x, 1/2+y, z; ^{iv}x, 2-y, 1/2+z; ^{v}2-x, 2-y, 1/2+z; ^{vi}2-x, y, z; ^{vii}2-x, y, 1+z; ^{viii}3/2-x, 3/2-y, 1/2+z; ^{ix}3/2-x, 3/2-y, -1/2+z; ^{x}-1/2+x, 3/2-y, -1/2+z; ^{xi}2-x, y, -1+z; ^{xii}x, y, -1+z

It is interesting to note that compound **1** contains multiple zinc metal centres, which possess the four different coordination numbers of three, four, five and six. A zinc containing MOF was reported by Liu *et al* in 2009,[5] which they claimed was the first complex to contain three kinds of coordination numbers for zinc ions in one structure.

Table 3.5: Experimental Zn-O bond lengths for **1** and literature Zn-O bond lengths

Bond	Length (Å)	Average Length (Å)	Bond Type
Zn1-O1	2.088(5)	2.01 ± 0.06* 1.990, 2.089, 2.096**	μ_3-OH
Zn2-O1	1.947(4)		
Zn3-O1	1.959(5)		
Zn4-O5	2.127(7)		
Zn5-O5	1.985(3)		
Zn6-O7	1.999(6)		
Zn7-O7	1.835(3)		
Zn8-O7	2.078(6)		
Zn1-O10	2.092(5)	2.00 ± 0.09* 2.03 ± 0.05**	Terminal carboxylate
Zn1-O16^{vii}	2.060(5)		
Zn1-O22^{viii}	2.080(5)		
Zn1-O28	2.161(5)		
Zn2-O17^{vii}	1.950(5)		
Zn2-O27	1.947(5)		
Zn2-O29	2.000(5)		
Zn3-O11	1.986(5)		
Zn3-O32^{ix}	2.041(6)		
Zn4-O13^{ii+iii}	2.089(5)		
Zn4-O31^{+i}	2.065(5)		
Zn5-O12^{iii}	1.986(5)		
Zn5-O14^{ix}	1.943(5)		
Zn5-O30	1.975(5)		
Zn6-O18	1.791(7)		
Zn7-O19B^{vi}	1.93(1)		
Zn7-O21^{v}	1.913(6)		
Zn7-O24A	1.98(1)		
Zn8-O20^{iv+v}	2.117(5)		
Zn8-O25^{+vi}	2.097(5)		
Zn3-O3	2.127(9)	2.09 ± 0.08* 2.08 ± 0.08**	5-coordinate Zn, terminal H_2O
Zn3-O4	1.995(8)		
Zn9-O34	2.043(6)	2.09 ± 0.08* 2.10 ± 0.05**	6-coordinate Zn, terminal H_2O
Zn9-O35	2.092(8)		
Zn9-O36	2.056(7)		
Zn1-O2A	2.094(5)	2.07 ± 0.09*	DMF
Zn1-O2B	2.057(5)		
Zn4-O6	2.106(8)		
Zn6-O8	2.12(1)		
Zn8-O9	2.062(7)		
Zn9-O37	2.082(8)		
Zn9-O38	2.095(8)		
Zn9-O39	2.065(8)		

* Values obtained from the CSD; ** Mean values reported in Orpen *et al*[4]

When Zn6 and Zn7 are present the O18^{vi}-C14^{vi}-O19^{vi} carboxylate is in the O19B^{vi} position. O19B^{vi} is coordinated to Zn7 and O18 is uncoordinated. O19 in the O18-C14-O19 carboxylate is in the O19A position and is uncoordinated while O18 is coordinated to Zn6

Related by symmetry: ^{i}1-x, y, z; ^{ii}-1/2+x, 1/2+y, z; ^{iii}3/2-x, 1/2+y, z; ^{iv}x, 2-y, 1/2+z; ^{v}2-x, 2-y, 1/2+z; ^{vi}2-x, y, z; ^{vii}2-x, y, 1+z; ^{viii}3/2-x, 3/2-y, 1/2+z; ^{ix}3/2-x, 3/2-y, -1/2+z; ^{x}-1/2+x, 3/2-y, -1/2+z; ^{xi}2-x, y, -1+z; ^{xii}x, y, -1+z

(Figure 3.8b). When the metal ions are in the Zn6^{vi} and Zn7^{vi} positions the reverse happens (Figure 3.8c). For clarity only the relevant atoms are labelled in Figure 3.8. For the same reason Zn8 is not shown in the figure. A similar situation occurs with the O24-C23-O25 carboxylate moiety. When in the Zn7 position the O24-C23-O25 carboxylate is in the O24A position, which is coordinated to Zn7 while the O24^{vi}-C23^{vi}-O25^{vi} carboxylate is in the O24B^{vi} position and O24B^{vi} is uncoordinated. O25 and O25^{vi} are always coordinated to Zn8.

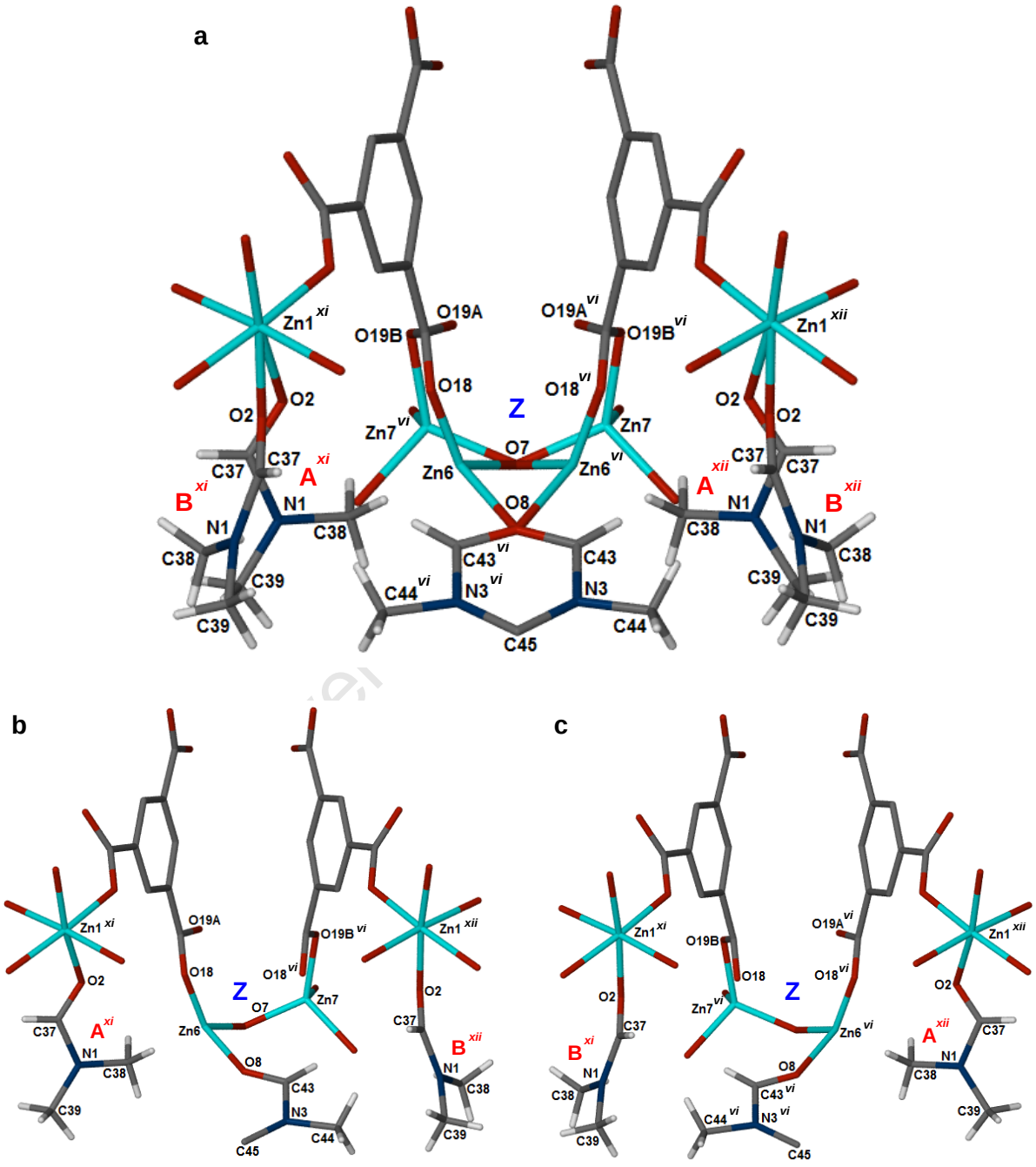

Figure 3.8: The disorder of **1**. **a)** The disorder of the O2^{xi} and O2^{xii} DMF molecules A and B and that of SBU **Z**, **b)** O2^{xi} DMF A, O2^{xii} DMF B and the corresponding disorder in SBU **Z** and **c)** O2^{xi} DMF B, O2^{xii} DMF A and the corresponding disorder in SBU **Z**

Related by symmetry: ^{i}1-x, y, z; ^{ii}-1/2+x, 1/2+y, z; ^{iii}3/2-x, 1/2+y, z; ^{iv}x, 2-y, 1/2+z; ^{v}2-x, 2-y, 1/2+z; ^{vi}2-x, y, z; ^{vii}2-x, y, 1+z; ^{viii}3/2-x, 3/2-y, 1/2+z; ^{ix}3/2-x, 3/2-y, -1/2+z; ^{x}-1/2+x, 3/2-y, -1/2+z; ^{xi}2-x, y, -1+z; ^{xii}x, y, -1+z

Figure 3.8a shows the disorder around the (*0, y, z*) mirror plane in SBU **Z** and the effect on the O2 DMF molecule. The disorder in SBU **Z** leads to disorder of the O2 DMF molecule. When SBU **Z** consists of Zn6 and Zn7 the O8 DMF is on the opposite side of the mirror plane to Zn6 (Figure 3.8b). The O2^{xi} DMF is coordinated to Zn1^{xi} in position A while the O2^{xii} DMF is coordinated to Zn1^{xii} metal centre in position B. When SBU **Z** contains Zn6^{vi} and Zn7^{vi} the O8^{vi} DMF is on the opposite side of the mirror plane to Zn6^{vi}. The O2^{xi} DMF molecule can no longer occupy position A and therefore shifts to position B while the O2^{xii} DMF molecule is now located in position A (Figure 3.8c). O2A and O2B are oriented at approximately 90° to one another.

1 forms a three-dimensional, anionic framework, shown in orange in Figure 3.9. Large channels (~11 Å in diameter) and small channels (~7 Å in diameter) extend along the [001] direction. The large channels are occupied by the $[Zn(DMF)_3(H_2O)_3]^{2+}$ cation and guest water molecules while the small channels are occupied by uncoordinated guest water molecules, the O8 DMF molecule coordinated to Zn6 and the coordinated water molecule O4. There are 2.96 water molecules modelled in the asymmetric unit of the structure.

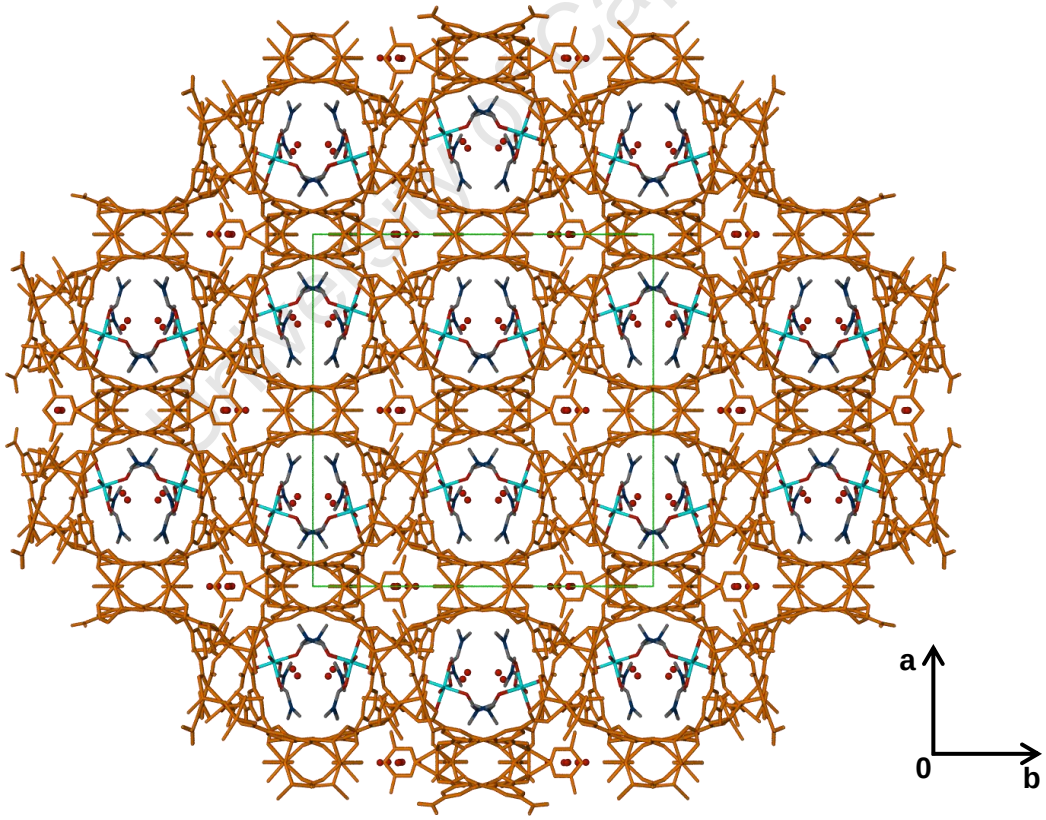

Figure 3.9: The packing diagram of **1** viewed along the [001] axis. The anionic framework is shown in orange

Related by symmetry: ^{i}1-x, y, z; ^{ii}-1/2+x, 1/2+y, z; ^{iii}3/2-x, 1/2+y, z; ^{iv}x, 2-y, 1/2+z; ^{v}2-x, 2-y, 1/2+z; ^{vi}2-x, y, z; ^{vii}2-x, y, 1+z; ^{viii}3/2-x, 3/2-y, 1/2+z; ^{ix}3/2-x, 3/2-y, -1/2+z; ^{x}-1/2+x, 3/2-y, -1/2+z; ^{xi}2-x, y, -1+z; ^{xii}x, y, -1+z

These water molecules are heavily disordered and can be removed at low temperatures, which suggests that they can move freely throughout the channels. They were modelled over nine positions with site occupancy factors (s.o.f.) ranging from 0.15 to 0.50. Seven of the nine positions are in the small channels and those seven positions correspond to a s.o.f. of 2.30. The other two positions are in the larger channel and correspond to a s.o.f. of 0.66.

The trimeric zinc clusters and the packing structure of **1** are very similar to those found in **MOF-CJ3**[6]. **MOF-CJ3** is also prepared from Zn(II) and H_3BTRI although under substantially different conditions: Zn(II) nitrate and H_3BTRI are dissolved in a solvent system of DMF/glacial acetic acid (HAc) (3:1 ratio, v/v) and held at 170 °C for four days. The unit cell dimensions, chemical content and symmetry of **MOF-CJ3** and **1** differ significantly and their PXRD patterns are different (see Section 3.3.3 – Powder X-ray Diffraction, Figure 3.13). While both are anionic the counter ion for **1** is $[Zn(DMF)_3(H_2O)_3]^{2+}$ while for **MOF-CJ3** the counter ion is (unobserved) H_3O^+. Both compounds contain guest water molecules located in the channels along [001]. The data collection for **MOF-CJ3** was performed at 293 K. This could explain why the guest water molecules were not modelled in this structure.

Figure 3.10 depicts the framework of **1** viewed down the [001] axis – shown in black – with an overlay in red of the symmetry elements present in the $Cmc2_1$ space group. The symbols are explained in the figure. The (0,0,z) and (1/2,1/2,z) twofold screw axes are located between **Z** SBUs. The (1/2,0,z) and (0,1/2,z) twofold screw axes are situated between **Y** SBUs. The twofold screw axes at (1/4,1/4,z), (1/4,3/4,z), (3/4,1/4,z) and (3/4,3/4,z) are sited between **X** SBUs.

Related by symmetry: [i]1-x, y, z; [ii]-1/2+x, 1/2+y, z; [iii]3/2-x, 1/2+y, z; [iv]x, 2-y, 1/2+z; [v]2-x, 2-y, 1/2+z; [vi]2-x, y, z; [vii]2-x, y, 1+z; [viii]3/2-x, 3/2-y, 1/2+z; [ix]3/2-x, 3/2-y, -1/2+z; [x]-1/2+x, 3/2-y, -1/2+z; [xi]2-x, y, -1+z; [xii]x, y, -1+z

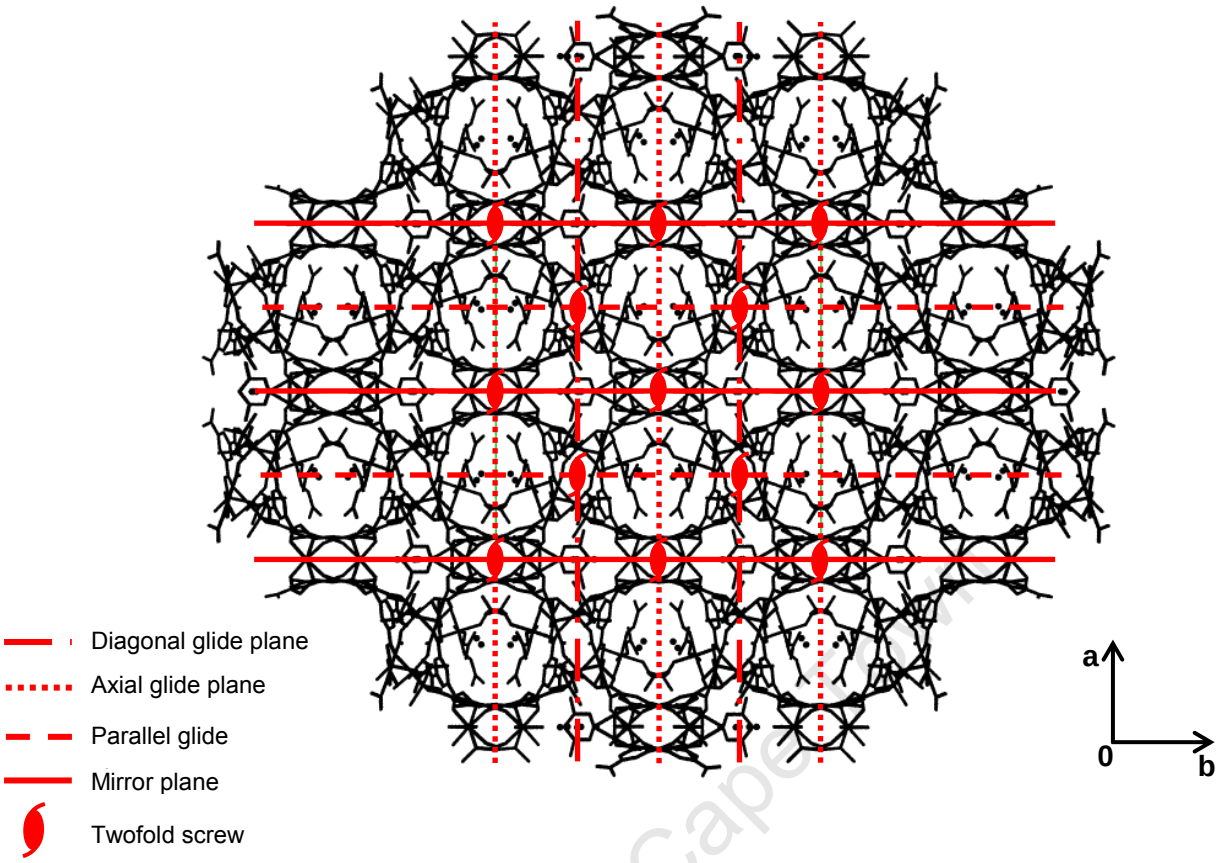

Figure 3.10: The packing diagram of 1 (black) viewed along the [001] axis with an overlay of the symmetry elements in the unit cell (red)

3.3.2 THERMAL ANALYSIS

The thermogravimetric (TG) trace (Figure 3.11, blue) shows three mass loss steps before decomposition: A, B and C. The range of each mass loss was determined by analysis of the first derivative of the TG trace with respect to temperature. Mass loss A (*ca* 20 – 45 °C) corresponds to the loss of the *ca* 2.30 guest water molecules located in the smaller channel running along [001] (calculated: 2.22%). Mass loss B (*ca* 45 – 120 °C) corresponds to the loss of the guest water molecules located in the larger channel running along [001] (with a s.o.f. of 0.66) as well as the coordinated water molecules: O3, O4, O34, O35 and O36 (calculated: 5.46%). O3 and O4 are located on the framework while O34, O35 and O36 are coordinated to the cation.

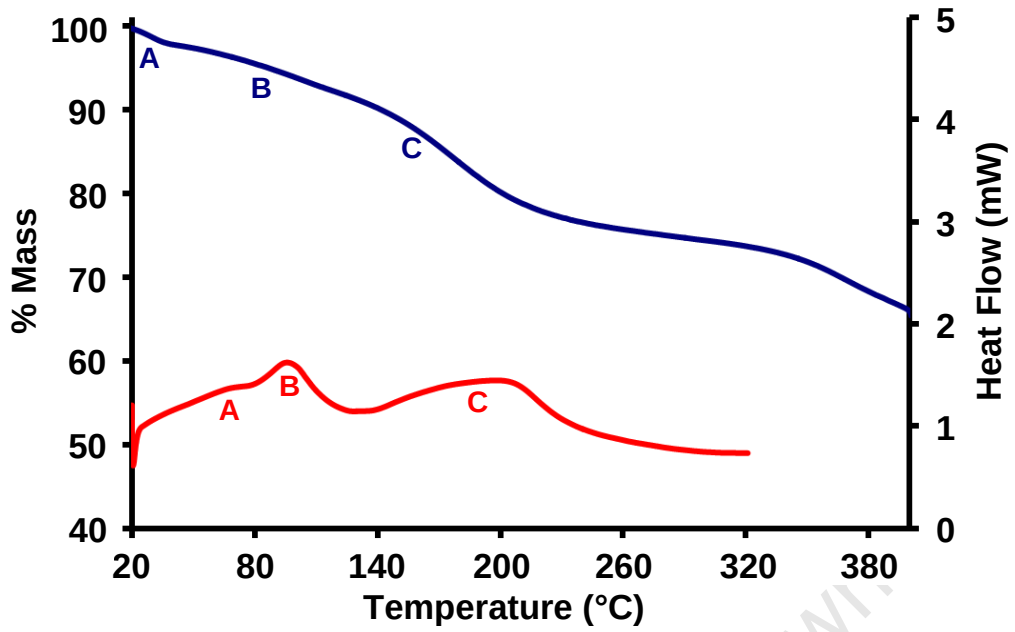

Figure 3.11: a) TG analysis of **1** and **b)** DSC analysis of **1** both with a heating rate of 10 °C.min^{-1}

Mass loss C (120 – 290 °C) corresponds to the loss of 4.5 of the 5.5 DMF molecules in the asymmetric unit (calculated: 17.63%). The O2 DMF molecule is the only DMF molecule not located in a channel. The O8 DMF is located in the small channels along [001] and the cation DMF molecules are located in the large channels along [001]. The O6 and O9 DMF molecules are located in a "channel" along [010] that consists solely of O6 and O9 DMF molecules. The one DMF that is not removed until decomposition is therefore likely to be the O2 DMF.

Three endotherms are visible in the differential scanning calorimetry (DSC) trace (Figure 3.11, red). See Table 3.6 for the DSC endotherm onset temperatures as well as the TG mass loss percentages. Endotherms A and B overlap. Endotherm A corresponds to the loss of the 2.30 H_2O molecules (located in the small channels along [001]) and starts as soon as the measurement begins. Endotherm B correlates with the loss of the remaining guest water molecules as well as the water molecules coordinated to the framework and the cation. Endotherm A appears as a shoulder on B and obscures the beginning of B. This prevents an accurate measurement of the onset temperature for B. Endotherm C corresponds with the loss of the 4.5 DMF molecules. The TGA and DSC results are presented in Table 3.6.

Table 3.6: TGA and DSC results for **1**

	TGA Results		DSC Results
	Calc. % Mass Loss	**Exp. % Mass Loss**	**T_{onset} (°C)**
2.30 H_2O	2.22	2.27	21
5.66 H_2O	5.46	5.36	*ca* 80
4.50 DMF	17.63	17.97	137

The thermal events visible in the hot-stage microscopy (HSM) are observed at temperatures higher than those in the TG and DSC analyses. This is due to many factors including crystal size, geometry of the analysis equipment and the different conditions of analysis. There is also a temperature gradient in the HSM. The sample is placed in the centre of the brass heating plate and the centre area is not heated directly. As a result the sample temperature can lag behind that reported by the apparatus.

The HSM was performed in a room at 27 °C. The sample is crystalline at room temperature (Figure 3.12a). The crystal starts to become opaque at approximately 80 °C upon the loss of the more strongly held guest water molecules and the coordinated water (Figure 3.12b). This corresponds to mass loss B in the TG analysis. The crystal continues to become progressively more opaque until 120 °C when all the water molecules have been removed. According to variable temperature PXRD (see Section 3.3.3, Figure 3.15) the sample is still crystalline at this temperature although it is no longer a single crystal. At 124 °C bubbles start to form (Figure 3.12c) corresponding with the loss of the DMF molecules. The sample begins to become amorphous at the same time. The bubbles continue with increasing temperature. It is interesting to note that the bubbles will eventually stop if the sample is held at 180 °C and that at this temperature 3.5 of the 5.5 DMF molecules have been removed.

The O34, O35 and O36 DMF molecules as well as the O8 DMF molecule (located in the large channel along [001]) are probably removed first. The crystal is completely opaque at 180 °C as shown in Figure 3.12d. The sample starts to bubble again at 216 °C due to the loss of the O6 and O9 DMF molecules. As the sample was not held at 180 °C during the TG analysis there is only one visible step for the loss of the DMF molecules in the TG trace. The loss of the O6 and O9 DMF molecules continues until approximately 300 °C and during this process decomposition begins. This is visible in the HSM as the edges of the crystal start to turn a brown colour at 243 °C (Figure 3.12e). The crystal decomposes above 300 °C and has turned completely brown by 400 °C (Figure 3.12f).

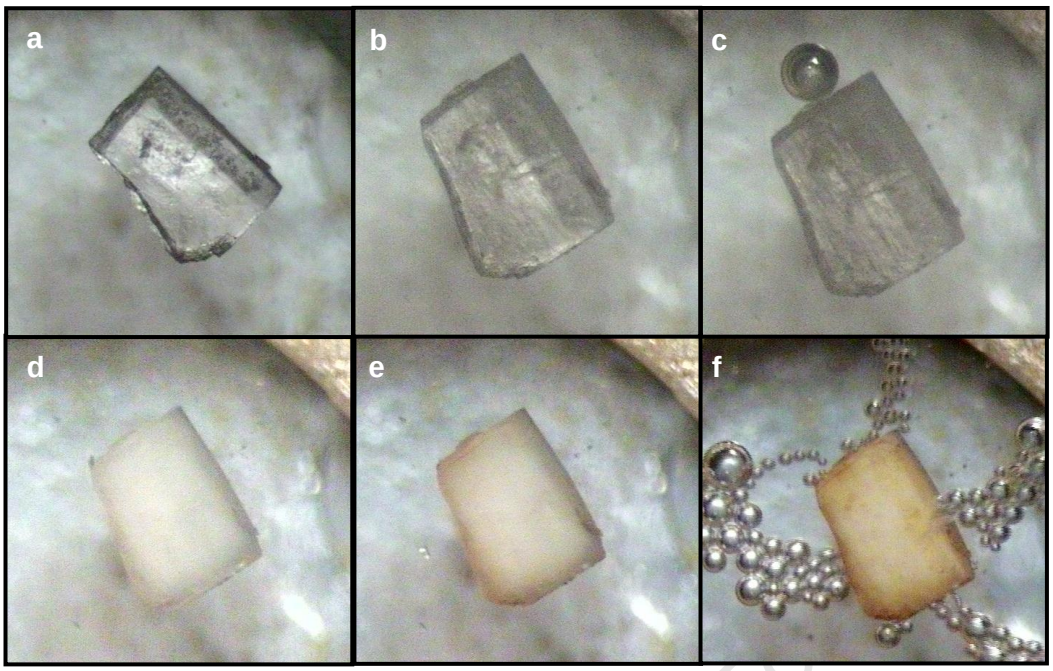

Figure 3.12: HSM pictures of **1** at **a)** 27 °C, **b)** 86 °C, **c)** 124 °C, **d)** 180 °C, **e)** 243 °C and **f)** 400 °C

Elemental analysis confirms the presence of 2.96 water molecules in the asymmetric unit. It correlates well with both the single crystal and the thermal analyses. Details are given in Table 3.7.

Table 3.7: Elemental analysis of $[(Zn_7C_{36}O_{26}H_{14})(H_2O)_5(C_3NOH_7)_{5.5}]\cdot 2.96H_2O$ (**1**)

	Calculated	Experimental
% C	33.80	33.68
% H	3.70	3.68
% N	4.13	4.81

3.3.3 POWDER X-RAY DIFFRACTION

The PXRD pattern of **MOF-CJ3** (Figure 3.13b, red) resembles that of **1** (Figure 3.13a, black) in the low 2θ range. From 2 – 15° 2θ all the peaks visible for **MOF-CJ3** are also visible for **1**. This corresponds with the similarity seen between the two compounds: the trimeric zinc clusters and packing structures. **1** has significant extra peaks at 7.9 and 14.6° 2θ as well as smaller ones at 4.4, 6.7 and 9.5° 2θ. Above 15° 2θ there are many more small peaks in the pattern for **1**. This corresponds with the lower symmetry found in compound **1** when compared to **MOF-CJ3**.

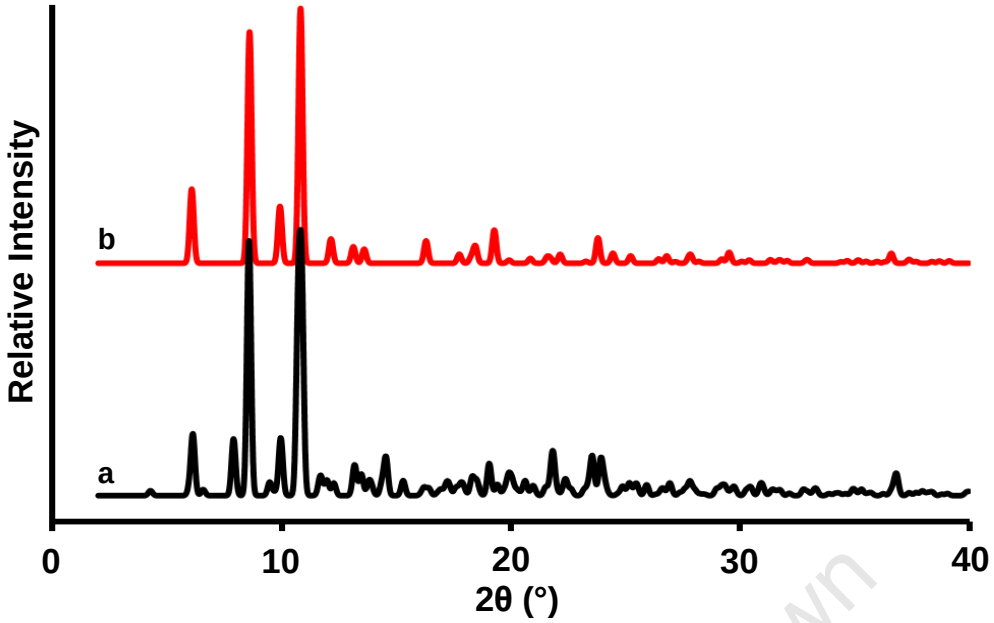

Figure 3.13: PXRD patterns calculated from single crystal data of **a) 1** and **b) MOF-CJ3**

The PXRD pattern obtained from the bulk material of **1** (Figure 3.14b, red) corresponds well with the pattern calculated from the single crystal data (Figure 3.14a, blue).

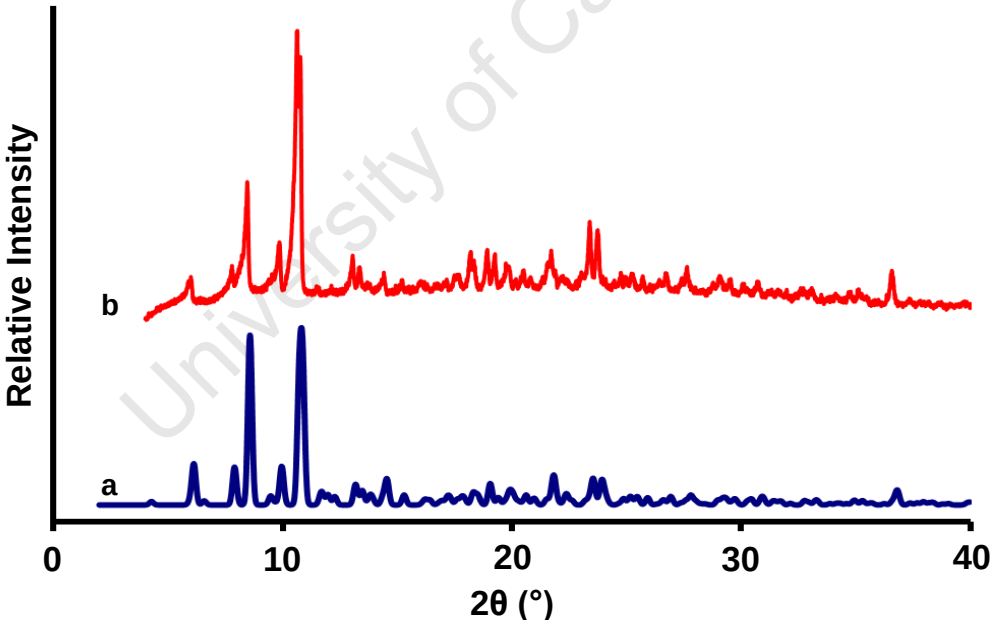

Figure 3.14: PXRD patterns of **1 a)** calculated from single crystal data and **b)** experimental

When **1** is heated crystallinity is lost (Figure 3.15). This corresponds with the loss of solvent molecules seen in the thermal analysis (Section 3.3.2 – Thermal Analysis). The sample is almost completely amorphous by 150 °C. The solvent molecules lost include guest and coordinated water molecules as well as coordinated DMF molecules.

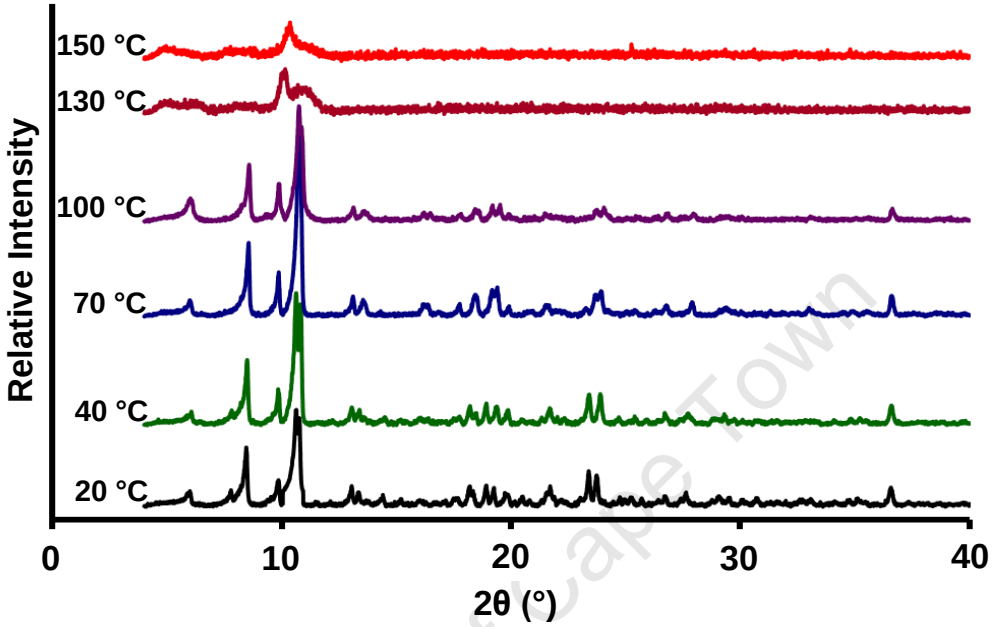

Figure 3.15: Variable temperature PXRD patterns of **1** from 20 – 150 °C

A sample of **1** was dried at 150 °C (**1a**). Upon exposure of a sample of **1a** to water vapour crystallinity begins to return. After one hour of exposure there are extra peaks in the PXRD pattern (Figure 3.16b). After 24 hours of exposure to water vapour crystallinity is regained (Figure 3.16c). The pattern does not vary with longer exposure. The PXRD pattern obtained does not match that observed for **1**. This is unsurprising as both DMF and H_2O molecules were lost upon heating but the sample was only exposed to water vapour. TG analysis on this rehydrated sample reveals that *ca* 24 water molecules are reabsorbed by the compound.

A sample of **1a** was also exposed to a mixture of DMF and H_2O vapour for 5 hours (Figure 3.16d). Crystallinity was regained and the PXRD pattern resembles that of **1** in some areas. There are differences however and the pattern has distinct differences from the water vapour sample as well. TG analysis revealed a 22.3% mass loss for the resolvated sample. The sorption is of both DMF and water and the mass loss steps are not distinct. The absorption of both DMF and water is implied by the fact that the pattern is different from the sample after exposure to just water vapour (Figure 3.16c) but that there are some similarities. However, the first derivative of the TG trace reveals two separate steps, one of *ca* 11.9% and the other of *ca* 10.5%. It is probable that the water would be removed before

the DMF molecules. The initial mass loss therefore corresponds to the loss of nine water molecules while the second mass loss corresponds to the loss of two DMF molecules.

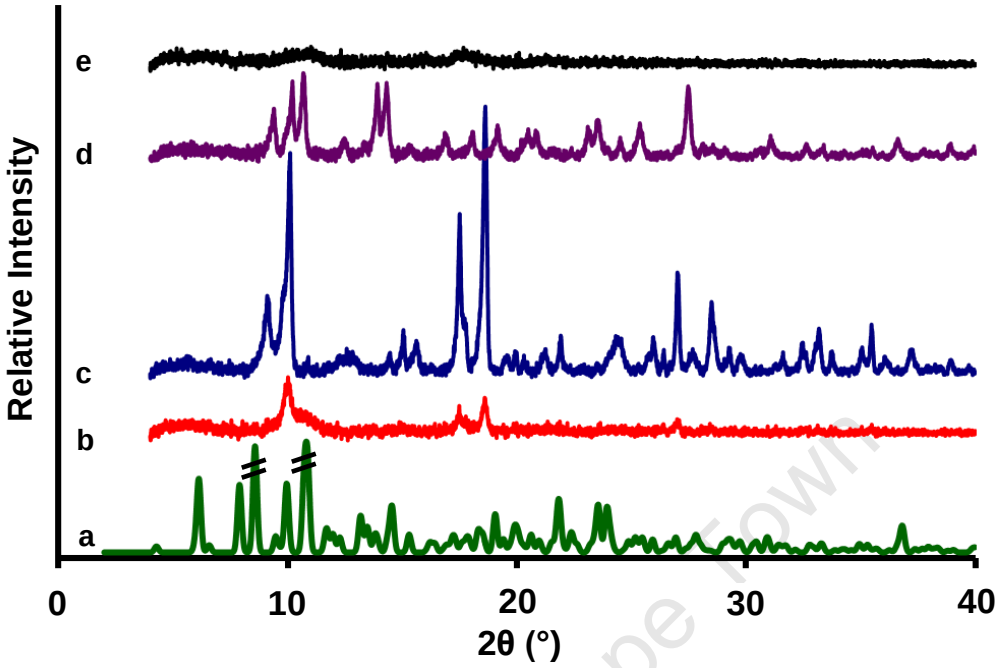

Figure 3.16: PXRD patterns of vapour diffusion experiments on dried samples of **1** (**1a**). **a)** Calculated **1**, **b)** after exposure of **1a** to water vapour for 1 hour, **c)** after exposure of **1a** to water vapour for 24 hours, **d)** after exposure of **1a** to DMF/H_2O vapour for 5 hours, **e)** control after heating to 180 °C

3.3.4 SUMMARY

Compound **1** was prepared reproducibly using a number of methods (see Section 3.1 – Preparation of Zinc(II) and 1,3,5-benzenetricarboxylate Compounds). This was confirmed using single-crystal and powder X-ray diffraction as well as thermal methods. **1** is similar to **MOF-CJ3** but has lower symmetry due to disorder and a different, larger counter cation. **1** loses crystallinity at higher temperatures but can regain it upon exposure to water vapour or a mixture of water and DMF vapour.

The topology of **1** is discussed in depth in Chapter 5 – Topological Studies.

3.4 [Zn(HCOO)(BTRI)$_{0.3}$(DMF)] (2)

3.4.1 SINGLE CRYSTAL X-RAY DIFFRACTION ANALYSIS

The hydrogen atoms were placed in idealised positions in a riding model. All hydrogen atoms were refined isotropically and assigned temperature factors that relate to the atom they are attached to. The temperature factors are 1.2 times the parent atom for phenyl and formate hydrogen atoms and 1.5 times the parent atom for methyl hydrogen atoms.

Table 3.8: Crystal data and refinement parameters of **2**

Empirical Formula	$C_7H_9NO_5Zn$
Formula weight (g.mol^{-1})	252.52
Temperature (K)	173(2)
Wavelength (Å)	0.71073
Crystal System	Trigonal
Space Group	$P\bar{3}$
a (Å)	13.933(2)
b (Å)	13.933(2)
c (Å)	8.064(2)
α (°)	90
β (°)	90
γ (°)	120
Volume (Å^3)	1355.8(4)
Z	6
Calculated Density (g.cm^{-3})	1.856
***μ* (mm^{-1})**	2.712
***F* (*000*)**	768
Crystal Size (mm)	0.40 x 0.40 x 0.15
***Θ* Range Scanned (°)**	2.92 – 31.51
Index Range	-20 < h < 20, -19 < k < 20, -11 < l < 11
No. Reflections Collected	41449
No. Unique Reflections	3032
R_{int}	0.0984
Data Completeness to θ_{max} (%)	99.9
Refinement Method	Full-matrix least-squares on F^2
Data/Restraints/Parameters	3032/0/129
Goodness-of-fit on F^2	1.079
Final *R* Indices [*I>2σ(I)*]	R_1 = 0.0279, wR_2 = 0.0779
***R* Indices (all data)**	R_1 = 0.0314, wR_2 = 0.0800
Largest Diff. Peak and Hole (*e.Å*$^{-3}$)	1.321, -0.627

The compound crystallises in the trigonal crystal system, in the space group $P\bar{3}$. **2** is a neutral two-dimensional metal-organic framework. Further crystallographic and refinement details are given in Table 3.8.

Figure 3.17 shows the asymmetric unit of **2** and Figure 3.18 the extended structure. Single-crystal X-ray diffraction reveals that **2** is a highly symmetrical molecule. Hexameric $[Zn_6(HCOO)_6(DMF)_6]$ clusters are connected by fully deprotonated 1,3,5-benzenetricarboxylate (BTRI) ligands to form neutral, two dimensional sheets parallel to the [110] plane.

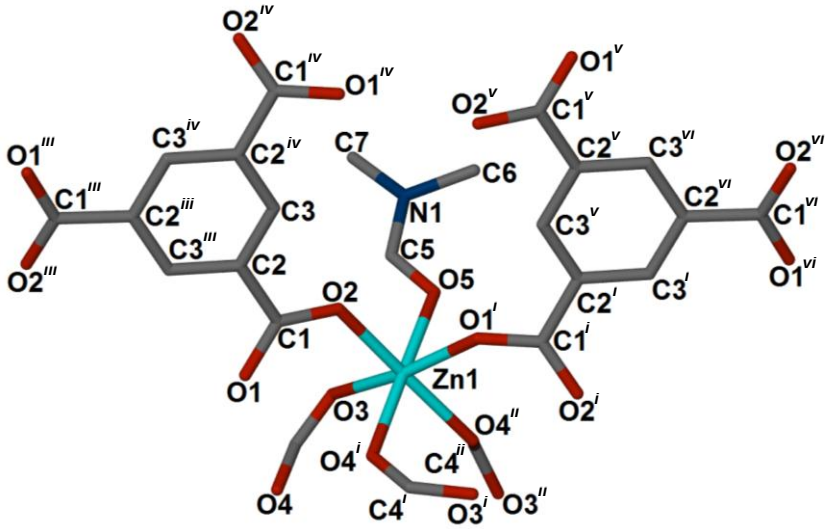

Figure 3.17: Compound **2** with the asymmetric unit and symmetry generated atoms labelled

Three DMF molecules are located on either side of a 2D-sheet interlocking with the DMF molecules on the adjacent sheet. The Zn1 metal centre is coordinated to the oxygen atom of two different BTRI ligands (O2 and $O1^{i}$), three oxygen atoms from three different formate ligands (O3, $O4^{i}$ and $O4^{ii}$) and the oxygen atom of one DMF molecule (O5). The formate is formed *in situ* by the hydrolysis of the DMF solvent molecules.

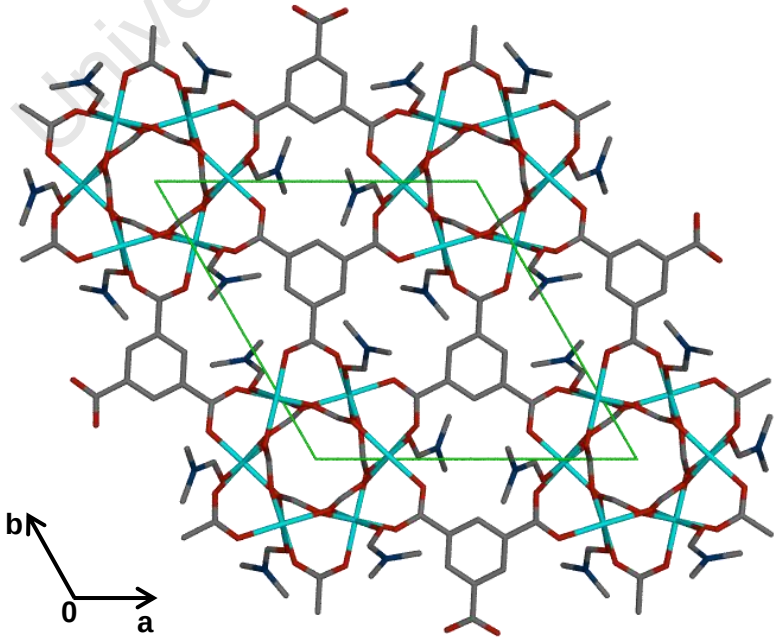

Figure 3.18: The packing diagram of **2** viewed along the [001] axis

Related by symmetry: ^{i}x-y, -1+x, 1-z; ^{ii}1-y, -1+x-y, z; ^{iii}2-y, x-y, z; ^{iv}2-x+y, 2-x, z; ^{v}2-x, 1-y, 1-z; ^{vi}y, 1-x+y, 1-z

The Zn1 metal centre assumes a slightly distorted octahedral geometry with axial-equatorial and equatorial-equatorial O-Zn-O angles ranging from 83.66(4) to 96.1(4)°. The O2-Zn1-O4^{ii} and O4^{i}-Zn1-O5 axial angles are close to 180°. The O1^{i}-Zn1-O3 axial angle is smaller than expected (168.82(4)°) due to the O3-C4-O4 formate moiety bridging two Zn1 metal centres.

A list of Zn-O bond lengths is given in Table 3.9. The full list of angles and bond lengths can be found in the supplementary material. The terminal carboxylate Zn-O bond lengths correspond well with those given in Orpen *et al.*[4] All the Zn-O distances agree well with those determined by a search of the CSD.

Table 3.9: Experimental Zn-O bond lengths for **2** and literature Zn-O bond lengths

Bond	Length (Å)	Average Length (Å)	Bond Type
Zn1-O1^{I}	2.034(2)	2.00 ± 0.09*	Terminal carboxylate
Zn1-O2	2.043(1)	2.03 ± 0.05**	
Zn1-O3	2.113(1)	2.08 ± 0.05*	Formate μ-O_2CH
Zn1-O4^{I}	2.132(1)		
Zn1-O4^{II}	2.119(1)		
Zn1-O5	2.151(1)	2.07 ± 0.09*	DMF

* Values obtained from the CSD; ** Mean values reported in Orpen *et al*[4]

Compound **2** is highly symmetrical with hexameric zinc clusters forming rings. Three zinc(II) metal centres lie above the plane and three zinc(II) metal centres lie below the plane of the ring. The zinc metal ions are connected by six bridging formate moieties each with a charge of 1-. The hexameric formate/zinc ion clusters act as SBUs connected by fully deprotonated BTRI units. For every zinc SBU there are two full BTRI units each with a charge of 3-. As a result the network is neutral overall.

Figure 3.19 shows the packing diagram of **2** viewed along the [100] axis. High-lighted in orange is one of the 2-dimensional sheets. Each zinc metal centre is coordinated to one DMF molecule, therefore each hexameric zinc cluster is coordinated to six DMF molecules. Three DMF molecules are to the left of the cluster and three DMF molecules are to the right of the cluster as seen in the figure. The DMF molecules on adjoining layers interlock.

Related by symmetry: ^{i}x-y, -1+x, 1-z; ^{ii}1-y, -1+x-y, z; ^{iii}2-y, x-y, z; ^{iv}2-x+y, 2-x, z; ^{v}2-x, 1-y, 1-z; ^{vi}y, 1-x+y, 1-z

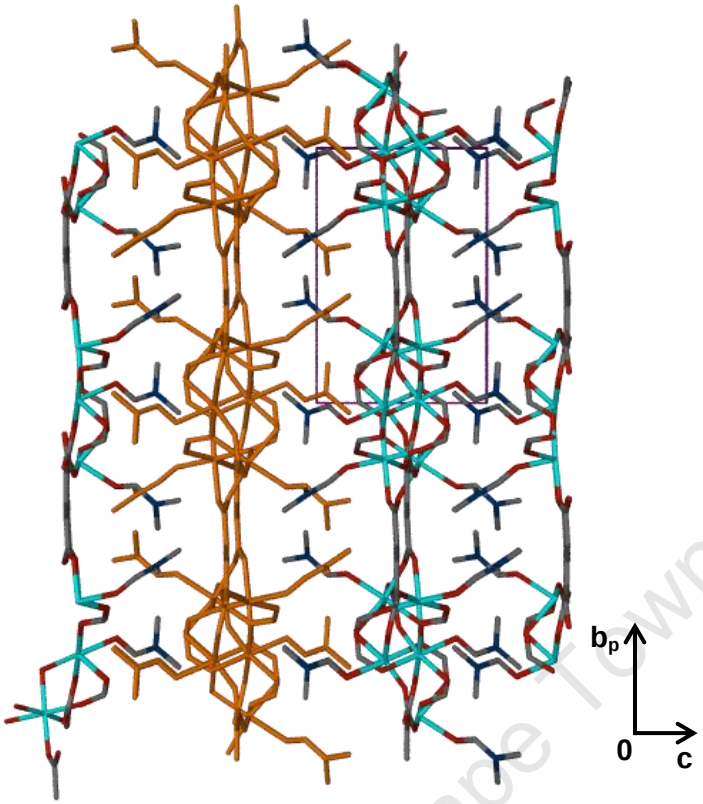

Figure 3.19: A packing diagram of **2** viewed along the [100] axis. One 2-dimensional layer is highlighted in orange. The packing looks identical when viewed along the [010] axis

Two similar structures have been previously reported. **MOF-CJ4** was prepared by He *et al*[6] using cobalt rather than a zinc metal salt. The method used is dissimilar to that used for **2** with a solvent system of DMF/glacial acetic acid and the solution being held at 170 °C for two days. $Mn_6(HCOO)_6(BTRI)_2(DMF)_6$ (**Mn-1**) was prepared by Chen *et al*[7] using a manganese metal salt. The structure of $[Mg_3(CHO_2)_3(C_9H_3O_6)(C_3H_7NO)_3]_n$ (**Mg-1**) is reported by Yeh *et al*[8] although the preparative conditions are not given. The crystal structures of **MOF-CJ4**, **Mn-1**, **Mg-1**, and **2** are isostructural.

Figure 3.20 depicts the symmetry elements present in **2** when viewed along the [001] axis. The network is shown in black while the symmetry elements are given in red. The circles represent centres of inversion. These are located between DMF molecules on adjoining SBUs. The red triangles with white circles in the centre represent the 3-fold inversion axes. The (0,0,z) axis is located at the centre of the hexameric zinc SBUs. The solid red triangles represent three-fold rotation axes. The (1/3,2/3,z) and (2/3,1/3,z) axes are located at the centre of the fully deprotonated BTRI units. There are six symmetrically different inversion centres in compound **2**. The (0,1/2,0) centre is located between the O5 DMF molecules. Due to the high symmetry of the structure the (1/2,0,0) and (1/2,1/2,0) centres are in the same

Related by symmetry: [i]x-y, -1+x, 1-z; [ii]1-y, -1+x-y, z; [iii]2-y, x-y, z; [iv]2-x+y, 2-x, z; [v]2-x, 1-y, 1-z; [vi]y, 1-x+y, 1-z

chemical environment as the inversion centre at (0,1/2,0). The (0,1/2,1/2) centre is also located between the DMF molecules but in the same plane as the metal centres. (1/2,0,1/2) and (1/2,1/2,1/2) are in the same chemical environment as (0,1/2,1/2).

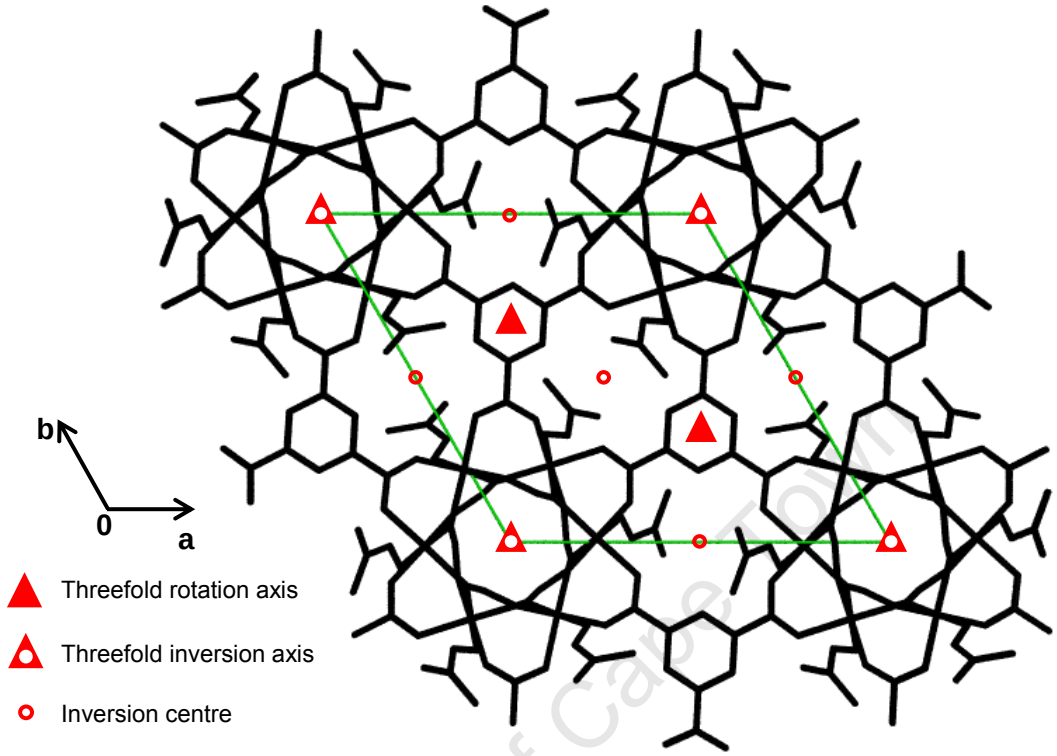

Figure 3.20: The packing diagram of **2** (black) viewed along the [001] axis with an overlay of the symmetry elements in the unit cell in red

3.4.2 THERMAL ANALYSIS

The TG trace (Figure 3.21, blue) shows four mass loss steps before decomposition although mass loss D is indistinct. If one considers the hexameric SBU there are six zinc metal centres, six DMF molecules, six formate anions and two BTRI units. The first mass loss A (*ca* 70 – 145 °C) of 15.03% corresponds to the loss of two DMF molecules and two formic acid molecules (calculated: 15.59%). The molecules lost are determined by establishing which reasonable combination of molecules in the asymmetric unit would give the percentage mass loss observed. Mass loss B (*ca* 145 - 190°C) corresponds to the loss of a further DMF molecule and another two formic acid molecules (experimental: 10.48%; calculated: 10.77%). The third mass loss C (*ca* 190 – 305 °C) matches the calculated loss of 14.54% for three DMF molecules. Mass loss D (*ca* 305 – 375 °C) correlates with the removal

of one more formic acid molecules before decomposition starts at just over 400 °C. All the details are given in Table 3.10.

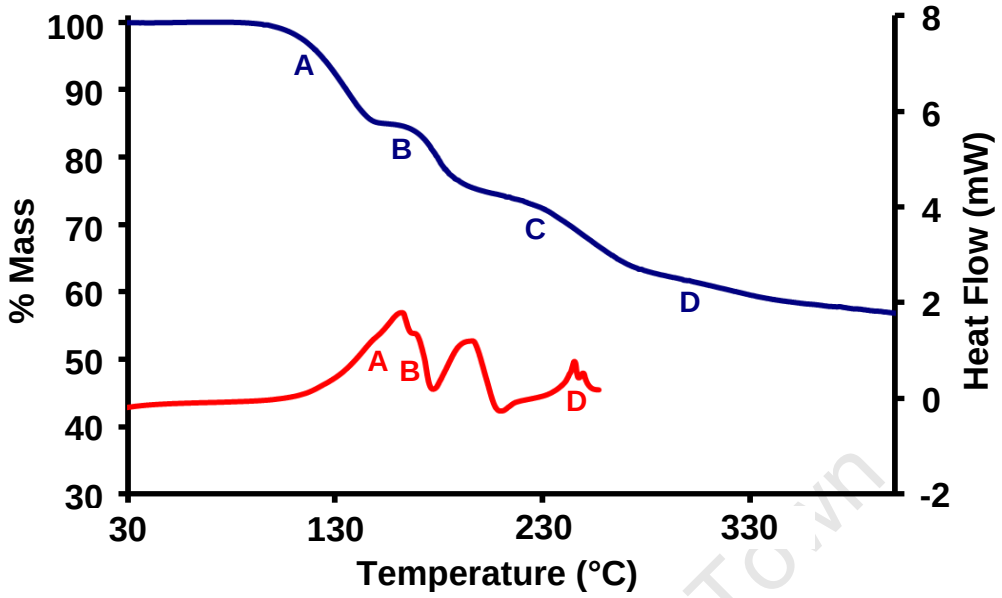

Figure 3.21: TG analysis of **2** and **b)** DSC analysis of **2** both with a heating rate of 20 °C.min^{-1}

As shown by the change in the variable temperature PXRD pattern (Section 3.4.3 – Powder X-ray Diffraction, Figure 3.25) there is a transformation in the structure of the compound as it is heated. As the formic acid molecules are lost there would be a change in the charge of the network. As a result it is probable that the compound undergoes a change in the coordination around the metal site.

Four endotherms are visible in the DSC trace (Figure 3.21, red) although endotherm B appears as a shoulder on endotherm A. Endotherms A and B correspond with mass losses A and B although the onset temperature of endotherm A is higher than the beginning of mass loss A. Endotherm C corresponds with the loss of the three DMF molecules and the onset temperature correlates well with the beginning of mass loss C. Endotherm D corresponds with mass loss D. The two peaks imply that the loss of the formic acid is not a one step process. The TGA and DSC results are presented in Table 3.10.

Table 3.10: TGA and DSC results for $[Zn(C_9H_3O_6)_{0.3}(CHO_2)(C_3H_7NO)]$ (**2**)

	TGA Results		DSC Results
	Calc. % Mass Loss	**Exp. % Mass Loss**	**T_{onset} (°C)**
2 DMF + 2 HCOOH	15.59	15.03	162
1 DMF + 2 HCOOH	10.77	10.48	*ca* 176
3 DMF	14.47	14.54	197
1 HCOOH	2.97	3.02	245

The thermal events visible in the HSM agree well with the onset temperatures obtained by DSC (Figure 3.22). The HSM was performed in a room at 29 °C and the sample was placed directly into silicone oil. The hexagonal morphology of the crystal is visible in Figure 3.22a. The crystal begins to become opaque at approximately 161 °C (Figure 3.22c) when the third DMF molecule and third and fourth formic acid molecules are lost. This matches the change observed in the variable temperature PXRD pattern. At 175 °C (Figure 3.22d) bubbles start to form, which is consistent with the loss of the remaining DMF molecules. By 188 °C the crystal has become completely opaque and bubbles are being formed continually. This persists until over 440 °C (Figure 3.22f). The crystals never become discoloured due to decomposition but remain opaque.

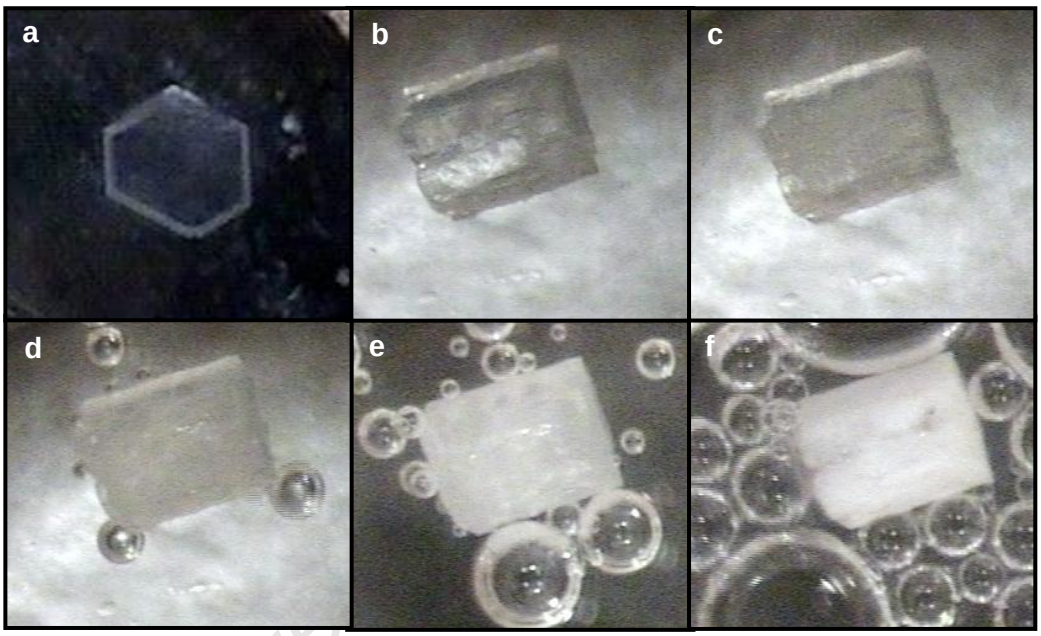

Figure 3.22: a) Side on view of crystal of **2**. HSM pictures of **2** at **b)** 29 °C, **c)** 161 °C, **d)** 175 °C, **e)** 188 °C, **f)** 447 °C

There is a slight discrepancy between the calculated and experimental elemental values. If one considers the presence of half a water molecule per asymmetric unit however the values correspond well. There is no evidence that compound **2** absorbs water. It is therefore probable that the sample was not completely dry (due to surface water) when the analysis was performed.

Table 3.11: Elemental analysis of[$Zn(C_9H_3O_6)_{0.3}(CHO_2)(C_3H_7NO)$] (**2**)

	Calculated 2	Calculated 2·0.5H_2O	Experimental
% C	33.30	32.15	32.71
% H	3.59	3.85	4.11
% N	5.55	5.36	5.36

3.4.3 POWDER X-RAY DIFFRACTION

The PXRD patterns of **MOF-CJ4**[6] (Figure 3.23b, red), **Mn-1**[7] (Figure 3.23c, blue) and **Mg-1**[8] (Figure 3.23d, green) are identical to that for compound **2** (Figure 2.23a, black). This confirms that all three compounds are isostructural. It is particularly interesting to note that while cobalt and manganese have similar van der Waals radii of approximately 2 Å and magnesium has a van der Waals radius of 1.73 Å, the van der Waals radii of zinc is significantly smaller at approximately 1.39 Å.[9]

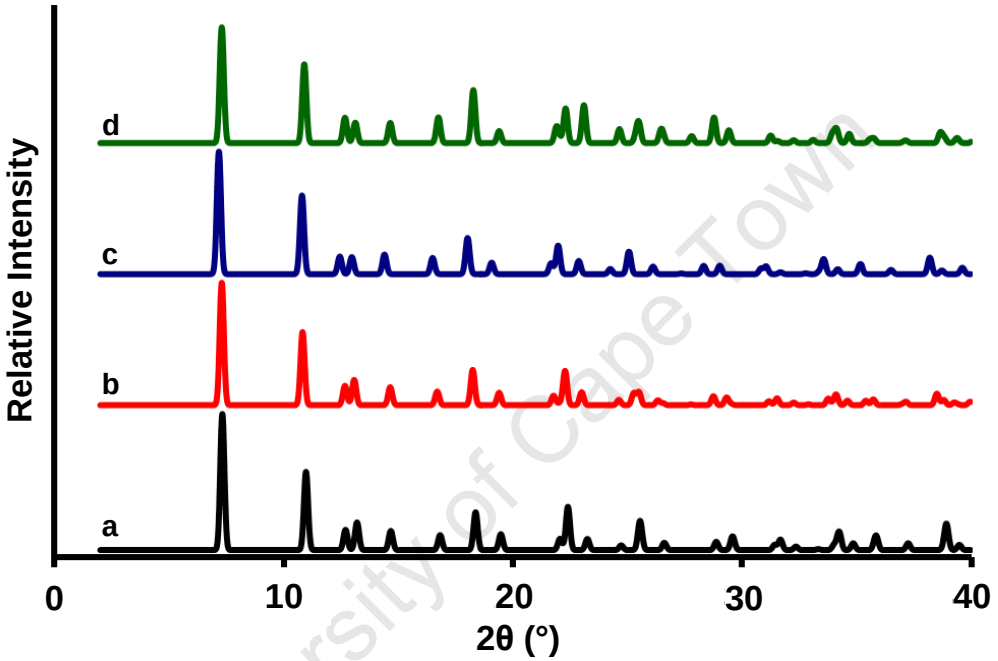

Figure 3.23: PXRD patterns calculated from single crystal data of **a) 2**, **b) MOF-CJ4**, **c) Mn-1** and **d) Mg-1**

The PXRD pattern calculated from the single crystal data (Figure 3.24a, blue) matches the pattern obtained from the bulk material of **2** (Figure 3.24b, red).

Heating compound **2** causes a change in the PXRD pattern as observed in Figure 3.25. Up to 100 °C the pattern remains consistent with the room temperature structure. The pattern obtained at 130 °C has extra peaks at 11.5 and 18.5° 2θ as well as a small extra peak at 13.5° 2θ. Otherwise the diffraction pattern is the same as that of the original compound. By 145 °C there are more changes and this continues until above 160 °C. At 190 °C the strong peak observed at approximately 7° 2θ begins to decrease and the fine detail above 12 2θ° has been lost completely. By 270 °C there are very few peaks left in the pattern with a trio of peaks at approximately 10° 2θ and the diminished peak at 7° 2θ the most distinct. The

patterns observed do not match directly with the pattern calculated from the single crystal diffraction data for the loss of DMF and formic acid molecules as observed in the TG analysis. This suggests that there may be a structural rearrangement occurring with heating.

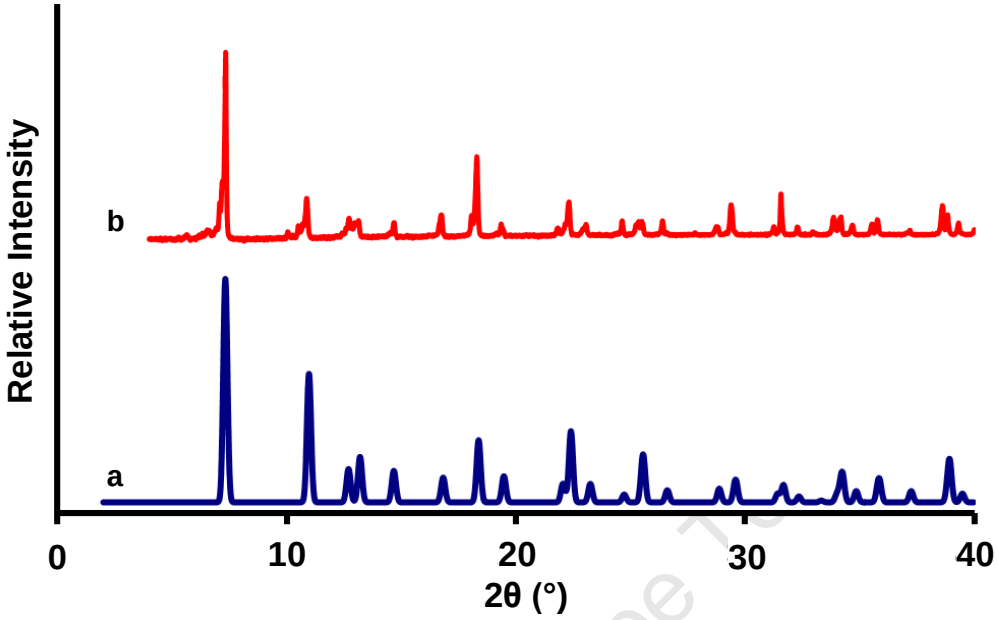

Figure 3.24: PXRD patterns of **2 a)** calculated from single crystal data and **b)** experimental

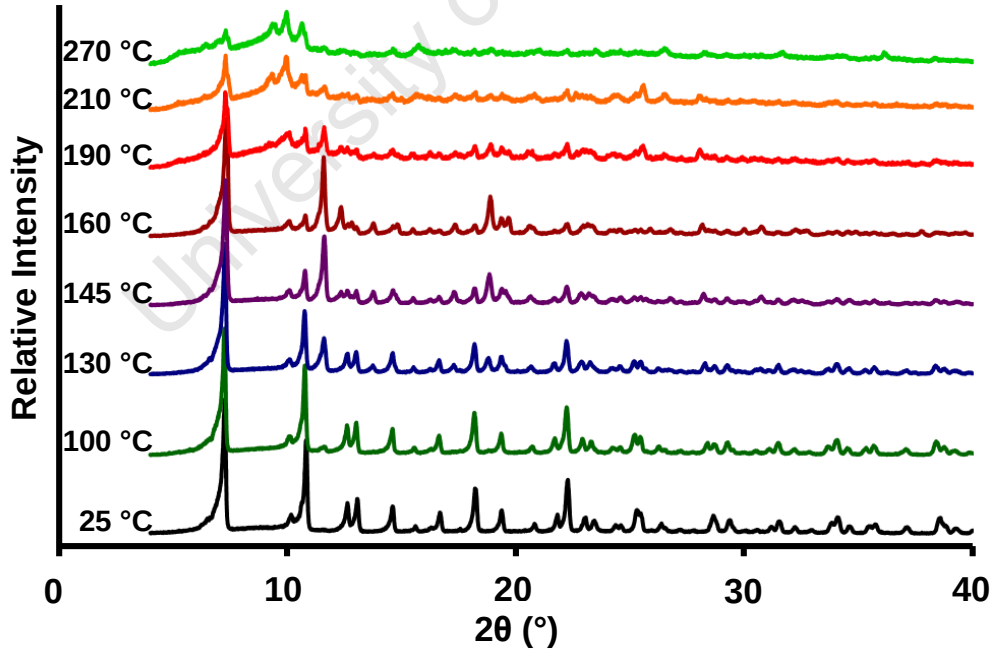

Figure 3.25: Variable temperature PXRD patterns of **2** from 25 – 270 °C

3.4.4 SUMMARY

Compound **2** was prepared using methods 1 – 4 (See Chapter 3.1 – Preparation of Zinc(II) and 1,3,5-benzenetricarboxylate Compounds). The structure of **2** was confirmed using single-crystal and PXRD as well as thermal methods. **2** retains its crystallinity until over 270 °C and appears to rearrange itself upon heating and the loss of formic acid molecules. **2** is isostructural with **MOF-CJ4** and **Mn-1** with the only difference being the metal ion. The topology of **2** is discussed fully in Chapter 5 – Topological Studies.

3.5 $[Zn_2(\mu_2\text{-}OH_2)(HBTRI)(BTRI)(H_2O)_2]\cdot DMA\cdot 3H_2O$ (3)

3.5.1 SINGLE CRYSTAL X-RAY DIFFRACTION ANALYSIS

The hydrogen atoms located on the framework and counter cation were placed in idealised positions in a riding model. These hydrogen atoms were refined isotropically and assigned temperature factors that relate to the atom they are attached to. The temperature factors are 1.2 times the parent atom for the phenyl, carboxylic acid, coordinated water and amine hydrogen atoms. The temperature factors are 1.5 times the parent atom for the methyl hydrogen atoms. Most of the hydrogen atoms on the guest water molecules were placed in idealised positions in a riding model with temperature factors of 1.2 times the oxygen atom. One of the hydrogen atoms was located in the electron difference Fourier map and refined using SHELXL-97.

The compound crystallises in the monoclinic crystal system, in the space group $P2_1$. **3** is an anionic metal-organic framework with a charge of 1-. The counter cation is *N*,*N*'-dimethylammonium and is formed *in situ* by the hydrolysis of DMF. Further crystallographic and refinement details are given in Table 3.12.

Table 3.12: Crystal Data and Refinement Parameters of **3**

Empirical Formula	$C_{20}H_{27}NO_{18}Zn_2$
Formula Weight (g.mol^{-1})	700.17
Temperature (K)	173(2)
Wavelength (Å)	0.71073
Crystal System	Monoclinic
Space Group	$P2_1$
a (Å)	7.8334(1)
b (Å)	17.2763(4)
c (Å)	9.445(1)
α (°)	90
β (°)	100.475(2)
γ (°)	90
Volume (Å^3)	1256.9 (1)
Z	2
Calculated Density (g.cm^{-3})	1.850
***μ* (mm^{-1})**	2.000
***F* (*000*)**	716
Crystal Size (mm)	0.60 x 0.30 x 0.30
***Θ* Range Scanned (°)**	3.11 – 28.30
Index Range	-10 < h < 10, -23 < k < 23, -12 < l < 12
No. Reflections Collected	56992
No. Unique Reflections	6232
R_{int}	0.0563
Data Completeness to θ_{max} (%)	99.7
Refinement Method	Full-matrix least-squares on F^2
Data/Restraints/Parameters	6232/6/386
Goodness-of-fit on F^2	1.085
Final *R* Indices [$I>2\sigma(I)$]	R_1 = 0.0265, wR_2 = 0.0620
***R* Indices (all data)**	R_1 = 0.0304, wR_2 = 0.0640
Largest Diff. Peak and Hole (*e*.Å^{-3})	0.473, -0.484

Figure 3.26 displays the asymmetric unit of **3**, which consists of two zinc metal centres (Zn1 and Zn2), one triply deprotonated BTRI unit (A), one doubly deprotonated HBTRI unit (B), three coordinated water molecules, three uncoordinated water molecules and one *N,N*-dimethylammonium (DMA) cation.

The Zn1 metal centre is coordinated to five oxygen atoms in a distorted trigonal bipyramidal fashion. O7 and O8 are both water molecules and are located in axial positions. O4^{i}, O10 and O12^{ii} are carboxylate oxygen atoms and are located in the equatorial positions. O8 bridges Zn1 and Zn2 distorting the O7-Zn1-O8 angle to 168.74(7)°. O8-Zn1-O4^{i} is significantly larger than the expected angle of 90° (102.11(8)°). This is due to the bridging O8 water molecule. The remaining O-Zn1-O axial-equatorial angles are approximately 90°. O10 is part of the O10-C10-O11 bridging carboxylate moiety, which results in a value of

Related by symmetry: ^{i}-1+x, y, -1+z; ^{ii}1-x, 1/2+y, 1-z; ^{iii}2-x, -1/2+y, 1-z; ^{iv}1+x, y, 1+z; ^{v}2-x, 1/2+y, 1-z; ^{vi}1-x, -1/2+y, 1-z; ^{vii}2-x, 1/2+y, 2-z; ^{viii}1-x, 1/2+y, -z; ^{ix}-x, -1/2+y, -z; ^{x}-x, 1/2+y, -z; ^{xi}2-x, -1/2+y, 2-z; ^{xii}1-x, -1/2+y, -z; ^{xiii}1+x, y, z; ^{xiv}3-x, -1/2+y, 2-z

131.99(8)° for O10-Zn1-O12^{ii} and of 98.92(8)° for O10-Zn1-O4^{i}. The expected values are approximately 120°.

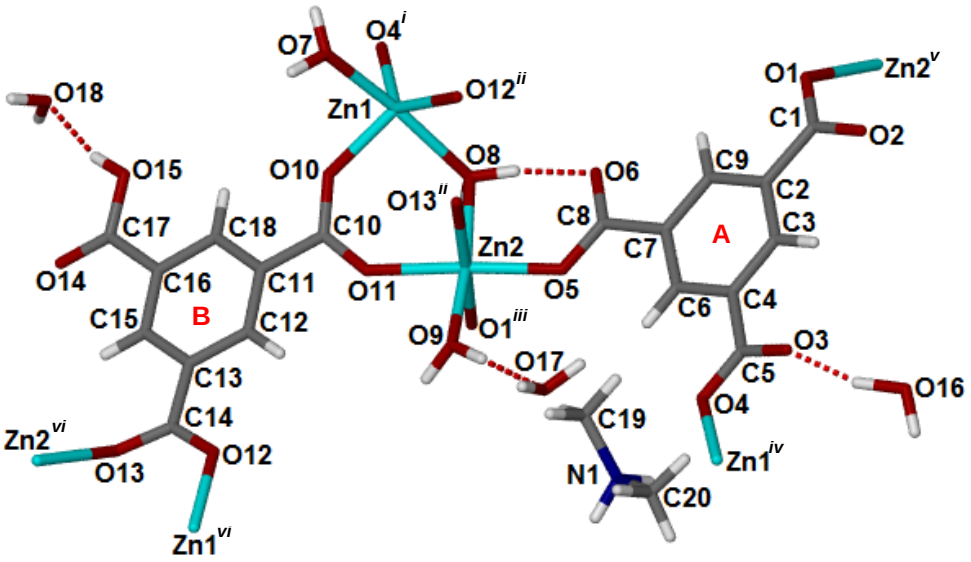

Figure 3.26: The asymmetric unit of **3**

Zn2 is coordinated through a distorted octahedron to six oxygen atoms. O8 and O9 are water molecules and O5, O11, O1^{iii} and O13^{ii} are terminal carboxylate oxygen atoms. O6 in the O5-C8-O6 carboxylate is hydrogen bonded to H8A of the bridging water molecule as well as H16B and H18A of the O16 and O18 water molecules. O2^{iii} in the O1^{iii}-C1^{iii}-O2^{iii} carboxylate is hydrogen bonded to H8B of the bridging water molecule. This results in an angle of 97.89(8)° for O1^{iii}-Zn2-O9 with the O1^{iii}-C1^{iii}-O2^{iii} carboxylate distorted towards the O8 water molecule. The O5-Zn2-O1^{iii} angle is larger than expected (94.41(8)°) for the same reason. To allow for the O8-H8A···O6 hydrogen bond the O6-C8-O5 carboxylate shifts away from the bridging water molecule. As a result O5-Zn2-O8 has an angle of 94.62(7)°. O11-Zn2-O9 is smaller than expected (83.65(8)°) due to the O10-C10-O11 carboxylate bridging Zn1 and Zn2 and the O9-H9A···O18^{iv} hydrogen bond. The other axial-equatorial O-Zn2-O angles range from 87.27(7) to 90.89(7)°.

O7 and O9 are terminal water molecules and the Zn-O distances of 2.115(2) and 2.095(2) Å correspond with the values reported in Orpen *et al*[4] for water terminally coordinated to 5- and 6-coordinate zinc metal ions respectively. O8 bridges Zn1 and Zn2 and the Zn-O distances of 2.205(2) and 2.275(2) Å correspond with the range of 2.100 – 2.326 Å described by Orpen for bridging water molecules. The terminal carboxylate Zn-O distances range from 1.977(2) to 2.116(2) Å, which correlates with the literature value of 2.033 Å. The Zn2-O1^{iii} bond is slightly longer than expected due to the O8-H8B···O2^{iii} hydrogen bond. The

Related by symmetry: ^{i}-1+x, y, -1+z; ^{ii}1-x, 1/2+y, 1-z; ^{iii}2-x, -1/2+y, 1-z; ^{iv}1+x, y, 1+z; ^{v}2-x, 1/2+y, 1-z; ^{vi}1-x, -1/2+y, 1-z; ^{vii}2-x, 1/2+y, 2-z; ^{viii}1-x, 1/2+y, -z; ^{ix}-x, -1/2+y, -z; ^{x}-x, 1/2+y, -z; ^{xi}2-x, -1/2+y, 2-z; ^{xii}1-x, -1/2+y, -z; ^{xiii}1+x, y, z; ^{xiv}3-x, -1/2+y, 2-z

Zn2-O13^{ii} bond is also longer than expected in order to preserve octahedral geometry (see the reference values in Table 3.13).

Table 3.13: Experimental Zn-O bond lengths for **3** and literature Zn-O bond lengths

Bond	Length (Å)	Average Length (Å)	Bond Type
Zn1-O8	2.204(2)	2.3 ± 0.1* 2.100 – 2.326**	μ-OH_2
Zn2-O8	2.276(2)		
Zn1-O7	2.115(2)	2.09 ± 0.08* 2.08 ± 0.08**	5-coordinate Zn, terminal H_2O
Zn2-O9	2.094(2)	2.09 ± 0.08* 2.10 ± 0.05**	6-coordinate Zn, terminal H_2O
Zn1-O4^{i}	2.025(2)	2.00 ± 0.09* 2.03 ± 0.05**	Terminal carboxylate
Zn1-O10	1.977(2)		
Zn1-O12^{ii}	2.001(2)		
Zn2-O1^{iii}	2.102(2)		
Zn2-O5	2.003(2)		
Zn2-O11	2.032(2)		
Zn2-O13^{ii}	2.116(2)		

* Values obtained from the CSD; ** Mean values reported in Orpen *et al*[4]

BTRI **A** is triply deprotonated with one oxygen atom from each carboxylate moiety (O1, O4 and O5) coordinated to Zn2^{v}, Zn1^{iv}, and Zn2, respectively. All three uncoordinated oxygen atoms form hydrogen bonds. O2 is part of the O8^{v}-H8B^{v}···O2 and the O17^{vii}-H17A^{vii}···O2 hydrogen bonds, with O8 the water molecule that bridges Zn1 and Zn2 and O17 a guest water molecule. O3 is involved in the O16-H16A···O3 and the O18^{ii}-H18B^{ii}···O3 hydrogen bonds, where O16 and O18 are both guest water molecules. O6 is part of the O8-H8A···O6, the O16^{i}-H16B^{i}···O6, and the O18^{viii}-H18A^{viii}···O6 hydrogen bonds. As previously mentioned, O8 is a bridging water molecule while O16 and O18 are guest water molecules.

HBTRI **B** is doubly deprotonated with one carboxylate group (O10-C10-O11) bridging Zn1 and Zn2 and O12-C14-O13 bridging Zn1^{vi} and Zn2^{vi}. The carboxylic acid moiety forms a hydrogen bond to a guest water molecule (O15-H15A···O18). A complete list of hydrogen bond distances and angles are given in Table 3.14.

Compound **3** is a three-dimensional metal-organic framework with water and the DMA cations located in channels extending along the [100] direction. The coordinated network carries a single negative charge, which is balanced by the DMA cation. The guest water molecules are secured in the channels by hydrogen bonds with the carboxylic acid moiety, the coordinated water molecules, and each other. The cation forms favourable hydrogen bonds with the anionic framework and H1A is located in a pocket formed by O9, O11 and O13. These atoms are all coordinated to the Zn2 metal ion as shown in Figure 3.27.

Related by symmetry: ^{i}-1+x, y, -1+z; ^{ii}1-x, 1/2+y, 1-z; ^{iii}2-x, -1/2+y, 1-z; ^{iv}1+x, y, 1+z; ^{v}2-x, 1/2+y, 1-z; ^{vi}1-x, -1/2+y, 1-z; ^{vii}2-x, 1/2+y, 2-z; ^{viii}1-x, 1/2+y, -z; ^{ix}-x, -1/2+y, -z; ^{x}-x, 1/2+y, -z; ^{xi}2-x, -1/2+y, 2-z; ^{xii}1-x, -1/2+y, -z; ^{xiii}1+x, y, z; ^{xiv}3-x, -1/2+y, 2-z

Table 3.14: Hydrogen-bond distances and angles for **3**

Donor-H···Acceptor	H···A (Å)	D···A (Å)	D-H···A (°)
O7 – H7A ··· O1^{vi}	2.14	2.924	171
O7 – H7B ··· O14^{ix}	1.89	2.782	172
O8 – H8A ··· O6	1.74	2.708	166
O8 – H8B ··· O2^{iii}	1.89	2.696	149
O9 – H9A ··· O18^{iv}	2.07	2.860	172
O9 – H9B ··· O17	1.83	2.729	175
O15 – H15A ··· O18	1.77	2.592	164
O16 – H16A ··· O3	1.64	2.614	160
O16 – H16B ··· O6^{iv}	1.87	2.762	159
O17 – H17A ··· O2^{x}	2.01	2.850	170
O18 – H18A ··· O6^{xi}	2.16	2.900	144
O18 – H18B ··· O3^{vi}	2.02	2.777	152
N1 – H1A ··· O9^{xii}	2.38	3.147	140
N1 – H1A ··· O11^{xii}	2.58	3.227	128
N1 – H1A ··· O13^{v}	2.09	2.820	135
N1 – H1B ··· O16^{xiii}	1.90	2.680	144

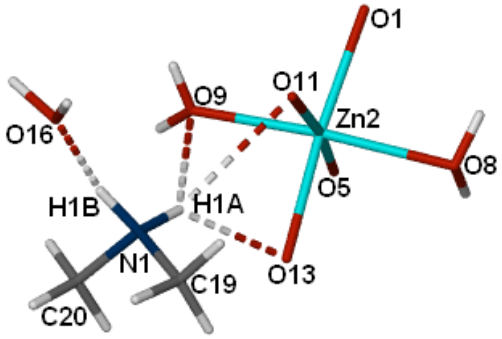

Figure 3.27: The DMA cation located in a pocket comprising O9, O11 and O13

The packing diagram of **3** is given in Figure 3.28. The anionic framework is depicted in orange. The DMA cation and guest water molecules are located in the channels along the [100] axis. The coordinated O9 water molecule also extends into the channels and helps to define them. The guest water molecules as well as the cation are plotted with van der Waals radii in Figure 3.28.

The thermal analysis – discussed fully in Section 3.5.2 – shows that the compound can accommodate additional water molecules. These are not observed in the single crystal structure. Void calculations were performed on the fully refined single crystal structure and there were no solvent accessible voids available to extra water molecules in the structure. It is therefore likely that these water molecules were not present in the single crystal when the data collection was performed.

Related by symmetry: ^{i}-1+x, y, -1+z; ^{ii}1-x, 1/2+y, 1-z; ^{iii}2-x, -1/2+y, 1-z; ^{iv}1+x, y, 1+z; ^{v}2-x, 1/2+y, 1-z; ^{vi}1-x, -1/2+y, 1-z; ^{vii}2-x, 1/2+y, 2-z; ^{viii}1-x, 1/2+y, -z; ^{ix}-x, -1/2+y, -z; ^{x}-x, 1/2+y, -z; ^{xi}2-x, -1/2+y, 2-z; ^{xii}1-x, -1/2+y, -z; ^{xiii}1+x, y, z; ^{xiv}3-x, -1/2+y, 2-z

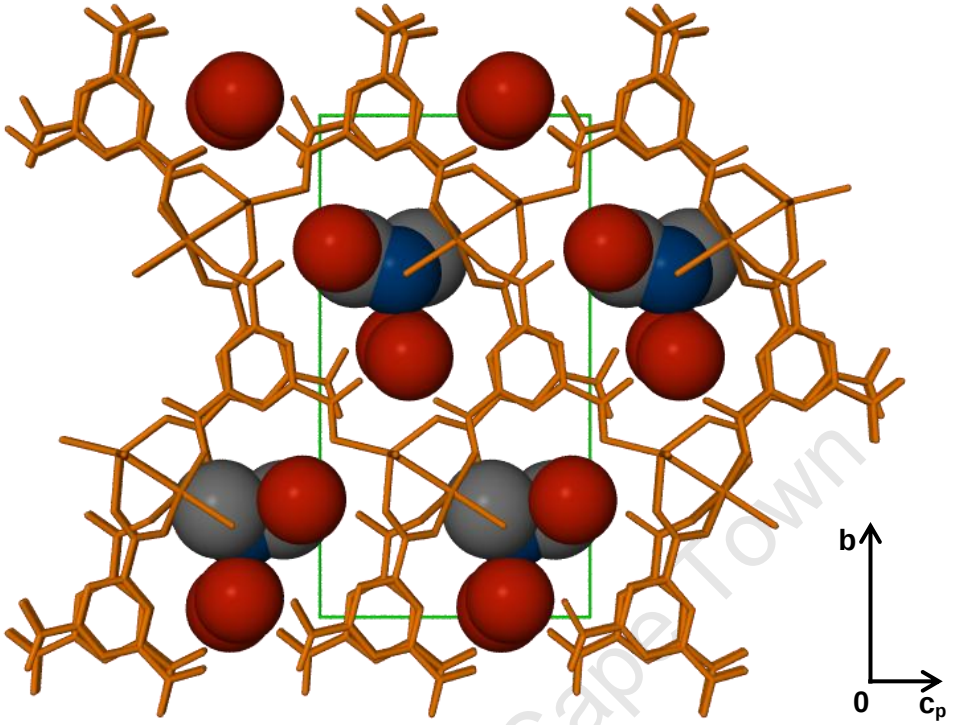

Figure 3.28: The packing diagram of **3** viewed along the [100] axis. The anionic framework is shown in orange. The DMA cation and guest water molecules are depicted with van der Waals radii

Figure 3.29 shows in black the framework of **3** when viewed along the [010] axis. Overlaid in red are the symmetry elements present in the $P2_1$ space group. The only symmetry elements present are twofold screw axes. There are four chemically different locations for the screw axes. The axis at (0,y,0) is located between O17 guest water molecules. This results in a channel of O17 water molecules down the b-axis. The (1/2,y,0) axis is located between DMA cations. The (0,y,1/2) axis is between the O6-C8-O5 carboxylate of two BTRI **A** units. The axis at (1/2,y,1/2) is situated between the O12-C14-O13 carboxylates of two HBTRI **B** units.

Related by symmetry: [i]-1+x, y, -1+z; [ii]1-x, 1/2+y, 1-z; [iii]2-x, -1/2+y, 1-z; [iv]1+x, y, 1+z; [v]2-x, 1/2+y, 1-z; [vi]1-x, -1/2+y, 1-z; [vii]2-x, 1/2+y, 2-z; [viii]1-x, 1/2+y, -z; [ix]-x, -1/2+y, -z; [x]-x, 1/2+y, -z; [xi]2-x, -1/2+y, 2-z; [xii]1-x, -1/2+y, -z; [xiii]1+x, y, z; [xiv]3-x, -1/2+y, 2-z

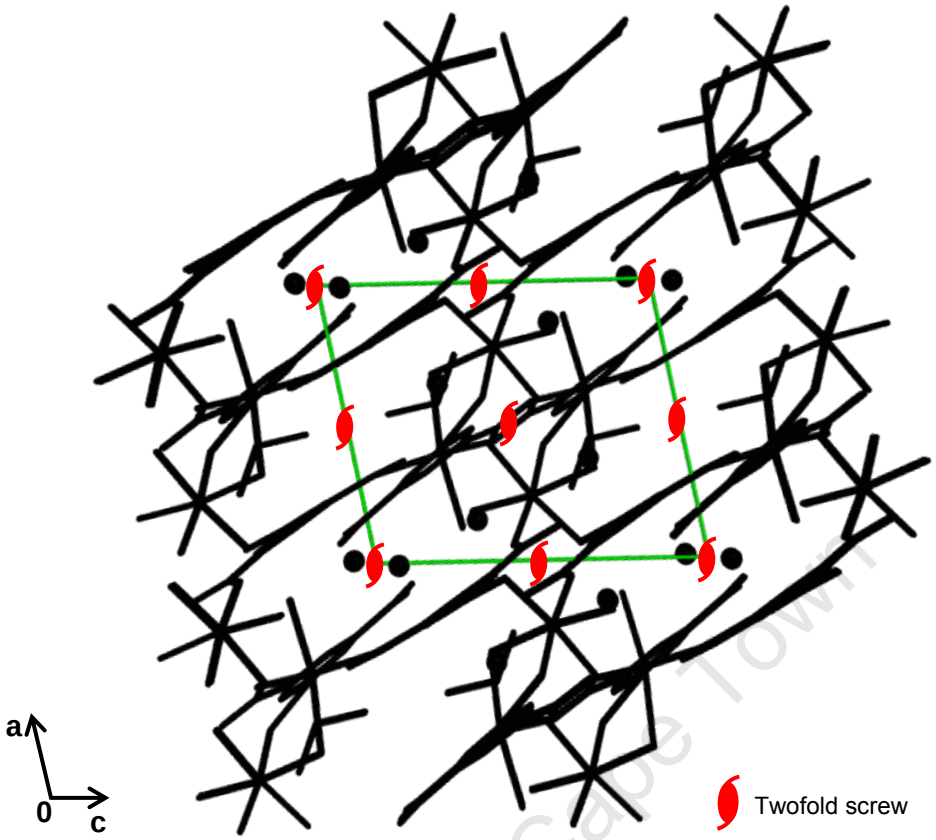

Figure 3.29: The packing diagram of **3** (black) viewed along the [010] axis with an overlay of the symmetry elements given in red

3.5.2 THERMAL ANALYSIS

The TG trace of compound **3**, shown in blue in Figure 3.30 comprises two mass loss steps, A and B. The first mass loss (*ca* 30 – 65 °C) corresponds to 0.85 water molecules that are not modelled in the single crystal structure (calculated: 2.14%). The sample is dried on filter paper before the experiment is performed and it is unlikely that these are surface water molecules. Mass loss A can vary from approximately 1.1% to greater than 2.3% from experiment to experiment. This correlates with a range of 0.45 – 0.90 extra water molecules per asymmetric unit. When a sample of **3** is held at 20 °C for two hours a mass loss of 3.1% is observed, which correlates to 1.25 waters. In fact compound **3** can contain up to 1.50 extra water molecules at 30 °C. This will be discussed in greater detail in Chapter 3.5.5 – Dehydration and Rehydration Studies. The loosely held and potentially very diffuse waters are not observed in the single crystal structure. Mass loss B (65 – 200 °C) corresponds to the loss of five water molecules (experimental: 12.75%, calculated: 12.59%). The three guest and the two terminally coordinated water molecules are removed. The M-O bonds for the

BTRI ligand are stronger than those for water allowing removal of the water molecules before decomposition.[10] Decomposition begins at approximately 240 °C.

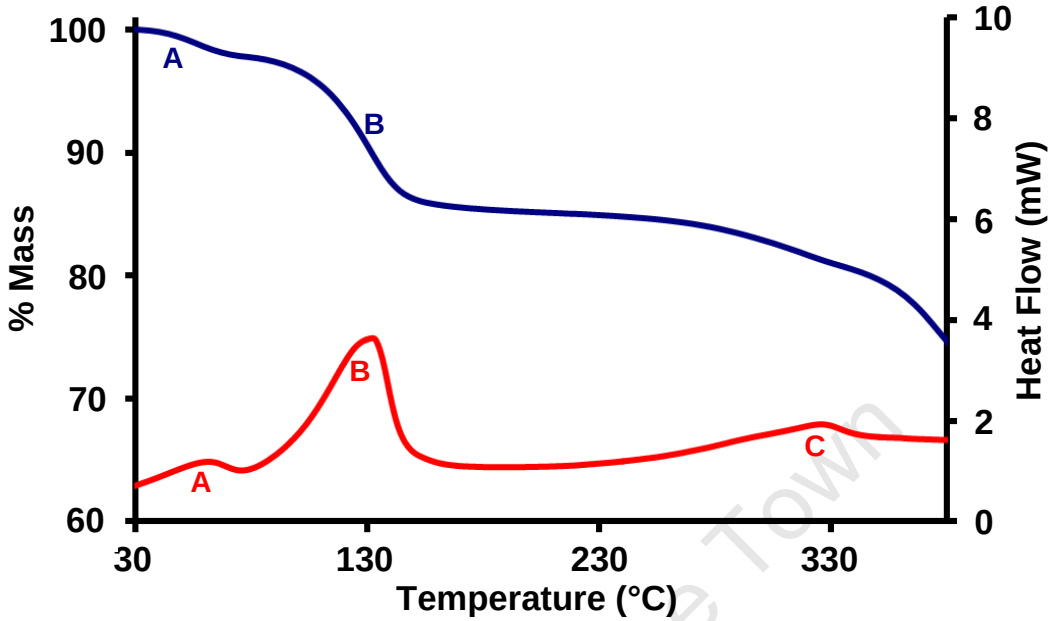

Figure 3.30: a) TG analysis of **3** and **b)** DSC analysis of **3** both with a heating rate of 10 °C.min^{-1}

Three endotherms are visible in the DSC trace (Figure 3.30, red). Endotherm A corresponds with the loss of the loosely bound water molecules. Endotherm A also has a low onset temperature implying that these water molecules are very loosely held within the channels. The large endotherm B at approximately 95 °C matches the loss of the five modelled water molecules. Endotherm C is a very weak, broad endotherm and relates to the decomposition of the compound.

Table 3.15: TGA and DSC results for **3**

	TGA Results (Blue)		DSC Results
	Calc. % Mass Loss	**Exp. % Mass Loss**	**T_{onset} (°C)**
0.85 H_2O	2.14	2.13	31
5.00 H_2O	12.59	12.75	95

HSM was performed in a room at 27 °C in silicone oil. The sample is crystalline at this temperature as seen in Figure 3.31a. Cracks start to form in the surface of the crystal at *ca* 85 °C. This coincides with the loss of the five modelled water molecules. The cracks completely cover the surface of the crystal by 100 °C (Figure 3.31b). This will be discussed further in Section 3.5.4 – Scanning Electron Microscopy. At 137 °C bubbles start to form due to solvent loss (Figure 3.31c). These bubbles continue until decomposition. The crystal is

completely opaque by 231 °C but has not begun to decompose (Figure 3.31d). Aside from the bridging O8 water molecule all water molecules are gone from the sample by this temperature. By 330 °C decomposition has begun as shown by the brown edges of the crystal in Figure 3.31e. This matches the TG trace. By 406 °C the crystal has turned completely brown and is bubbling continuously. This decomposition is shown in Figure 3.31f.

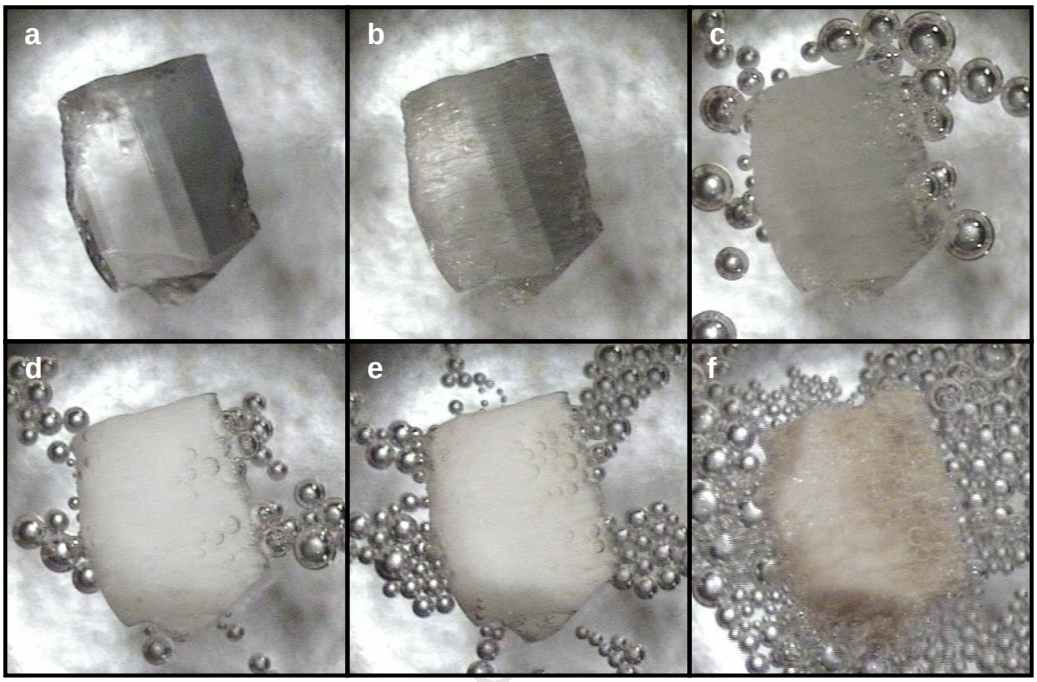

Figure 3.31: Hot-stage microscopy pictures of **3** at **a)** 27 °C, **b)** 100 °C, **c)** 137 °C, **d)** 231 °C, **e)** 330 °C, **f)** 406 °C

Elemental analysis confirms the presence of the five modelled water molecules. The sample was exposed to the air before analysis allowing the removal of any extra water molecules. There was sufficient time between removal from the mother liquor and the elemental analysis for any of the previously mentioned loosely held water molecules to be lost. The flexibility of the channels and their ability to contain additional water molecules will be discussed in more detail later in this section.

Table 3.16: Elemental analysis of $[(Zn_2C_{20}NO_{13}H_{17})(H_2O)_2]\cdot 3H_2O$ (**3**)

	Calculated	**Experimental**
% C	34.31	34.34
% H	3.89	4.10
% N	2.00	1.72

3.5.3 POWDER X-RAY DIFFRACTION

The peaks in the calculated pattern (Figure 3.32a, blue) are observed at higher 2θ values than those in the experimental trace (Figure 3.32b, red). This is due to contraction of the crystal upon cooling during data-collection on the single crystal X-ray diffractometer. This occurs whenever data collection is performed at low temperatures. The shift is particularly noticeable for compound **3** due to the flexibility of the structure. The two PXRD traces correspond well however, which confirms that the single crystal is representative of the bulk sample.

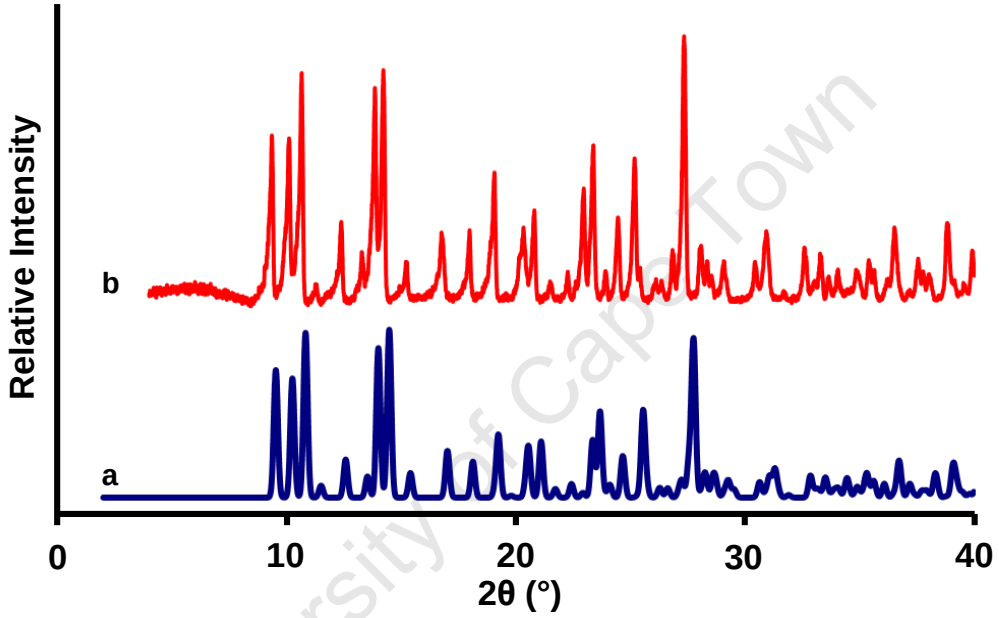

Figure 3.32: PXRD patterns of **3 a)** calculated from single crystal data and **b)** experimental

Upon heating compound **3** loses crystallinity as shown in Figure 3.33. This corresponds with the loss of solvent molecules observed in the thermal analysis (see Section 3.5.2). By 160 °C the sample is almost completely amorphous. The solvent molecules lost are the three guest water molecules and the two coordinated terminal water molecules.

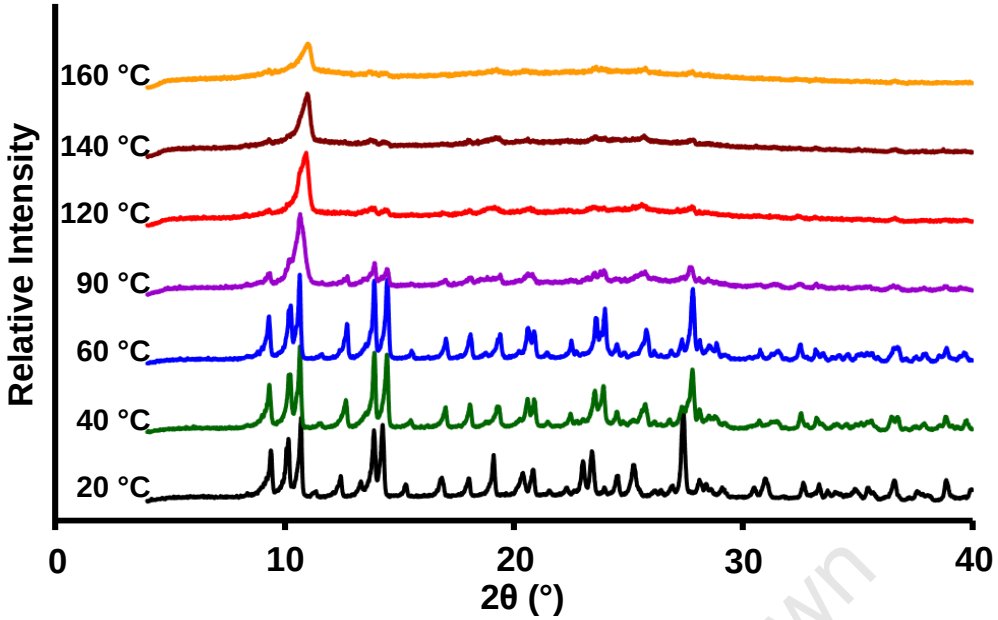

Figure 3.33: Variable temperature PXRD patterns of **3** from 20 – 160 °C

Crystals of **3** were ground to a fine powder (Figure 3.34a) and heated to 160 °C. The powder became almost amorphous as shown in Figure 3.34b. This powder was then exposed to water vapour. After thirty minutes crystallinity was regained. After 24 hours the PXRD pattern obtained from the rehydrated sample matches that of compound **3**. This is shown in Figure 3.34c. Longer exposure of up to 72 hours resulted in no further changes in the PXRD pattern.

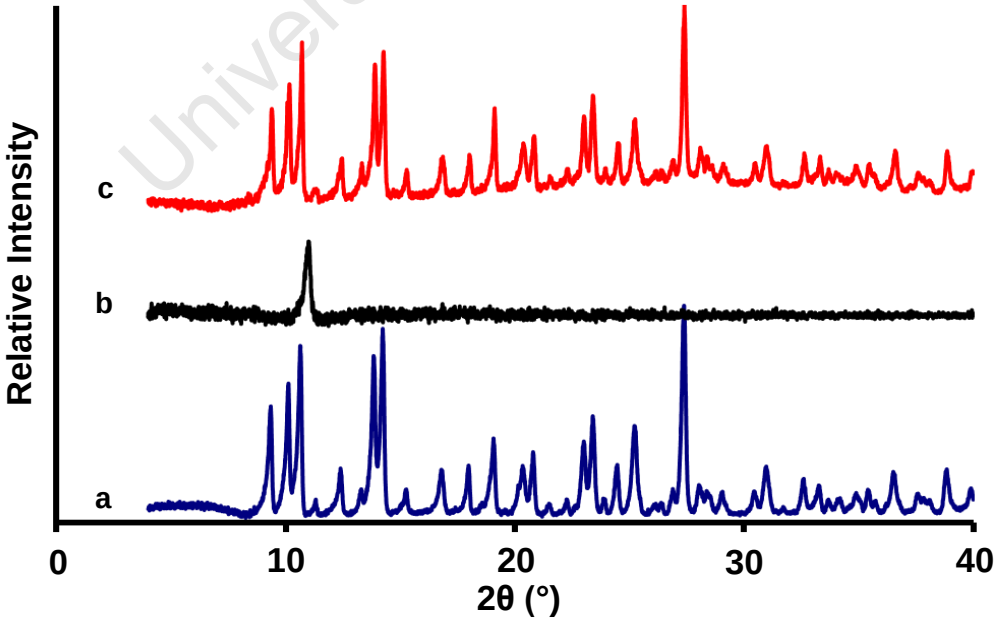

Figure 3.34: PXRD patterns of vapour diffusion experiments of **3**. **a)** Sample of **3** before drying, **b)** control after heating to 160 °C and **c)** sample after exposure to water vapour for 24 hours

3.5.4 SCANNING ELECTRON MICROSCOPY (SEM)

Variable temperature PXRD reveals that **3** is almost amorphous when heated to 160 °C. The original structure is regained after exposure to water vapour for thirty minutes. Scanning electron microscopy[11] (SEM) was performed on crystals of **3** before heating (Figure 3.35a), after heating (Figure 3.35b) and upon rehydration (Figure 3.35c).

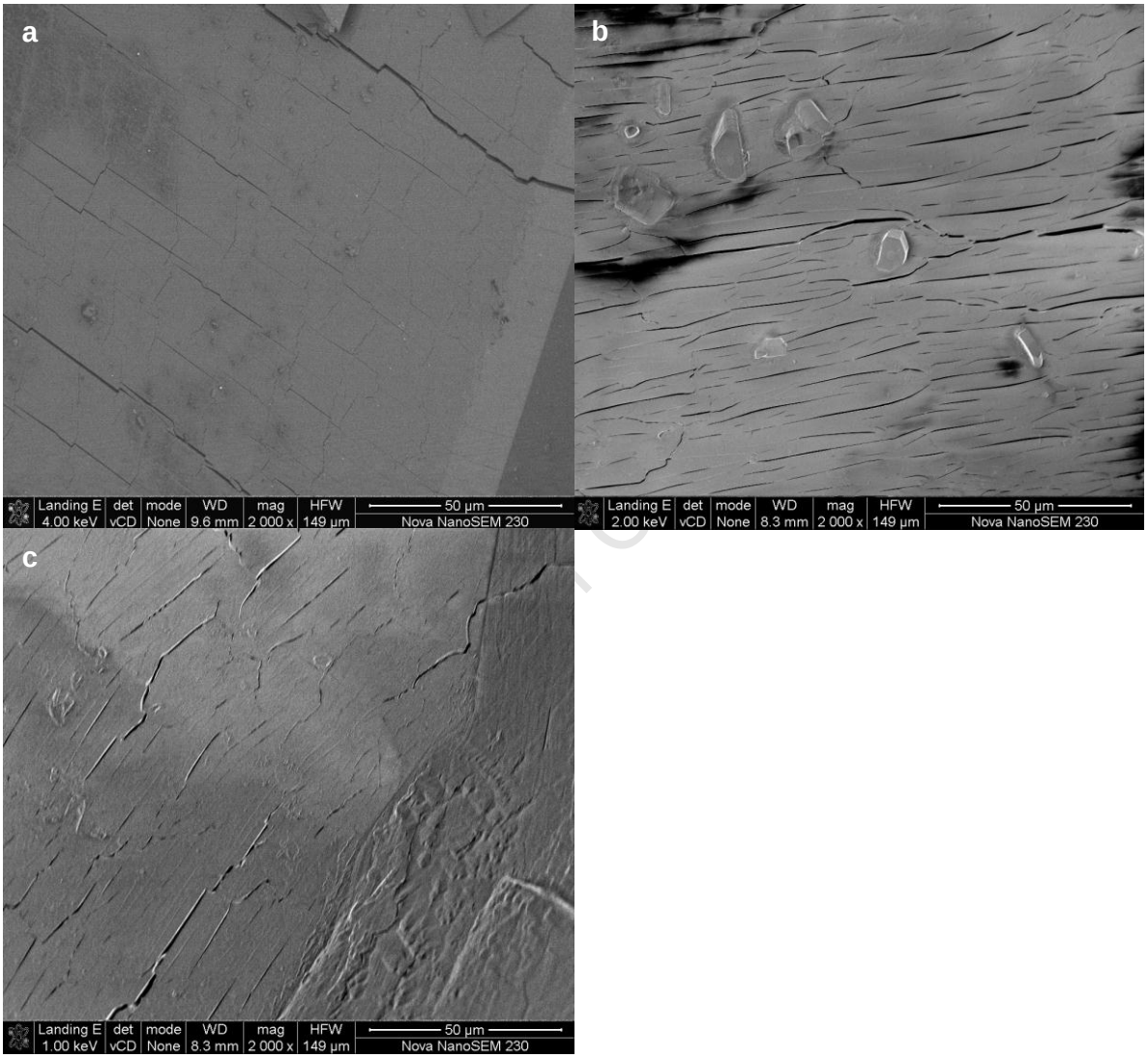

Figure 3.35: Scanning electron microscopy (SEM) pictures of **3**. **a)** Straight from the mother liquor, **b)** after heating to 160 °C and **c)** after exposure to water vapour and rehydration

Single crystal XRD models three guest and two terminally coordinated water molecules. Thermogravimetric analysis demonstrates the possibility of additional absorbed water molecules located in the channels. Three guest water molecules are modelled in the single crystal structure. Platon[12,13] shows no further accessible void space in the structure, which implies that **3** is flexible when absorbing additional water molecules.

All SEM experiments are performed under vacuum and this vacuum facilitates the removal of the extra water in a short period of time. The extra water molecules are lost if left under nitrogen at 20 °C and could therefore be removed easily under vacuum. This is probably the reason for the few large cracks seen in Figure 3.35a. The extra water is held loosely enough that when removed under ambient conditions the crystal remains undeformed and highly single crystal.

Upon heating to 160 °C the cracks in the surface of the crystal become more pronounced covering the entire area. These cracks are shown in Figure 3.35b. They are highly regular and extend along the same direction. Dehydrated crystals of **3** were exposed to water vapour and the result is given in Figure 3.35c. There are some cracks remaining in the surface, probably due to the high vacuum. However, the majority of the cracks are no longer present. Light “scars” are visible on the surface where water has been reabsorbed into the channels. The structure has healed itself upon rehydration.

When the packing diagram of **3** is viewed down the [100] axis there are obvious channels, shown in Figure 3.36.

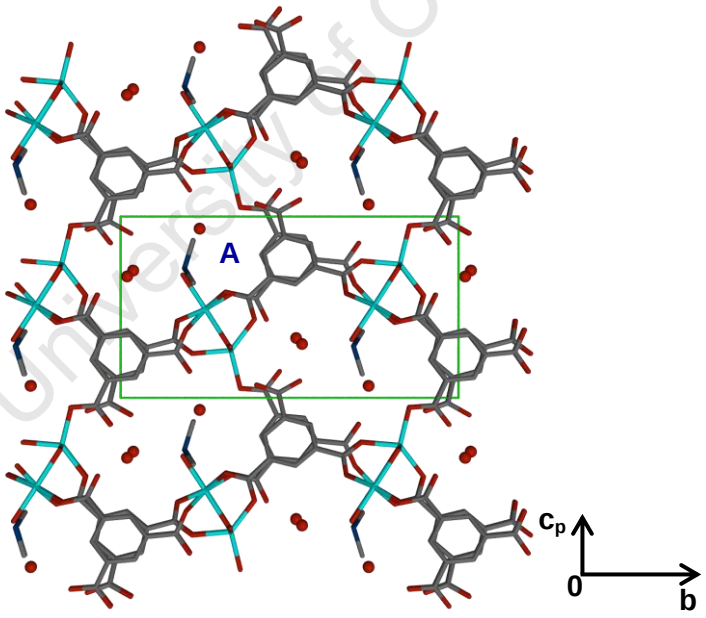

Figure 3.36: The packing diagram of **3** viewed down the [100] axis

The three guest water molecules O16, O17 and O18 are located in the channels labelled A in the diagram. O9 helps to shape the channel and as such is situated near O16, O17 and O18. O16 and O18 are located away from the cation and could easily be removed from the structure via this channel.

There are smaller channels shown in Figure 3.37, that extend along the [100] axis. The guest water molecules O17, O18, and O19 as well as the O7 and O9 coordinated water molecules are located in this channel. These channels are another pathway for water to exit the structure. When compound **3** is dehydrated it is likely that the structure contracts along these channels. It is the shrinking of these channels that causes the cracks in the surface of the crystal seen in the SEM images. When the dehydrated sample is exposed to water vapour again the channels expand to accommodate the water and the sample regains crystallinity. When a single crystal of compound **3** is exposed to excess water or water vapour the channels expand and extra water is absorbed. The structure is not stable in that state and so loses the guest molecules when the source of excess water is removed. This is why only three guest water molecules are modelled in the single crystal structure.

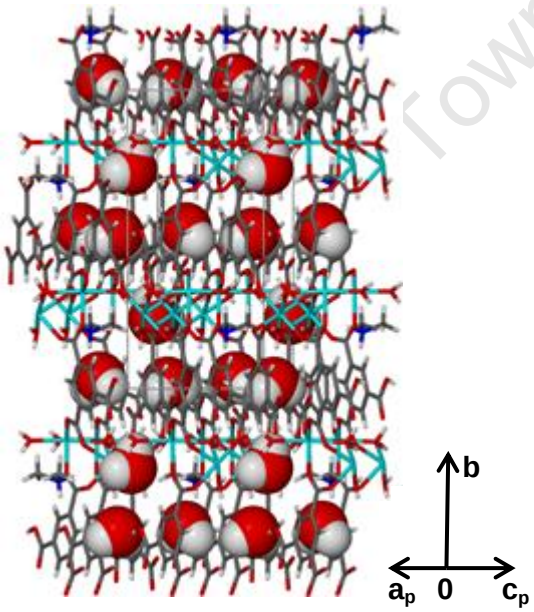

Figure 3.37: a) Packing diagram of **3** viewed onto the (0 0 $\bar{1}$) face

Figure 3.38b shows the crystal morphology of **3** obtained by face-indexing of the crystal. Figure 3.38c is an SEM image in the same orientation showing that the cracks run along the largest, (0 0 $\bar{1}$), face of the crystal. When the channels shrink upon dehydration, as previously described, the cracks seen in Figure 3.35 are produced in a uniform manner across the (0 0 $\bar{1}$) surface of the crystal.

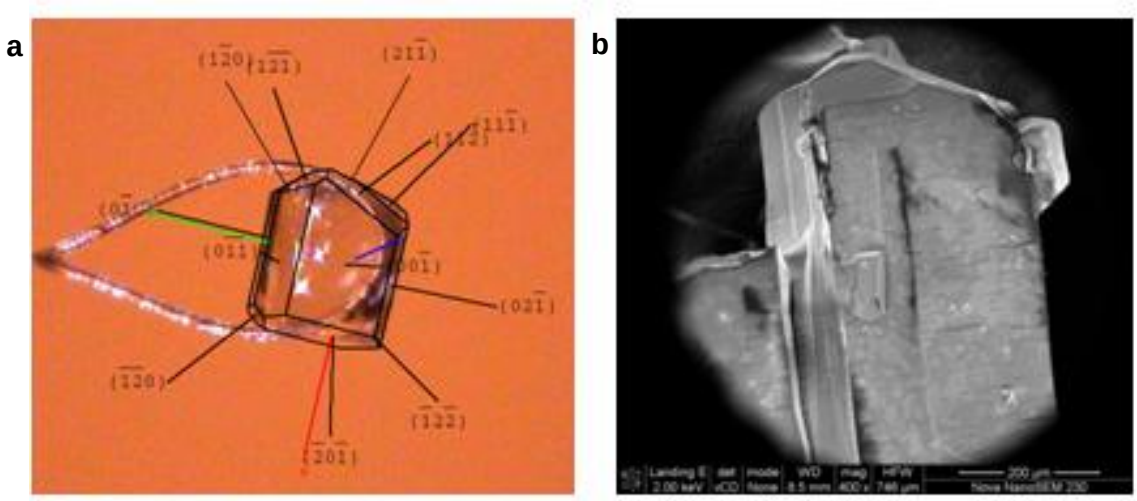

Figure 3.38: a) A face-indexed crystal of **3**, **b)** SEM image of the crystal in the same orientation showing the orientation of cracks across the (0 0 $\bar{1}$) face

3.5.5 DEHYDRATION AND REHYDRATION STUDIES

Full kinetic studies could not be performed on compound **3** due to the difficulty of preparing sufficient amounts of high quality sample. A rehydration experiment was performed on a sample of **3** in a similar manner to the kinetics experiments outlined in Chapter 2.8 – Kinetics. The water vapour level in the brass container was allowed to equilibrate for two hours with the temperature kept at a constant 30 °C throughout the experiment. A sample of **3** was dried on TG apparatus at 160 °C until the TG trace indicated that five water molecules were removed. 172 mg (0.282 mmol) of the sample was then placed on the balance and under the container. The balance was zeroed and the increase in mass over the next two hours was recorded.

Figure 3.39a shows that 33 mg of water is absorbed by the sample over two hours. 33 mg corresponds to 1.832 mmol of water absorbed by the sample. As 0.282 mmol of sample was present this equates to 6.5 water molecules absorbed by the sample per asymmetric unit.

There are only five water molecules modelled in the single crystal structure that can be removed. This, coupled with the thermal analysis, indicates that the compound can expand to contain an extra 1.5 water molecules. The amount of extra water absorbed by **3** confirms that the water molecules are very loosely held and can be removed from the structure at ambient temperatures. The dehydration/rehydration experiment was performed under high vapour pressure conditions and therefore the maximum amount of water molecules that could be absorbed at 30 °C was measured.

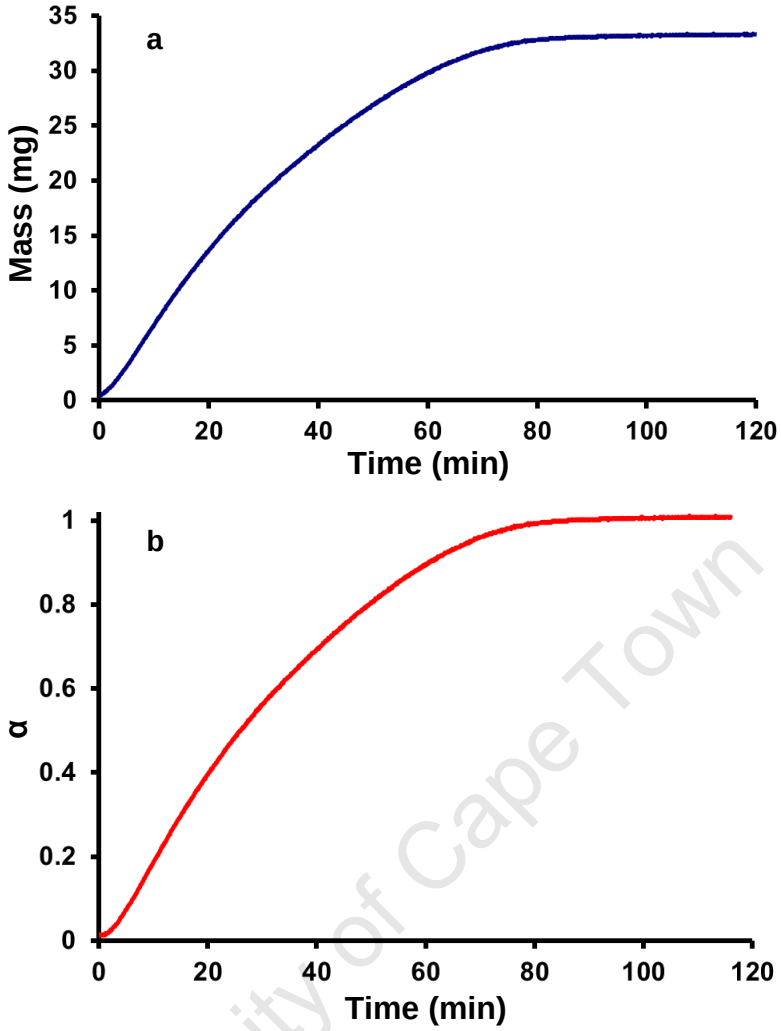

Figure 3.39: a) The mass of water absorbed by a sample of **3** over 120 minutes and **b)** α, the extent of the reaction over 120 min. The reaction was performed at a constant 30 °C

Figure 3.39b shows the extent of the reaction, α, as defined in Chapter 2.8 - Kinetics. A variety of mathematical expressions were used to evaluate the α versus time curve. These expressions are derived from suggested mechanisms for numerous solid-state processes. The contracting area equation (1) fit the data best with a correlation coefficient of 0.9998 and a rate constant (k) of 1.1565 x 10^{-2}. This equation is described as a two-dimensional advancement of the phase boundary by Byrn *et al*.[14] It is applied where the reaction is assumed to proceed from the surface of a circular disk or cylinder inward. This fits well with the assumption that the water molecules enter the compound via channels as previously discussed.

$$1 - (1 - \alpha)^{1/2} = kt \qquad (1)$$

3.5.6 GAS SORPTION STUDIES

Gas sorption studies were performed on compound **3**. The method is as described in Chapter 2.5 – Gas Sorption. These experiments were performed at Stellenbosch University. Unfortunately the apparatus used broke before further tests could be run and was not functional again in the time frame of this project. The reproducibility of these results has therefore not been investigated. We were also unable to retest and explore further any unusual results. Sorption experiments were done under vacuum on approximately 65 mg of dehydrated **3**. The percent absorption by weight (wt%) was calculated and plotted against the pressure. The pressure on the sample was then reduced and desorption data was collected.

Figure 3.40 shows the results for each of the three gases attempted. For carbon dioxide (CO_2) gas (Figure 3.40b) the experiment was performed at 20 °C. For both nitrogen (N_2) gas (Figure 3.40a) and hydrogen (H_2) gas (Figure 3.40c) the experiment was performed at 0 °C.

In all three cases there is strong hysteresis displayed with almost no change in the absorption percentage for hydrogen gas when the pressure is reduced to 0 bar. It is also possible that there may be a chemical interaction taking place upon absorption that prevents the gas molecules from leaving the host. Regardless of the heating temperature the compound became amorphous upon dehydration and so could not be crystallographically characterised.

N_2 gas (Figure 3.40a) is absorbed to a maximum of 0.48 wt% at 0 °C and 20 bar. There are reports in the literature of up to 7.6 wt%.[15] However, those results were obtained at a temperature of -195 °C. CO_2 gas (Figure 3.40b) is absorbed to a maximum of 0.96 wt% at 20 °C and 20 bar. This is not significant with respect to the literature with an example by Arstad *et al*[16] absorbing up to 60 wt% at 25 °C and 25 bar. Our result is due to the large size of CO_2 when compared to water. The cation is located in the channels along [100] and may obstruct the entry of CO_2 into the cavities.

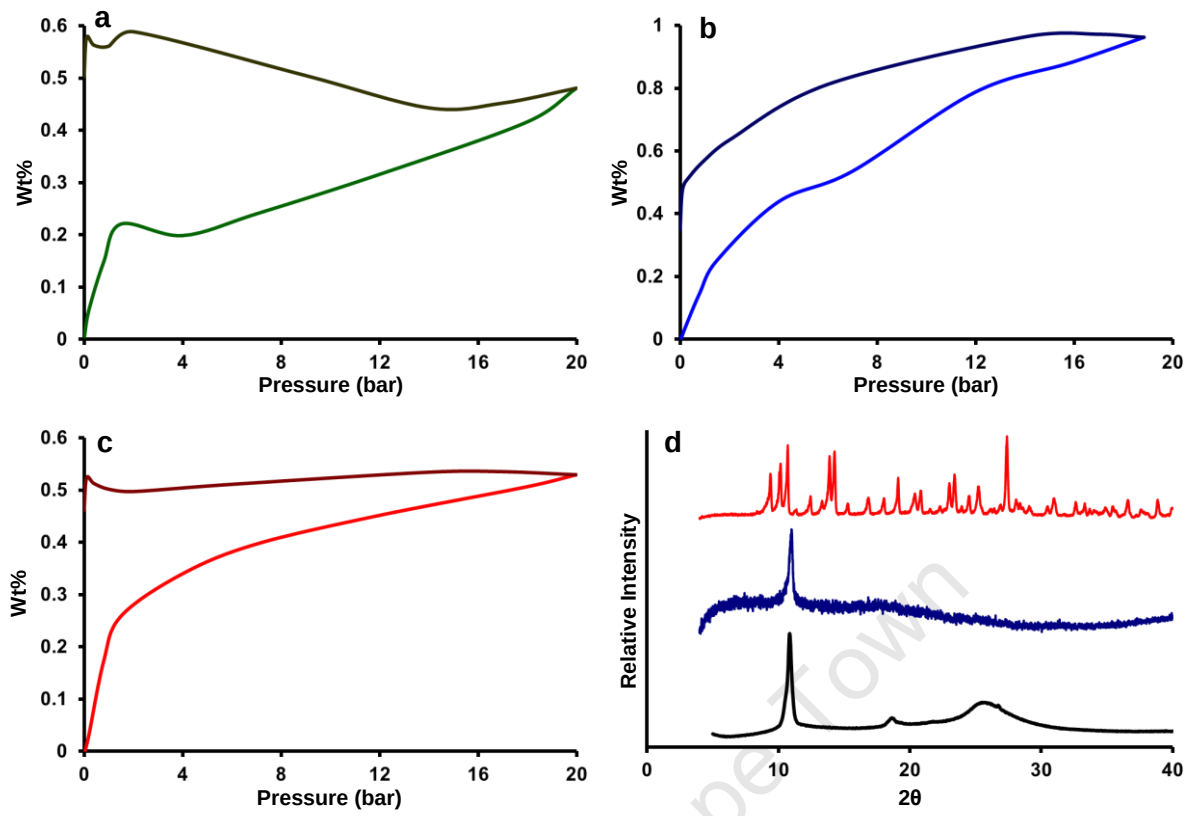

Figure 3.40: Sorption and desorption diagrams for compound **3** with **a)** N_2 gas, **b)** CO_2 gas and **c)** H_2 gas. **d)** The PXRD pattern of **3** in red, after heating in blue and after absorption of H_2 in black

H_2 absorption studies are often done at very low temperatures and high pressures. The absorption of 6.9 wt% achieved by Dincă *et al*[17] for their manganese and benzenetristetrazole compound is a good example. Their sorption experiment was performed at -196 °C and 90 bar. In this experiment we obtained an maximum uptake of 0.53 wt% at 0 °C and 20 bar pressure. Sagara *et al*[18] demonstrate up to 2.0 wt% absorption for **IRMOF-8** at room temperature and 10 bar. These values are comparable to those achieved with **3**.

A sample of **3** that had been exposed to H_2 gas was analysed on a PXRD and this is shown in Figure 3.40d. The red trace shows the experimental PXRD pattern for compound **3**. The blue trace is of compound **3** after heating to 160 °C (**3a**) and the black trace shows the sample of **3a** after exposure to H_2 gas. The pattern remains almost amorphous indicating that the H_2 gas molecules are not large enough to force the previously described channels to expand. This means the original structure is not restored.

3.5.7 SUMMARY

Compound **3** was produced via a number of methods (see Section 3.1 – Preparation of Zinc(II) and 1,3,5-benzenetricarboxylate Compounds). This was confirmed with single-crystal, PXRD and thermal methods. **3** loses crystallinity at high temperatures but can be dehydrated and rehydrated. Compound **3** is able to expand as necessary to accommodate extra water molecules and can contain a total of 4.5 guest water molecules. Cracks form on the surface of the crystal with dehydration but close again with rehydration implying that the structure breathes and the surface heals itself. Compound **3** absorbs CO_2 and N_2 to a low degree and demonstrates a reasonable affinity to the absorption of H_2 gas.

The topology of **3** is discussed in detail in Chapter 5 – Topological Studies.

3.6 [Gd(BTRI)(H_2O)$_6$] (4)

3.6.1 SINGLE CRYSTAL X-RAY DIFFRACTION ANALYSIS

The aromatic hydrogen atoms were placed in idealised positions in a riding model, refined isotropically and assigned a temperature factor of 1.2 times the parent atom. The hydrogen atoms on the terminal water molecules were located and refined using SHELXL-97. All of the hydrogen atoms were refined isotropically and where the hydrogen atom did not refine satisfactorily a temperature factor of 1.2 times the parent atom was assigned.

Compound **4** crystallises in the monoclinic crystal system, in the space group *Cc*. **4** is a neutral coordination polymer and forms one-dimensional chains. The chains are connected by hydrogen bonds between the water molecules and uncoordinated carboxylate moiety. Crystal data and refinement parameters are provided in Table 3.17.

Table 3.17: Crystal Data and Refinement Parameters of **4**

Empirical Formula	$C_9H_{15}GdO_{12}$
Formula Weight (g.mol^{-1})	472.46
Temperature (K)	173(2)
Wavelength (Å)	0.71073
Crystal System	Monoclinic
Space Group	*Cc*
a (Å)	11.3160(3)
b (Å)	17.8157(5)
c (Å)	7.1635(2)
α (°)	90
β (°)	118.972(1)
γ (°)	90
Volume (Å^3)	1263.45(6)
Z	4
Calculated Density (g.cm^{-3})	2.484
***μ* (mm^{-1})**	5.320
***F* (*000*)**	916
Crystal Size (mm)	0.60 x 0.15 x 0.10
***Θ* Range Scanned (°)**	3.10 – 26.02
Index Range	-13 < h < 13, -21 < k < 21, -8 < l < 8
No. Reflections Collected	18562
No. Unique Reflections	2482
R_{int}	0.0822
Data Completeness to θ_{max} (%)	99.8
Refinement Method	Full-matrix least-squares on F^2
Data/Restraints/Parameters	2482/21/242
Goodness-of-fit on F^2	1.076
Final *R* Indices [*I>2σ(I)*]	R_1 = 0.0243, wR_2 = 0.0544
***R* Indices (all data)**	R_1 = 0.0263, wR_2 = 0.0558
Largest Diff. Peak and Hole (*e*.Å^{-3})	1.219, -1.079

The asymmetric unit of **4** is given in Figure 3.41 with the hydrogen atoms omitted for clarity. The asymmetric unit consists of one fully deprotonated BTRI unit, one nine-coordinated gadolinium(III) metal centre and six terminal water molecules. The gadolinium metal centre is coordinated to three carboxylate oxygen atoms (O4^{i}, O5^{ii} and O6) and six water molecules and has tricapped trigonal prismatic geometry.[20] The O1-C1-O2 carboxylate moiety of the BTRI unit is uncoordinated. This carboxylate is deprotonated as demonstrated by the near equal O1-C1 and O2-C1 bond lengths of 1.261(7) and 1.260(7) Å respectively. The O3-C5-O4 carboxylate is unidentate with O3 uncoordinated and O4 coordinated to the Gd1^{iii} metal centre. The O5-C8-O6 carboxylate is bidentate and bridges two Gd1 metal centres with O5 coordinated to Gd1^{iv} and O6 coordinated to Gd1. Each BTRI unit connects three different metal centres and so extends the one-dimensional chains along [20$\bar{2}$].

Related by symmetry: ^{i}1+x, y, 1+z; ^{ii}1/2+x, 1/2-y, 1/2+z; ^{iii}-1+x, y, -1+z; ^{iv}-1/2+x, 1/2-y, -1/2+z; ^{v}x, -y, -1/2+z; ^{vi}1/2+x, 1/2+y, z; ^{vii}1+x, -y, 1/2+z; ^{viii}1+x, -y, 3/2+z; ^{ix}x, -y, 1/2+z; ^{x}1/2+x, 1/2+y, 1+z

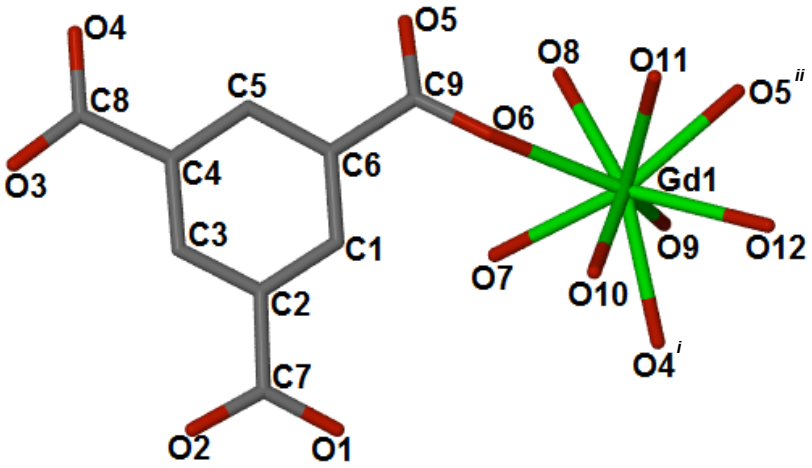

Figure 3.41: The asymmetric unit of **4** with hydrogen atoms omitted

The Gd-O distances observed for the carboxylate moieties correspond with those found for terminal carboxylates coordinated to gadolinium metal centres in the CSD. The Gd-O distances for the terminal water molecules agree well with the literature[4] and CSD values for nine-coordinated metal centres. Full details of these bond distances are given in Table 3.18.

Table 3.18: Experimental Zn-O bond lengths for **4** and literature Zn-O bond lengths

Bond	Length (Å)	Average Length (Å)	Bond Type
Gd1-O4^{I}	2.372(4)	2.39 ± 0.06*	Terminal Carboxylate
Gd1-O5^{II}	2.386 (4)		
Gd1-O6	2.447(4)		
Gd1-O7	2.428(4)	2.42 ± 0.05* 2.44 ± 0.07**	9-coordinate Gd, terminal H_2O
Gd1-O8	2.414(4)		
Gd1-O9	2.505(4)		
Gd1-O10	2.495(4)		
Gd1-O11	2.506(4)		
Gd1-O12	2.462(4)		

* Values obtained from the CSD; ** Mean values reported in Orpen *et al*[4]

The BTRI units bridge metal centres to form parallel, one-dimensional chains. The chains extend along [20$\bar{2}$] and are staggered. The uncoordinated O1-C1-O2 carboxylates are located between the gadolinium metal centres on the adjoining chains ±1/2 along the *b*- and *c*-axes (Figure 3.42a). Figure 3.42b shows the chains stacking next to each other as they extend along [20$\bar{2}$]. The chains are also stacked on top of one another along [010].

Related by symmetry: ^{i}1+x, y, 1+z; ^{ii}1/2+x, 1/2-y, 1/2+z; ^{iii}-1+x, y, -1+z; ^{iv}-1/2+x, 1/2-y, -1/2+z; ^{v}x, -y, -1/2+z; ^{vi}1/2+x, 1/2+y, z; ^{vii}1+x, -y, 1/2+z; ^{viii}1+x, -y, 3/2+z; ^{ix}x, -y, 1/2+z; ^{x}1/2+x, 1/2+y, 1+z

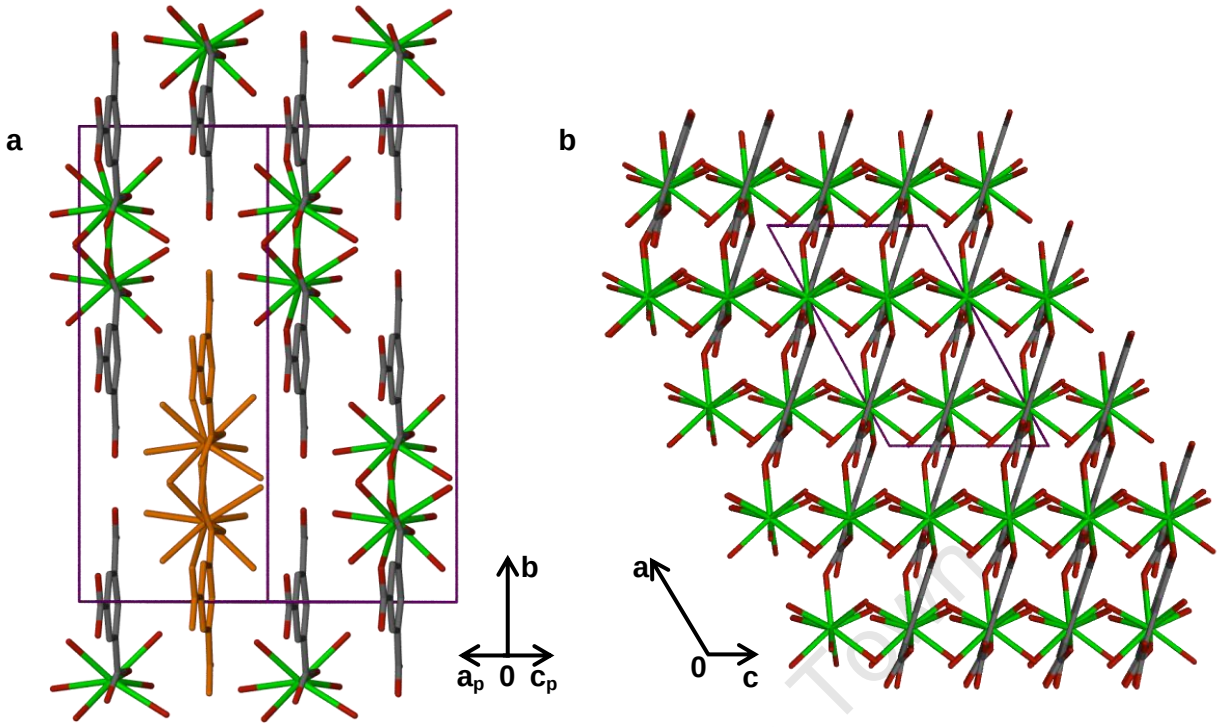

Figure 3.42: The 1-dimensional chains of **4 a)** extending along [20$\bar{1}$] with one chain shown in orange and **b)** viewed down [010]

The BTRI units occupy two positions along *b*, labelled A and B in Figure 3.43. When viewed along [001] it can be seen that the phenyl rings in position A of one chain superimpose on the phenyl rings in position B of the next chain. This chain is located half a unit cell along the *b*-axis and half a unit cell along the *c*-axis. This results in a stacking of the carboxylate moieties.

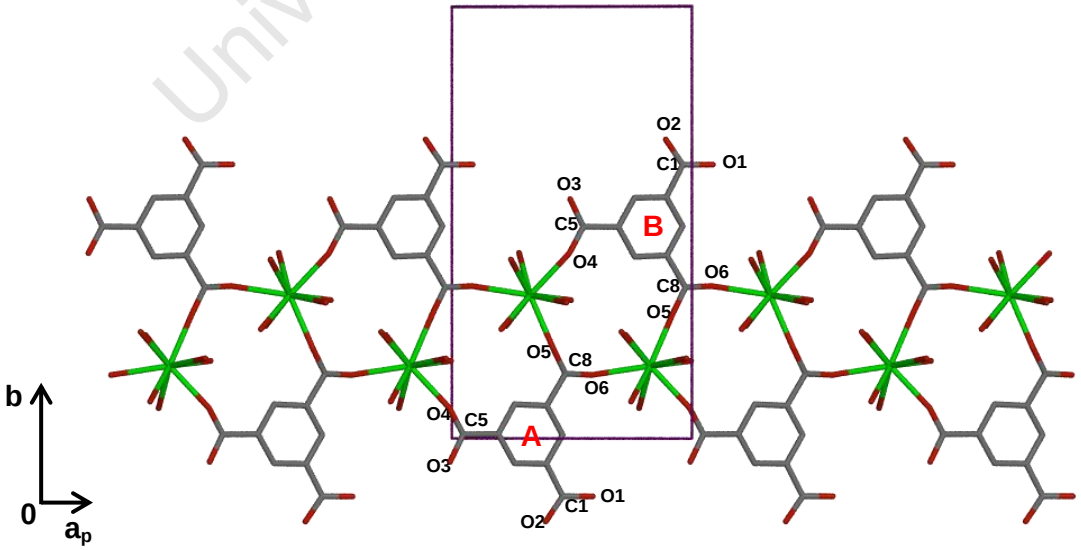

Figure 3.43: The 1-dimensional chains of **4** viewed down [001]. They extend along [20$\bar{1}$]

Related by symmetry: [i]1+x, y, 1+z; [ii]1/2+x, 1/2-y, 1/2+z; [iii]-1+x, y, -1+z; [iv]-1/2+x, 1/2-y, -1/2+z; [v]x, -y, -1/2+z; [vi]1/2+x, 1/2+y, z; [vii]1+x, -y, 1/2+z; [viii]1+x, -y, 3/2+z; [ix]x, -y, 1/2+z; [x]1/2+x, 1/2+y, 1+z

The uncoordinated carboxylate moiety is positioned between the bidentate carboxylate in an O6-C8-O5/O1-C1-O2/O6-C8-O5 fashion. Due to this stacking the uncoordinated O1-C1-O2 carboxylate is located between two carboxylates coordinated to metal centres. The metal centres have six terminally coordinated water molecules and as a result O1-C1-O2 is located in a pocket of water molecules: O7, O8 and O9 from one chain and O10, O11 and O11* from another. The unidentate carboxylates stack in an O3-C5-O4/O4-C5-O3/O3-C5-O4 manner. Due to the alternation of O3 and O4 along [001], O3 is situated in a pocket of water molecules. These are O9 from one chain and O10 and O12 from another. The water pockets are demonstrated in Figure 3.44.

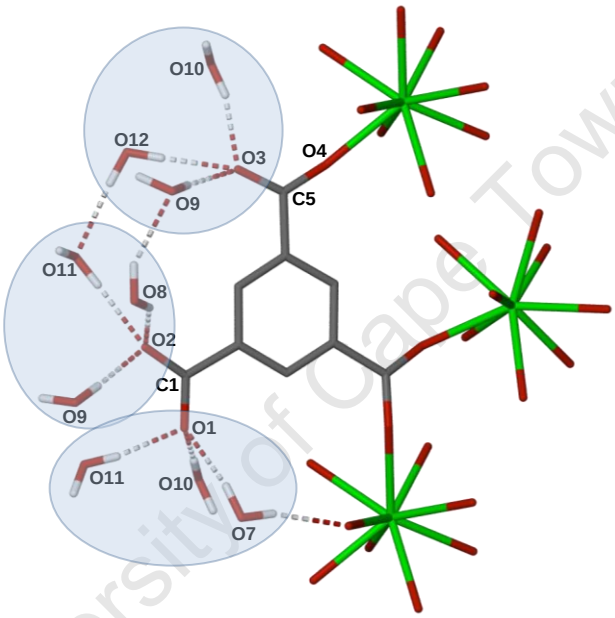

Figure 3.44: O1, O2 and O3 located in the water pockets formed by coordinated water molecules from the adjoining 1-dimensional chains

There is extensive hydrogen bonding between the O1-C1-O2 carboxylate oxygen atoms and the water molecules on the adjoining chains. There are also hydrogen bonds between water molecules further binding the chains together. Full hydrogen bonding details are provided in Table 3.19. The hydrogen atoms on the water molecules were located and placed based on electron density in the difference Fourier map and as a result some of the hydrogen bond angles deviate from the ideal 180°. The contact distances are well within the normal range and there are hydrogen bonds present.

Related by symmetry: [i]1+x, y, 1+z; [ii]1/2+x, 1/2-y, 1/2+z; [iii]-1+x, y, -1+z; [iv]-1/2+x, 1/2-y, -1/2+z; [v]x, -y, -1/2+z; [vi]1/2+x, 1/2+y, z; [vii]1+x, -y, 1/2+z; [viii]1+x, -y, 3/2+z; [ix]x, -y, 1/2+z; [x]1/2+x, 1/2+y, 1+z

Table 3.19: Hydrogen-bond distances and angles for **4**

Donor-H···Acceptor	H···A (Å)	D···A (Å)	D-H···A (°)
O7 − H7A ··· O10^{v}	1.98	2.803	163
O7 − H7B ··· O1^{v}	1.89	2.714	164
O8 − H8A ··· O2^{vi}	2.01	2.775	149
O8 − H8B ··· O5	2.31	2.983	137
O8 − H8B ··· O9^{iv}	2.16	2.871	141
O9 − H9A ··· O2^{vi}	1.86	2.706	177
O9 − H9B ··· O3^{vii}	2.13	2.976	171
O10 − H10A ··· O3^{viii}	1.85	2.676	165
O10 − H10B ··· O1^{ix}	1.91	2.757	172
O11 − H11A ··· O2^{x}	1.96	2.804	173
O11 − H11B ··· O1^{ix}	1.90	2.742	171
O12 − H12A ··· O11^{ii}	2.00	2.847	174
O12 − H12B ··· O3^{viii}	1.90	2.738	177

There are π-π interactions between the phenyl rings on adjacent chains (Figure 3.45). When the structure is viewed along [001] these phenyl rings appear superimposed but they are offset by 1.168 Å. The contact distance between centroids placed at the centre of the phenyl rings is 3.599 Å. These π-π interactions help to strengthen the three-dimensional supramolecular framework formed by the hydrogen bonds.

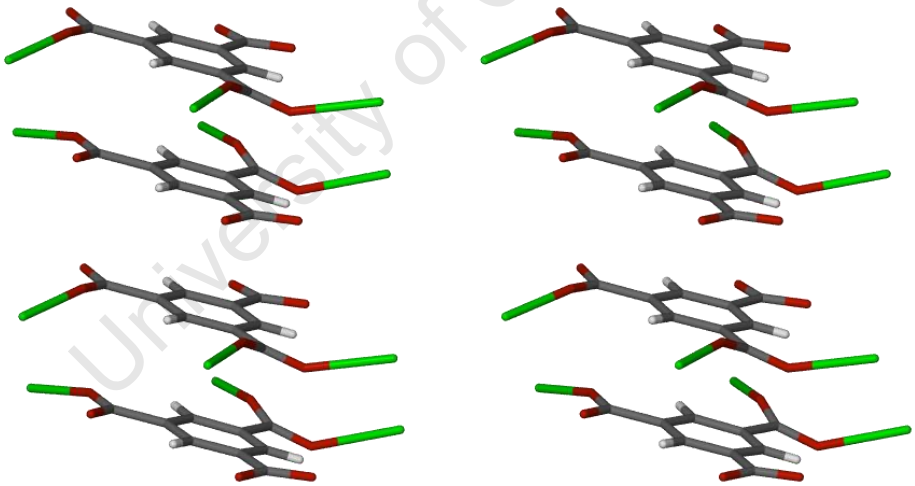

Figure 3.45: A stereo diagram showing the π-π interactions of the phenyl rings in **4**

Compound **4** is isostructural with two previously reported structures. Y(BTRI)(H_2O)$_6$ (**Y-1**) was prepared by Daiguebonne et al[19] in 1999. The method of preparation was significantly different to that used for 4. A solution of Y(III) chloride was diffused through the ammonium salt of H3BTRI. [La(BTRI)(H2O)6]n (**La-1**) was prepared by Wen et al[20] in 2005 from La(NO3)3·3H2O, H3BTRI and Na2CO3 in water. The solution was held at 160 °C for three days before being slowly cooled to room temperature.

Related by symmetry: ^{i}1+x, y, 1+z; ^{ii}1/2+x, 1/2-y, 1/2+z; ^{iii}-1+x, y, -1+z; ^{iv}-1/2+x, 1/2-y, -1/2+z; ^{v}x, -y, -1/2+z; ^{vi}1/2+x, 1/2+y, z; ^{vii}1+x, -y, 1/2+z; ^{viii}1+x, -y, 3/2+z; ^{ix}x, -y, 1/2+z; ^{x}1/2+x, 1/2+y, 1+z

3.6.2 THERMAL ANALYSIS

The TG and DSC traces for compound **4** are given in Figure 3.46. There is only one obvious mass loss evident in the TG trace. There is a change in the slope at approximately 130 °C however as confirmed by the first derivative with respect to temperature leading to the two mass losses A and B. Mass loss A (*ca* 35 – 130 °C) is 18.99% and corresponds with the loss of 5 of the coordinated water molecules (calculated: 19.06%). Mass loss B (*ca* 130 – 300 °C) correlates with the loss of the final water molecule (calculated: 3.84%). The change in slope is due to different energy requirements for the removal of the final water molecule. All details are given in Table 3.20.

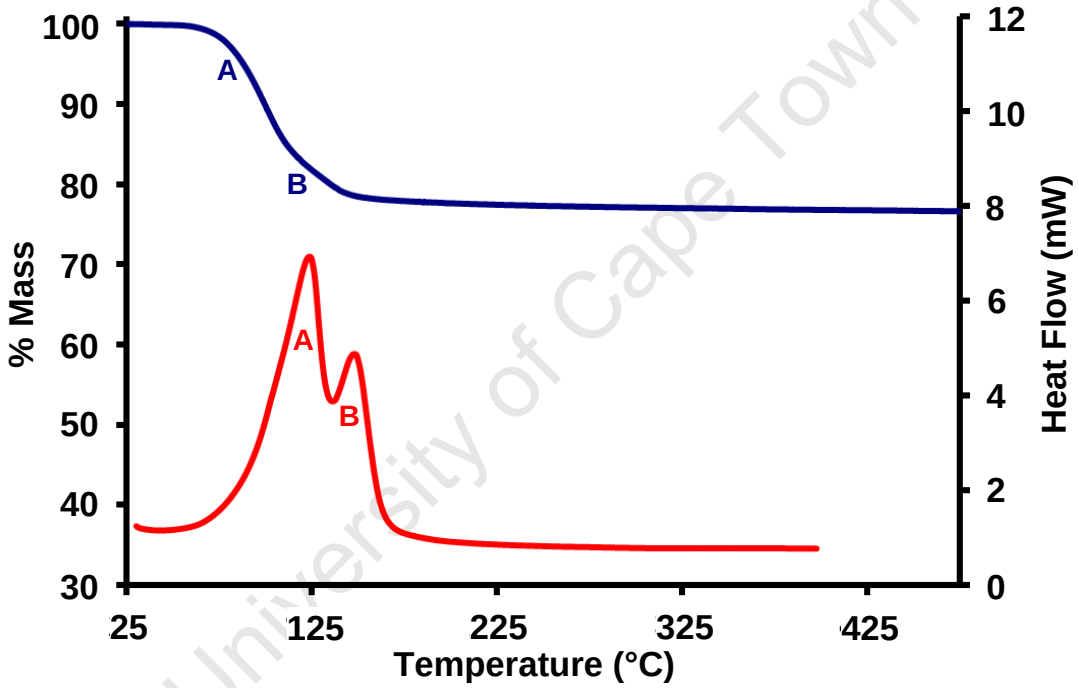

Figure 3.46: TG analysis of **4** and **b)** DSC analysis of **4** both with a heating rate of 20 °C.min^{-1}

The DSC curve displays two endotherms, A and B. B appears as a large shoulder on endotherm A. The onset temperatures of both endotherms correspond well with the loss of the coordinated water molecules. It is interesting to note that endotherm B is relatively large considering it coincides with the loss of only one water molecule. This is most likely due to a structural rearrangement occurring at that point. The variable temperature PXRD – Section 3.6.3, Figure 3.49 – shows this structural rearrangement. This will be discussed fully in that section.

Table 3.20: TGA and DSC results for **4**

	TGA Results		DSC Results
	Calc. % Mass Loss	**Exp. % Mass Loss**	**T_{onset} (°C)**
5 H_2O	19.06	18.99	97
1 H_2O	3.81	3.84	*ca* 155

Elemental analysis of **4** is a good match for the modelled structure. A sample of **4** was heated to 200 °C and then exposed to air for 72 hours at room temperature (**4a**). The elemental analysis on this sample shows that one water molecule has been absorbed. This suggests this network either prefers to include all six water molecules or only one water molecule.

Table 3.21: Elemental analysis of $[(GdC_9O_6H_3)(H_2O)_6]$ (**4**) and sample of **4** after heating to 200 °C and exposure to air for 72 hours ($[(GdC_9H_6O_3)(H_2O)]$) (**4a**)

	Compound 4		Compound 4a	
	Calculated	**Experimental**	**Calculated**	**Experimental**
% C	22.88	22.38	28.27	27.75
% H	3.20	3.75	1.32	1.46

3.6.3 POWDER X-RAY DIFFRACTION

The PXRD patterns calculated for the **La-1**[20] (Figure 3.47b) and **Y-1**[19] (Figure 3.47c) compounds mentioned in Section 3.6.1 (Single Crystal X-ray Diffraction Analysis) are exceedingly similar to the pattern calculated from the single crystal data of **4** (Figure 3.47a). This is due to these three compounds being isostructural. All the diffraction peaks for **La-1** have a slightly lower ° 2θ value than the equivalent diffraction peak for **4** and **Y-1**. Aside from that the patterns are identical up to the peaks at *ca* 2.6° 2θ. Again **Y-1** matches **4** to a large degree. The pattern of the four peaks between *ca* 23.6 and 25.5° 2θ for **La-1** however is quite different to those found for **4** and **Y-1**. There are also some minor differences between the three structures in the fine detail above 25.5° 2θ. Their crystal structures match closely with only the metal ion being different.

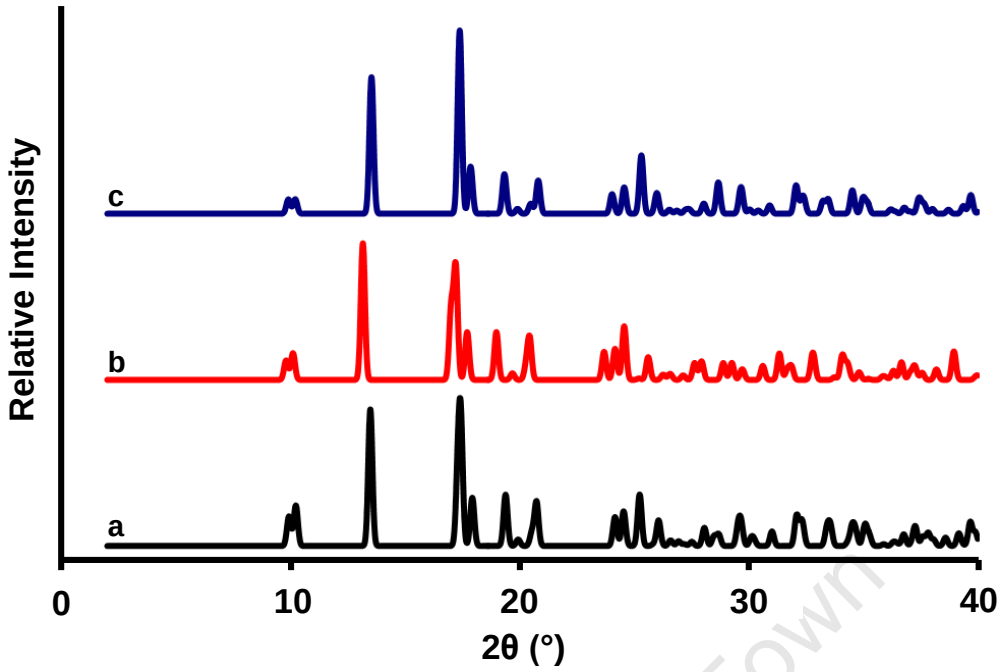

Figure 3.47: PXRD patterns calculated from single crystal data of **a) 4**, **b) La-1** and **c) Y-1**

The PXRD pattern calculated from the single crystal data of **4** (Figure 3.48a, blue) matches that obtained from the bulk material (Figure 3.48b, red). The bulk material is generally a fine, crystalline powder.

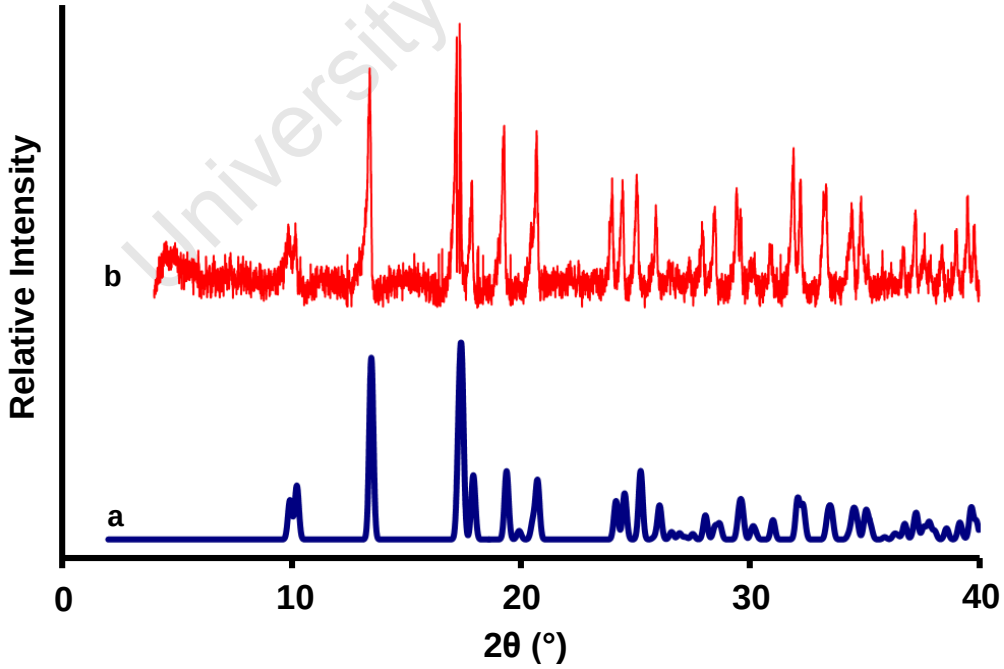

Figure 3.48: PXRD patterns of **4 a)** calculated from single crystal data and **b)** experimental

Variable temperature PXRD shows an interesting variation in the crystallinity of compound **4**. Up to 50 °C the structure of **4** is retained as can be seen in Figure 3.49. Coinciding with the removal of the first water molecule there is a significant change in the PXRD pattern with much of the fine detail being lost. This continues until 110 °C where the compound appears almost amorphous. After 110 °C however there is an increase in the intensity of the peaks observed at approximately 11, 16 and 20° 2θ. This increase in crystallinity coincides with the loss of five of the water molecules implying that the structure – containing one water molecule at this stage – is able to undergo some rearrangement at this point. The increase in the 11, 16 and 20° 2θ peaks continues until 200 °C where maximum peak intensity is reached. After the removal of all water molecules from the compound at approximately 200 °C the peaks reduce in size marginally but remain present indicating that the rearrangement that has occurred, remains.

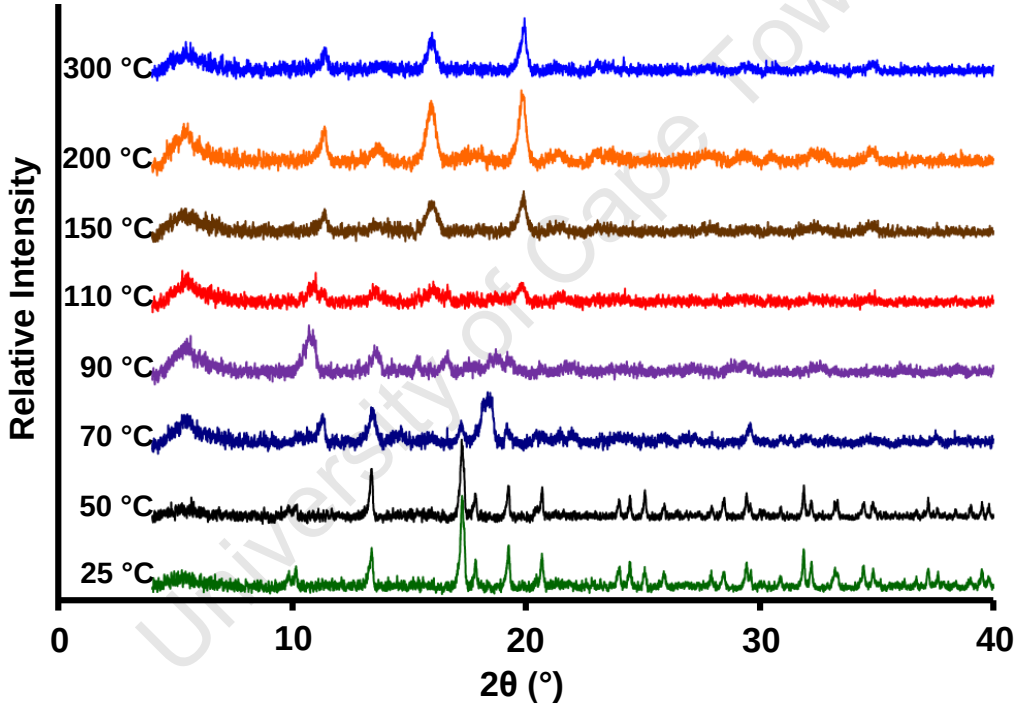

Figure 3.49: Variable temperature PXRD patterns of **4** from 25 – 300 °C

This continuation of the rearranged structure shows that the uptake of one water molecule after dehydration (as seen in Section 3.6.2 – Thermal Analysis) is probable. The structure does not change further and therefore there must be space to accommodate that one water molecule.

3.6.4 KINETIC STUDIES

For the full details of the kinetic studies see Chapter 2.8– Kinetics. Experiments were performed at 25 °C and 30 °C for water vapour and at 25 °C for ethanol vapour. In each case the vapour level was allowed to equilibrate at the desired temperature before the experiment was started. The sample was sieved for these experiments to give particle sizes of between 38 – 45 µm.

To test the effect of exposure to air on the sample, as well as any increase in this effect due to sieving (increased surface area) TG analysis was performed on samples of **4**. Figure 3.50a (blue) shows the TG trace for a sample of compound **4** taken directly from the mother liquor and dried on filter paper. TG analysis was performed immediately on the dried sample. As described in Section 3.6.2 (Thermal Analysis) **4** loses 6 water molecules (calculated: 22.88%, experimental: 22.38%). Compound **4** undergoes a structural transformation with the loss of water molecules (Section 3.6.3 – Powder X-ray Diffraction, Figure 3.49) but is stable until at least 500 °C.

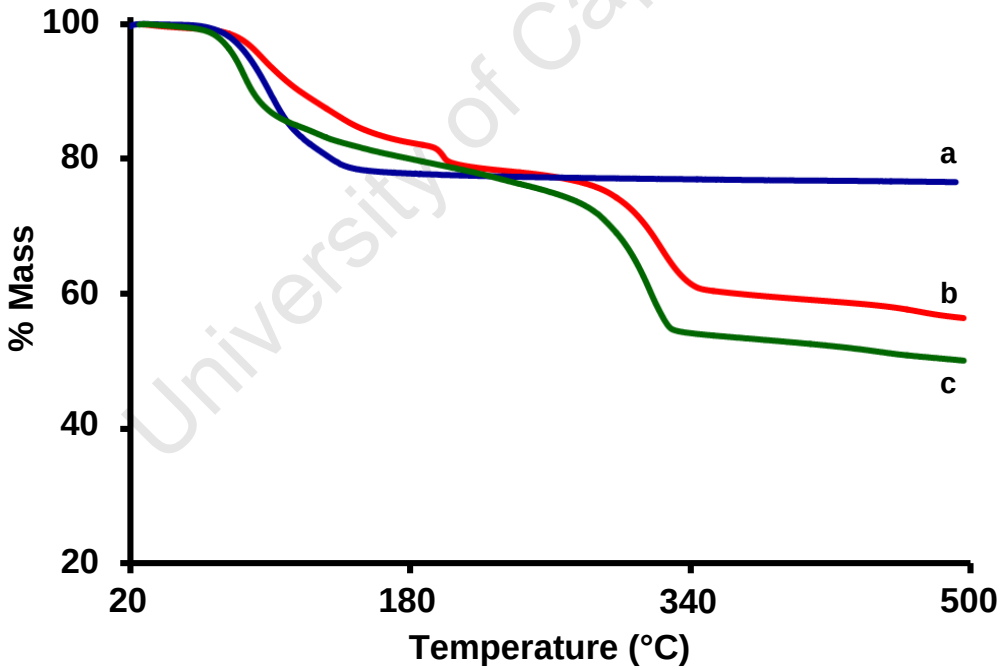

Figure 3.50: TG traces for compound **4**. **A)** Compound **4** taken straight from the mother liquor and dried on filter paper (heating rate: 20 °C.min^{-1}), **b)** compound **4** exposed to air for 2 days to allow thorough drying (**4a**) (heating rate: 10°C.min^{-1}), **c)** thoroughly dried compound **4a** after sieving (**4b**) (heating rate: 10 °C.min^{-1})

Figure 3.50b (red) shows the TG trace for a sample of **4** removed from the mother liquor and then placed on filter paper and allowed to dry thoroughly over several days (**4b**). It is necessary to dry a sample thoroughly before sieving. The dry, not sieved **4b** was then

analysed using TG apparatus. The loss of 6 water molecules is observed for **4b** (experimental: 22.49% by *ca* 260 °C) but in a reproducible two-step process. Decomposition begins at approximately 270 °C.

The fact that compound **4b** decomposes at *ca* 270 °C while compound **4** is stable to 500 °C shows that exposure of compound **4** to air for an extended period of time results in a loss of structural integrity. Figure 3.50c (green) shows the TG trace for a sieved sample of **4b** (**4c**). The profile of **4c** is similar to that of **4b** although the loss of water is no longer a two-step process. The six water molecules are lost by 225 °C indicating that the increase in surface area results in the loss of water molecules at a lower temperature. Decomposition starts at approximately 240 °C.

Figure 3.51a shows the TG trace for a sieved sample of **4c** heated to 500 °C at 10 °C.min^{-1}. The sample starts to decompose at approximately 22 minutes (which corresponds to a temperature of *ca* 240 °C. Figure 3.51b shows the TG trace for a sample of **4c** held at 200 °C for an extended period of time. The decomposition evident in Figure 3.51a no longer occurs with only a 1.5% mass loss observed between 40 and 160 minutes. The sample is marginally yellow after removal from the TG apparatus indicating that a slight decomposition may have occurred.

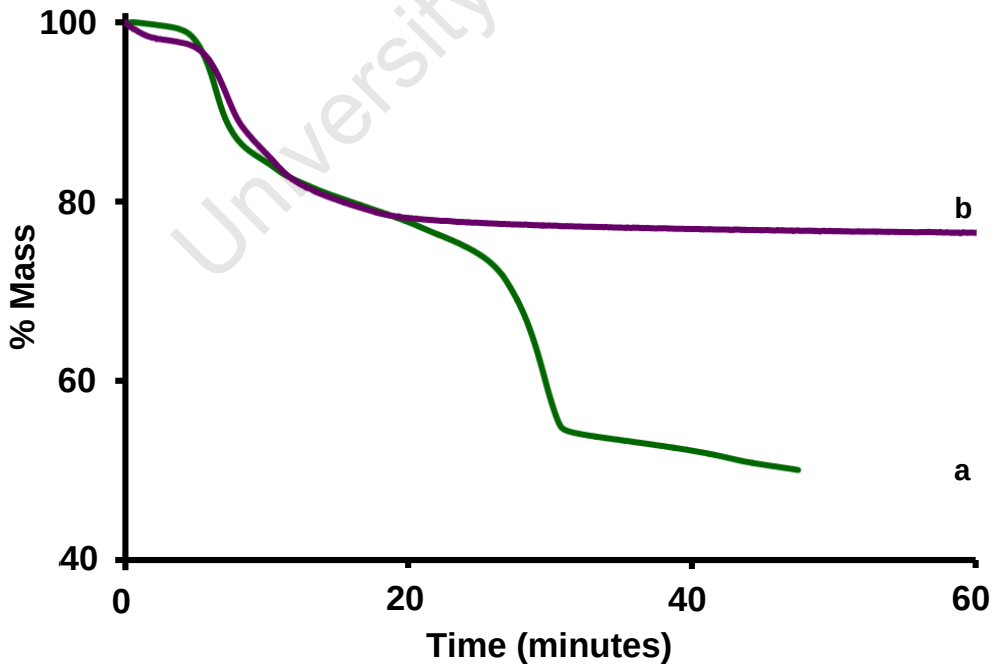

Figure 3.51: TG traces for a sieved sample of compound **4 a)** heated to 200 °C at 10 °C.min^{-1} and held at that temperature and **b)** heated to 500 °C at 10 °C.min^{-1}

Samples were therefore dried at 200 °C for 40 minutes for each experiment. This corresponds to the loss of all six water molecules (experimental: 23.03%, calculated: 22.88%) It was essential that the sample was not held for longer than 40 minutes at 200 °C due to the decreased integrity of compound **4** upon drying and sieving. Due to this sensitivity a new sample of **4c** was dehydrated for each experiment.

Compound **4c** could potentially reabsorb water at a fast rate. The following method was therefore used:

- The brass container was placed around the balance with water or ethanol in the chambers.
- This was allowed to equilibrate at 25 or 30 °C and the balance was zeroed.
- The monitoring apparatus was started and only then was the dehydrated sample removed from the oven.
- This sample was immediately placed onto the balance within the brass container.
- The balance was not rezeroed at this stage in order for an accurate measurement of the initial mass to be obtained.

The data provided in the following figures are corrected for the initial mass of the sample. For Figures 3.52 – 3.54: a) is a plot of the number of water or ethanol molecules absorbed per asymmetric unit with time; b) shows α (the extent of the reaction) against time; c) shows the PXRD patterns of the samples as well as other relevant PXRD traces; d) gives the TG trace for the samples. For the water absorption experiments (Figures 3.52 and 3.53) run 1 is given in green and run 2 is given in brown or orange. For the ethanol absorption experiments (Figure 3.54) run 1 is given in blue while run 2 is shown in red.

Figure 3.52 shows the results of the kinetics experiments with H_2O at 25 °C. The absorption profiles of runs 1 and 2 do not match exactly (Figure 3.52a) with 7 water molecules absorbed in run 1 and 6 absorbed in run 2. However the extent of reaction profiles for both runs (Figure 3.52b) are very similar. The two-dimensional diffusion model equation[14] (2) is obtained with a fit of 0.9978 and 0.9979 for runs 1 and 2 respectively. These values were calculated from the inclusion of 0 – 6 water molecules as we believe the extra water is due to surface absorption. Equation (2) applies when the rate is controlled by two-dimensional diffusion from the surface of a disk or cylinder. The rate constant values (k) are given in Table 3.22 at the end of this section.

$$(1 - \alpha)\ln(1 - \alpha) + \alpha = kt \qquad (2)$$

After both samples are exposed to the water vapour all the diffraction peaks from the original PXRD pattern are obtained (Figures 3.52c, (ii) and (iii)) showing that the structural change observed at 200 °C (Figure 3.52c, (v)) is reversible to some degree. There are also additional peaks at 14.2, 14.8 and 16.4° 2θ suggesting that there are some differences between the rehydrated sample and the original compound **4**. The water uptake is stable as shown in Figure 3.52d, which is the trace obtained from the second run sample after exposure to air for 12 hours at room temperature. TG analysis on the samples gives a 22.4% mass loss by 500 °C. This corresponds to the loss of 6 water molecules (calculated: 22.9%). Any surface water is apparently lost upon removal of the sample from the brass container and the environment of high water vapour pressure. TG analysis indicates that the instability observed in the original sieved sample (Figures 3.50 and 3.51) is reduced when the sample is rehydrated. The sample does not fully decompose by 500 °C and is stable until 250 °C and the loss of the final water molecule. The TG trace of the rehydrated sample exposed to air overnight behaves in exactly the same way confirming that the change in structure is stable.

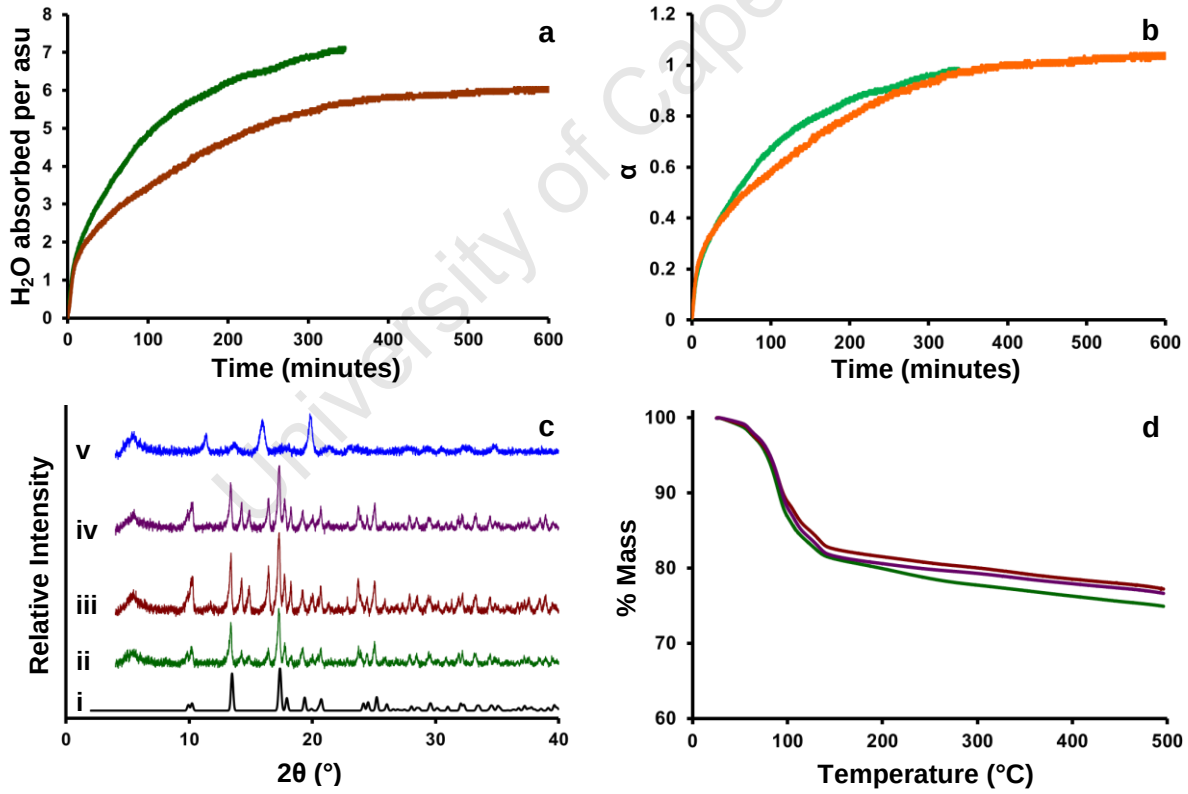

Figure 3.52: Kinetics studies of **4c** with H_2O at 25 °C. **a)** Number of water molecules absorbed per asymmetric unit with time, run 1 in green, run 2 in brown. **b)** The extent of the reaction (α) with time, run 1 in green, run 2 in orange. **c)** PXRD traces of: **(i)** Calculated pattern for **4**, **(ii)** run 1, **(iii)** run 2, **(iv)** run 2 after exposure to air for 12 hours at room temperature and **(v) 4** after heating to 200 °C. **d)** TG traces of the samples, run 1 in green, run 2 in brown, and run 2 after exposure to air for 12 hour in purple (heating rate for all runs: 10 °C.min^{-1})

Figure 3.53 displays the results of the kinetics experiment with H_2O at 30 °C. By 120 minutes 4.5 water molecules are absorbed for run 1, while 5.5 are absorbed for run 2. Additional water molecules are absorbed in both runs after 120 minutes but a change in the slope at this point implies that the extra water is due to surface absorption. It is possible that the additional water absorbed in run 2 compared to run 1 is due to a change in surface area as this is not constant for every experiment despite attempts at consistency. Although the number of water molecules absorbed do not match for the two runs the extent of reaction profiles (Figure 3.53b) correspond well to one another. The two-dimensional advancement of a phase boundary model[14] (3) is obtained with a fit of 0.9953 and 0.9982 for runs 1 and 2 respectively. The extent of reaction was taken from the beginning of the run to the absorption of 4.5 and 5.5 water molecules for runs 1 and 2 respectively. The model does not match that observed for the experiments at 25 °C.

$$1 - (1 - \alpha)^{½} = kt \qquad (3)$$

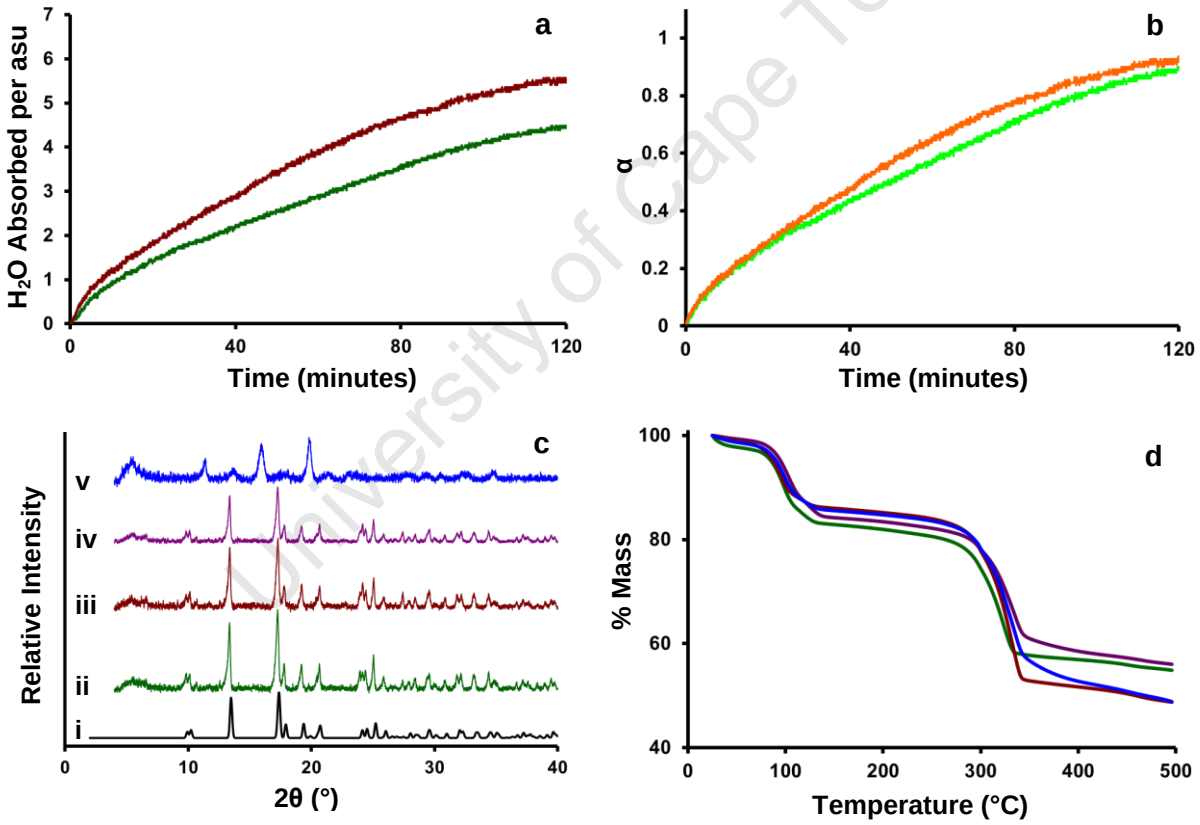

Figure 3.53: Kinetics studies of **4c** with H_2O at 30 °C. **a)** Number of water molecules absorbed per asymmetric unit with time, run 1 in green, run 2 in brown. **b)** The extent of the reaction (α) with time, run 1 in green, run 2 in orange. **c)** PXRD traces of: **(i)** Calculated pattern for **4**, **(ii)** run 1, **(iii)** run 2, **(iv)** run 2 exposure to air for 12 hours and **(v) 4** after heating to 200 °C. **d)** TG traces of the samples, run 1 in green, run 1 after exposure to air for 7 weeks in purple, run 2 in brown, run 2 after exposure to air for 12 hours in blue (heating rate for all runs: 10 °C.min^{-1})

For both runs 1 and 2 the original PXRD diffraction pattern is obtained after exposure to water vapour at 30 °C (Figure 3.53c (ii) and (iii)). Unlike with absorption at 25 °C there are no diffraction peaks in the PXRD trace aside from those for compound **4**. The transformation back to compound **4** is stable as shown by the PXRD pattern of the run 2 sample exposed to air overnight (Figure 3.53c (iv)). The pattern once again matches compound **4**. TG analysis for run 1 (Figure 3.53d, green) shows that 4.5 water molecules are removed by 225 °C (calculated: 18.20%, experimental: 17.91%). This implies that the additional water absorbed in the kinetics experiments were surface water. In contrast although more water was absorbed during run 2 (Figure 3.53d, brown) only 3.5 water molecules were removed by 225 °C (calculated: 14.75%, experimental: 15.09). This implies that the reason more water was absorbed in run 2 (for example greater surface area) also allowed that water to be removed more easily. The water retained immediately after removal for the high vapour pressure environment is not lost with longer exposure to air. Figure 3.53d, purple shows run 1 after exposure to air for 7 weeks while Figure 3.53d, blue shows run 2 after exposure to air for 12 hours. In both instances almost identical TG traces to the original samples are obtained. The main difference is that the decomposition peak at approximately 340 °C is not as sharp in the samples after exposure.

Figure 3.54 gives the results of the kinetics experiment with ethanol at 25 °C. Approximately 1 ethanol molecule is absorbed per asymmetric unit. Although the absorption versus time profiles (Figure 3.54a) do not look the same, the extent of reaction profiles are similar (Figure 3.54b). The extent of reaction profile matches the one-dimensional diffusion model equation[14] (4) with a fit of 0.9960 and 0.9957 for runs 1 and 2 respectively. These values were calculated from a time of 0 minutes to the inclusion of 1 ethanol molecule. The one-dimensional diffusion model implies that the ethanol cannot access the cavities in the same manner as the water molecules.

$$\alpha^2 = kt \qquad (4)$$

The PXRD pattern after exposure to ethanol is not similar to that for compound **4** and some changes from the dehydrated structure are observed (Figure 3.54c, (ii)). The peak at 10° 2θ has increased in intensity. A new, low intensity peak has appeared at 11.8° 2θ. The distinctive peak at 16.2° 2θ from the dehydrated sample is still present in the sample exposed to ethanol vapour. Both the original compound **4** and the dehydrated sample show a peak at 19.5° 2θ, which is no longer present in the sample exposed to ethanol vapour. Peaks that were visible between 24 and 25.2° 2θ in the original sample, but not for the dehydrated sample, are once again present in Figure 3.54c, (ii) though with less fine detail.

The TG trace for each run, as well as the corresponding first derivative with respect to temperature (%.°C^{-1}) is given in Figure 3.54d. Before 230 °C the profiles of runs 1 and 2 match perfectly and the mass loss of 3.4% corresponds to the loss of 0.3 ethanol molecules (calculated: 3.6%). This implies that the compound is only stable with one ethanol molecule for every three asymmetric units. Excess ethanol molecules are lost as soon as the sample is removed from the high vapour pressure environment. The traces do not match that of the sieved sample (Figure 3.54d, black) below 230 °C. This is unsurprising as the sieved sample contains water. At approximately 230 °C there is a large mass loss. This is bigger for run 1 than for run 2. The shape of the profiles and the temperature of this mass loss matches that of decomposition in the sieved sample. Both samples are fully decomposed by 500 °C. The first derivative profiles of both runs correspond well at decomposition with that of the sieved sample.

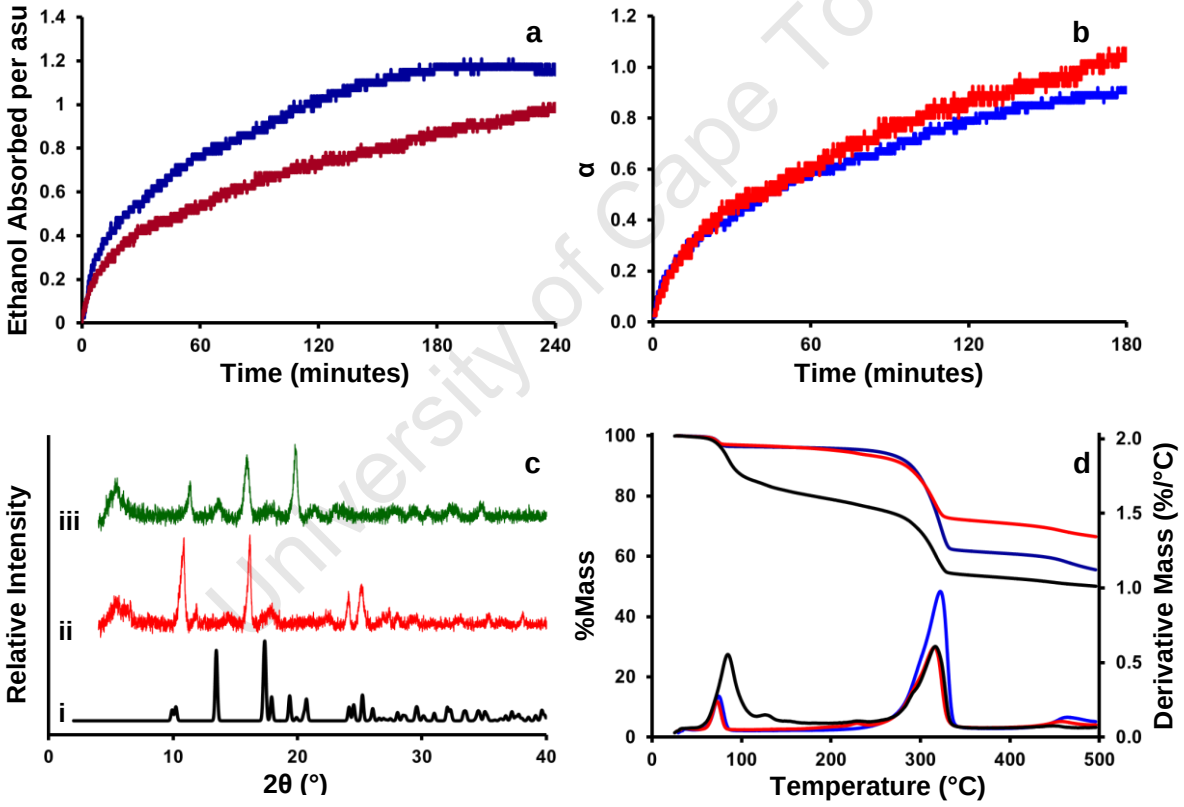

Figure 3.54: Kinetics studies of **4** with ethanol at 25 °C. **a)** Number of ethanol molecules absorbed per asymmetric unit with time, run 1 in blue, run 2 in brown. **b)** The extent of the reaction (α) with time, run 1 in blue, run 2 in red **c)** PXRD traces of:**(i)** Calculated pattern for **4**, **(ii)** run 1, **(iii) 4** after heating to 200 °C. **d)** TG traces and first derivatives with respect to sample temperature. Run 1 is in blue, run 2 is in red and the sieved sample before dehydration is in black (heating rate for all runs: 10 °C.min^{-1})

The rate constants obtained for runs 1 and 2 performed at 25 °C with water are very similar. The rate constants for the runs at 30 °C are not that dissimilar although the value for run 2 is larger than that for run 1. This is unsurprising as more water is absorbed in run 2 than in run

1 in the same time frame. For the ethanol experiment at 25 °C the rate constants obtained are similar although run 2 has the larger rate constant. All the values are given in Table 3.22.

Table 3.22: Rate constants (k) for the absorption of water into dehydrated samples of compound **4**

	H_2O		Ethanol
	25 °C ($.s^{-1}$)	**30 °C ($.s^{-1}$)**	**25 °C ($.s^{-1}$)**
Run 1	2.7762×10^{-3}	6.8974×10^{-3}	4.7602×10^{-3}
Run 2	2.5669×10^{-3}	7.6292×10^{-3}	5.9836×10^{-3}

3.6.5 SUMMARY

Compound **4** is obtained in every experiment where gadolinium nitrate and H_3BTRI were combined. Thermal analysis shows that there is a change in the energy required when removing the final of six water molecules. This is confirmed with variable temperature PXRD where a structural rearrangement occurs when all but one water molecule is removed from the structure. This rearrangement persists after the removal of the final water molecule. Exposure to air damages the integrity compound **4** and sieving intensifies this problem. The integrity can be partially regained through dehydration and rehydration at 25 °C although the original structure is not regained. The original structure can be obtained through rehydration at 30 °C but the same decomposition temperature is observed as that found for the sieved sample before dehydration. Dehydrated samples of compound **4** can absorb ethanol but only 0.3 ethanol molecules are stable out of the high vapour pressure environment.

3.7 TRANSFORMATION OF 3 INTO 4

Compounds **3** and **4** were fully discussed in Sections 3.5 and 3.6 respectively. They can both be prepared by multiple methods as was reviewed in Section 3.1. Compound **4** can also be prepared from compound **3** by placing crystals of compound **3** into a solution of gadolinium nitrate as will be discussed in this section. It is noted that similar work has been recently published by Cui *et al*.[21]

3.7.1 CHANGE OF PXRD TRACE OVER TIME AT CONSTANT CONCENTRATION

Gadolinium nitrate was dissolved in a 1:1, v/v DMF/H_2O solvent system to obtain a concentration of 0.1 mol.dm^{-3}. Single crystals of **3** were submerged in the gadolinium nitrate solution at room temperature. The results are shown in Figure 3.55. An approximate crystal size is given where relevant. Over time the sample transforms from compound **3** to compound **4**. The single crystals of **3** retain their shape but lose single crystallinity and as a result PXRD experiments were used to demonstrate the transformation. The degree of crystallinity changes for each experiment due to different samples being selected for each pattern.

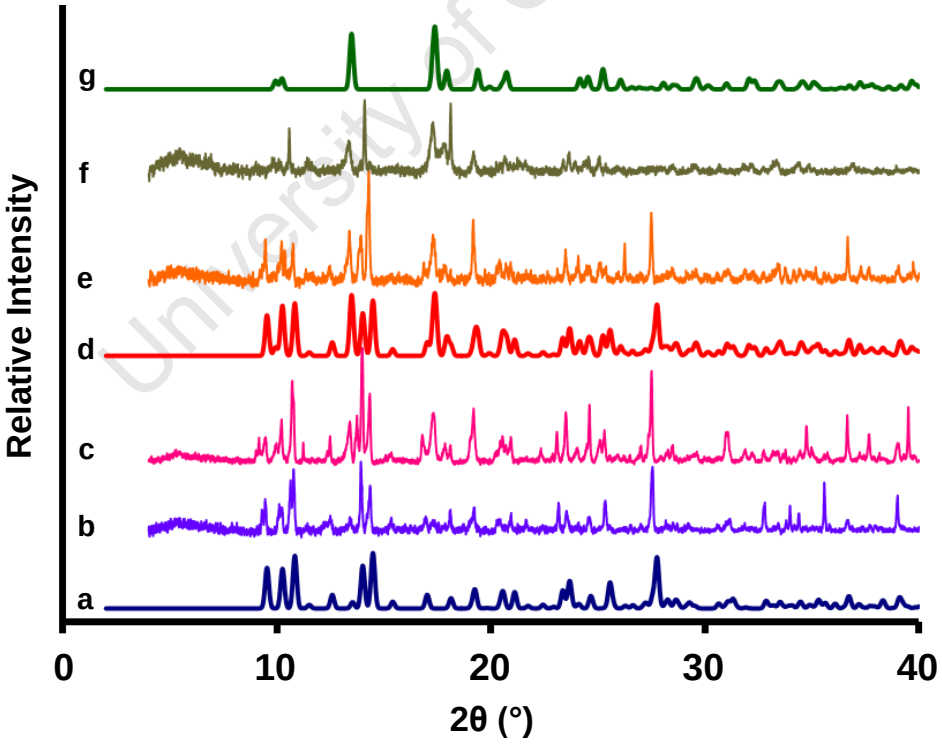

Figure 3.55: Variation in the PXRD pattern of **3** when placed into a 0.1 mol.dm^{-3} DMF/H_2O solution of $Gd(NO_3)_3$. **a)** Calculated pattern of **3**, **b)** 4 hours in solution, **c)** 24 hours in solution, **d)** 50:50 combination of the calculated patterns of **3** and **4**, **e)** 3 days in solution, **f)** 7 weeks in solution and **g)** the calculated pattern of **4**

A hot-stage microscopy study of a single crystal placed into a 0.1 mol.dm^{-3} DMF/H_2O solution of gadolinium nitrate is shown in Figure 3.58 in Section 3.7.2. For each PXRD pattern a different sample was removed from the solution. Figure 3.55a shows the calculated pattern of compound **3**. After four hours of submersion the PXRD pattern obtained matches the pattern calculated for **3** (Figure 3.55b). After 24 hours (Figure 3.55c) the pattern retains the peaks consistent with **3** and new peaks have emerged. The most notable of these is the peak at approximately 17.2° 2θ. After 72 hours the PXRD pattern obtained (Figure 3.55e) is a very good match for the combination of the calculated patterns for **3** and **4**. This combination is depicted in Figure 3.55d. The most prominent peaks in the calculated pattern for **3** are at 9.5, 10.2, 10.5, 14, 14.2 and 20.6° 2θ. Figure 3.55f contains some peaks from compound **3** but these are dramatically reduced. By this time the sample had been submerged in the gadolinium solution for seven weeks. The majority of the peaks match those found in compound **4**. The peaks at 13.3 and 17.3° 2θ are particularly conspicuous. The characteristic peaks of **3**, normally observed at 9.5 and 27.7° 2θ, have disappeared entirely. The peaks at 10.5 and 14° 2θ are still present however.

Figure 3.56 shows that crystal size has a visible effect on the amount of time taken for the transformation to take place. The samples retained their shape with submersion but lost single crystallinity and were therefore studied using PXRD. Figure 3.56b shows the PXRD trace obtained from a large (*ca* 2.0 x 1.2 x 0.9 mm) crystal submerged in a 0.1 mol.dm^{-3} solution for four weeks. The pattern contains all the significant peaks of compound **3** as well as those around 13.4 and 17.5° 2θ that are indicative of compound **4**.

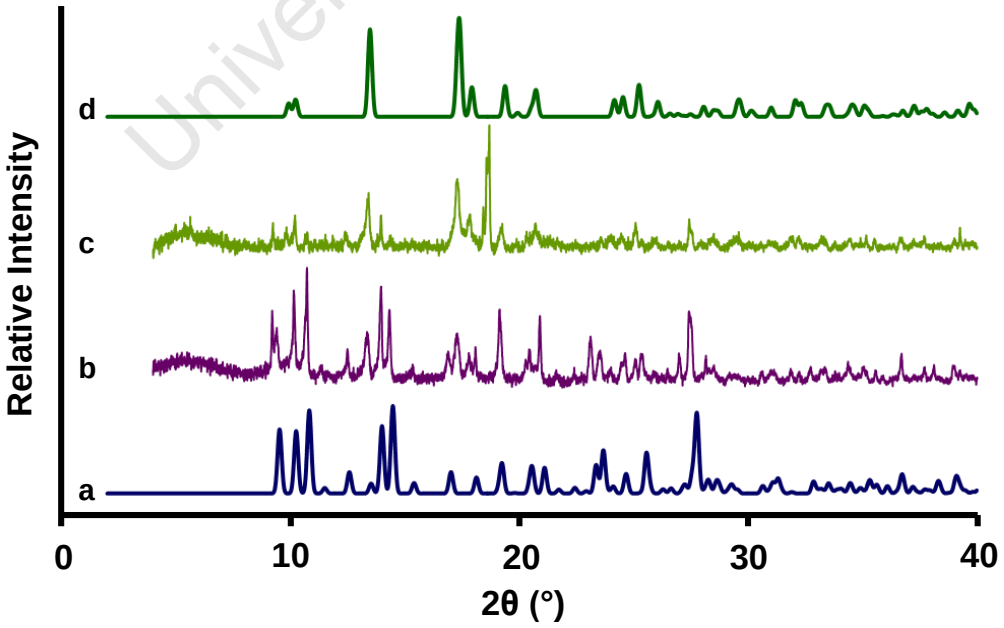

Figure 3.56: The effect of crystal size on the PXRD pattern of **3** when placed into a 0.1 mol.dm^{-3} DMF/H_2O solution of $Gd(NO_3)_3$. **a)** Calculated pattern of **3**, **b)** large crystal in solution for 4 weeks, **c)** small crystal in solution for 2 weeks and **d)** the calculated pattern of **4**

Figure 3.56c shows the PXRD trace obtained from a small (*ca* 0.6 x 0.3 x 0.2 mm) sample immersed in the solution for two weeks. The peaks for compound **3** have almost disappeared and those around 13.4 and 17.5° 2θ have increased. The pattern matches that calculated for compound **4** more closely than that of the larger crystal submerged for longer. Seven weeks of submersion in the 0.1 mol.dm^{-3} solution resulted in the majority of the sample being transformed to compound **4**. Hot-stage microscopy evidence for the effect of size is shown in Figure 3.59 in Section 3.7.2.

Separate samples with sizes of approximately 1.0 x 0.6 x 0.4 mm were submerged in solutions with a range of concentrations. The results are given in Figure 3.57. Figure 3.57b is the pattern obtained from the sample in 0.1 mol.dm^{-3} solution for 24 hours. Some new peaks have emerged in the pattern but the majority of peaks are those of compound **3**. Figure 3.57c represents a sample placed in a 0.15 mol.dm^{-3} solution for 29 hours. The peaks representative of compound **4** are apparent although there are a few peaks (10.5 and 14.3° 2θ) indicative of compound **3** still remaining. Based on the PXRD trace and results shown in Figure 3.59 of Section 3.7.2 the majority of the sample has transformed with only the centres of the original crystals remaining as compound **3**. Figure 3.57d and Figure 3.57e are for samples of **3** placed into 0.20 and 0.25 mol.dm^{-3} solutions respectively. In both cases the samples were submerged for approximately one day in the solution. A complete transformation to compound **4** is evident in both PXRD traces even in such a relatively short time frame.

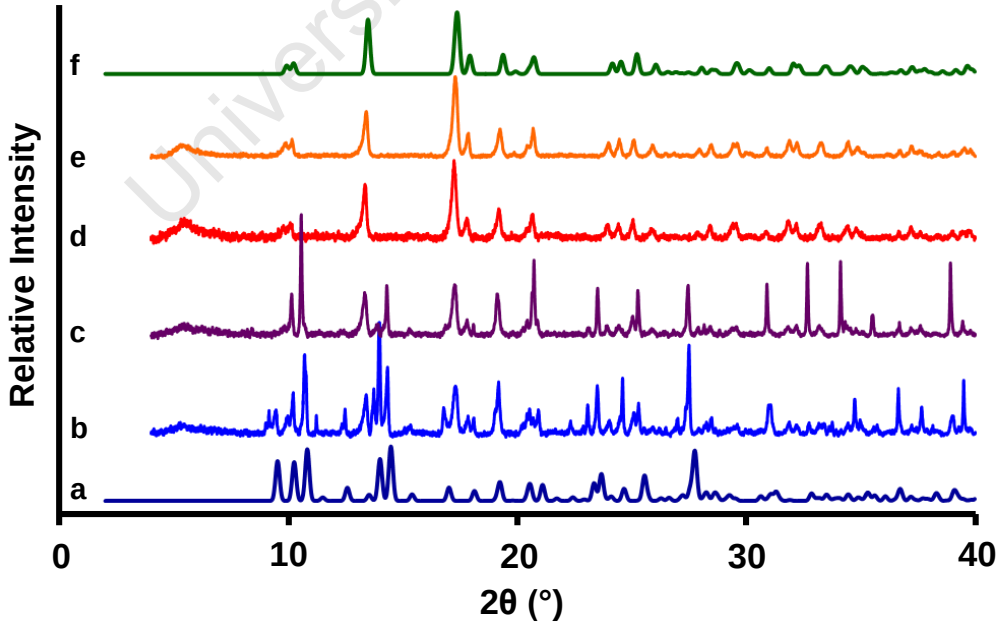

Figure 3.57: PXRD results of the effect of concentration of the gadolinium nitrate solution on the transformation of compound **3** to compound **4**. **a)** The calculated pattern for compound **3**, **b)** 24 hours in a 0.1 mol.dm^{-3} solution, **c)** 29 hours in a 0.15 mol.dm^{-3} solution, **d)** 24 hours in a 0.2 mol.dm^{-3} solution, **e)** 20 hours in 0.25 mol.dm^{-3} solution and **f)** the calculated pattern for compound **4**

However, the higher concentrations of the solutions resulted in the sample disintegrating. Examples of this disintegration are depicted in Figures 3.59 and 3.60 in Section 3.7.2.

3.7.2 CHANGE OF CRYSTAL APPEARANCE OVER TIME AT CONSTANT CONCENTRATION

The following experiments were performed on a HSM apparatus. The HSM was used to keep the temperature constant. A crystal of **3** (*ca* 0.80 x 0.65 x 0.40 mm in size) was submerged in a 0.1 mol.dm^{-3} DMF/H_2O solution of gadolinium nitrate and viewed under the hot-stage microscope. The results are presented in Figure 3.58. For PXRD results corresponding to compound **3** submerged in a 0.1 mol.dm^{-3} solution over a period of 7 weeks see Figure 3.55 in Section 3.7.1. Figure 3.58a shows the single crystal of **3** before being placed into the solution. Immediately following the addition of the gadolinium nitrate solution the crystal starts to become opaque. Figures 3.58b to 3.58k document the progress of that change over 4.5 hours.

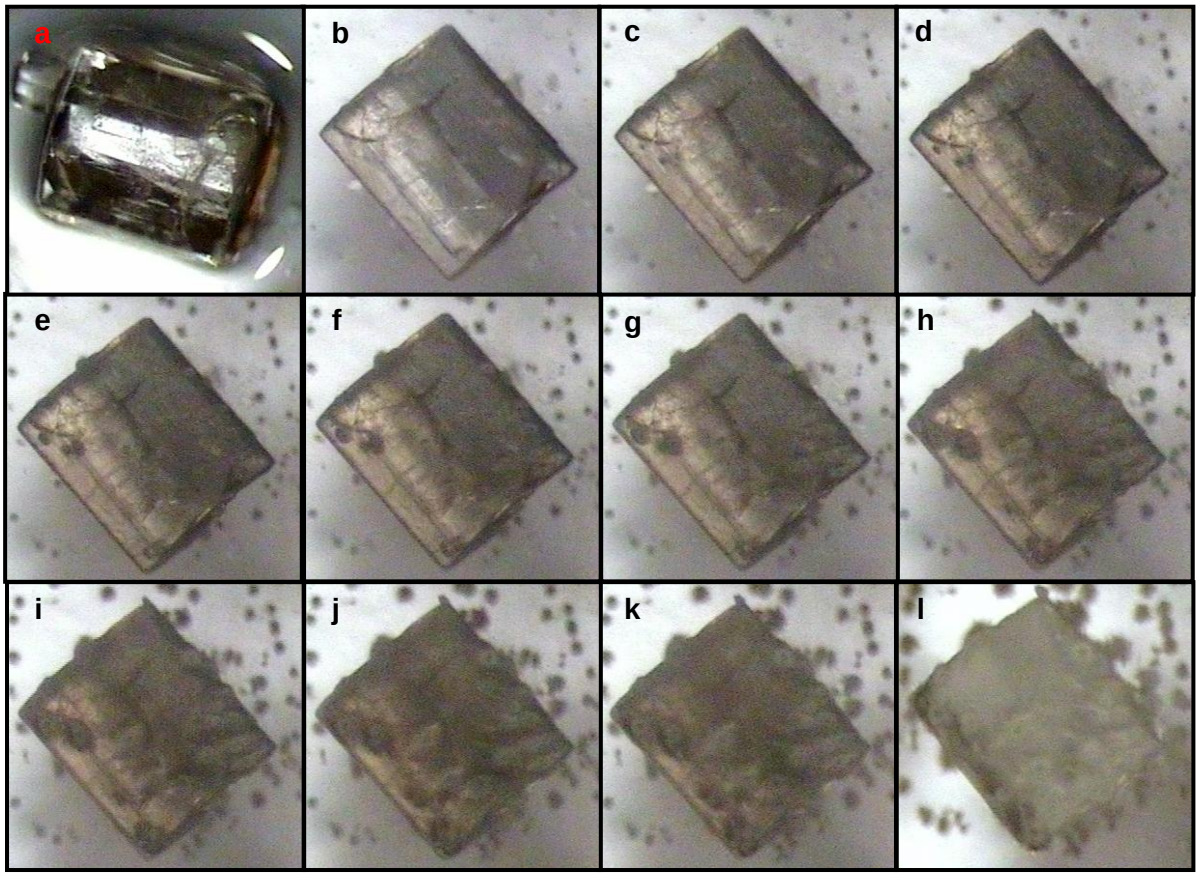

Figure 3.58: Hot-stage microscopy pictures showing the transition over 2.5 days of a *ca* 0.80 x 0.65 x 0.40 mm crystal of **3** placed into a 0.1 mol.dm^{-3} DMF/H_2O solution of $Gd(NO_3)_3$. **a)** Before addition of the solution, **b)** – **k)** over 4.5 hours and **l)** after 2.5 day of immersion

After approximately 30 minutes a dark mark appears on the surface of the crystal (Figure 3.58d). This grows over time and spreads across the surface of the crystal. By 4.5 hours of submersion the crystal is completely dark as shown in Figure 3.58k. The shape of the sample is retained however and at no point does the sample dissolve into the solution and recrystallise. The picture seen in Figure 3.58l is the same crystal after 2.5 days in the gadolinium solution. The shape of the crystal has been retained and it is now completely opaque and white. This picture matches at minimum the PXRD trace shown in Figure 3.55d, which is the combination of both compounds **3** and **4**. It can therefore be inferred that the transformation is at least partially a solid-state one. Figure 3.55e (Section 3.7.1) shows partial transformation after three days. As the crystal observed in Figure 3.58 is relatively small (*ca* 0.80 x 0.65 x 0.40 mm) a larger transformation from **3** to **4** may have occurred. The sample that was submerged in a 0.1 mol.dm^{-3} solution for seven weeks (Figure 3.55f, Section 3.7.1) retained the shape of the original crystal of compound **3**.

Figures 3.59 and 3.60 show the transformation of larger crystals when placed in 0.15 mol.dm^{-3} (Figure 3.59) and 0.25 mol.dm^{-3} (Figure 3.61) DMF/H_2O solutions of gadolinium nitrate.

Figure 3.59a–c are of smaller crystals approximately 0.40 x 0.20 x 0.15 mm in size. Figure 3.59a is the crystal of **3** within five minutes of submersion in the 0.15 mol.dm^{-3} solution. The crystal has already begun to turn opaque and small flecks of white are visible on the surface.

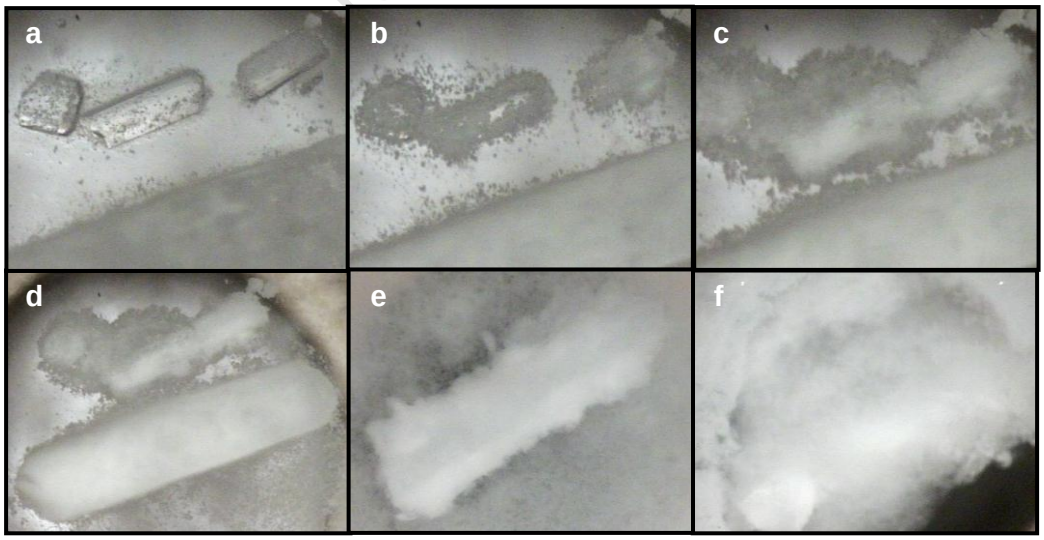

Figure 3.59: Hot-stage microscopy pictures showing the transition over 11.5 hours of a crystal of **3** placed into a 0.15 mol.dm^{-3} DMF/H_2O solution of $Gd(NO_3)_3$. **a)** – **c)** small crystals over approximately 1.5 hours and **d) – e)** a large crystal over a further 10 hours of submersion

After twenty minutes (Figure 3.59b) of immersion the surface is covered with white flecks and after an hour and twenty minutes the original shape of the crystal is almost indistinguishable. At this point the magnification was decreased and a larger crystal (*ca* 1.8 x 0.6 x 0.45 mm) was focused on. This is due to the effect of size on the length of time necessary for transformation to take place (see Figure 3.56, Section 3.7.1). The larger crystal is completely opaque but still retains its original shape. This transformation process continues slowly and after approximately six hours the larger crystal also begins to lose shape. After 11.5 hours the sample has completely disintegrated. No more changes are visible in the HSM pictures but it is probable from the results shown in Figure 3.57c (Section 3.7.1) that the feathery compound **4** particles surround small crystals of compound **3**.

Figure 3.60a is an approximately 2.00 x 0.85 x 0.65 mm size crystal of **3** before submersion. Immediately after the gadolinium nitrate solution is added (Figure 3.60b) the crystal begins to become opaque and within 15 minutes a white substance has formed on the surface of the crystal (Figure 3.60c). After 1 hour the crystal is almost indistinguishable as shown in Figure 3.60e. More white precipitate is formed on the crystal until no vestiges of the crystal shape remain as seen in Figure 3.60g. This process continues until, after 8.5 hours, no more precipitate is formed (Figure 3.60h). The precipitate is compound **4** forming on the surface of the compound **3** crystal.

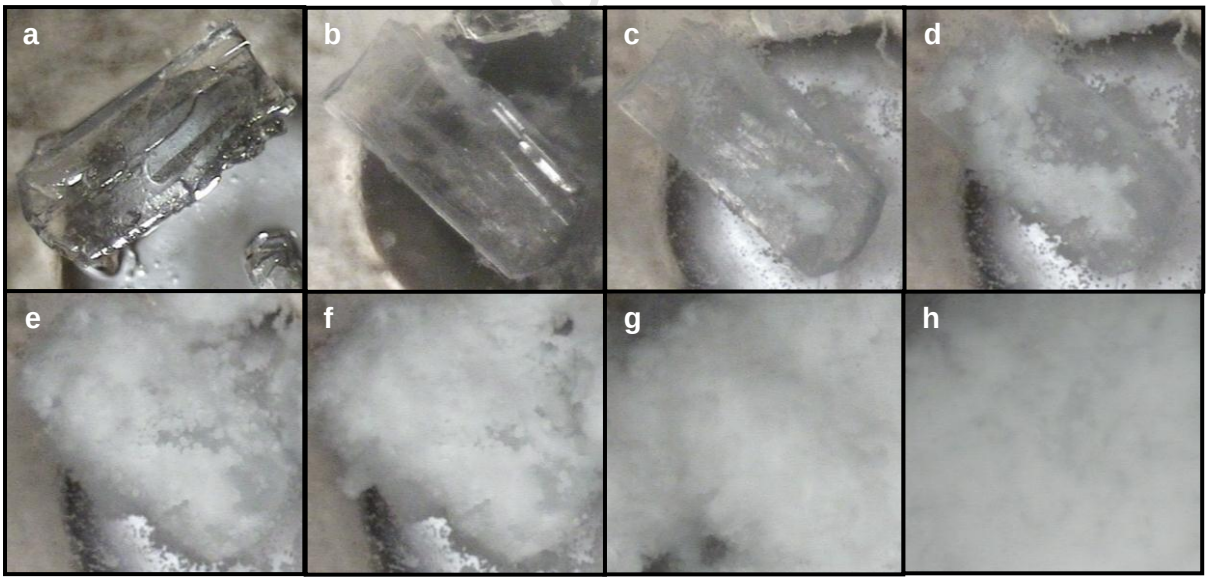

Figure 3.60: Hot-stage microscopy pictures showing the transition over 8.5 hours of a crystal of **3** placed into a 0.25 mol.dm^{-3} DMF/H_2O solution of $Gd(NO_3)_3$. **a)** Before addition of the solution and **b) – h)** over 8.5 hours of submersion

When the concentration of the gadolinium solution is too high compound **4** breaks away from the remaining crystal (compound **3**) allowing the next layer of crystal to transform. This

continues until the crystal of **3** no longer remains and the sample is entirely compound **4**. The higher the concentration used the faster this process. For the 0.1 mol.dm^{-3} the process decelerates after the initial conversion. The surface of the crystal is completely transformed to compound **4** and as this does not separate from the rest of the sample it is a slower process for the transformation to continue. This is confirmed in Section 3.7.1, Figure 3.55 as even after 7 weeks of immersion the crystal has not completely transformed in the 0.1 mol.dm^{-3} solution. For both the 0.20 and 0.25 mol.dm^{-3} there is complete transformation within 24 hours (see Figure 3.57d and e). At these higher concentrations the edges of the crystals transform to **4** and peel off and the sample no longer maintains its original shape.

3.7.3 TEST FOR TRANSFORMATION OF **4** INTO **3**

Zinc sulphate was dissolved in a 1:1, v/v DMF/H_2O solvent system to obtain a concentration of 0.25 mol.dm^{-3}. A sample of **4** was placed into this solution and left submerged for three days. The sample was then tested through PXRD as shown in Figure 3.61. This was done in order to determine whether a transformation from **4** to **3** was possible if there was a high concentration of the zinc salt in solution. It was also done to determine if compound **4** formed from **3** due solely to the high concentration of the gadolinium salt or if compound **4** was in fact the more favoured structure. As can been seen in Figure 3.61b the PXRD trace of the sample after submersion is a very good match for compound **4** and no peaks for compound **3** are visible.

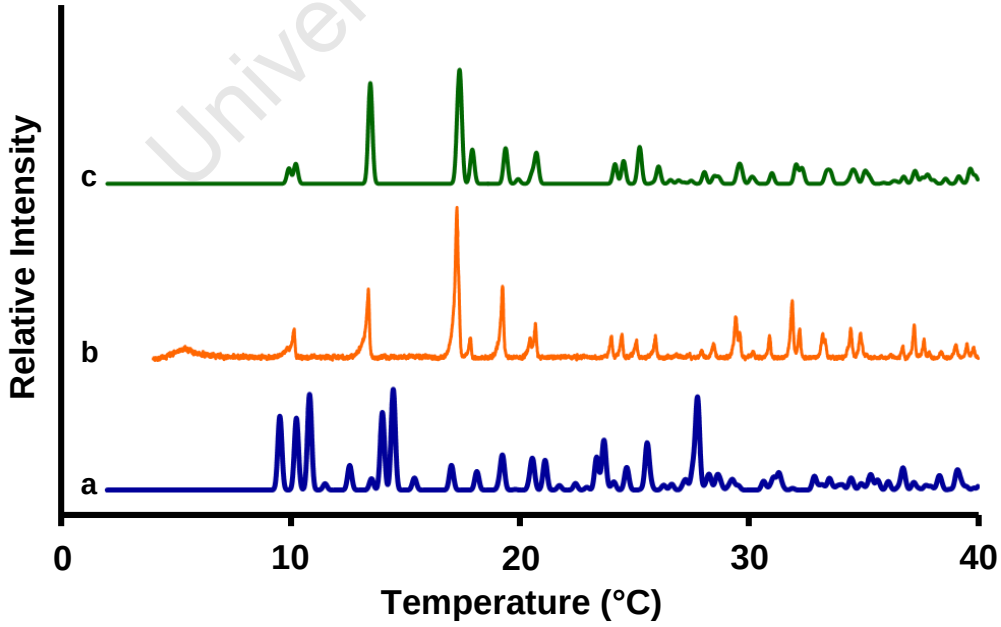

Figure 3.61: a) The calculated PXRD pattern of compound **3**, **b)** the PXRD trace obtained for a sample of **4** submerged in a 0.25 mol.dm^{-3} DMF/H_2O solution of zinc sulphate for three days and **c)** the calculated PXRD pattern of compound **4**

3.7.4 SUMMARY

When compound **3** is submerged in a solution of gadolinium nitrate it converts to compound **4**. There is the possibility that there is no exchange of metal cations but rather only a structural change. The two metal ions have very different coordination modes and so it seems unlikely that they would adopt such similar structures. There is also the fact that this exchange does not occur spontaneously in a zinc solution, or even in air, but only when the crystal is exposed to a solution containing gadolinium cations. Compound **3** is remarkably stable in both the mother liquor and in air, lasting many months without signs of degradation beyond a loss of single crystallinity in air. This leads to the conclusion that some sort of exchange has taken place. This is at least a partially solid-state transformation. Although single crystallinity is lost the crystal morphology is retained when the concentration is low enough. Compound **4** is generally microcrystalline, when formed in DMF, or forms long thin needles, when formed in DEF, (see Section 3.1). As compound **4** retains the morphology of compound **3** (a large rectangle) when formed in low concentration solutions it is probable that the compound does not dissolve in the DMF and recrystallise. At higher concentrations it is possible that the sample recrystallizes out of the DMF/H_2O solution. Compound **4** will not transform into compound **3** when placed in a solution of zinc sulphate but instead retains the structure of compound **4**.

3.8 REFERENCES

1. S. Chatterjee, V. R. Pedireddi, A. Ranganathan and C. N. R. Rao, *J. Mol. Struct.,* 2000, **520**, 107.

2. Paratone N oil, (Exxon Chemical Co., Tx, USA).

3. Cambridge Structural Database and Cambridge Structural Database System, Version 5.32, Cambridge Crystallographic Data Centre, University Chemical Laboratory, Cambridge, England, February 2011.

4. A. G. Orpen, L. Brammer, F. H. Allen, O. Kennard, D. G. Watson and R. Taylor, *J. Chem. Soc. Dalton. Trans.,* 1989, S1.

5. H. -Y. Liu, B. Zhao, W. Shi, Z. -J. Zhang, P. Cheng, D. -Z. Liao and S. -P. Yan, *Eur. J. Inorg. Chem.,* 2009, 2599.

6. J. He, Y. Zhang, Q. Pan, J. Yu, H. Ding and R. Xu, *Microporous and Mesoporous Materials,* 2006, **90**, 145.

7. J. Chen, M. Ohba and S. Kitagawa, *Chem. Lett.,* 2006, **35**, 526.

8. C. -T. Yeh, H. -K. Liu, C. -J. Lin and C. -H. Lin, *Acta Cryst. E,* 2010, **E66**, m1289.

9. http://www.ccdc.com.ac.uk/products/csd/radii, accessed 7 October 2011.

10. O. M. Yaghi, H. Li and T. L. Groy, *J. Am. Chem. Soc.,* 1996, **118**, 9096.

11. *Electron Microscope Unit, University of Cape Town*.

12. A. L. Spek, Program PLATON, A Multipurpose Crystallographic Tool, Version 10500, © 1980 - 2000, Utrecht University, The Netherlands.

13. A. L. Spek, *J. Appl. Cryst.,* 2003, **36**, 7.

14. S. R. Byrn, R. R. Pfeiffer and J. G. Stowell, in *Solid-State Chemistry of Drugs,* SSCI, Inc., Indiana, USA, 1999, pp.443.

15. N. L. Rosi, J. Kim, M. Eddaoudi, B. Chen, M. O'Keeffe and O. M. Yaghi, *J. Am. Chem. Soc.,* 2005, **127**, 1504.

16. B. Arstad, H. Fjellvåg, K. O. Kongshaug, O. Swang and R. Blom, *Adsorption,* 2008, **14**, 755.

17. M. Dincă, A. Dailly, Y. Liu, C. M. Brown, D. A. Neumann and J. R. Long, *J. Am. Chem. Soc.,* 2006, **128**, 16876.

18. T. Sagara, J. Ortony and E. Ganz, *J. Chem. Phys.,* 2005, **123**, 214707.

19. C. Daiguebonne, O. Guilloa, Y. Gérault, A. Lecerf and K. Boubekeur, *Inorg. Chim. Acta,* 1999, **284**, 139.

20. Y. -H. Wen, J. -K. Cheng, Y. -L. Feng, J. Zhang, Z. -J. Li and Y. -G. Yao, *Chinese J. Struct. Chem.,* 2005, **24**, 1440.

21. X.. Cui, A. N. Khlobystov, X. Chen, D. H. Marsh, A. J. Blake, W. Lewis, N. R. Champness, C. J. Roberts, M. Schröder, *Chem. Eur. J.,* 2009, **15**, 8861.

Chapter 4

5-Nitroisophthalate Compounds

Three compounds prepared from 5-nitroisophthalic acid and gadolinium(III) nitrate hexahydrate are discussed in this chapter. No complexes were obtained from 5-nitroisophthalic acid and zinc(II) sulphate heptahydrate. The sections are divided by compound and the full characterisation using single crystal and powder X-ray diffraction, thermal analysis is given in the relevant section for each compound.

Three new compounds were prepared from 5-nitroisophthalic acid (H_2NIA) and gadolinium(III) nitrate hexahydrate. $[Gd(NIA)_{1.5}(DMF)_2]\cdot DMF$ (**5**), $[Gd_2(NIA)_3(DMF)_4]\cdot 2.67H_2O$ (**6**) and $[Gd_4(NIA)_6(DMF)_{5.5}(H_2O)_3]\cdot 4DMF\cdot H_2O$ (**7**). The powder X-ray diffraction patterns (PXRD) calculated from single crystal data for each of these compounds are given in Figure 4.1. Further details of the methods of preparation are provided in Section 4.1.

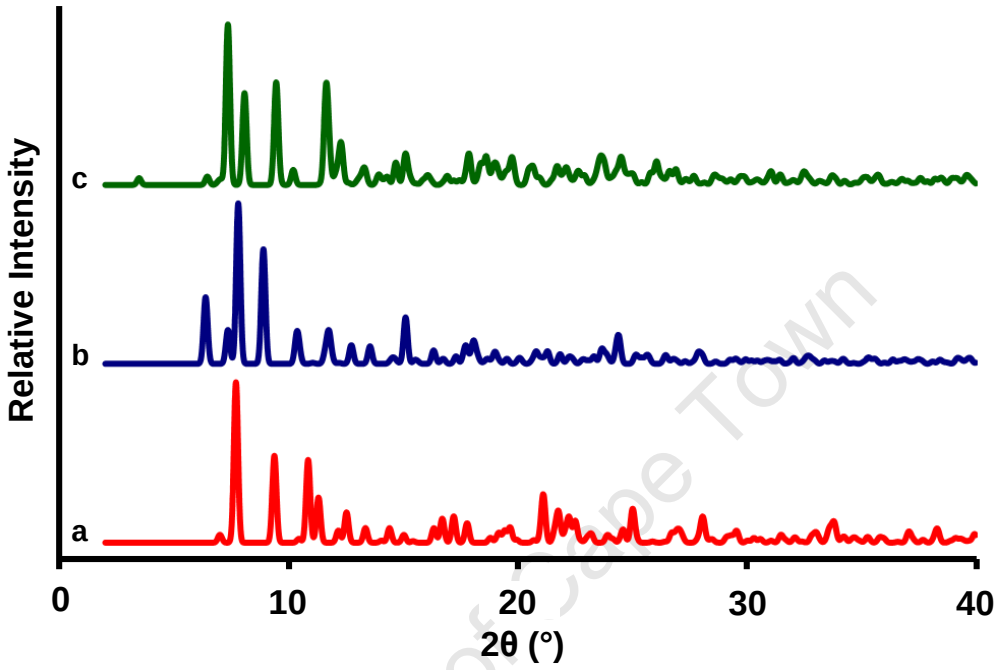

Figure 4.1: The PXRD patterns calculated from single crystal data for **a) 5** – red, **b) 6** – blue and **c) 7** – green

Attempts were made to prepare compounds from H_2NIA and zinc(II) sulphate heptahydrate but these were unsuccessful. Very thin plate-like crystals were visible in the reaction container. They could be due to the ligand alone or complexation may have occurred. These dissolved when handled however, and no analyses could be performed. Approximately 500 coordination polymers containing a transition metal and 1,3-benzenedicarboxylate are reported in the Cambridge Structural Database.[1] In comparison only *ca* 110 coordination polymers are reported that contain transition metals and H_2NIA. The majority of these structures contain a mixture of ligands with the additional ligand most often coordinating through a nitrogen atom. Only thirteen of these compounds contain H_2NIA only as a ligand.[2-11] Two of those thirteen contain zinc metal ions demonstrating that zinc-NIA structures are plausible.[2,7] However, zinc nitrate[7] was used for the preparation of one while zinc chloride was used for the preparation of the other.[2] The methods were also significantly different to those used in this thesis with both compounds prepared using aqueous solutions, high-pressure sealed bombs and high temperatures.

4.1 PREPARATION OF GADOLINIUM(III) AND 5-NITROISOPHTHALATE COMPOUNDS

Several methods were employed in the preparation of compounds **5**, **6** and **7** and these are listed below. In methods 1a and 1b H_2NIA was dissolved in a given amount of *N*,*N*'-dimethylformamide (DMF) and gadolinium(III) nitrate hexhydrate was dissolved in an equal volume of water. In methods 2a, 2b, 2c and 3 both starting materials were dissolved in equal volumes of DMF. The starting materials were dissolved at 60 °C with stirring for all methods. The two solutions were then filtered into the same vial.

Method 1:

1. The vial was closed and sealed with parafilm
2. Placed in an oil bath and held at 60 °C for 24 hours
3. Cooled to room temperature over 48 hours (0.83 °C/hour)
4. The vial was partially opened to the atmosphere once cooled to room temperature to allow for slow evaporation

For method 1a a metal to ligand ratio of 1:1 was used while for method 1b a ratio of 2:3 was used.

Method 2:

1. The vial was closed and sealed with parafilm
2. Placed in an oven at 80 °C
3. Kept at 80 °C until crystals formed

A metal to ligand ratio of 1:1 was used for method 2a, while for method 2b a ratio of 2:1 was used and for method 2c a ratio of 1:2 was used.

Method 3:

1. The vial was closed and sealed with parafilm
2. Placed in a Dewar containing water at a temperature of 70 °C
3. The Dewar was sealed and allowed to cool slowly
4. The vial was partially opened to the atmosphere once cooled to room temperature to allow for slow evaporation

A 1:1 metal to ligand ratio was used for method 3.

For all methods a 1:1 v/v ratio of the either the H_2O/DMF or DMF/DMF solvent system was used. The amount of solvent used to dissolve each starting material was varied from 0.5 – 2.5 ml in increments of 0.5 ml. This resulted in a total volume of 1 – 5 ml increasing in increments of 1 ml. Some experiments using method 1b were performed with a 0.5 ml solvent volume in the final solution. Methods 1a and 1b used H_2O to dissolve the metal salt and DMF to dissolve the ligand. Methods 2a – 3 used DMF as the solvent for both the metal salt and the ligand.

The compounds obtained for methods 1a, 2a and 3 at varying concentrations are given in Table 4.1. The concentration reported is that for all starting materials in the final solution. There are no obvious trends with concentration for any of these methods. Methods 2a and 3 produce compound **5** in a large majority. Method 1a yields mostly compound **6** although the majority of samples obtained were of poor diffraction quality.

Table 4.1: Concentrations and results for the gadolinium-NIA compounds using methods 1a, 2a and 3

Concentration ($mol.dm^{-3}$)	Method 1a	Method 2a	Method 3
0.032±2	6	5	5
0.038±2	7	5	5
0.047±2	6	5	5
0.063±3	6/7	5	5
0.076±2	5	6	5
0.095±5	5	5/6	5
0.114±2	6	5	5
0.127±3	6	6	5/6
0.142±2	5	5	5
0.154±6	6	5	5
0.190±9	6	5/6	5
0.222±2	5	5	5
0.237±2	6	5	5
0.253±6	6	7	5
0.266±2	6	5	5
0.285±5	6	6	5
0.317±3	6	5	5
0.332±3	-	5	6
0.38±1	6	5	5
0.443±4	6	5	-
0.475±5	6	5	5
0.570±9	6	-	5
0.665±5	6	-	-
0.760±9	6	-	5/6
0.95±1	6	-	-

* "/" indicates a mixture of compounds were obtained, No attempt to determine relative amounts was made

The compounds produced for methods 1b, 2b and 2c at varying concentrations are given in Table 4.2. As the ratio of metal to ligand is not 1:1 for any of these methods the concentration of starting materials is not reported as a single value. Rather the concentration

of each starting material in the final solution is given. Again there are no clear trends although both 2b and 2c yield compound **5** for the majority of experiments. The metal to ligand ratio in compounds **5**, **6** and **7** is 2:3. However, the metal to ligand ratio in the starting solution does not appear to have a large effect on the results. Method 1b uses the same metal to ligand ratio of 2:3 that is found in the final compounds. It appears to favour the formation of compound **6**, however method 1a produces compound **6** in a larger percentage (Figure 4.2a) than method 1b despite 1a having a metal to ligand ratio of 1:1.

Table 4.2: Concentrations (in mol.dm^{-3}) and results for the gadolinium-NIA compounds using methods 1b, 2b and 2c.

Method 1b (M:L, 2:3)			Method 2b (M:L, 2:1)			Method 2c (1:2)		
Gd	H_2NIA	Result	Gd	H_2NIA	Result	Gd	H_2NIA	Result
0.0120±4	0.019±1	5	0.0191±4	0.009±1	Amorphous	0.0191±4	0.038±1	5
0.015±1	0.024±1	6	0.024±1	0.012±1	Amorphous	0.024±1	0.047±1	5
0.020±1	0.032±2	5/6	0.0381±4	0.019±1	Amorphous	0.0318±7	0.063±2	5
0.0239±4	0.038±1	6	0.0476±6	0.024±1	Amorphous	0.0381±4	0.076±1	5
0.030±1	0.047±2	6	0.064±1	0.032±2	5	0.0476±4	0.095±1	5
0.0359±4	0.057±1	6	0.0953±4	0.047±1	5	0.0572±4	0.114±1	5
0.040±1	0.063±2	5/6	0.1143±4	0.057±1	5	0.064±1	0.126±2	5
0.045±1	0.071±1	6	0.1429±6	0.071±1	5	0.071±1	0.142±1	5
0.060±2	0.095±5	5/6	0.191±2	0.095±5	5/7	0.095±2	0.189±5	5/6
0.090±1	0.142±2	6	0.238±1	0.118±2	Amorphous	0.119±1	0.237±1	5
0.120±4	0.189±9	5/6	0.254±1	0.126±2	6	0.159±1	0.316±2	5
0.179±2	0.284±5	5	0.286±2	0.142±5	5	0.191±2	0.379±5	5
0.239±4	0.379±9	5/7	0.318±1	0.158±2	5	0.238±2	0.474±5	5
0.359±4	0.568±9	7	0.381±2	0.189±5	5/7	0.476±2	0.947±5	5
			0.476±2	0.237±5	Amorphous			
			0.572±2	0.284±5	Amorphous			
			0.953±2	0.474±5	Amorphous			

* "/" indicates a mixture of compounds were obtained, no attempt to determine relative amounts was made; ** Concentrations reported are for the relevant starting material in the final solution

Figure 4.2 shows the results obtained for all methods with compounds **5**, **6** and **7** given in red, blue, and green, respectively. The percentage of the total experiments that produced each compound is given in Figure 4.2a. Figure 4.2b shows the total number of experiments performed and the number of experiments that produced each compound. Tables 4.1 and 4.2 do not reflect all experiments but only whether a product was formed at a specific concentration. As a result there may be some discrepancies between the total number of experiments for each method (Figure 4.2b) and the number of products shown in the tables. The experiments that resulted in amorphous material have not been included in the figures. The trends observed for each method are described in greater detail in the following sections. These trends are based on the number of experiments at a specific concentration in which a compound was formed. When more than one compound was formed in a single experiment it is taken into account. When mixtures of crystals occurred in a single vial the

relative amounts of each compound were not determined. Studies were performed with PXRD.

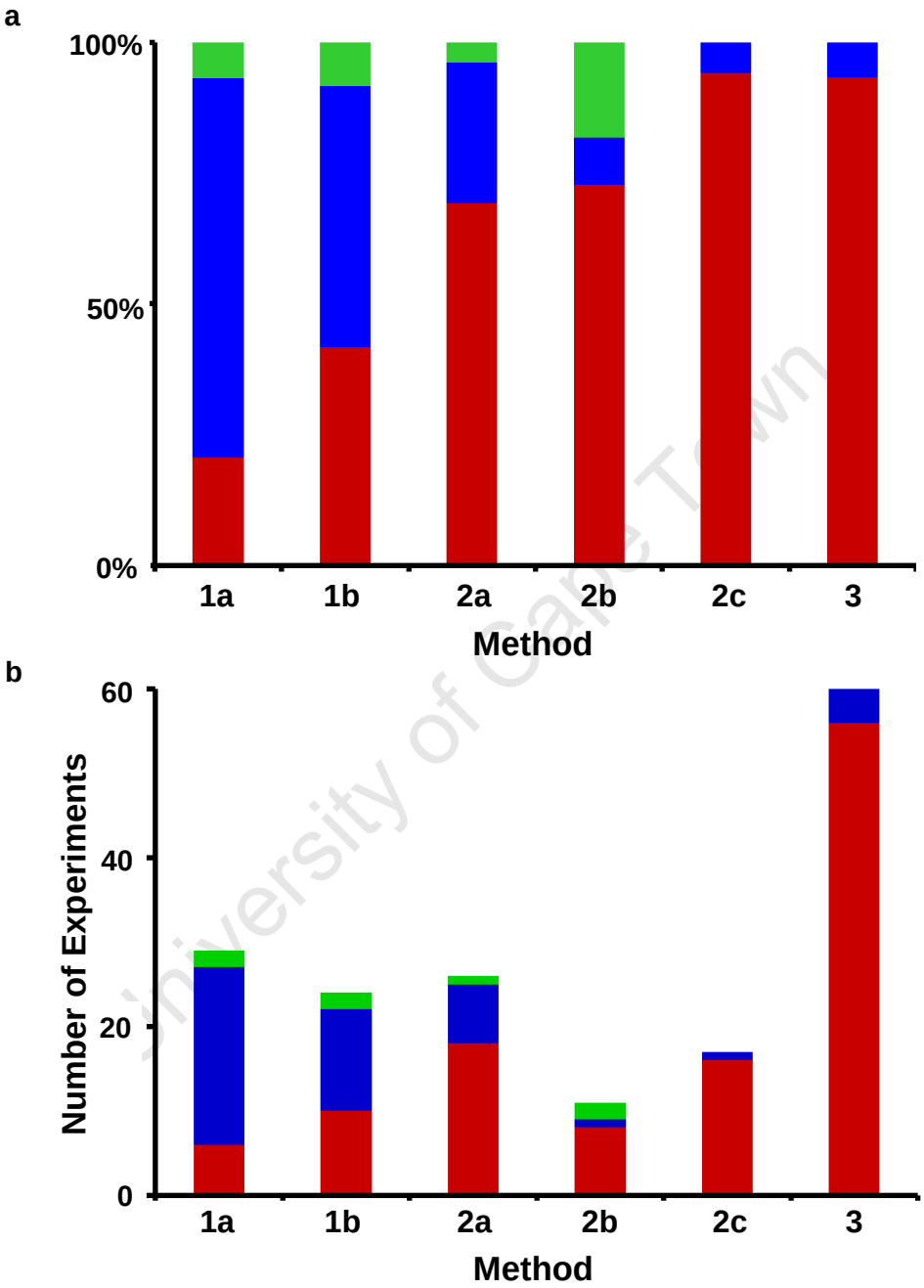

Figure 4.2: The number of times that compounds **5**, **6** and **7** were obtained for each method in terms of **a)** percentage and **b)** number of experiments. Compound **5** is shown in red, compound **6** in blue and compound **7** in green

4.1.1 METHOD 1

For methods 1a and 1b the sample is held at 60 °C for 24 hours before being cooled slowly to room temperature. The metal to ligand ratio is varied but does not appear to have much effect on the outcome of the reaction. Approximately the same ratio of the three compounds is obtained with both the 1:1 (1a) and 2:3 (1b) methods. There is no clear trend in the yield with respect to concentration of the starting materials. For method 1a compound **7** was formed at low concentrations but only in two experiments. Compound **6** is formed the majority of the time and over a range of concentrations. Compound **5** is not produced as often as **6** and appear to form at lower concentrations. For method 1b compound **7** was formed at high concentrations, but again only in two experiments. Compounds **5** and **6** are both spread over a large concentration range with compound **5** having the larger range for this method. More experiments resulted in compound **6** than compound **5** as was found for method 1a.

4.1.2 METHOD 2

For methods 2a, 2b and 2c the vial containing the sample is held at 80 °C and held at that temperature until crystals grow. The metal to ligand ratio is varied and this appears to have some effect. For all three methods the majority product is compound **5**. For method 2a one experiment produced compound **7** while compound **7** was obtained in two experiments for method 2b. Compound **6** was produced for experiments with all three methods, generally at concentrations in the middle of the range. In general the quality of samples obtained from methods 2a, 2b and 2c was poor. Method 2b often produced only amorphous material.

4.1.3 METHOD 3

For method 3 a 1:1 metal to ligand ratio is used. The samples are allowed to cool slowly to room temperature immediately after the two solutions are combined. Compound **5** was produced almost exclusively with only four experiments giving compound **6**. These are spread across the concentration range and therefore no correlations between concentration and product can be determined. The largest number of experiments were performed with method 3 and results were consistent. None of compound **7** was formed in any of the experiments using method 3.

4.1.4 SUMMARY

Compound **5** was formed with all methods and using methods 2a, 2b, 2c and 3 it was the majority product. It appears that compound **5** is the thermodynamically favoured product. When the solution was cooled immediately (method 3) compound **5** is formed almost exclusively. However, even with a constant input of heat (methods 2a – 2c) compound **5** was the majority product. The solutions were held at elevated temperatures for methods 1a and 1b. In these methods the high temperature was combined with controlled, slow cooling resulting mostly in compound **6**. It is a combination of both high temperatures and controlled cooling that allows compound **6** to form. Compound **7** forms sporadically and is much more unlikely to form than either **5** or **6**. The trends found are unsurprising when the structures of compounds **5**, **6** and **7** are studied. The structure of **5** is much more symmetrical and will be favoured. Compound **6** is also quite symmetrical, although it has reduced symmetry compared to **5**. Rotation around a C-C bond is required for **6** to form. This rotation is perhaps more likely to occur at higher temperatures. Slow cooling of the substance after the rotation has had a chance to occur is more likely to result in compound **6** (methods 1a and 1b). Compound **7** requires the rotation to have occurred in some of the secondary-building units (SBUs) and not to have occurred in others. This reduces the symmetry of the structure further. As a result it is unsurprising that so few experiments produced compound **7**. See the structure descriptions in this chapter as well as Chapter 5.7 (The Relationship Between **5** and **6**) for further details.

It is interesting to note that although compounds **5**, **6** and **7** all have metal to ligand ratios of 2:3 when compound **5** is formed it is usually the only material produced. For compounds **6** and **7** the crystals are often obtained with a mixture of starting materials and poor quality, almost amorphous material.

4.2 DATA COLLECTION PROCEDURE FOR 5-NITROISOPHTHALATE COMPOUNDS

Compounds **6** and **7** formed conglomerates of single crystals and were therefore cut to isolate a monocrystaline fragment of suitable size for data collection. All crystals of **5**, **6** and **7** were immediately covered in Paratone N oil[12] to prevent degradation and the loss of solvent molecules. The crystal was then placed on the rigid mounting of a nylon loop to allow for low-temperature data collection. The single crystal X-ray diffraction data were collected at 173(2) K using MoKα radiation. For compounds **5** and **6** this was done on the Nonius Kappa CCD diffractometer. For compound **7** this was done on the Bruker KAPPA APEX II DUO

diffractometer. For full details see Chapter 2.5.1 – Single Crystal X-ray Diffraction. Full data collections parameters are given for each compound in the relevant sections of this chapter.

4.3 $[Gd(NIA)_{1.5}(DMF)_2]\cdot DMF$ (5)

4.3.1 SINGLE CRYSTAL X-RAY DIFFRACTION ANALYSIS

The hydrogen atoms were placed in idealised positions in a riding model. They were refined isotropically and assigned temperature factors relating to the atom they are attached to. The temperature factors are 1.2 times the parent atom for phenyl hydrogen atoms and 1.5 times the parent atom for methyl hydrogen atoms.

Compound **5** crystallises in the monoclinic crystal system, in the space group *C*2/*c*. **5** is a neutral metal-organic framework. Crystal data and refinement paratmeters are given in Table 4.3.

Table 4.3: Crystal data and refinement parameters of **5**

Empirical Formula	$C_{21}H_{25.5}GdN_{4.5}O_{12}$
Formula Weight (g.mol^{-1})	690.21
Temperature (K)	173(2)
Wavelength (Å)	0.71073
Crystal System	Monoclinic
Space Group	*C*2/*c*
a (Å)	21.622(4)
b (Å)	16.800(3)
c (Å)	16.317(3)
α (°)	90
β (°)	119.628(4)
γ (°)	90
Volume (Å^3)	5152(2)
Z	8
Calculated Density (g.cm^{-3})	1.780
***μ* (mm^{-1})**	2.645
***F* (*000*)**	2744
Crystal Size (mm)	0.30 x 0.25 x 0.20
***Θ* Range Scanned (°)**	2.82 – 30.51
Index Range	-30 < h < 22, -23 < k < 21, -11 < l < 23
No. Reflections Collected	32987
No. Unique Reflections	7835
R_{int}	0.0225
Data Completeness to θ_{max} (%)	99.7
Refinement Method	Full-matrix least-squares on F^2
Data/Restraints/Parameters	7835/0/355
Goodness-of-fit on F^2	1.060
Final *R* Indices [*I*>2σ(*I*)]	R_1 = 0.0193, wR_2 = 0.0484
***R* Indices (all data)**	R_1 = 0.0240, wR_2 = 0.0507
Largest Diff. Peak and Hole (*e*.Å^{-3})	1.195, -0.981

Figure 4.3 shows the asymmetric unit of **5** with hydrogen atoms excluded for clarity. The asymmetric unit consists of one gadolinium metal ion, one and a half fully deprotonated NIA molecules, two coordinated DMF molecules and one guest DMF molecule.

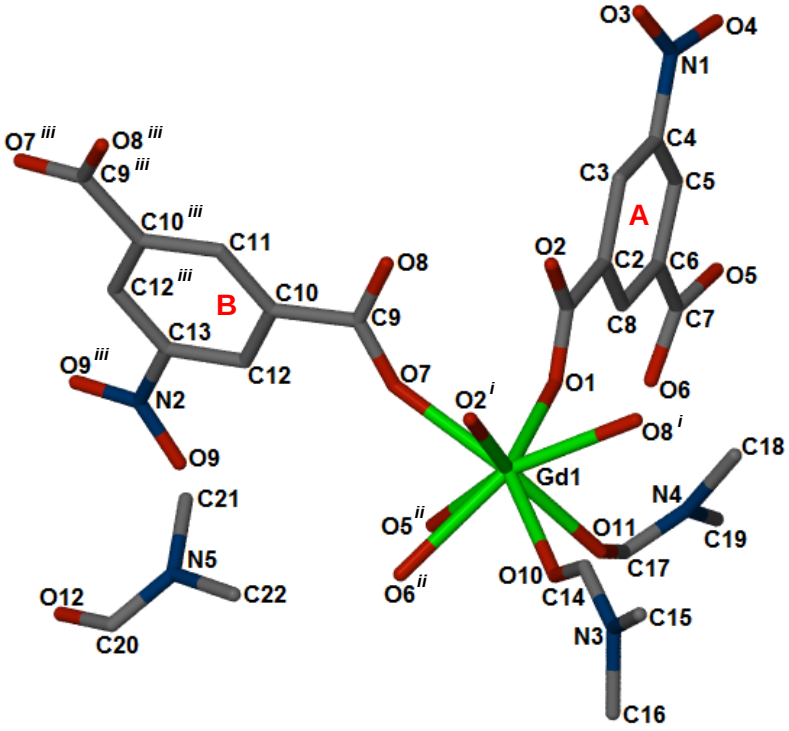

Figure 4.3: The asymmetric unit of **5** with the hydrogen atoms omitted for clarity

The Gd1 metal ion is coordinated to 8 oxygen atoms in a distorted square, antiprismatic manner as shown in Figure 4.4. Four oxygen atoms are from bridging carboxylate moieties (O1, O2^{i}, O7, O8^{i}), two are from a bidentate, chelating carboxylate moiety (O5^{ii}, O6^{ii}) and two are from DMF molecules (O10, O11). O1, O2^{i}, O7 and O8 form one square and are given in blue in the figure while O5^{ii}, O6^{ii}, O10 and O11 form the other square and are shown in purple. Gd-O distances are given in Table 4.4 and correlate well with previously reported structures found in the Cambridge Structural Database[1] (CSD).

Table 4.4: Experimental Gd-O bond lengths for **5** and literature Gd-O bond lengths

Bond	Length (Å)	Average Length (Å)	Bond Type
Gd1-O1	2.387(2)	2.35 ± 0.06*	Terminal Carboxylate
Gd1-O2^{i}	2.323(1)		
Gd1-O7	2.353(2)		
Gd1-O8^{i}	2.390(1)		
Gd1-O5^{ii}	2.514(1)	2.52 ± 0.09*	Chelating Carboxylate
Gd1-O6^{ii}	2.448(1)		
Gd1-O10	2.362(2)	2.38 ± 0.04*	DMF
Gd1-O11	2.439(2)		

* Values obtained from the CSD

Related by symmetry: ^{i}1/2-x, 1/2-y, -z; ^{ii}x, 1-y, 1/2+z; ^{iii}1-x, y, 1/2-z; ^{iv}x, 1-y, -1/2+z; ^{v}1/2+x, 1/2-y, 1/2+z; ^{vi}-1/2+x, 1/2-y, -1/2+z; ^{vii}1/2-x, -1/2+y, -1/2-z; ^{viii}x, -y, -1/2+z; ^{ix}-x, y, -1/2-z; ^{x}1/2-x, 1/2+y, 1/2-z; ^{xi}1/2+x, 1/2-y, 1/2+z; ^{xii}1/2-x, -1/2+y, 1/2-z

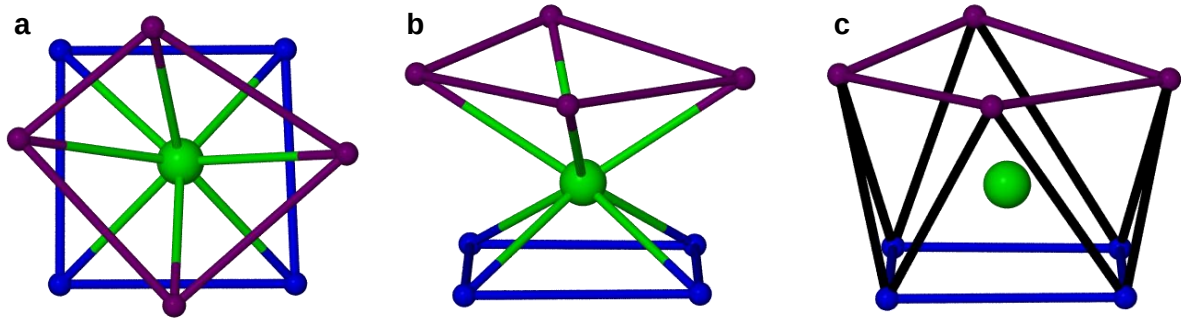

Figure 4.4: The distorted square antiprismatic geometry adopted by the Gd1 metal centre. The O5^{ii}, O6^{ii}, O10 and O11 oxygen atoms are shown in purple while the O1, O2^{i}, O7 and O8^{i} oxygen atoms are shown in blue. **a)** shows the top and bottom square faces of the antiprism, **b)** shows the a side on view of the two faces, **c)** shows the square antiprism with the Gd1 metal centre located at the centre

The O1-C1-O2 carboxylate moiety of NIA A bridges Gd1 and Gd1^{i} and is singly coordinated to each metal centre. The O5-C7-O6 carboxylate moiety is coordinated to Gd1^{iv} in a bidentate fashion. NIA B is located on a twofold rotation axis with C11, C13 and N2 situated on the twofold axis. The O7-C9-O8 carboxylate moiety is related to the O7^{iii}-C9^{iii}-O8^{iii} carboxylate by the twofold rotation axis. The O7-C9-O8 carboxylate bridges Gd1 and Gd1^{i} while O7^{iii}-C9^{iii}-O8^{iii} bridges Gd1^{iii} and Gd1^{v}. The nitro groups are uncoordinated for both NIA A and NIA B.

Four fully deprotonated NIA units – two NIA A and two NIA B – bridge the Gd1 and Gd1^{i} metal dimer in a paddle-wheel fashion (see Chapter 1.2.2 – Secondary-Building Units). A further two NIA A units are bound in a bidentate fashion through one carboxylate moiety to each metal centre. The Gd1/Gd1^{i} metal pair acts as a secondary-building unit (SBU) comprising the four bridging NIA units, two bidentate chelating NIA units and four DMF molecules. This secondary-building unit, with DMF molecules omitted for clarity, is shown in Figure 4.5. Each NIA unit acts as a connector to another SBU and the SBUs are joined in an octahedral fashion. The topology that arises from this SBU is discussed in greater detail in Chapter 5 – Topological Studies.

5 forms a three-dimensional framework with channels along the [010] direction. These channels are occupied by coordinated (O10, O11) and guest (O12) DMF molecules. The O10 and O11 coordinated DMF molecules also lie in channels along [001]. The coordinated DMF molecules help to shape the channels along the [010] and [001] directions. The DMF molecules can be removed at elevated temperatures but after the removal of the first DMF the structure starts to change and eventually collapses. For further details see Sections 4.3.2 and 4.3.3 – Thermal Analysis and Powder X-ray Diffraction.

Related by symmetry: ^{i}1/2-x, 1/2-y, -z; ^{ii}x, 1-y, 1/2+z; ^{iii}1-x, y, 1/2-z; ^{iv}x, 1-y, -1/2+z; ^{v}1/2+x, 1/2-y, 1/2+z; ^{vi}-1/2+x, 1/2-y, -1/2+z; ^{vii}1/2-x, -1/2+y, -1/2-z; ^{viii}x, -y, -1/2+z; ^{ix}-x, y, -1/2-z; ^{x}1/2-x, 1/2+y, 1/2-z; ^{xi}1/2+x, 1/2-y, 1/2+z; ^{xii}1/2-x, -1/2+y, 1/2-z

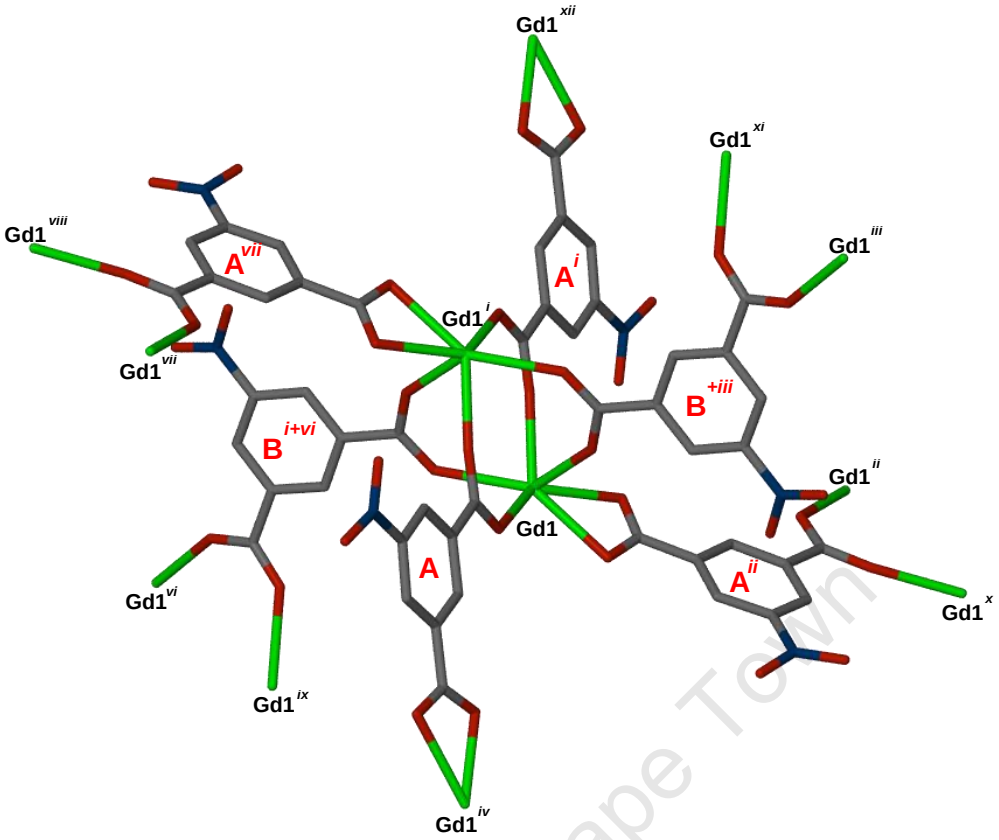

Figure 4.5: The Gd1/Gd1^{i} secondary-building unit (SBU) of compound **5** where NIA A, NIA A^{i}, NIA B/B^{iii} and NIA B^{i}/B^{vi} form the paddle-wheel and NIA A^{ii} and NIA A^{vii} are axially coordinated. The DMF molecules are omitted for clarity

Figure 4.6 shows the framework of **5** viewed along the [010] axis. The framework is shown in black and the symmetry elements present in the *C*2/*c* space group are given in red. The symbols are explained in the figure. The inversion centres at (0,0,0), (0,1/2,0), (0,0,1/2), (0,1/2,1/2), (1/2,0,1/2), (1/2,1/2,1/2), (1/2,0,0) and (1/2,1/2,0) are located in the centre of the channels along [010] and between the nitrogen atoms of O10 DMF molecules. The (1/4,1/4,0), (3/4,3/4,0), (1/4,3/4,1/2) and (3/4,1/4,1/2) inversion centres are between the metal centres in the Gd1 dimers. The (1/4,3/4,0), (3/4,1/4,0), (1/4,1/4,1/2) and (3/4,3/4,1/2) inversion centres are located between the nitro moieties of two NIA A units.

The four different positions for the twofold rotation axes are (0,y,1/4), (0,y,3/4), (1/2,y,1/4) and (1/2,y,3/4). All pass through C11, C13 and N2 of the NIA B unit. The four positions for the twofold screw axes are (1/4,y,1/4), (1/4,y,3/4), (3/4,y,1/4) and (3/4,y,3/4). These all pass between the benzene rings of NIA A units. There are no solvent accessible voids for compound **5** aside from those containing the O10, O11 and O12 DMF molecules. This was determined by the program Platon.[13,14]

Related by symmetry: ^{i}1/2-x, 1/2-y, -z; ^{ii}x, 1-y, 1/2+z; ^{iii}1-x, y, 1/2-z; ^{iv}x, 1-y, -1/2+z; ^{v}1/2+x, 1/2-y, 1/2+z; ^{vi}-1/2+x, 1/2-y, -1/2+z; ^{vii}1/2-x, -1/2+y, -1/2-z; ^{viii}x, -y, -1/2+z; ^{ix}-x, y, -1/2-z; ^{x}1/2-x, 1/2+y, 1/2-z; ^{xi}1/2+x, 1/2-y, 1/2+z; ^{xii}1/2-x, -1/2+y, 1/2-z

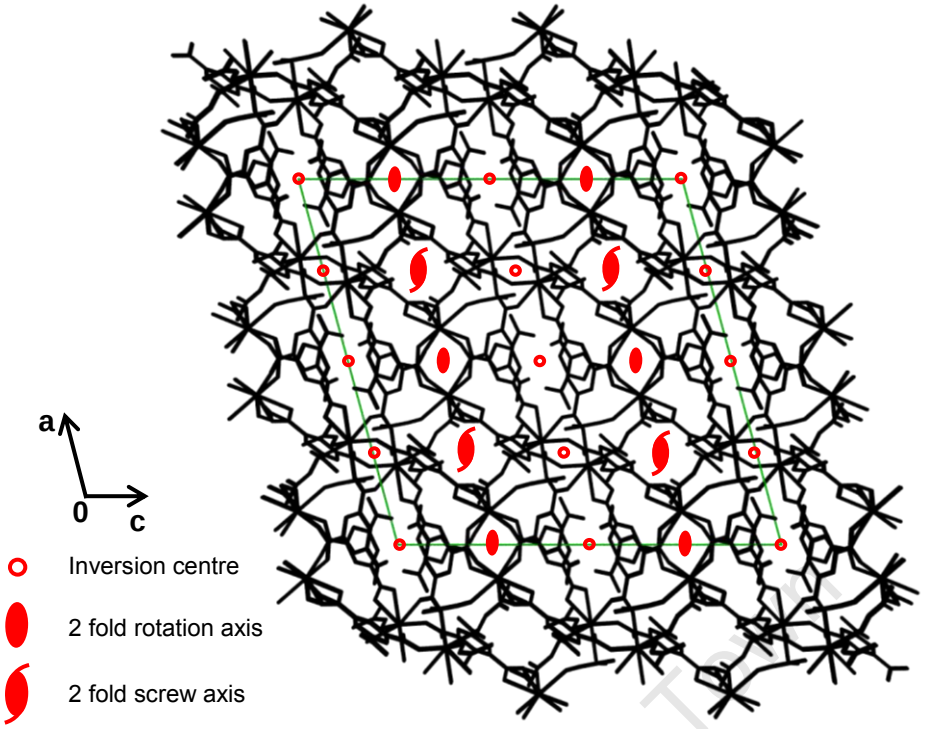

Figure 4.6: The packing diagram of **5** as viewed down [010] is shown in black with an overlay of the symmetry elements in the unit cell given in red

The packing diagram of compound **5** viewed along [100], [010] and [001] is given in Figures 4.7a, b, and c respectively with the guest O12 DMF molecules omitted. A void space of 1026.6 Å^3 per unit cell is determined when the O12 guest DMF molecule is deleted from the structure. This fits well with expectations as there are 8 O12 DMF molecules per unit cell. The omission of this DMF has no visual effect on the packing diagram along [100] and [010] in terms of available space. There are holes visible along [001] but they are small despite the large void volume calculated. This implies that the coordinated DMF molecules cap the channels containing guest DMF molecules.

Figure 4.8a shows the packing diagram of **5** (viewed along [001]) with the coordinated O11 and the guest O12 DMF molecules omitted. There are channels visible along [001] (calculated void space: 1779.3 Å^3 per unit cell). Figure 4.8b gives the packing diagram of **5** (viewed along [010]) with the coordinated O10 and the guest O12 DMF molecules removed. There are channels visible along [010] and the calculated void space is 1938.8 Å^3 per unit cell. Therefore one of the coordinated O10 or O11 DMF molecules needs to be removed, at least partially, before the guest O12 DMF molecule can leave the structure.

Related by symmetry: ^{i}1/2-x, 1/2-y, -z; ^{ii}x, 1-y, 1/2+z; ^{iii}1-x, y, 1/2-z; ^{iv}x, 1-y, -1/2+z; ^{v}1/2+x, 1/2-y, 1/2+z; ^{vi}-1/2+x, 1/2-y, -1/2+z; ^{vii}1/2-x, -1/2+y, -1/2-z; ^{viii}x, -y, -1/2+z; ^{ix}-x, y, -1/2-z; ^{x}1/2-x, 1/2+y, 1/2-z; ^{xi}1/2+x, 1/2-y, 1/2+z; ^{xii}1/2-x, -1/2+y, 1/2-z

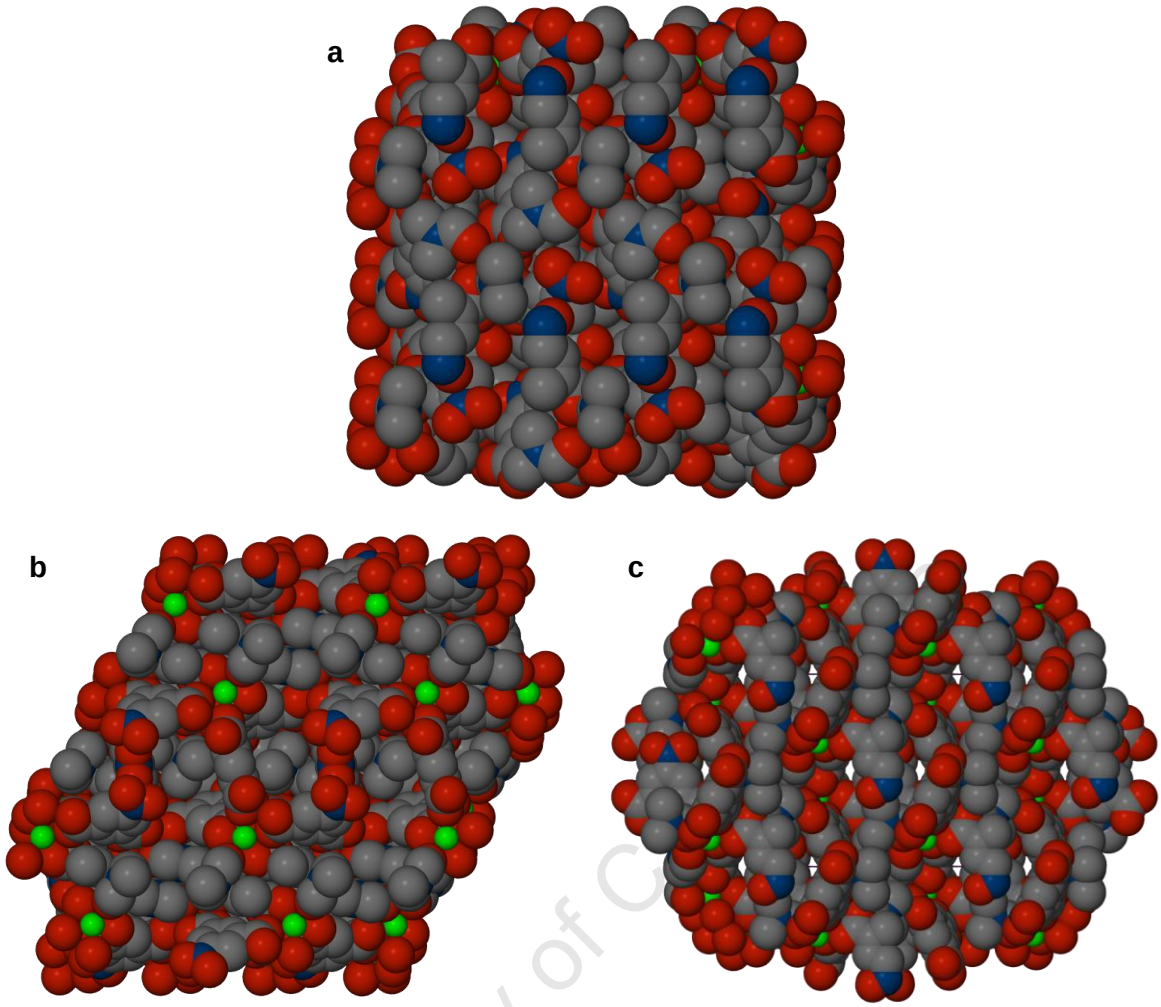

Figure 4.7: Packing diagrams of compound **5** shown with van der Waals radii and the guest O12 DMF molecules omitted. **a)** Viewed along [100], **b)** viewed along [010] and **c)** viewed along [001]

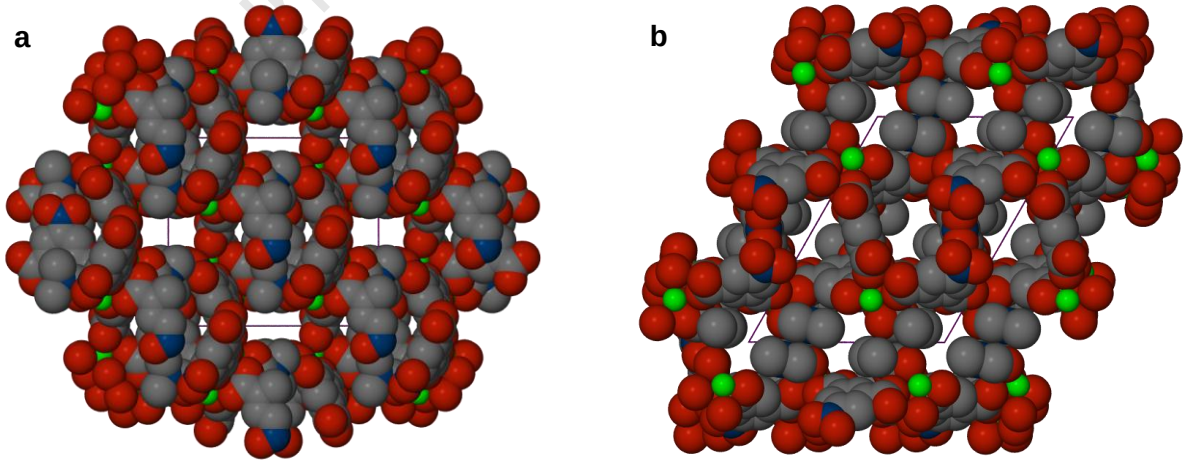

Figure 4.8: The packing diagrams of compound **5** shown with van der Waals radii. **a)** Viewed along [001] with the O11 and O12 DMF molecules omitted. **b)** Viewed along [010] with the O10 and O12 DMF molecules omitted

It is interesting to note that the 1026.6 Å^3 void space found with the removal of the O12 guest DMF molecule as well as the void space of 1938.8 Å^3 for the removal of the O10 and O12 DMF molecules are reported by Platon as existing in four discrete "pockets" within in the unit cell. These pockets are 257 and 485 Å^3 and must account for two and four DMF molecules per pocket respectively. The 1779.3 Å^3 void space reported by Platon after the removal of the O11 and O12 DMF molecules is not reported as discrete pockets but rather one void space. It is possible that the structure distorts with the removal of the DMF molecules (as evidenced by PXRD) to allow the O12 DMF molecule to leave. This will be discussed further in Section 4.3.3 – Powder X-ray Diffraction.

Compound **5** is isostructural with the **1-Eu**, **2-Pr**, **3-Sm** compounds reported by Wang *et al*[15] as well as the **1-Nd**, **2-Dy** and **3-Ho** compounds reported by Chen *et al*[16]. Compound **5** was prepared under different conditions. For further details see Section 4.3.3 – Powder X-ray Diffraction, Figure 4.11.

4.3.2 THERMAL ANALYSIS

The thermogravimetric (TG) trace (Figure 4.9, blue) shows five mass loss steps: A, B, C, D and E. Mass loss A (*ca* 25 – 98 °C) corresponds to the loss of half a DMF molecule (calculated: 5.30%, experimental: 5.43%). This is probably one of the coordinated DMF molecules (see Section 4.3.1 – Single Crystal X-ray Diffraction Analysis). Mass loss B (*ca* 98 – 140 °C) corresponds to the loss of one DMF molecule (calculated: 10.56%, experimental: 10.64%). The removal of half of either the O10 or O11 coordinated DMF molecules allows the O12 DMF to be removed resulting in the sharpest mass loss in the TG trace before decomposition. Mass losses C and D (*ca* 140 – 335 °C) are not well defined and together correspond to the loss of 1.5 DMF molecules (calculated: 15.86%, experimental: 15.31%). Mass loss C probably corresponds to the remainder of the DMF molecules removed before guest loss (mass loss B) while mass loss D corresponds to the other coordinated DMF molecule. The first four mass losses are close together and it is probable that the losses of the different DMF molecules overlap rather than occurring in clearly defined steps. The loss of the final DMF molecules ends at approximately 335 °C and almost directly after this temperature decomposition begins (mass loss E).

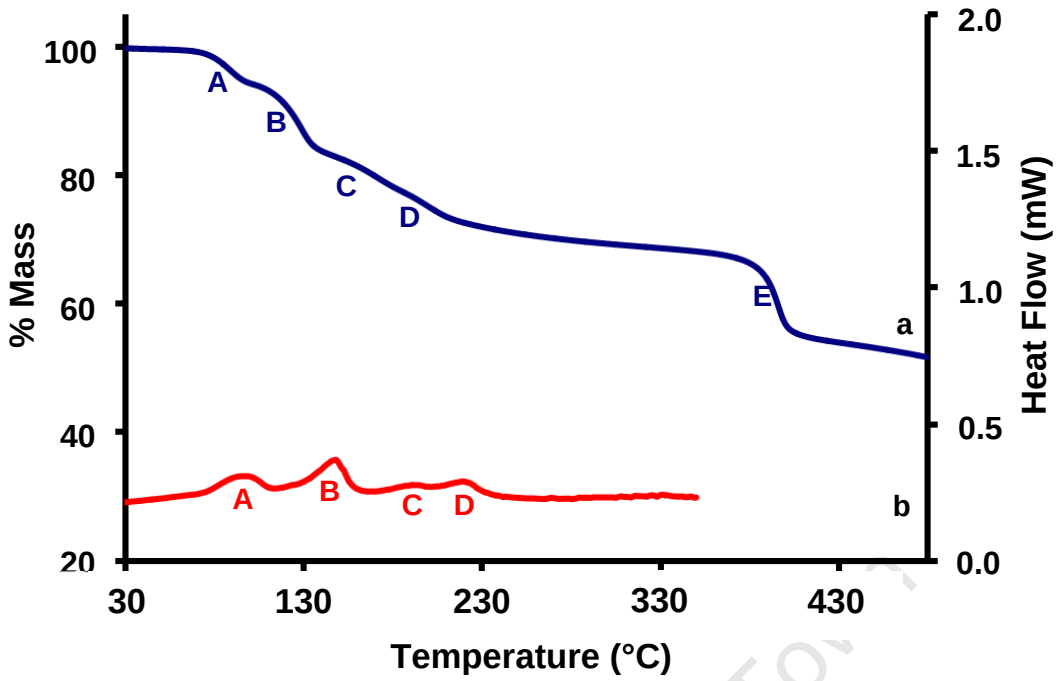

Figure 4.9: a) The TG trace and **b)** the DSC trace of compound **5** (heating rates: 2 and 10 °C.min^{-1}) respectively

The DSC trace correlates well with the TG. Four endotherms coincide with the loss of the solvent molecules. Endotherm C appears as a shoulder on endotherm D making the onset temperature of D difficult to determine. All four endotherms are very close together and have similar energy requirements. This confirms that the process of solvent loss is similar for all three DMF molecules. The peak for endotherm B is slightly sharper than those for A, B and C. Mass loss B in the TG trace is also the steepest mass loss. The profile of endotherm B may be due to the structural rearrangement undergone by **5** to allow for guest removal. The DSC was measured to decomposition. Full mass loss and onset temperature details for the TG and DSC experiments are given in Table 4.5.

Table 4.5: TGA and DSC results for compound **5**

	TGA Results		DSC Results
	Calc. % Mass Loss	**Exp. % Mass Loss**	**T_{onset} (°C)**
0.5 DMF	5.30	5.43	77
1.0 DMF	10.56	10.64	128
0.5 DMF	5.30	15.31	180
1.0 DMF	10.56		*ca* 205

Hot-stage microscopy was performed in a room at 26 °C. Compound **5** retains single crystallinity until above 44 °C (Figure 4.10a). Upon loss of the first half DMF molecule at approximately 77 °C (see DSC results, Table 4.5) the crystal begins to become opaque

(Figure 4.10b). This continues until after the loss of 1.5 DMF molecules and by 148 °C (Figure 4.10d) the crystal is completely opaque. The compound is stable when heated beyond 176 °C (Figure 4.10e) and only begins to discolour at *ca* 250 °C (Figure 4.10f). With the removal of the last of the DMF solvent molecules the crystal becomes discoloured and decomposition begins (Figure 4.10g). The crystal is completely decomposed by 400 °C as shown in Figure 4.10h.

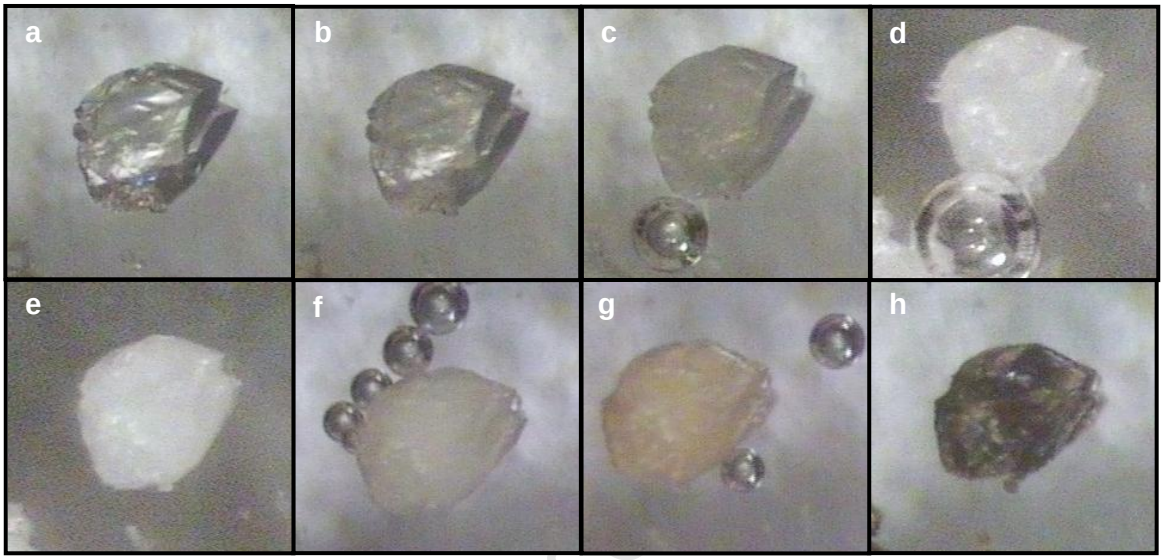

Figure 4.10: HSM pictures of **5** at **a)** 44 °C, **b)** 74 °C, **c)** 99 °C, **d)** 148 °C, **e)** 176 °C, **f)** 255 °C, **g)** 316 °C and **h)** 400 °C

Elemental analysis (Table 4.6) suggests that sample lost some of the DMF molecules before the analysis was performed. With elemental analysis the sample is often exposed to air for a long period of time. To confirm the theory that some DMF has been lost before analysis a sample of **5** was dried on filter paper and exposed to air for 3.5 days. TG analysis was then performed on the dried sample (**5a**). The profile of the TG trace obtained after 100 °C was similar to that of **5** although the mass loss steps are not as distinct as those observed for **5** (Figure 4.9). Overall 2.4 DMF molecules were removed from the structure by 325 °C (calculated: 27.1%, experimental: 26.9%). This implies that approximately 0.6 of a DMF molecule per asymmetric unit was lost upon exposure to air for an extended period of time. It is probable that the amount of DMF lost is dependent on the time the sample was exposed to air. The calculated value for **5** as well as for the loss of 0.6 (**5a**) and 0.5 (**5b**) DMF molecules are given in Table 4.6.

Table 4.6: Elemental analysis of $[Gd(C_{12}N_{1.5}O_9H_{4.5})(C_9N_3O_3H_{21})]$ (**5**), $[Gd(C_{12}N_{1.5}O_9H_{4.5})(C_{7.2}N_{2.4}O_{2.4}H_{16.8})]$ (**5a**) and $[Gd(C_{12}N_{1.5}O_9H_{4.5})(C_{7.5}N_{2.5}O_{2.5}H_{17.5})]$ (**5b**)

	Calculated 5	Calculated 5a	Calculated 5b	Experimental
% C	36.54	35.68	35.83	35.26
% H	3.72	3.32	3.39	4.03
% N	9.13	8.45	8.57	9.02

4.3.3 POWDER X-RAY DIFFRACTION

The PXRD pattern calculated from the single crystal data of compound **5** (Figure 4.11a) is in good agreement with that of **1-Eu**, **2-Pr** and **3-Sm** reported by Wang *et al*[15] in 2010 (Figures 4.11b-d) as expected from isostructural compounds. Wang added 0.06 mmol of 4,4'-bipyridyl and 0.2 mmol of NIA to 0.1 mmol of $Eu(NO_3)_3{\cdot}6H_2O$, $Pr(NO_3)_3{\cdot}6H_2O$ and $Sm(NO_3)_3{\cdot}6H_2O$, respectively. The starting materials were dissolved in 3 ml DMF and 1 ml ethanol at room temperature and left in a 50 mL tube at 60 °C for 4 days until colourless crystals formed. Compound **5** is also isostructural with **1-Nd**, **2-Dy** and **3-Ho** reported by Chen *et al*[16] in 2010 (Figure 4.11e-g). Again a mixture of DMF and ethanol was used. 4,4'-bipyridine was used to direct the structure for **1-Eu**, **2-Pr** and **3-Sm** while 2,2'-bipyridine was used to direct the structure for **1-Nd**, **2-Dy** and **3-Ho**. It was not necessary to use a templating material to prepare compound **5** showing that these compounds could be prepared in a more efficient manner.

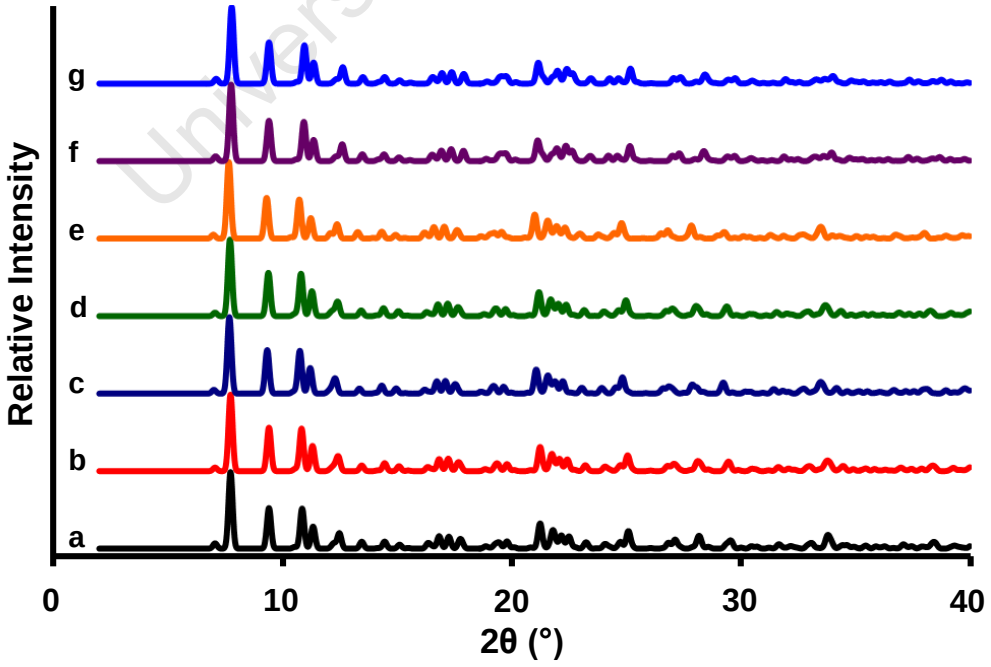

Figure 4.11: PXRD patterns calculated from the single crystal data of **a) 5**, **b) 1-Eu**, **c) 2-Pr**, **d) 3-Sm**, **e) 1-Nd**, **f) 2-Dy** and **g) 3-Ho**

The PXRD pattern obtained from the bulk material of **5** (Figure 4.12b, red) corresponds well with the pattern calculated from the single crystal data (Figure 4.12a, blue).

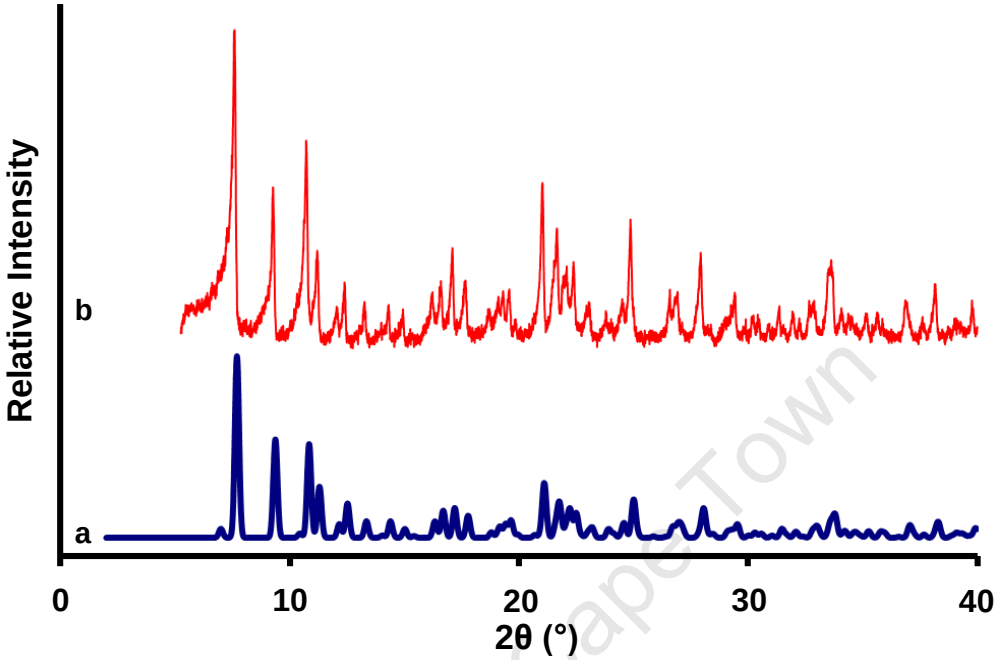

Figure 4.12: PXRD patterns of **5 a)** calculated from single crystal data and **b)** experimental

When compound **5** is heated it loses crystallinity (Figure 4.13). This corresponds with the loss of the solvent molecules seen in the thermal analysis (see Section 4.3.2 – Thermal Analysis). A structural rearrangement is seen between 75 and 110 °C. This coincides with the removal of the first half coordinated DMF and probably allows the removal of the guest DMF molecule as previously discussed. There is another change in the PXRD pattern between 110 and 150 °C which corresponds with the loss of the guest DMF molecule. There is only a slight change in the pattern between 150 and 175 °C. 175 °C corresponds with the beginning of mass loss C (see Section 4.3.2 – Thermal Analysis, Figure 4.9) and the removal of the remaining 1.5 DMF molecules. The compound is almost completely amorphous by 200 °C which indicates that the final DMF molecule is required to retain any crystallinity.

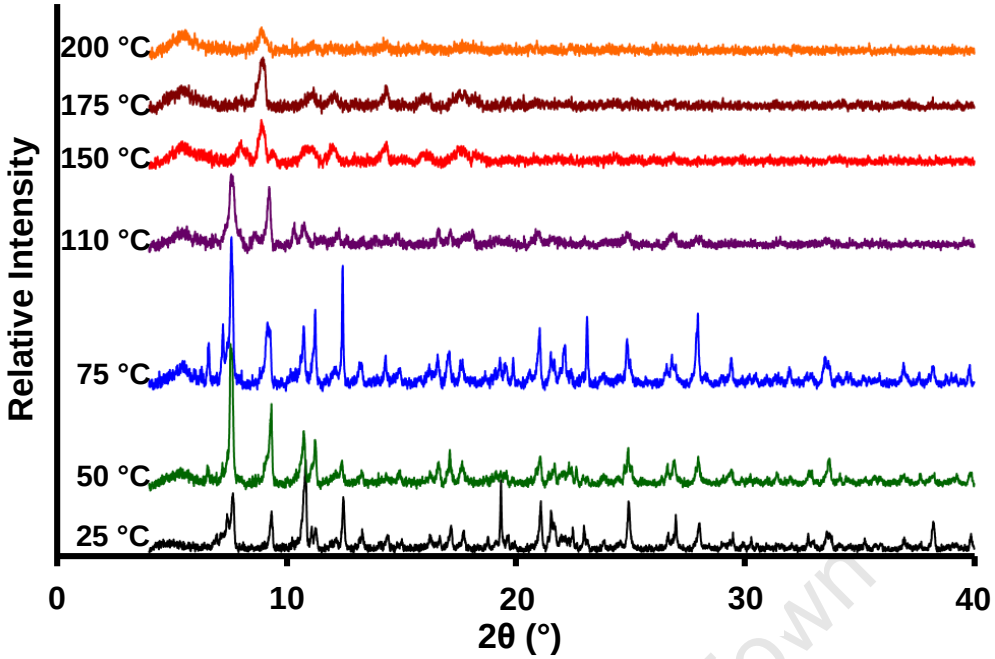

Figure 4.13: Variable temperature PXRD patterns of **5** from 25 – 200 °C

A sample of **5** was heated at 110 °C for approximately 30 hours. The PXRD pattern of the sample after heating is given in Figure 4.14c. This pattern is very similar to that obtained after heating to 150 °C (Figure 4.14d). The mass loss at this stage corresponds to the loss of two DMF molecules from **5** (calculated: 21.2%, experimental: 21.2%). This partially desolvated sample (**5c**) was exposed to DMF vapour for 36 hours (see Figure 4.14b). TG analysis shows that one DMF molecule has been absorbed in the resolvated sample (**5d**). A mass loss corresponding to the loss of 2 DMF molecules by 325 °C is found (calculated: 23.7%, experimental: 24.1%). The resolution is not particularly clear for **5d** but there are many similarities between the original compound **5** (Figure 4.14a) and the resolvated compound **5d**. The most noticeable differences are the presence of an extra peak at 9° 2θ and a small peak at 7.7° 2θ. These are both present in the dehydrated sample **5c**. The composition of each compound **5**, **5c** and **5d** are given in Table 4.7.

Table 4.7: The composition of compounds **5**, **5c** and **5d**

Compound	Composition
5	$[Gd(NIA)_{1.5}(DMF)_2]\cdot DMF$
5c	$[Gd(NIA)_{1.5}(DMF)]$
5d	$[Gd(NIA)_{1.5}(DMF)]\cdot DMF$

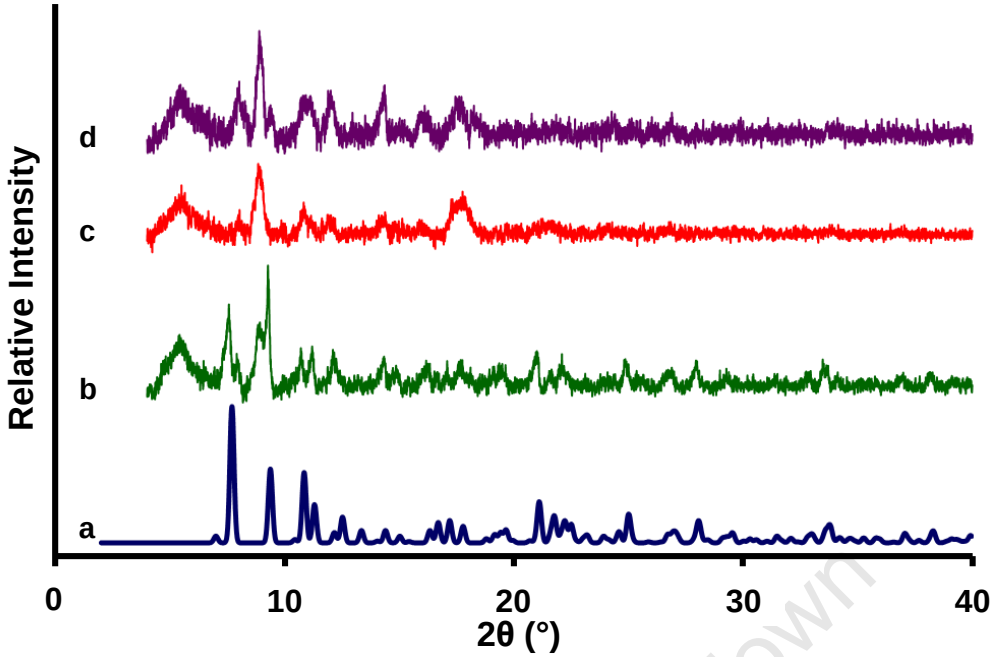

Figure 4.14: PXRD patterns of vapour diffusion experiments of **5**. **a)** Calculated **5**, **b)** after exposure of desolvated sample **5c** to DMF vapour for 36 hours (**5d**), **c)** after heating of **5** at 110 °C for 30 hours (**5c**) and **d)** compound **5** after heating to 150 °C

4.3.4 SUMMARY

Compound **5** was prepared using a number of methods (see Section 4.1 – Preparation of Gadolinium(III) and 5-nitroisophthalate Compounds). The best quality single crystals of **5** were obtained from methods 1a, 1b and 3. Those grown at high temperature (methods 2a-c) were of poorer quality. Compound **5** was much more likely to form when cooled immediately to room temperature (method 3) rather than held at a high temperature for any length of time. The reproducible preparation of **5** was confirmed using single crystal and PXRD analysis as well as thermal techniques. There are many compounds prepared from lanthanide salts and H_2NIA found in the literature that are isostructural to **5**.[15,16] Compound **5** can be partially desolvated and partially resolvated with heating and exposure to DMF vapour.

Octahedral networks from lanthanide metal ions and H_2NIA ligands have been found to have rhombohedral pores accessible to DMF.[15,16]

4.4 $[Gd_2(NIA)_3(DMF)_4]\cdot 2.67H_2O$ (6)

4.4.1 SINGLE CRYSTAL X-RAY DIFFRACTION ANALYSIS

The hydrogen atoms located on the framework of compound **6** were placed in idealised positions in a riding model. All hydrogen atoms were refined isotropically and assigned temperature factors that relate to the atom they are attached to. The temperature factors are 1.2 times the parent atom for phenyl hydrogen atoms and 1.5 times the parent atom for methyl hydrogen atoms. The hydrogen atoms on the guest water molecules were not modelled.

Compound **6** crystallises in the monoclinic crystal system, in the space group *C*2/*c*. **6** is a neutral metal-organic framework. Further details are given in Table 4.8.

Table 4.8: Crystal Data and Refinement Parameters of **6**

Empirical Formula	$C_{36}H_{42.4}Gd_2N_7O_{24.7}$
Formula Weight (g.mol^{-1})	1282.34
Temperature (K)	173(2)
Wavelength (Å)	0.71073
Crystal System	Monoclinic
Space Group	*C*2/*c*
a (Å)	24.9427(2)
b (Å)	16.9411(2)
c (Å)	25.2889(2)
α (°)	90
β (°)	105.208(1)
γ (°)	90
Volume (Å^3)	10311.8(2)
Z	8
Calculated Density (g.cm^{-3})	1.652
***μ* (mm^{-1})**	2.636
***F* (*000*)**	5062
Crystal Size (mm)	0.30 x 0.20 x 0.15
***Θ* Range Scanned (°)**	1.58 – 27.48
Index Range	-32 < h < 32, -21 < k < 21, -32 < l < 32
No. Reflections Collected	180368
No. Unique Reflections	11826
R_{int}	0.0824
Data Completeness to θ_{max} (%)	99.9
Refinement Method	Full-matrix least-squares on F^2
Data/Restraints/Parameters	11826/0/616
Goodness-of-fit on F^2	1.130
Final *R* Indices [$I>2\sigma(I)$]	R_1 = 0.0402, wR_2 = 0.1040
***R* Indices (all data)**	R_1 = 0.0538, wR_2 = 0.1139
Largest Diff. Peak and Hole (*e*.Å^{-3})	1.732, -2.087

Figure 4.15 shows the asymmetric unit of **6** with hydrogen atoms and guest water molecules omitted. The oxygen atoms of the coordinated DMF molecules are given although the rest of the molecule is not shown. The asymmetric unit consists of two gadolinium(III) metal centres, three deprotonated NIA anions, four coordinated DMF molecules and 2.67 guest water molecules.

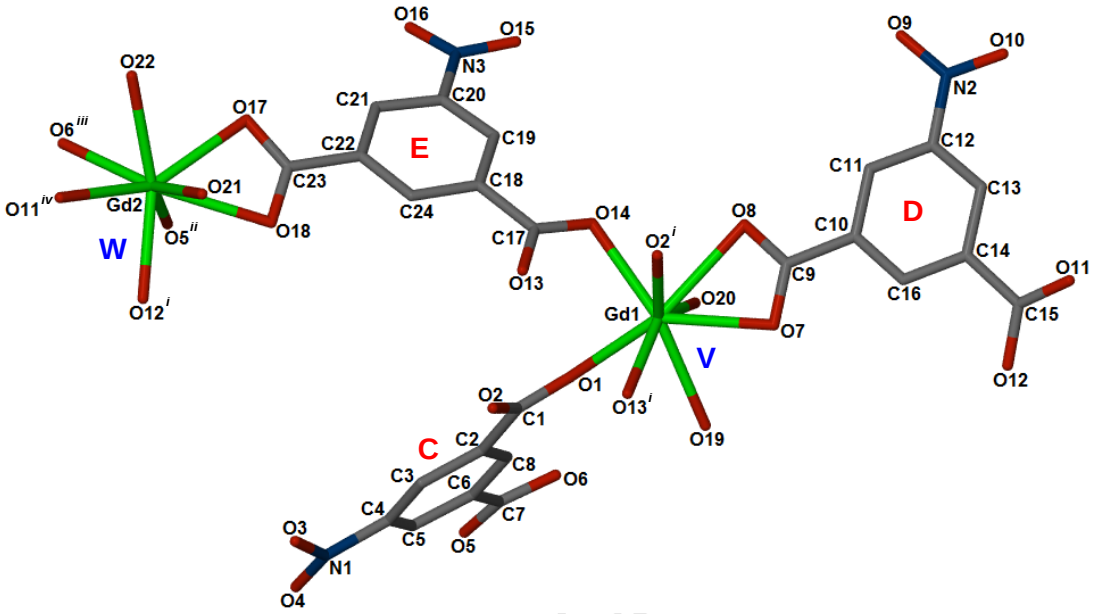

Figure 4.15: The asymmetric unit of **6** with the hydrogen atoms and guest water molecules omitted for clarity. Only the oxygen atoms of the coordinated DMF molecules are shown

The Gd1 metal centre is coordinated to 8 oxygen atoms in a distorted square, antiprismatic fashion. Four of the oxygen atoms are from singly coordinated, bridging carboxylate moieties (O1, O2^{i}, O13^{i}, O14), two are from a bidentate, chelating carboxylate moiety (O7, O8) and two are from DMF molecules (O19, O20). The Gd2 metal centred also coordinates in a distorted square, antiprismatic manner to 8 oxygen atoms. Four of the oxygen atoms are from singly coordinated, bridging carboxylate moieties (O5^{ii}, O6^{iii}, O11^{iv}, O12^{i}), two are from a bidentate, chelating carboxylate moiety (O17, O18) and two DMF molecules (O21, O22). The O-Gd1-O and O-Gd2-O angles are similar to those obtained around the Gd1 metal centre in compound **5**. Gd-O distances are shown in Table 4.9 and these correlate well with previously reported structures.[1]

Both metal centres form paddle-wheel secondary-building units (SBUs) as shown in Figure 4.16. SBU **V** is based on the Gd1/Gd1^{i} dimer (Figure 4.16a) while SBU **W** is based on the Gd2/Gd2^{v} dimer (Figure 4.16b). Each SBU comprises four bridging NIA units, two doubly coordinated NIA units and four DMF molecules. The coordination of NIA units to the metal centres in **6** is similar to that found in **5**. The difference in the structures is obvious when the

Related by symmetry: ^{i}1/2-x, 3/2-y, -z; ^{ii}1-x, 2-y, -z; ^{iii}x, 2-y, -1/2+z; ^{iv}1/2+x, 3/2-y, -1/2+z; ^{v}1-x, y, -1/2-z; ^{vi}x, 2-y, 1/2+z; ^{vii}-1/2+x, 3/2-y, 1/2+z; ^{viii}-1/2+x, -1/2+y, z; ^{ix}1/2-x, -1/2+y, -1/2-z; ^{x}1/2+x, 1/2+y, z; ^{xi}1/2-x, 1/2+y, -1/2-z; ^{xii}1-x, y, 1/2-z; ^{xiii}1/2-x, -1/2+y, 1/2-z; ^{xiv}1/2+x, -1/2+y, z; ^{xv}1/2+x, 3/2-y, 1/2+z

connectivity of the SBUs is examined. SBU **V** acts as a square planar connector while SBU **W** acts as a tetrahedral connector. The topology that arises from these SBUs will be discussed further in Chapter 5 - Topological Studies.

Table 4.9: Experimental Gd-O bond lengths for **6** and literature Gd-O bond lengths

Bond	Length (Å)	Average Length (Å)	Bond Type
Gd1-O1	2.417(3)	2.35 ± 0.06*	Terminal Carboxylate
Gd1-O2^{i}	2.386(3)		
Gd1-O13^{i}	2.338(3)		
Gd1-O14	2.405(3)		
Gd2-O5^{ii}	2.410(4)		
Gd2-O6^{iii}	2.303(3)		
Gd2-O11^{iv}	2.442(3)		
Gd2-O12^{i}	2.247(4)		
Gd1-O7	2.391(3)	2.52 ± 0.09*	Chelating Carboxylate
Gd1-O8	2.506(3)		
Gd2-O17	2.444(3)		
Gd2-O18	2.476(4)		
Gd1-O19	2.443(4)	2.38 ± 0.04*	DMF
Gd1-O20	2.422(3)		
Gd2-O21	2.396(4)		
Gd2-O22	2.407(4)		

* Values obtained from the CSD

One carboxylate moiety of NIA C bridges Gd1 and Gd1^{i} while the other carboxylate moiety bridges a Gd2^{ii} and Gd2^{vi} dimer. One carboxylate moiety of NIA D is doubly coordinated to Gd1 while the other carboxylate moiety bridges Gd2^{i} and Gd2^{vii}. One carboxylate moiety of NIA E is doubly coordinated to Gd2 while the other carboxylate moiety bridges Gd1 and Gd1^{i}. As a result all the Gd1 and Gd2 metal centres are bridged by both a NIA D and a NIA E anion, which results in SBU V and W both acting as four-connectors. The nitro groups are not coordinated for any of the NIA units.

The Gd1-O7 bond length is slightly shorter than expected for a bidentate chelating Gd-O bond length (2.391(3) Å). The Gd2-O12^{i} is also shorter than expected while the Gd2-O11^{iv} bond length is longer than expected (2.247(4) and 2.442(3) Å respectively). It is interesting to note that O7, O11 and O12 all belong to NIA D. NIA D bridges Gd1 and Gd2^{i}. NIA E^{i} also bridges Gd1 and Gd2^{i}. The "side" of NIA D that is closest to NIA E^{i} (see Figure 4.16a) contains the short Gd1-O7 and Gd2^{i}-O12 bonds. The strength of these bonds results in a lengthening of the Gd2^{vii}-O11 bond as well.

Related by symmetry: ^{i}1/2-x, 3/2-y, -z; ^{ii}1-x, 2-y, -z; ^{iii}x, 2-y, -1/2+z; ^{iv}1/2+x, 3/2-y, -1/2+z; ^{v}1-x, y, -1/2-z; ^{vi}x, 2-y, 1/2+z; ^{vii}-1/2+x, 3/2-y, 1/2+z; ^{viii}-1/2+x, -1/2+y, z; ^{ix}1/2-x, -1/2+y, -1/2-z; ^{x}1/2+x, 1/2+y, z; ^{xi}1/2-x, 1/2+y, -1/2-z; ^{xii}1-x, y, 1/2-z; ^{xiii}1/2-x, -1/2+y, 1/2-z; ^{xiv}1/2+x, -1/2+y, z; ^{xv}1/2+x, 3/2-y, 1/2+z

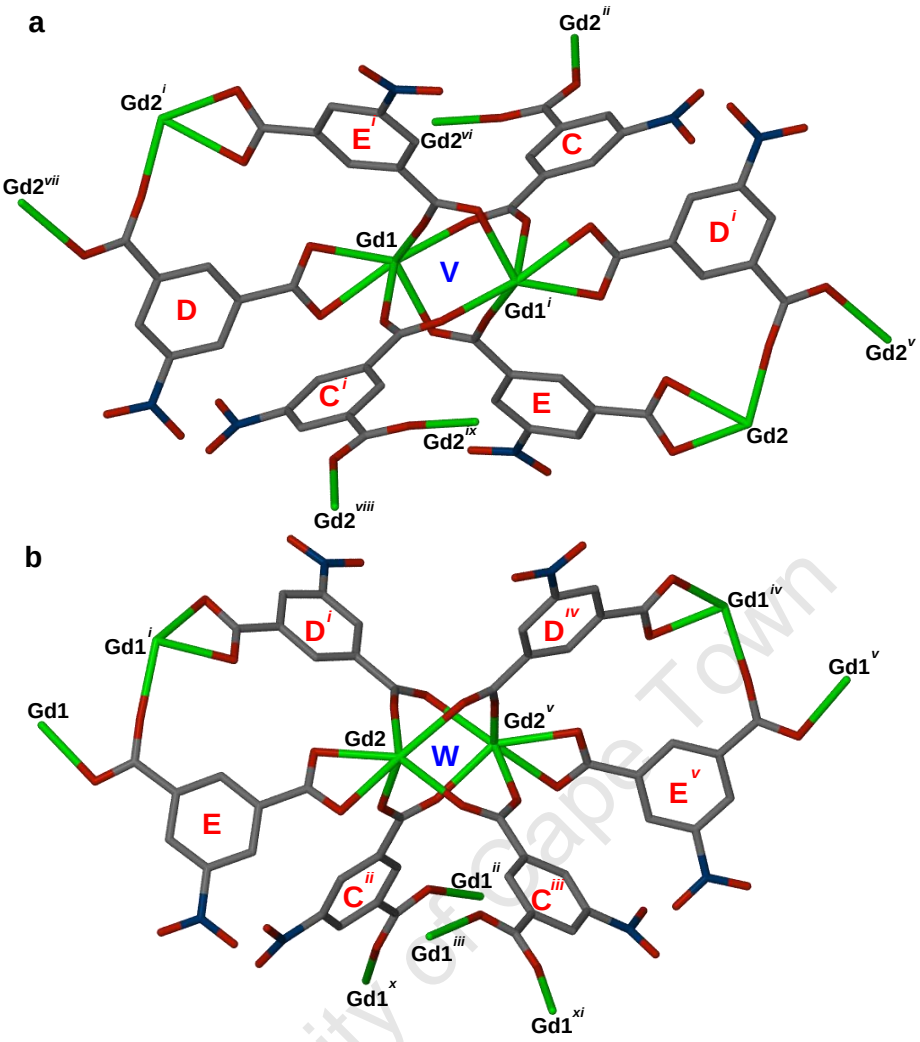

Figure 4.16: The SBUs of compound **6**. **a)** NIA C, NIA C^{i}, NIA E and NIA E^{i} form the paddle-wheel and NIA D and NIA D^{i} are axially coordinated in SBU V while **b)** NIA C^{ii}, NIA C^{iii}, NIA D^{i} and NIA D^{iv} form the paddle-wheel and NIA E and NIA E^{v} are axially coordinated in SBU W. DMF and guest water molecules are omitted for clarity

There are 2.67 water molecules modelled in the asymmetric unit of the single crystal structure. These are disordered over six positions and possess site occupancy factors (s.o.f.) ranging from 0.32 – 0.68. Four of these water molecules (O23, O24, O25, O26) have a cumulative s.o.f. of 1.88. These are located in a roughly cube shaped pocket formed by the network. The edges of the cube are formed by NIA C, NIA C^{xii}, NIA D^{xiii} and NIA D^{xiv}, NIA E^{i} and NIA E^{xv} as shown in Figure 4.17a and b. The symmetry generated O23^{xii}, O24^{xii}, O25^{xii} and O26^{xii} water molecules are also located in this pocket. This results in a cumulative s.o.f of 3.77 water molecules in the cavity. The remaining two water molecules O27 and O28 are located in another open space in the network (Figure 4.17c and d). The edges of this space are formed by NIA C, NIA C^{ii}, NIA D^{i}, NIA D^{x}, NIA E and NIA E^{ii} as well as the O22^{v}

Related by symmetry: ^{i}1/2-x, 3/2-y, -z; ^{ii}1-x, 2-y, -z; ^{iii}x, 2-y, -1/2+z; ^{iv}1/2+x, 3/2-y, -1/2+z; ^{v}1-x, y, -1/2-z; ^{vi}x, 2-y, 1/2+z; ^{vii}-1/2+x, 3/2-y, 1/2+z; ^{viii}-1/2+x, -1/2+y, z; ^{ix}1/2-x, -1/2+y, -1/2-z; ^{x}1/2+x, 1/2+y, z; ^{xi}1/2-x, 1/2+y, -1/2-z; ^{xii}1-x, y, 1/2-z; ^{xiii}1/2-x, -1/2+y, 1/2-z; ^{xiv}1/2+x, -1/2+y, z; ^{xv}1/2+x, 3/2-y, 1/2+z

and O22[vi] DMF molecules. The symmetry generated O27[ii] and O28[ii] water molecules are also located in this cavity. This results in a cumulative s.o.f. of 1.58 in the cavity.

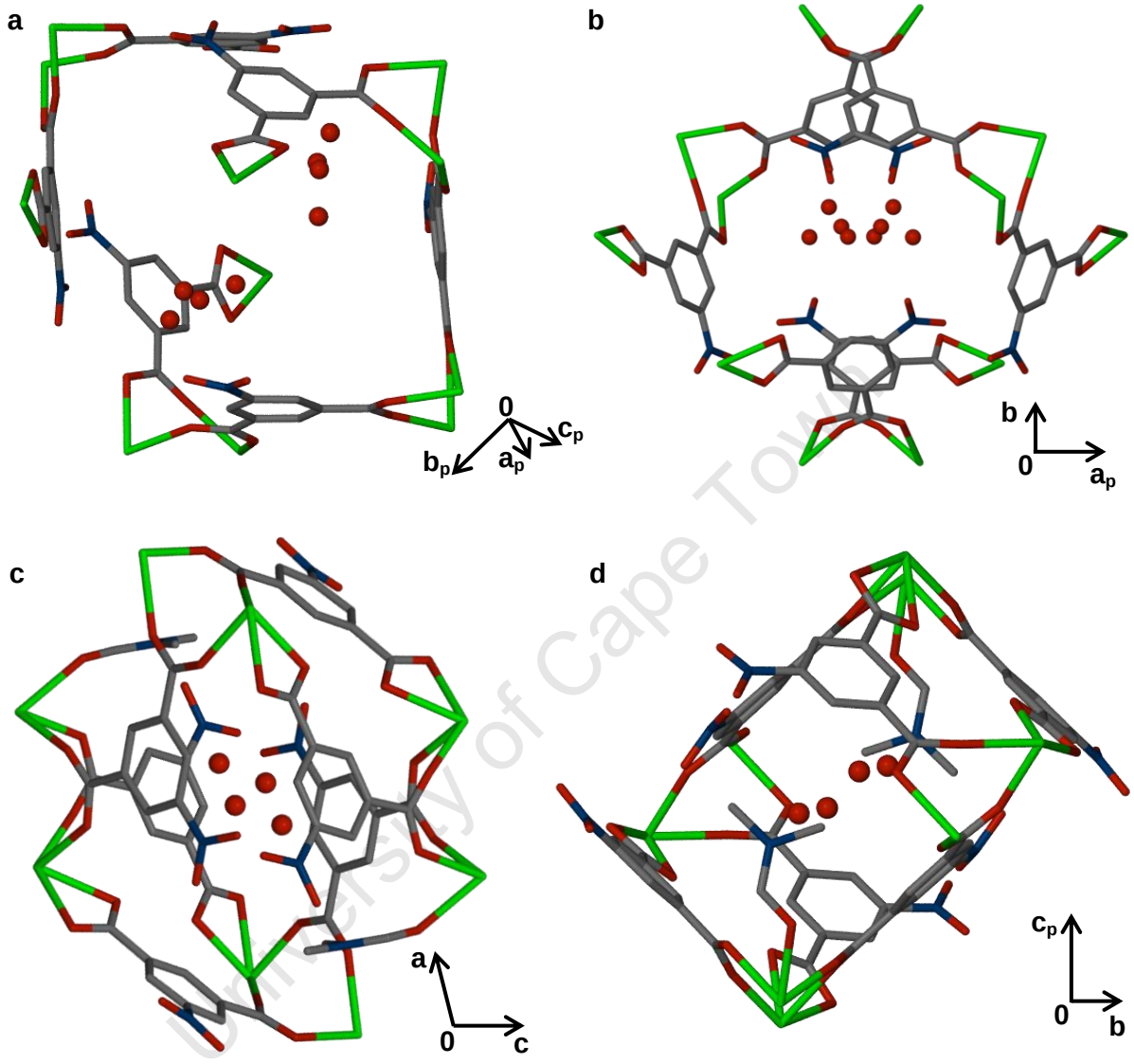

Figure 4.17: a) and **b)** show the O23, O24, O25, O26 and symmetry generated O23[xii], O24[xii], O25[xii] and O26[xii] water molecules located in a cavity formed between six NIA units. **c)** and **d)** show the O27, O28 and symmetry generated O27[ii] and O28[ii] water molecules located in a cavity formed by six NIA units and the O22[v] and O22[vi] DMF molecules.

In addition to the guest water molecules modelled in the crystal structure, compound **6** has a total solvent accessible void space of 632 Å^3 per unit cell as determined through the program Platon.[13, 14] This void space manifests as discrete pockets within the structure with the largest void space approximately 110 Å^3. This void space is shown in blue in Figure 4.18a. These spaces are found within the cavities that contain the guest water molecules described previously. There is an open space within the O27/O28 water cavity and two discrete open

Related by symmetry: [i]1/2-x, 3/2-y, -z; [ii]1-x, 2-y, -z; [iii]x, 2-y, -1/2+z; [iv]1/2+x, 3/2-y, -1/2+z; [v]1-x, y, -1/2-z; [vi]x, 2-y, 1/2+z; [vii]-1/2+x, 3/2-y, 1/2+z; [viii]-1/2+x, -1/2+y, z; [ix]1/2-x, -1/2+y, -1/2-z; [x]1/2+x, 1/2+y, z; [xi]1/2-x, 1/2+y, -1/2-z; [xii]1-x, y, 1/2-z; [xiii]1/2-x, -1/2+y, 1/2-z; [xiv]1/2+x, -1/2+y, z; [xv]1/2+x, 3/2-y, 1/2+z

spaces within the cavity containing the O23-O26 water molecules. Figure 4.18b shows the relevant water molecules with van der Waals radii. The water molecules and void space fit together well. The modelled water molecules are very diffuse with s.o.f ranging from 0.32 – 0.68. It is probable that the water molecules are able to move in the cavities. There is some residual electron density present in the O23-O26 cavity indicating the possibility of additional water being present there.

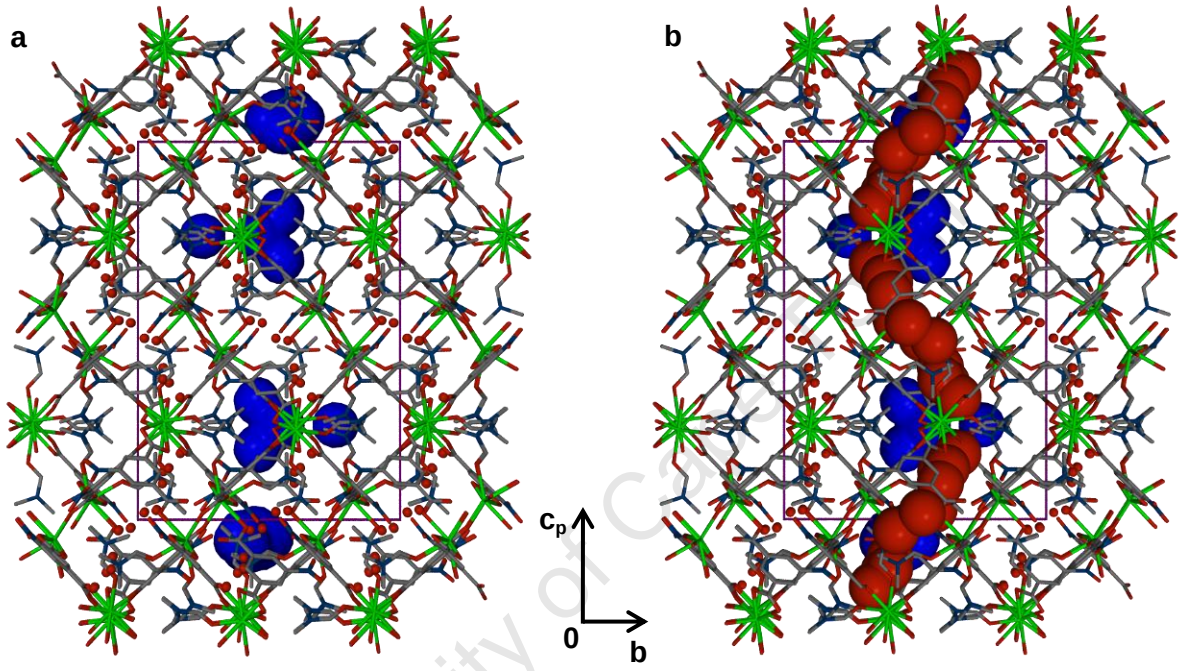

Figure 4.18: The packing diagram of **6** viewed along [100] with the Connelley surface shown in blue. **a)** The water molecules are shown with 0.2x their van der Waals radii and **b)** the relevant water molecules are given with van der Waals radii

Figure 4.19 shows the framework of compound **6** in black with an overlay in red of the symmetry elements present in the space group *C*2/*c*. The inversion centres at (0,0,0), (1/2,1/2,0), (0,0,1/2) and (1/2,1/2,1/2) are located between the nitro moieties of two NIA D units. The (1/4,3/4,0), (3/4,1/4,0), (1/4,1/4,1/2) and (3/4,3/4,1/2) centres of inversion are located in the centre of Gd1 metal dimers. The (1/4,1/4,0), (3/4,3/4,0), (1/4,3/4,1/2) and (3/4,1/4,1/2) inversion centres are between the nitro moieties of two NIA E units. The (0,1/2,0), (1/2,0,0), (0,1/2,1/2) and (1/2,0,1/2) inversion centres are in the centre of the O27, O27^{ii}, O28 and O28^{ii} water molecules, in the centre of the previously mentioned “pockets”.

The (0,y,1/4), (0,y,3/4), (1/2,y,1/4) and (1/2,y,3/4) twofold rotation axes are parallel to the *b*-axis through the centre of the Gd2 metal dimers. The (1/4,y,1/4), (1/4,y,3/4), (3/4,y,1/4) and (3/4,y,3/4) twofold screw axes progress through the centre of a spiral along the *b*-axis formed

Related by symmetry: ^{i}1/2-x, 3/2-y, -z; ^{ii}1-x, 2-y, -z; ^{iii}x, 2-y, -1/2+z; ^{iv}1/2+x, 3/2-y, -1/2+z; ^{v}1-x, y, -1/2-z; ^{vi}x, 2-y, 1/2+z; ^{vii}-1/2+x, 3/2-y, 1/2+z; ^{viii}-1/2+x, -1/2+y, z; ^{ix}1/2-x, -1/2+y, -1/2-z; ^{x}1/2+x, 1/2+y, z; ^{xi}1/2-x, 1/2+y, -1/2-z; ^{xii}1-x, y, 1/2-z; ^{xiii}1/2-x, -1/2+y, 1/2-z; ^{xiv}1/2+x, -1/2+y, z; ^{xv}1/2+x, 3/2-y, 1/2+z

by the O19, O21 and O22 DMF molecules. The screw axes are also located near NIA E units.

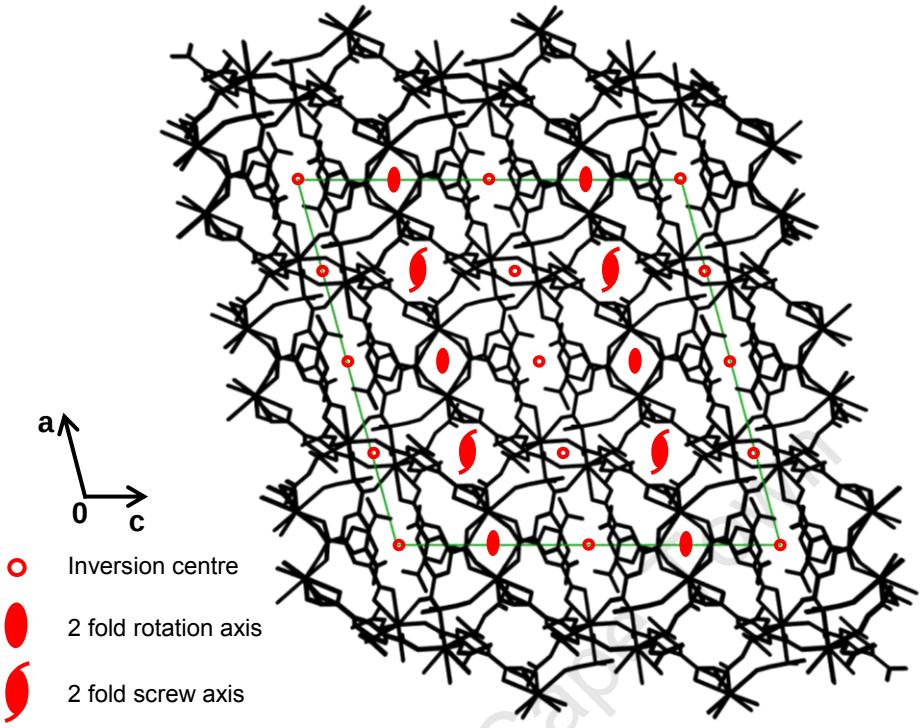

Figure 4.19: The packing diagram of **6** viewed down [010] and shown in black. The symmetry elements in the unit cell are depicted as a red overlay. Guest water molecules are omitted for clarity

4.4.2 THERMAL ANALYSIS

The TG trace of compound **6** is shown in blue in Figure 4.20. There are three mass loss steps visible in the trace. Mass loss A is small compared to mass losses B and C. Mass loss A (*ca* 30 – 116 °C) corresponds to the loss of 1.88 guest water molecules (calculated: 2.67%, experimental: 2.37%). 2.67 water molecules are modelled in the single crystal structure. This confirms that the water is able to move freely through the cavities mentioned in Section 4.4.1. It is possible that each single crystal of compound **6** has a different water content. The calculated mass losses correspond to $[Gd_2(NIA)_3(DMF)_4]\cdot 1.88H_2O$ (**6a**) as no mass loss is observed beyond 60 °C implying no extra water was present during the experiment. The difference in water content between **6** and **6a** of 0.79 water molecules corresponds to the s.o.f. of the O27 and O28 water molecules. Mass loss B (*ca* 116 – 250 °C) corresponds to the loss of the four coordinated DMF molecules (calculated: 23.06%, experimental 23.03%). Upon the loss of the DMF the structure begins to decompose immediately as demonstrated by mass loss B blending into mass loss C. Complete decomposition occurs with the loss of

another 1.00 NIA units in mass loss C (calculated 16.49%, experimental 16.40% from 250 – 375 °C). Full details for both the TG and DSC traces are given in Table 4.10.

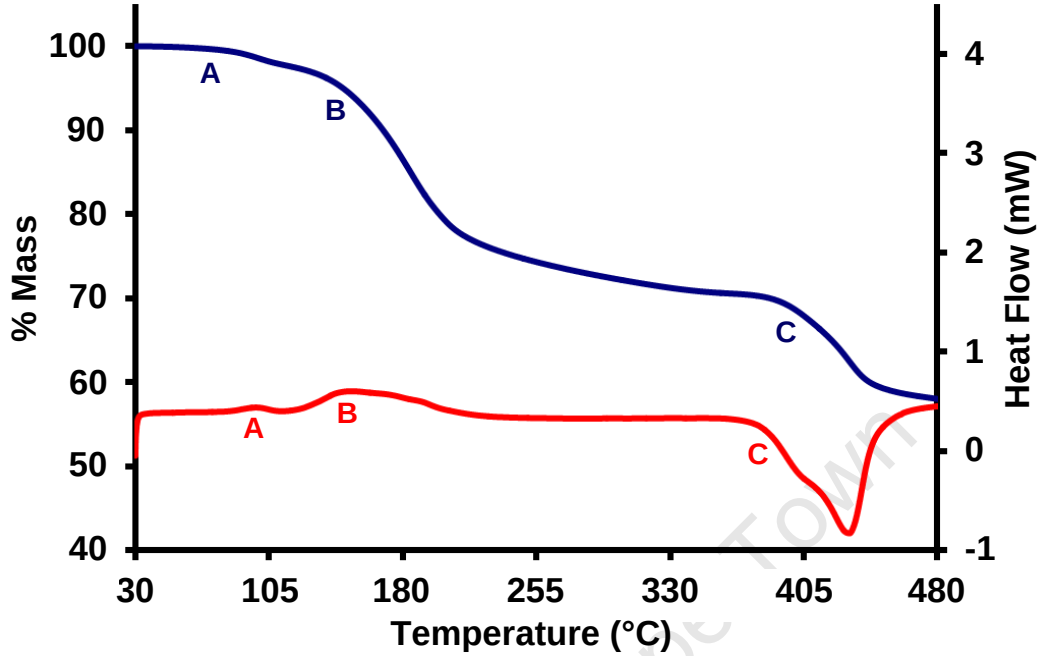

Figure 4.20: a) The TG analysis of **6** and **b)** the DSC analysis of **6** both heated at 10 °C.min^{-1}

The DSC trace correlates well with the TG. Two endotherms, A and B, coincide with the loss of solvent molecules. The exotherm C corresponds with decomposition. The DSC shows a broad, low energy endotherm (B) corresponding to the loss of DMF molecules. Energy is released when the compound decomposes as shown by exotherm C.

Table 4.10: TGA and DSC results for **6a**

	TG Results		DSC Results
	Calc. % Mass Loss	**Exp. % Mass Loss**	**T_{onset} (°C)**
1.88 H_2O (A)	2.67	2.37	85
4.00 DMF (B)	23.06	23.03	124
1.00 H_2NIA (C)	16.49	16.40	393

Hot-stage microscopy (HSM) experiments were started at 30 °C. The sample is crystalline at room temperature but starts to lose single crystallinity when removed from the mother liquor (Figure 4.21a). With the removal of the guest water molecule the sample becomes more opaque (Figure 4.21b) and it is completely white by 157 °C as shown in Figure 4.21c. The first bubble is visible in Figure 4.21c at 157 °C and this corresponds with the removal of DMF molecules. The crystal remains opaque and white above 200 °C (Figure 4.21e) and at this temperature the majority of the DMF molecules have been removed. There is a slight

discolouration seen in the sample at 268 °C (Figure 4.21f). This temperature matches the transition from all DMF being lost to the start of decomposition (between mass losses B and C on the TG trace). By 319 °C there is definite discolouration of the sample as shown in Figure 4.21g. The decomposition continues and the large decomposition steps seen in both the TG and DSC are obvious in HSM at 392 °C (Figure 4.21i) with the sample a dark brown colour.

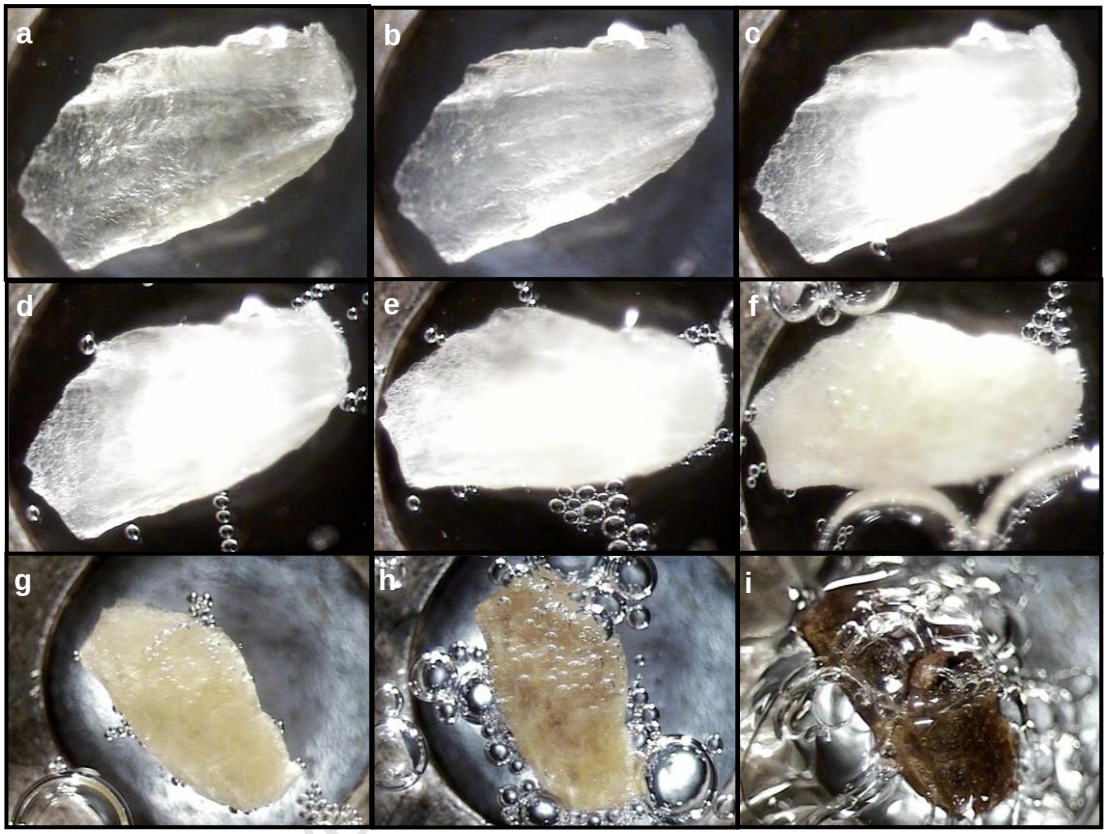

Figure 4.21: Hot-stage microscopy pictures of **6** at **a)** 30 °C, **b)** 80 °C, **c)** 157 °C, **d)** 182 °C, **e)** 200 °C, **f)** 268 °C, **g)** 319 °C, **h)** 356 °C and **i)** 392 °C

Elemental analysis (Table 4.11) corresponds well with the calculated values for compound **6a**. This confirms the presence of approximately 1.88 water molecules when the experiment was performed. For both TG and elemental analyses the sample was dried thoroughly on filter paper to remove surface solvent before the experiments were performed. For the single crystal data collection the crystal was placed quickly into paratone oil and then immediately cooled to prevent solvent loss. It is possible that the water not observed in the TG and elemental analyses is only loosely held in the structure and removed easily at ambient temperatures. The water content may vary with each crystal being examined. The calculated values for **6** and **6a** are provided in Table 4.11.

Table 4.11: Elemental Analysis for $[Gd_2(C_{24}N_3O_{18}H_9)(C_{12}N_4O_4H_{28})]\cdot 2.67H_2O$ (**6**) and $[Gd_2(C_{24}N_3O_{18}H_9)(C_{12}N_4O_4H_{28})]\cdot 1.88H_2O$ (**6a**)

	Calculated 6	Calculated 6a	Experimental
% C	33.72	34.10	34.54
% H	3.33	3.24	3.94
% N	7.65	7.73	8.33

4.4.3 POWDER X-RAY DIFFRACTION

The PXRD pattern obtained from the bulk material of **6** (Figure 4.22b, red) corresponds well with the pattern calculated from the single crystal data (Figure 4.22a, blue). A search of the Cambridge Structural Database revealed no isostructural compounds for compound **6**.

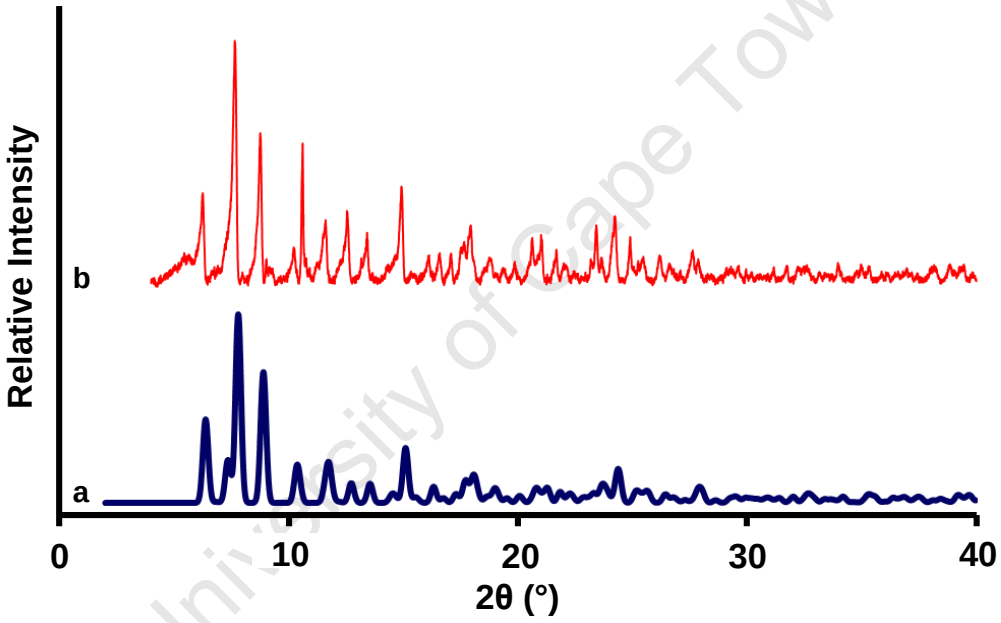

Figure 4.22: PXRD patterns of **6 a)** calculated from single crystal data and **b)** experimental

4.4.4 SUMMARY

As for compound **5** the gadolinium metal ions in compound **6** appear to absorb the X-rays resulting in poor PXRD patterns. This absorption presents a problem with regular variable temperature PXRD experiments as no diffraction pattern is obtained for a sample placed in a capillary tube even if a pattern was obtained with the same sample on a flat holder. See Chapter 2.5.2 – Powder X-ray Diffraction for more details. Variable temperature PXRD for compound **5** were obtained by heating the sample in TG apparatus before performing the PXRD experiment with a flat holder. However, the majority of sample obtained for compound

6 was of poor quality and did not produce good diffraction patterns. Compound **6** was also not obtained in large amounts. As a result variable-temperature experiments could not be performed on **6** through regular methods and there was insufficient of **6** to perform the experiments in the same manner as for compound **5**. The water content of **6** appears to be variable with the O27 and O28 water molecules easily removed at ambient temperatures.

The relationship between compounds **5** and **6** in terms of topological studies is discussed in greater detail in Chapter 5 – Topological Analysis.

4.5 $[Gd_4(NIA)_6(DMF)_{5.5}(H_2O)_3]\cdot 4DMF\cdot H_2O$ (7)

4.5.1 SINGLE CRYSTAL X-RAY DIFFRACTION ANALYSIS

The hydrogen atoms on the framework were either placed in idealised positions in a riding model or located based on electron density peaks in the density map. All hydrogen atoms were refined isotropically. Most were assigned temperature factors that relate to the atom they are attached to. The temperature factors are 1.2 times the parent atom for phenyl and water hydrogen atoms and 1.5 times the parent atom for methyl hydrogen atoms. The temperature factor was allowed to freely refine for certain hydrogen atoms attached to water molecules. Some of the water hydrogen atoms were not modelled.

Compound **7** crystallises in the triclinic crystal system, in the space group $P\bar{1}$. **7** comprises 6 fully deprotonated NIA anions each with a charge of 2- and four Gd(III) metal centres. It is a neutral coordination polymer. Crystal data and refinement details are given in Table 4.12. Despite absorption correction procedures being applied to the data there were still several large residual electron density peaks. These are all located around the metal centres.

Figure 4.23 shows the asymmetric unit of **7** with hydrogen atoms, guest water molecules and guest DMF molecules omitted. Only the oxygen atoms of the coordinated DMF molecules are shown. The asymmetric unit consists of four metal centres, six NIA units, five and a half coordinated DMF molecules, four guest DMF molecules, three coordinated water molecules and one guest water molecule.

Table 4.12: Crystal Data and Refinement Parameters of **7**

Empirical Formula	$C_{76.5}H_{92.5}Gd_4N_{15.5}O_{49.5}$
Formula Weight (g.mol^{-1})	2650.16
Temperature (K)	173(2)
Wavelength (Å)	0.71073
Crystal System	Triclinic
Space Group	$P\bar{1}$
a (Å)	14.324(2)
b (Å)	15.317(2)
c (Å)	25.468(3)
α (°)	87.994(2)
β (°)	85.151(2)
γ (°)	63.419(2)
Volume (Å^3)	4979(1)
Z	2
Calculated Density (g.cm^{-3})	1.768
***μ* (mm^{-1})**	2.733
***F* (*000*)**	2624
Crystal Size (mm)	0.43 x 0.28 x 0.18
***Θ* Range Scanned (°)**	1.59 – 28.45
Index Range	-19 < h < 19, -20 < k < 20, -34 < l < 34
No. Reflections Collected	190792
No. Unique Reflections	24969
R_{int}	0.0336
Data Completeness to θ_{max} (%)	99.3
Refinement Method	Full-matrix least-squares on F^2
Data/Restraints/Parameters	24969/17/1303
Goodness-of-fit on F^2	1.127
Final *R* Indices [$I>2\sigma(I)$]	R_1 = 0.0480, wR_2 = 0.1141
***R* Indices (all data)**	R_1 = 0.0576, wR_2 = 0.1216
Largest Diff. Peak and Hole (e.Å^{-3})	6.049, -2.347

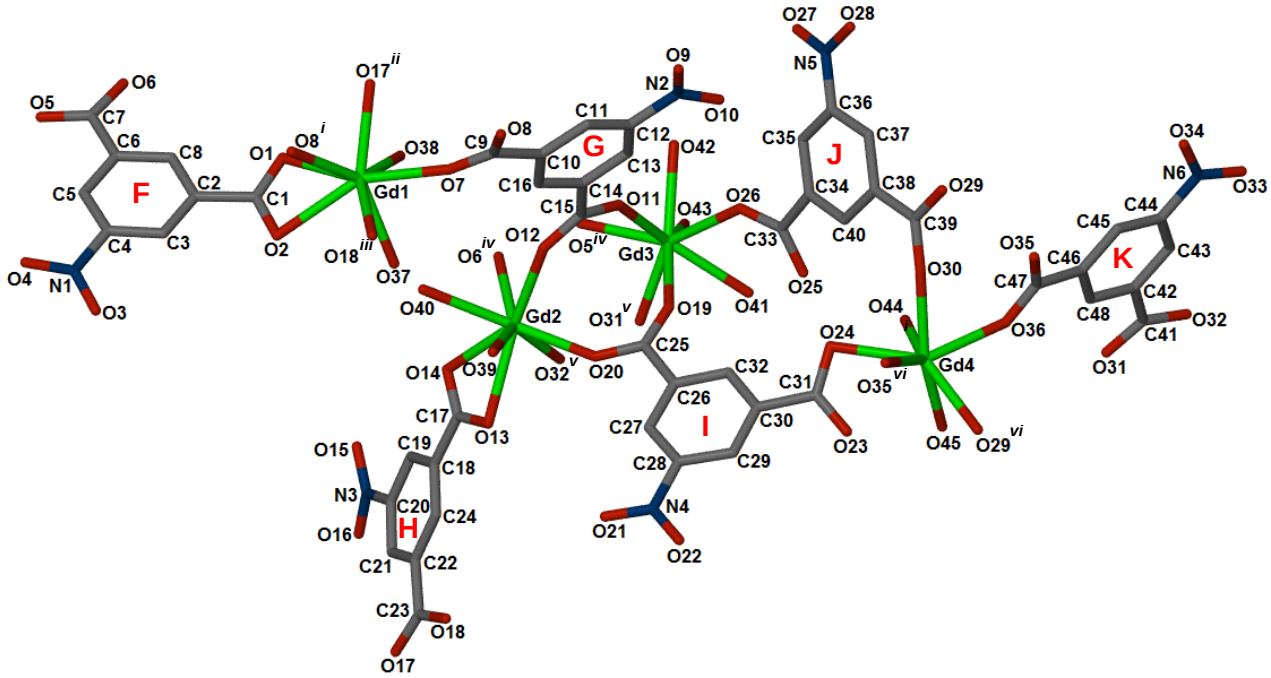

Figure 4.23: The asymmetric unit of **7** with hydrogen atoms, DMF molecules and guest water molecules omitted for clarity. The oxygen atoms of the coordinated DMF molecules are shown

Related by symmetry: [i]-x, 1-y, -z; [ii]-1+x, 1+y, z; [iii]1-x, -y, -z; [iv]1-x, 1-y, -z; [v]1-x, -y, 1-z; [vi]-x,-y,1-z; [vii]-1+x, y, z; [viii]1+x, -1+y, z; [ix]1+x, y, z

The Gd1, Gd2 and Gd3 metal centres are coordinated to 8 oxygen atoms. For Gd1 four oxygen atoms are from bridging carboxylates (O7, O8^{i}, O17^{ii}, O18^{iii}), two are from the O1-C1-O2 chelating carboxylate, one is from the O37 water molecule and one is from the O38 DMF molecule. For the Gd2 metal centre four oxygen atoms are from bridging carboxylates (O6^{iv}, O12, O20, O32^{v}), two are from the O13-C17-O14 chelating carboxylate and two are from the O39 and O40 coordinated DMF molecules. For the Gd3 metal centre four oxygen atoms are from bridging carboxylates (O5^{iv}, O11, O19, O31^{v}), one is from the unidentate carboxylate moiety (O26), one is from the coordinated water molecule O41 and two are from the O42 and O43 coordinated DMF molecules. Gd4 is coordinated to 7 oxygen atoms with four from bridging carboxylates (O29^{vi}, O30, O35^{vi}, O36), O24 from the unidentate O23-C31-O24 carboxylate moiety, one from the coordinated O44 water molecule and one from a coordinated DMF molecule (O45). Full details of bond lengths are given in Table 4.13.

Table 4.13: Experimental Gd-O bond lengths for **7** and literature Gd-O bond lengths

Bond	Length (Å)	Average Length (Å)	Bond Type
Gd1-O37	2.462(5)	2.42 ± 0.05*	Terminal Water
Gd3-O41	2.413(4)		
Gd4-O44	2.484(4)		
Gd1-O7	2.294(4)	2.35 ± 0.06*	Terminal Carboxylate
Gd1-O8^{i}	2.372(4)		
Gd1-O17^{ii}	2.359(4)		
Gd1-O18^{iii}	2.350(4)		
Gd2-O6^{iv}	2.356(4)		
Gd2-O12	2.382(4)		
Gd2-O20	2.315(4)		
Gd2-O32^{v}	2.386(4)		
Gd3-O5^{iv}	2.386(4)		
Gd3-O11	2.328(4)		
Gd3-O19	2.363(4)		
Gd3-O26	2.422(4)		
Gd3-O31^{v}	2.328(4)		
Gd4-O24	2.387(4)		
Gd4-O35^{vi}	2.391(4)		
Gd4-O29^{vi}	2.427(4)		
Gd4-O30	2.368(4)		
Gd4-O36	2.386(4)		
Gd1-O1	2.430(4)	2.52 ±0.09*	Chelating Carboxylate
Gd1-O2	2.516(4)		
Gd2-O13	2.519(4)		
Gd2-O14	2.472(4)		
Gd1-O38	2.418(4)	2.38 ± 0.04*	DMF
Gd2-O39	2.378(6)		
Gd2-O40	2.496(5)		
Gd3-O42	2.433(4)		
Gd3-O43	2.421(4)		
Gd4-O45	2.353(5)		

* Values obtained from the CSD

Related by symmetry: ^{i}-x, 1-y, -z; ^{ii}-1+x, 1+y, z; ^{iii}1-x, -y, -z; ^{iv}1-x, 1-y, -z; ^{v}1-x, -y, 1-z; ^{vi}-x,-y,1-z; ^{vii}-1+x, y, z; ^{viii}1+x, -1+y, z; ^{ix}1+x, y, z

The Gd1 metal centre forms a dimer with the Gd1^{i} metal centre. Gd2 and Gd3 act as a dimer and the Gd4 metal centre forms a dimer with the Gd4^{vi} metal centre. The distance between the Gd4 metal ions in each dimer is 4.0428(7) Å. This distance is significantly shorter than the Gd1-Gd1^{i} and Gd2-Gd3 distances (4.448 and 4.512 Å respectively). There have been reports of Gd-Gd distances as close as 3.866(1) Å.[17] The bridging NIA units have the same paddle-wheel motif as those found in compounds **5** and **6**. The SBUs formed by each of the Gd1/Gd1^{i}, Gd2/Gd3 and Gd4/Gd4^{vi} metal dimers are shown in Figure 4.24a, b, and c, respectively. The Gd2-O40 bond length is longer than the average seen in the Cambridge Structural Database[1] (CSD). O40 belongs to a coordinated DMF molecule and it may have partial coordinated and partial guest character leading to a longer Gd-O distance.

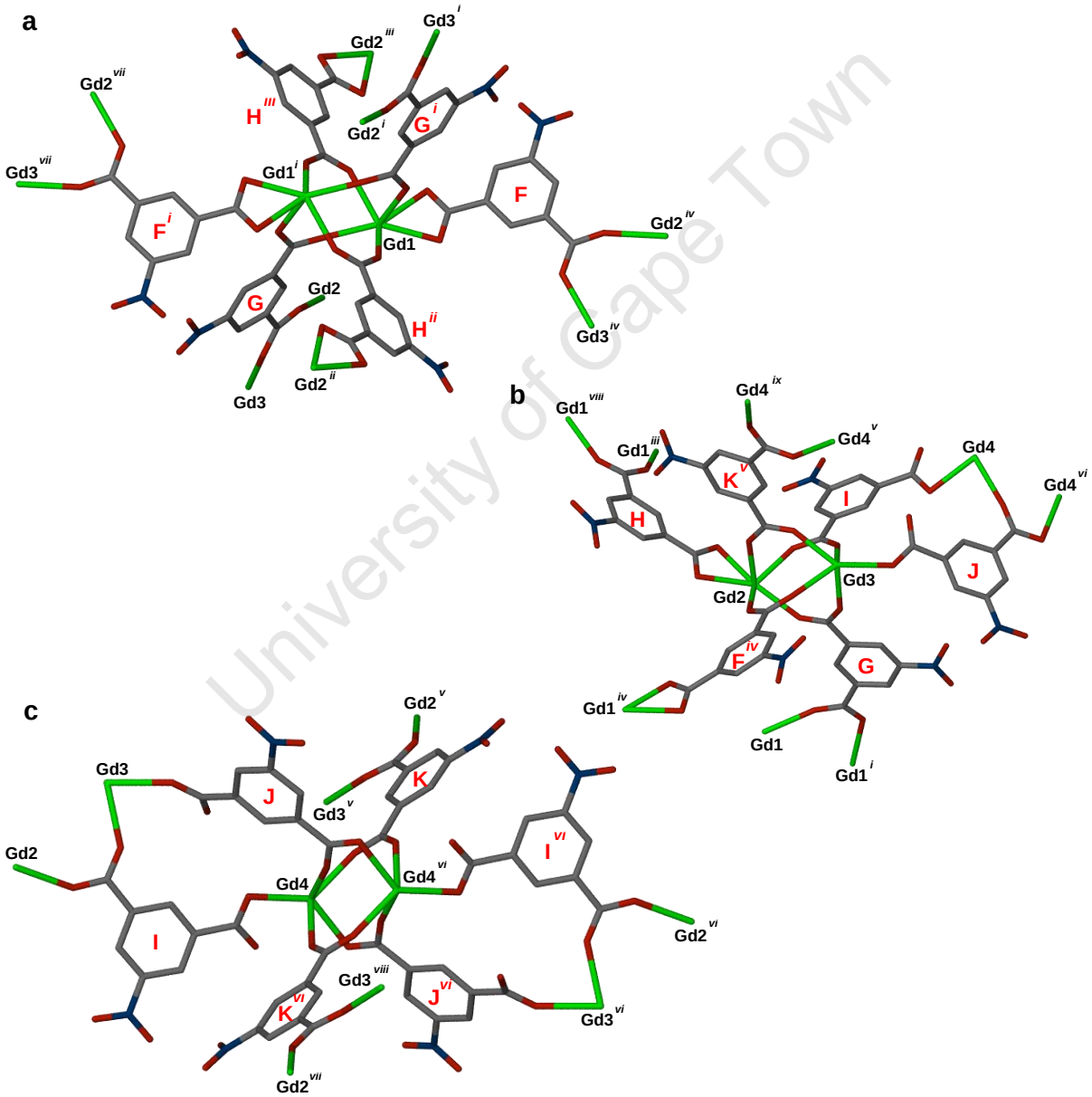

Figure 4.24: The SBUs of compound **7**. **a)** NIA G, NIA G^{i}, NIA H^{ii} and NIA H^{iii} form the paddle-wheel and NIA F and NIA F^{i} are axially coordinated in the Gd1/Gd1^{i} SBU, **b)** NIA F^{iv}, NIA G, NIA I and NIA K^{v} form the paddle-wheel and NIA H and NIA J are axially coordinated in the Gd2/Gd3 SBU and **c)** NIA J, NIA J^{vi}, NIA K and NIA K^{vi} form the paddle-wheel and NIA I and NIA I^{vi} in the Gd4/Gd4^{vi} SBU

Related by symmetry: ^{i}-x, 1-y, -z; ^{ii}-1+x, 1+y, z; ^{iii}1-x, -y, -z; ^{iv}1-x, 1-y, -z; ^{v}1-x, -y, 1-z; ^{vi}-x,-y,1-z; ^{vii}-1+x, y, z; ^{viii}1+x, -1+y, z; ^{ix}1+x, y, z

The O1-C1-O2 carboxylate of NIA F is doubly coordinated to the Gd1 metal centre. The O5-C7-O6 carboxylate is a bridge in the Gd2/Gd3 dimer with O5 coordinated to Gd3^{iv} and O6 coordinated to Gd2^{iv}. The O7-C9-O8 carboxylate of NIA G bridges a Gd1 dimer with O7 coordinated to Gd1 and O8 coordinated to Gd1^{i}. The O11-C15-O12 carboxylate bridges the Gd2/Gd3 metal centre pair with O11 coordinated to Gd3 and O12 coordinated to Gd2. The O13-C17-O14 carboxylate moiety of NIA H is chelated to the Gd2 metal centre. The O17-C23-O18 carboxylate bridges a Gd1 dimer with O17 coordinated to Gd1^{viii} and O18 coordinated to Gd1^{iii}.

The O19-C25-O20 carboxylate of NIA I bridges the Gd2/Gd3 dimer with O19 coordinated to Gd3 and O20 coordinated to Gd2. O24 is coordinated to Gd4 while O23 is uncoordinated. O26 in NIA J is coordinated to the Gd3 metal centre while O25 is uncoordinated. The O29-C39-O30 carboxylate moiety bridges the Gd4 dimer with O29 coordinated to Gd4^{vi} and O30 coordinated to Gd4. The O31-C41-O32 carboxylate of NIA K bridges the Gd2/Gd3 metal pair with O31 coordinated to Gd3^{v} while O32 is coordinated to Gd2^{v}. The O35-C47-O36 carboxylate bridges a Gd4 dimer with O35 coordinated to Gd4^{vi} and O36 coordinated to Gd4.

There are four guest DMF molecules (O46, O47, O48 and O49). The O46, O47 and O48 DMF molecules all have full site occupancy. The O49 DMF molecule is disordered over two positions with a ratio of approximately 0.8:0.2 s.o.f for the two disordered positions. There is also a guest O50 water molecule, which has full site occupancy.

Figure 4.25 shows in black the framework of compound **7**. The symmetry elements present in the $P\bar{1}$ space group are overlaid in red. The only symmetry elements present in compound **7** are inversion centres. The inversion centre at (0,0,0) is located between the nitro moieties of two NIA H units while that at (0,1/2,1/2) is located between the nitro moieties of two NIA J. The inversion centres at (1/2,0,0), (1/2,1/2,0) and (1/2,0,1/2) are situated between two Gd2, two Gd1 and two Gd4 metal ions in adjacent dimers, respectively. The inversion centre at (1/2,1/2,1/2) is positioned between two coordinated O45 DMF molecules. The inversion centres at (0,0,1/2) and (0,1/2,0) are located at the centre of Gd4/Gd4* and Gd1/Gd1* dimers respectively.

Related by symmetry: ^{i}-x, 1-y, -z; ^{ii}-1+x, 1+y, z; ^{iii}1-x, -y, -z; ^{iv}1-x, 1-y, -z; ^{v}1-x, -y, 1-z; ^{vi}-x,-y,1-z; ^{vii}-1+x, y, z; ^{viii}1+x, -1+y, z; ^{ix}1+x, y, z

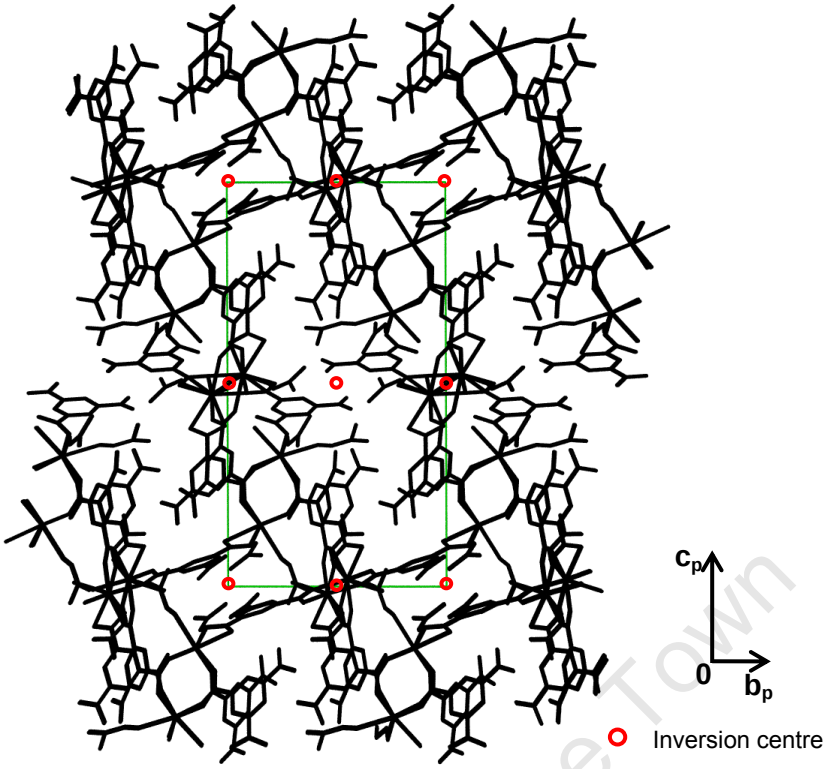

Figure 4.25: The packing diagram of **7** (black) viewed down [100] with an overlay in red of the symmetry elements present in the unit cell. Guest DMF and water molecules are omitted for clarity

4.5.2 THERMAL ANALYSIS

The TG trace (Figure 4.26a, blue) displays four mass loss steps. Step A (*ca* 20 – 73 °C) corresponds to the loss of the one guest water molecule (O50) and the one guest DMF molecule – potentially the O46 or O48 DMF molecules as these are both located close to the guest water molecule in the structure (calculated: 3.44%, experimental: 3.39%). Step B (*ca* 73 – 130 °C) corresponds to the loss of the other three guest DMF molecules (O47, O48, O49) as well as the three coordinated water molecules (O37, O41, O44) (calculated: 10.31%, experimental: 10.43%). Step C (*ca* 140 – 331 °C) corresponds to the loss of the 5.5 coordinated DMF molecules (calculated: 15.17%, experimental: 15.06%), which continues until 350 °C. Degradation of compound **7** starts as soon as step B is complete and coordinated DMF molecules begin to be removed. Mass loss D (*ca* 331 – 450 °C) corresponds with the structure decomposing completely as two of the NIA units are removed (calculated: 15.78%, experimental: 15.53%). The TG and DSC trace details are given in Table 4.14.

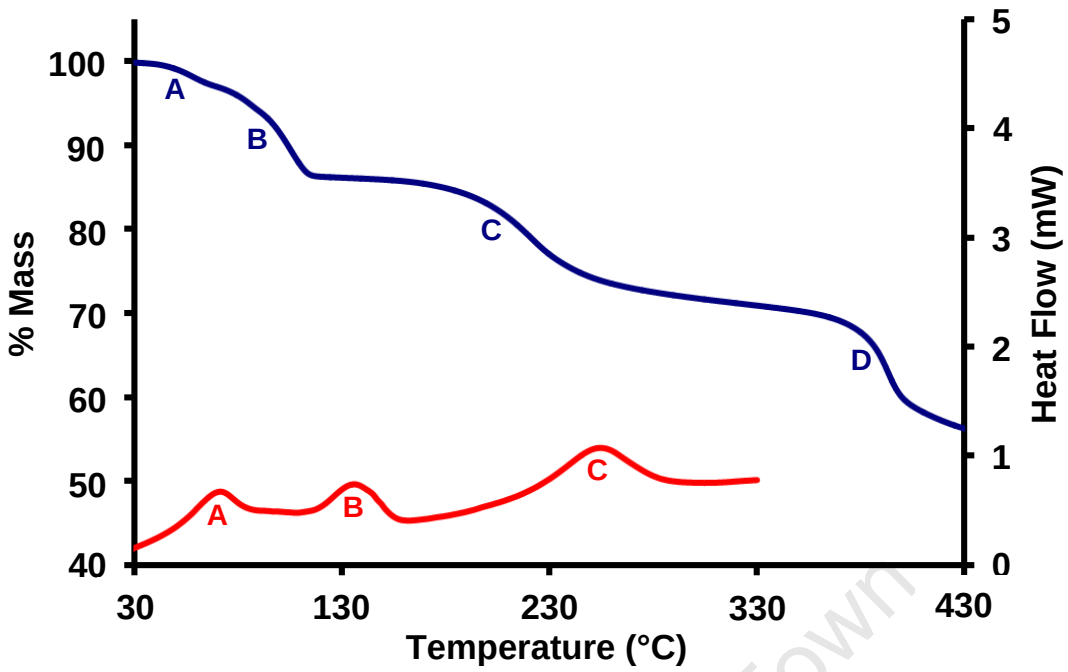

Figure 4.26: a) TG analysis of **7** and **b)** DSC analysis of **7** (heating rates: 2 and 10 °C.min^{-1} respectively)

The DSC trace (Figure 4.26, red) correlates well with the TGA. Three distinct endotherms (A, B and C) correspond to the loss of solvent molecules. Endotherm A corresponds with the loss of the one guest water and one of the guest DMF molecules. Endotherm B correlates with the loss of the remaining DMF guest molecules and the coordinated water molecules. The onset temperature of B is an approximation as the beginning of the peak is obscured by endotherm A. Endotherm C corresponds with the loss of the coordinated DMF molecules and the beginning of decomposition of compound **7**. The DSC experiment was not taken to complete decomposition.

Table 4.14: TGA and DSC results for **7**

	TG Results		DSC Results
	Calc. % Mass Loss	**Exp. % Mass Loss**	**T_{onset} (°C)**
1 H_2O&1 DMF	3.44	3.39	47
3 H_2O&3 DMF	10.31	10.43	*ca* 118
6 DMF	15.17	15.06	214.6
2 H_2NIA	15.78	15.53	-

The sample is crystalline at room temperature (28 °C) as seen with HSM (Figure 4.27). Despite the degradation observed at relatively low temperatures it is stable to over 50 °C as shown in Figure 4.27b. The crystal maintains that crystallinity with the removal of the first DMF molecule and guest water molecule with only a crack showing on the surface of the crystal at 75 °C (Figure 4.27c). After that temperature cracks continue to form on the crystal

with continued heating and loss of guest DMF molecules. By 110 °C (Figure 4.27e) the surface is criss-crossed with cracks. When all the guest DMF molecules have been removed at 129 °C (Figure 4.27f) a dark mark appears on the surface indicating the beginning of decomposition. This mark continues across the surface of the crystal until the entire crystal is opaque and decomposed by 150 °C (Figure 4.27g). This does not change upon the loss of the coordinated DMF molecules. The crystal begins to disintegrate at higher temperatures as shown in Figure 4.27h. This corresponds with mass loss D on the TG. This confirms that the structure is completely decomposed by that temperature.

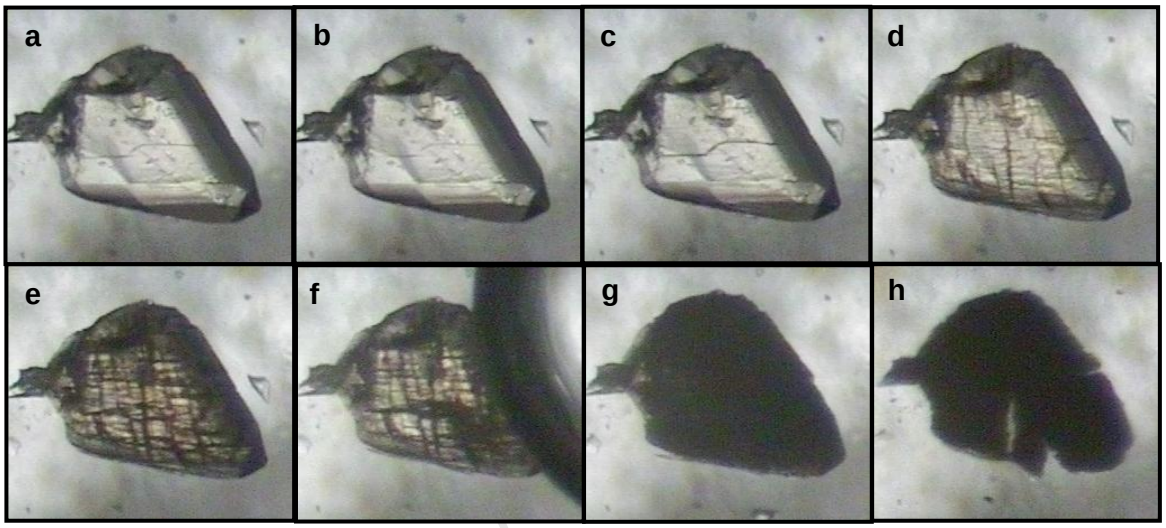

Figure 4.27: HSM pictures of **7** at **a)** 28 °C, **b)** 50 °C, **c)** 75 °C, **d)** 100 °C, **e)** 110 °C, **f)** 129 °C, **g)** 150 °C and **h)** 370 °C

As with compounds **5** and **6** elemental analysis suggests that guest molecules are lost, or exchanged, in compound **7** under ambient conditions if exposed to air for an extended period of time. This could not be tested with **7** specifically due to insufficient sample. If one guest DMF is lost and two additional guest water molecules are absorbed before the elemental analysis was performed (**7a**) a reasonable correlation between experimental and calculated is obtained. The calculated values for both **7** and **7a** are provided in Table 4.15.

Table 4.15: Elemental analysis of $[Gd_4(C_{48}N_6O_{36}H_{18})(C_{16.5}N_{5.5}O_{8.5}H_{44.5})]\cdot 4(C_3NOH_7)\cdot 4(H_2O)$ (**7a**)

	Calculated 7	Calculated 7a	Experimental
% C	34.67	33.78	33.41
% H	3.51	3.45	3.84
% N	8.19	7.77	8.04

4.5.3 SUMMARY

PXRD analysis of compound **7** was not included as the bulk samples obtained were generally a mixture of poorly crystalline powder and single crystals. This resulted in poor quality PXRD patterns that could not easily be interpreted. Instead of PXRD analysis single crystal analysis was performed on several crystals in a vial to determine whether compound **7** had been obtained.

Compound **7** has an interesting structural topology that contains elements of both compounds **5** and **6**. This will be discussed in greater detail in Chapter 5 – Topological Analysis.

4.6 REFERENCES

1. Cambridge Structural Database and Cambridge Structural Database System, Version 5.32, Cambridge Crystallographic Data Centre, University Chemical Laboratory, Cambridge, England, February 2011.

2. H. Xu and Y. Li, *J. Mol. Struct.,* 2004, **693**, 11.

3. H. -P. Xiao, X. -H. Li, Q. Shi, W. -B. Zhang, J. G-. Wang and A. Morsali, *J. Coord. Chem.,* 2008, **61**, 2905.

4. H. Abourahma, B. Moulton, V. Kravtsov and M. J. Zaworotko, *J. Am. Chem. Soc.,* 2002, **124**, 9990.

5. A. D. Burrows, C. G. Frost, M. F. Mahon, M. Winsper, C. Richardson, J. P. Attfield and J. A. Rodgers, *Dalton Trans.,* 2008, 6788.

6. M. Su, Z. -D. Huang, H. Sun, G. Yang and S. W. Ng, *Acta Cryst. E,* 2010, **E66**, m1220.

7. J. Tao, X. Yin, Y. -B. Jiang, L. -F. Yang, R. -B. Huang and L. -S. Zheng, *Eur. J. Inorg. Chem.,* 2003, 2678.

8. Y. Huang, B. Yan and M. Shao, *J. Solid State Chem.,* 2009, **182**, 657.

9. Y. Zhao, M. Padmanabhan, Q. Gong, N. Tsumori, Q. Xu and J. Li, *Chem. Commun.,* 2011, **47**, 6377.

10. J. Ye, P. Zhang, K. Ye, W. Yin, L. Ye, G. Yang and Y. Wang, *Inorg. Chem. Commun.,* 2006, **9**, 744.

11. S. P. Chen, Y. X. Ren and S. L. Gao, *Russ. J. Coord. Chem.,* 2008, **34**, 301.

12. Paratone N oil, (Exxon Chemical Co., Tx, USA).

13. A. L. Spek, *J. Appl. Cryst.,* 2003, **36**, 7.

14. A. L. Spek, Program PLATON, A Multipurpose Crystallographic Tool, Version 10500, © 1980 - 2000,, Utrecht University, The Netherlands.

15. G. Wang, T. Song, Y. Fan, W. Wan, J. Xu and L. Wang, *Inorg. Chem. Commun.,* 2010, **13**, 935.

16. S. -P. Chen, Y. -X. Ren, W. -T. Wang and S. -L. Gao, *Dalton Trans.,* 2010, **39**, 1552.

17. L. Cañadillas-Delgado, O. Fabelo, J. Cano, J. Pasán, F. S. Delgado, F. Lloret, M. Julve and C. Ruiz-Pérez, *CrystEngComm,* 2009, **11**, 2131.

Chapter 5

Topological Studies

The topological analyses of each of the seven compounds presented previously in this thesis are given in this chapter. Comparisons are made between these topologies and structures reported in the literature that display the same network. Where applicable new networks are fully analysed and described.

The nets of **1**, **2**, **3**, **5**, **6** and **7** were analysed with SYSTRE[1] and checked against the Reticular Chemistry Structural Resource,[2,3] (RCSR), and the EPINET[4] databases. Compound **4** forms a three-dimensional net through hydrogen bonding and was therefore not fully investigated.

Full SYSTRE, TOPOS[5,6] and OLEX[7] output for all new topologies are given in the supplementary material. A guide to network analysis can be found in a recent monograph.[8]

5.1 $[Zn_6(\mu_3\text{-}OH)_2(BTRI)_4(DMF)_{2.5}(H_2O)_2]\cdot[Zn(H_2O)_3(DMF)_3]\cdot 2.96H_2O$ (1)

Compound **1** has a binodal six- and three-connected network (as defined in Figure 5.1). The asymmetric unit of **1** is given in Figure 5.2 with the A, B, C and D BTRI units as well as the X, Y and Z secondary-building units (SBUs) labelled. This is an unprecedented topology with the short symbol $(4.6^2)_2(4^2.6^{10}.8^3)$. As described in Chapter 3.3 the structure consists of three trimeric $[Zn_3(OH)(BTRI)_6]$ (SBUs) X, Y and Z. Each SBU is coordinated to six fully deprotonated BTRI units. The asymmetric unit contains four BTRI units all with full site occupancy. BTRI A connects to one X SBU and two Y SBUs. BTRI B coordinates to one X SBU and two Z SBUs. BTRI C connects to two X SBUs and one Z SBU. BTRI D coordinates to two X SBUs and one Y SBU.

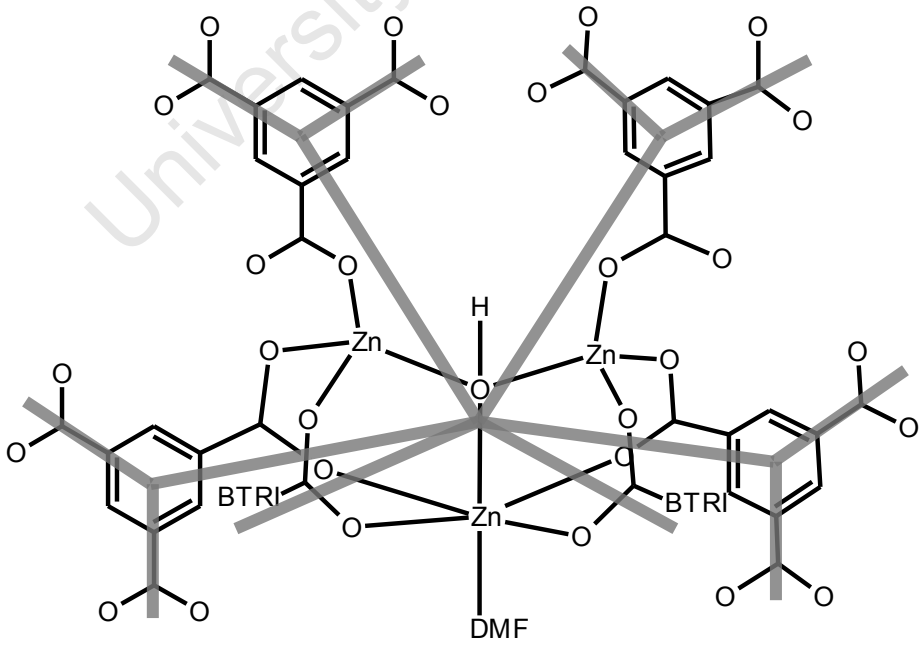

Figure 5.1: A schematic view of the three- and six-connected nodes in compound **1**. The **Y** SBU is depicted here but the nodes at SBU **X** and **Z** are topologically identical

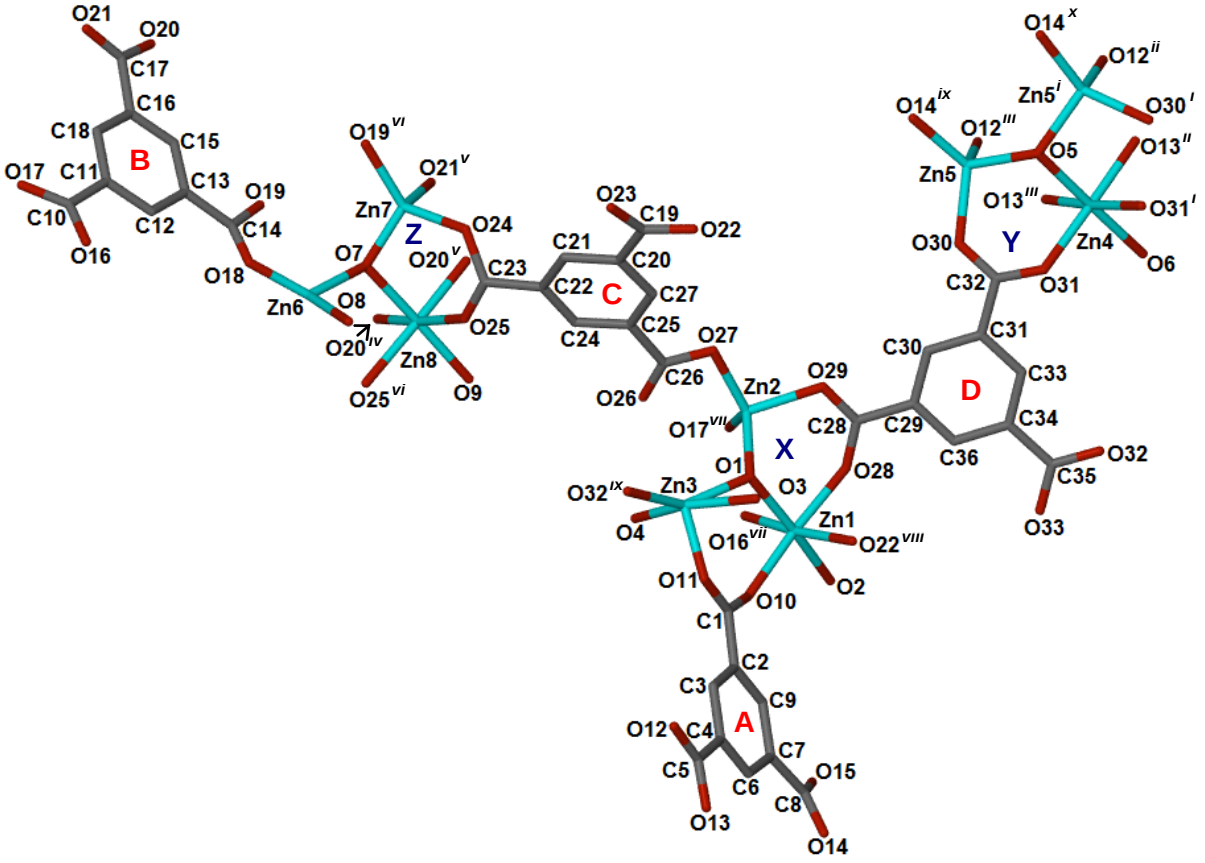

Figure 5.2: The asymmetric unit of **1** with DMF molecules, guest water molecules and counter cation omitted, the oxygen atoms of the DMF molecules as shown

A node placed within the metal cluster SBUs joins six BTRI units, which results in six-connected intersections. A node placed in the centre of each BTRI unit joins to three SBUs, which results in three-connected intersections. Each of the six-connected nodes was found to be equivalent (node 1). The three-connected nodes were also topologically equivalent (node 2). This leads to two distinct nodes within the structure. There are three trimeric zinc SBU within the asymmetric unit, however SBU Y and SBU Z are located on the (*1/2, y, z*) and (*0, y, z*) mirror planes respectively. Each of the four type 2 nodes have full site occupancy. This leads to a ratio of 1:2 for nodes 1 and 2.

Figure 5.3a shows the topological net of **1** as it appears in this structure. The six-connected nodes are shown in blue (node 1) and the three-connected nodes are shown in red (node 2). The channels mentioned in Chapter 3.3 are exaggerated by the net diagram. The link angles for node 1 fall into four areas: 42±4°, 85±7°, 101±6°, 135±7°. The node 1 located within SBUs Y and Z are highly symmetrical as both SBU are located on mirror planes. Node 2 coordinates in a distorted trigonal planar/trigonal pyramidal manner with two link angles of close to 120° and one of between 100 and 112° depending on the BTRI unit.

Related by symmetry: [i]1-x, y, z; [ii]-1/2+x, 1/2+y, z; [iii]3/2-x, 1/2+y, z; [iv]x, 2-y, 1/2+z; [v]2-x, 2-y, 1/2+z; [vi]2-x, y, z; [vii]2-x, y, 1+z; [viii]3/2-x, 3/2-y, 1/2+z; [ix]3/2-x, 3/2-y, -1/2+z; [x]-1/2+x, 3/2-y, -1/2+z

In its most symmetric form, see Figure 5.3b, the net comprises prismatic six-coordination, with two of the "sides" flattened to give link angles of only 43°, and Y-shaped trigonal nodes with angles of 130, 135° and 95°.

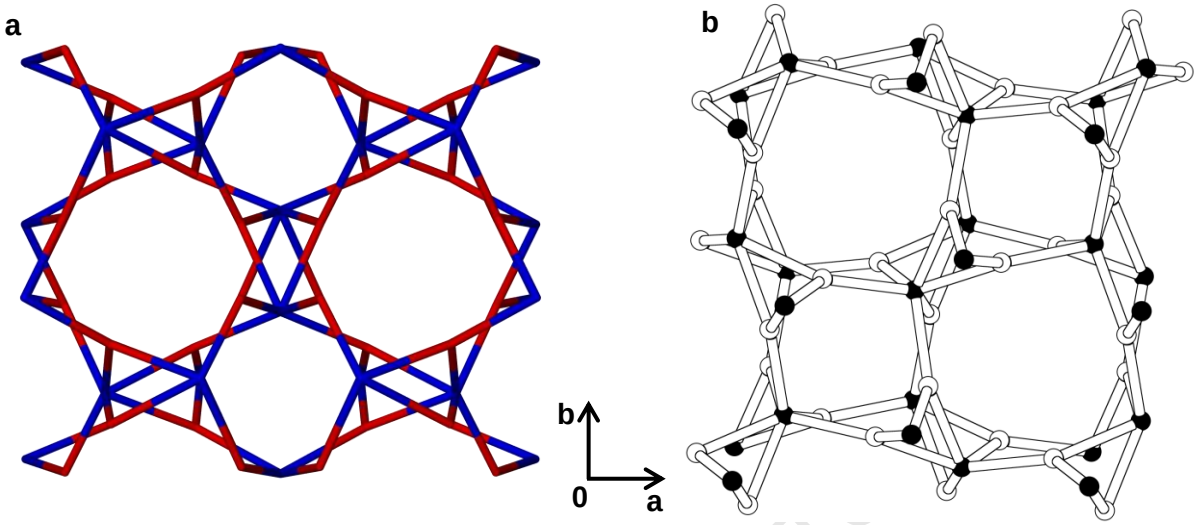

Figure 5.3: Network analysis of compound **1**. **a)** The net of **1** with node 1 shown in blue and node 2 given in red. **b)** The ideal form of the net with black circles for node 1 and white circles for node 2

The complete short and long symbols for **1** are $(4.6^2)_2(4^2.6^{10}.8^3)$ and $4{\cdot}4{\cdot}6{\cdot}6{\cdot}6{\cdot}6{\cdot}6{\cdot}6{\cdot}6{\cdot}6{\cdot}6_2{\cdot}6_2{\cdot}8_2{\cdot}8_2{\cdot}8_7$, $4{\cdot}6_2{\cdot}6_2$ respectively with a CD10 value of 1242.3333. This net has been accepted into the RCSR database as the **sab**-net. The CD10 value is defined as the sum of the first 10 shells of topological neighbours with a weighted average given where more than one type of node is present. The total includes the original node as well.

5.2 [Zn(HCOO)(BTRI)$_{0.3}$(DMF)] (2)

The asymmetric unit of **2** is given in Figure 5.4a. Each metal centre coordinates to two fully deprotonated BTRI units, three formate anions and a DMF molecule.

As described in Chapter 3.4 the zinc metal ions form hexameric clusters. These act as flat six-connected SBUs. Node 1 is placed at the centre of the cluster as shown in Figure 5.4b and is therefore a six-connected node. Node two is placed at the centre of the BTRI units, which act as three-connected nodes.

Node 1 is shown in red and node 2 in blue in Figure 5.4c. The three- and six-connected nodes join to form two-dimensional sheets parallel to the [001] plane. All angles around node 1 are approximately 60° and all of those around node 2 are around 120°. The two-

dimensional layers are parallel to one another and form the $(4^3)(4^6)$-**kgd** net. The complete long symbol for **2** is 4·4·4, 4·4·4·4·4·4·6·6·6·6·6·6·8_2·8_2·8_2 with a CD10 value of 251.0000.

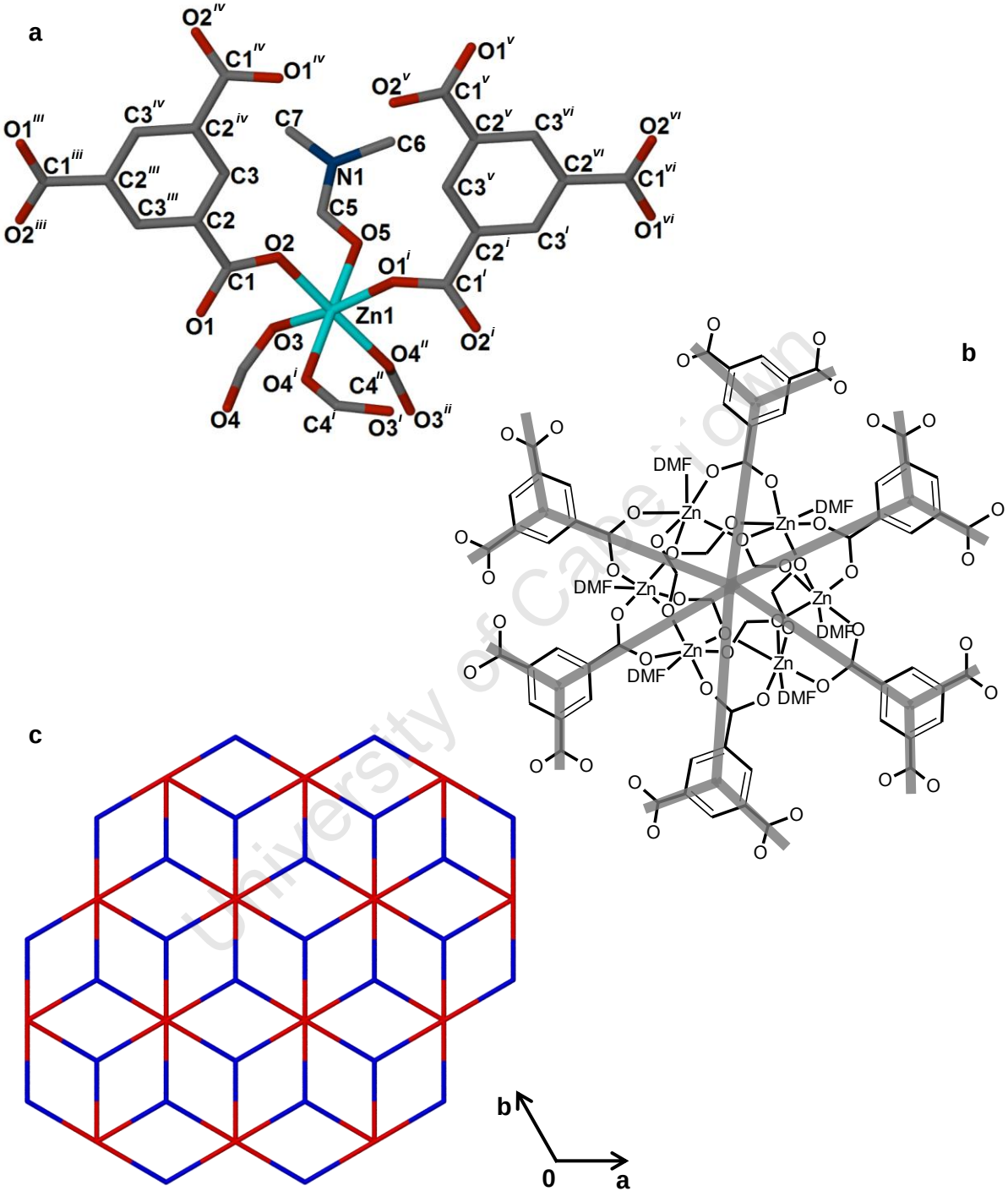

Figure 5.4: a) The asymmetric unit of **2**, **b)** a schematic representation of the hexameric zinc cluster and the three- and six- connected nodes and **c)** the topological net of **2** with node 1 in red and node 2 in blue

Related by symmetry: ^{i}x-y, -1+x, 1-z; ^{ii}1-y, -1+x-y, z; ^{iii}2-y, x-y, z; ^{iv}2-x+y, 2-x, z; ^{v}2-x, 1-y, 1-z; ^{vi}y, 1-x+y, 1-z

5.3 $[Zn_2(\mu_2\text{-}OH_2)(HBTRI)(BTRI)(H_2O)_2]\cdot DMA\cdot 3H_2O$ (3)

The asymmetric unit of **3** is given in Figure 5.5 with the fully deprotonated BTRI unit labelled A and the doubly deprotonated HBTRI unit labelled B. Compound **3** has a binodal five- and three-connected network as defined in Figure 5.6. This is of an unprecedented topology with short symbol $(6^3)(6^9.8)$.

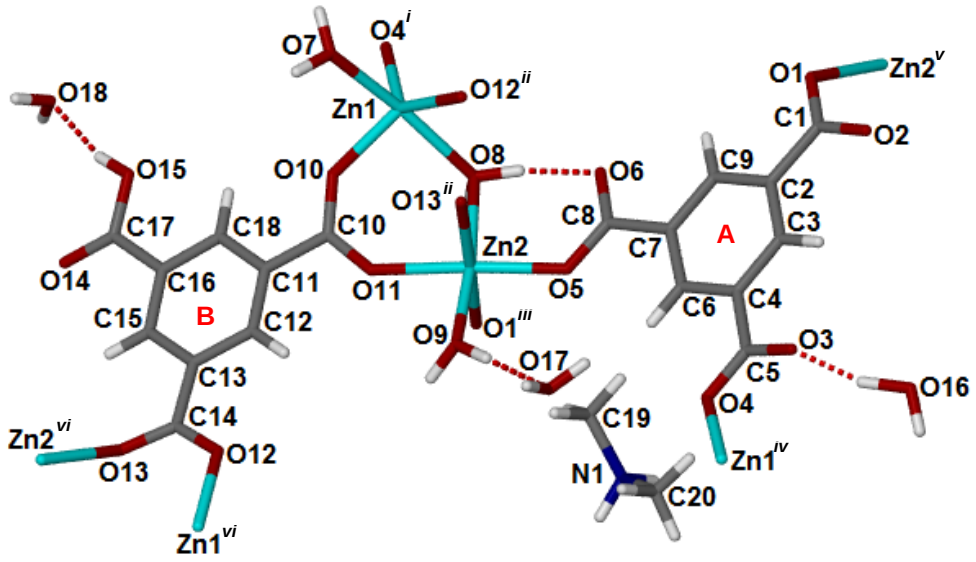

Figure 5.5: The asymmetric unit of **3**

The Zn1/Zn2 metal dimer is bridged by two HBTRI B units. The Zn1 metal centre is singly coordinated to one BTRI A unit and the Zn2 metal centre is singly coordinated two BTRI A units. Node 1 is placed between the Zn1/Zn2 metal centres. BTRI A coordinates to two Zn2 metal centres and one Zn1 metal centre. Node 2 is placed in the centre of BTRI A and is three-connected. The HBTRI B unit bridges a Zn1/Zn2 metal dimer with each carboxylate moiety but does not coordinate through the protonated carboxylic acid. As a result HBTRI B is treated as a bridge rather than a node.

Node 1 is a five-connected node and is linked to two type 1 nodes and three type 2 nodes. Node 2 is a three-connected node and is joined to three node 1. The topology for this net is given in Figure 5.7a with the five-connected nodes shown in blue and the three-connected nodes shown in red. In its most symmetric form, Figure 5.7b, this net has almost ideal trigonal coordination for the three-connected node and distorted trigonal-bipyramidal coordination for the five-connected node.

Related by symmetry: ^{i}-1+x, y, -1+z; ^{ii}1-x, 1/2+y, 1-z; ^{iii}2-x, -1/2+y, 1-z; ^{iv}1+x, y, 1+z; ^{v}2-x, 1/2+y, 1-z; ^{vi}1-x, -1/2+y, 1-z

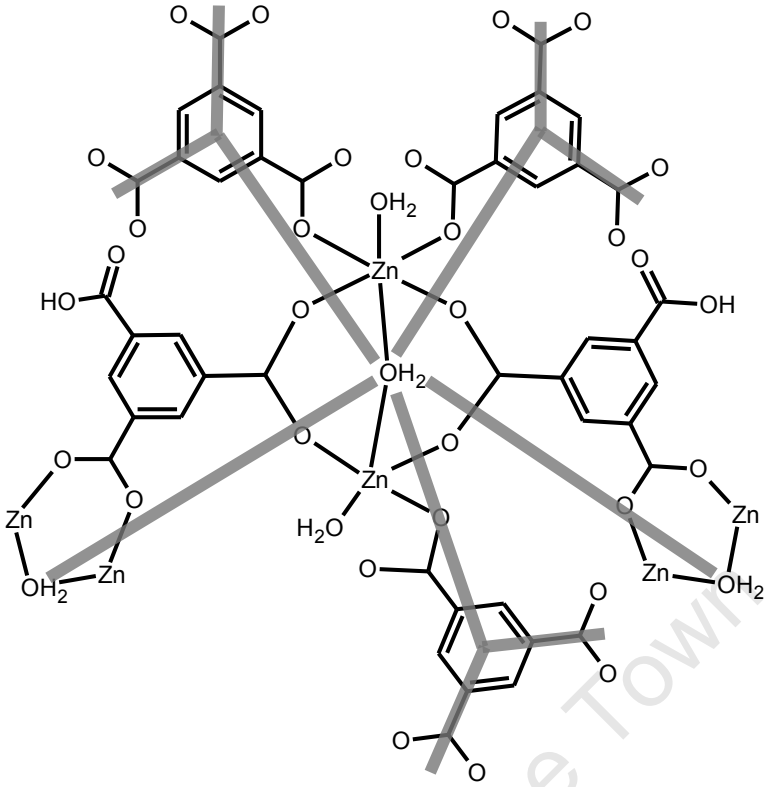

Figure 5.6: A schematic diagram of the three- and five-connected nodes with the five-connected node located between the Zn1/Zn2 metal centres

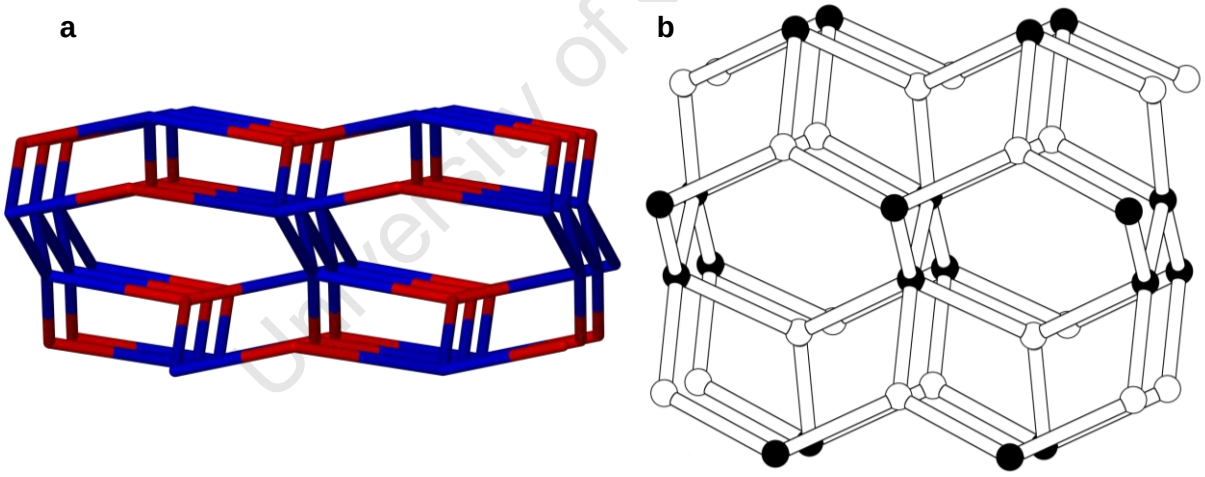

Figure 5.7: a) Network analysis of compound **3**. **a)** The net found for **3** with node 1 given in blue and node 2 given in red. **b)** The ideal form of the net with node 1 as black circles and node 2 as white circles

The fairly common five- and three-connected **hms** and **bnn** nets have one link between the five-connected nodes in the axial position and one in the equatorial position. The net found in compound **3** has both links between the five-connected nodes in the axial positions. The five-connected node can form ten different connections as explained in Chapter 1.7 – Topology. One of these links has an eight membered ring as the smallest ring. This is a

"shortcut" however, as it includes another connection. This eight membered ring is therefore written as * in the long symbol notation.

The complete short and long symbols for **3** are $(6^3)(6^9.8)$ and $6{\cdot}6{\cdot}6{\cdot}6_2{\cdot}6_2{\cdot}6_2{\cdot}6_2{\cdot}6_2{\cdot}6_2{\cdot}*$, $6_3{\cdot}6_3{\cdot}6_3$ with a CD10 value of 1242.0000. This net has been accepted into the RCSR database as the **kdd** network. Subsequently, $\{Cu(L1){\cdot}2H_2O{\cdot}1.5DMF\}_\infty$ (where L1 is 5-(pyridine-4-yl)isophthalic acid) reported by Xiang *et al* in Inorganic Chemistry in 2011[9] was also shown to contain the **kdd**-net topology.

5.4 [Gd(BTRI)(H$_2$O)$_6$] (4)

The asymmetric unit of compound **4** is given in Figure 5.8 with the hydrogen atoms omitted for clarity. Compound **4** packs as one-dimensional chains along the [20$\bar{2}$] axis. These chains are strongly hydrogen bonded together (see Chapter 3.6 for full details). As a result the network topology of **4** can be considered as three-dimensional.

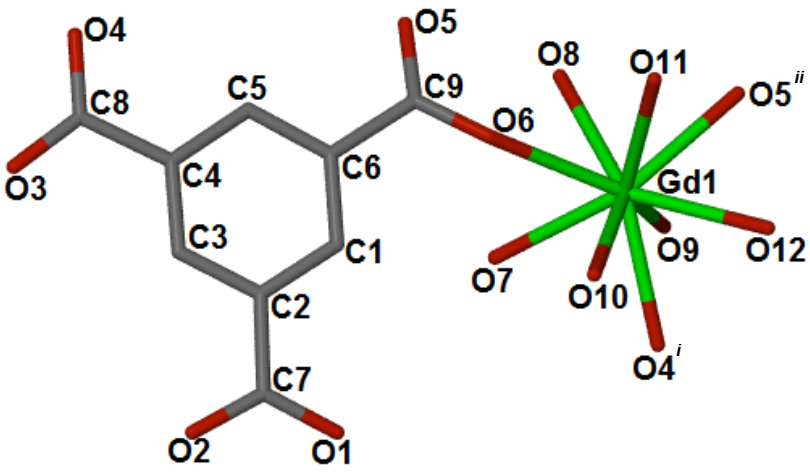

Figure 5.8: The asymmetric unit of **4** with hydrogen atoms omitted for clarity

There is one topological 9-connected node for compound **4**. This is located in two different chemical environments in the asymmetric unit. The two environments are the centre of the fully deprotonated BTRI unit and the gadolinium(III) metal ion. These are shown in purple and green respectively in Figure 5.9.

Figure 5.9a depicts the network of **4** viewed along [001]. From this perspective the net appears similar to the **kgd** net described previously. The "BTRI node" appears to be 6-connected while the "metal centre node" appears to be 3-connected. Figure 5.9b shows the nodes viewed along [010]. Two of the connections overlap when viewed down [010] and

Related by symmetry: ^{i}1+x, y, 1+z; ^{ii}1/2+x, 1/2-y, 1/2+z

therefore the nodes appear 8-connected. This net was formed through hydrogen-bonds and was therefore not analysed further.

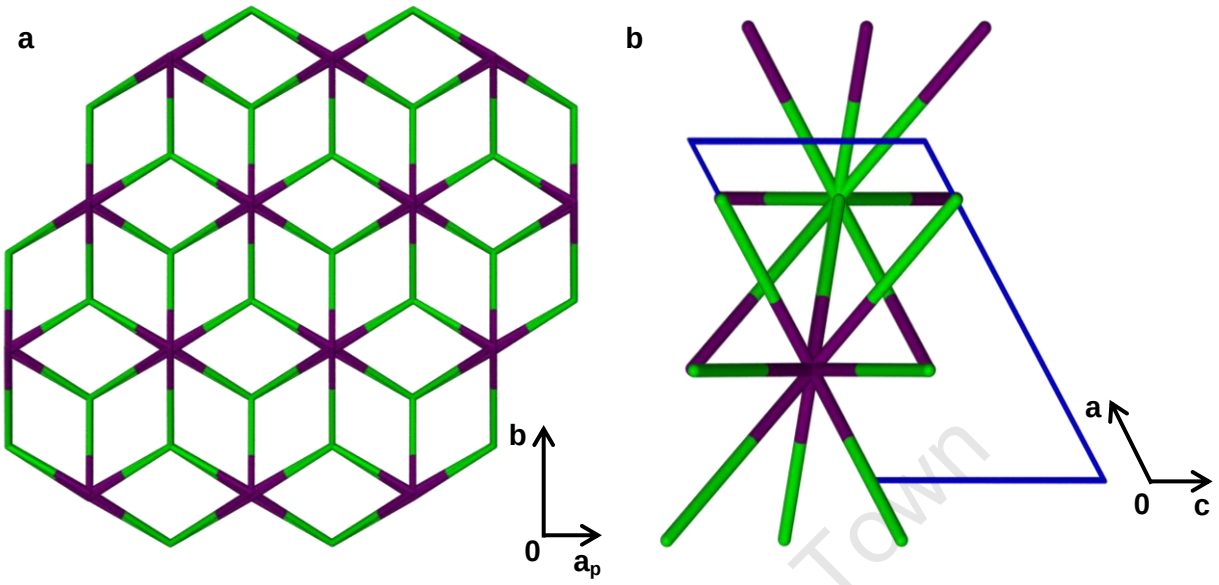

Figure 5.9: Network analysis of compound **4**. **a)** The net found for **4** with the node at the centre of the ligand given in purple and the metal centre node give in green. **b)** Both nodes are topologically equivalent as seen when viewed along [010]

5.5 $[Gd(NIA)_{1.5}(DMF)_2]\cdot DMF$ (5)

The asymmetric unit of compound **5** is given in Figure 5.10 with the NIA units A and B labelled. The Gd1 metal ions form metal pairs in a paddle-wheel motif as described in Chapter 4.

The topological net of **5** is given in Figure 5.11. The node is the centroid between Gd1 and Gd1*. This is shown in schematic form in Figure 5.12. The node connects to six identical paddle-wheel SBUs through four NIA A and two NIA B units. One carboxylate moiety of NIA A coordinates in a bidentate manner to a Gd1 metal centre while the other carboxylate bridges a Gd1/Gd1* pair. NIA B is located on the (*1/2, y, 1/4*) mirror plane and both carboxylates bridge a Gd1/Gd1* dimer. The six-connected node has distorted octahedral geometry. All axial-axial angles are 180° but the axial-equatorial and equatorial-equatorial angles range from 78.5 – 101.5°.

As the node is six-connected there are fifteen different rings that can be formed between node pairs. Twelve of these rings are four-membered rings. The other three are six-

* next to a metal denotes a generic symmetry generated atom

membered rings but as those rings are shortcuts and pass through another node pair they are written as * in the long symbol notation.

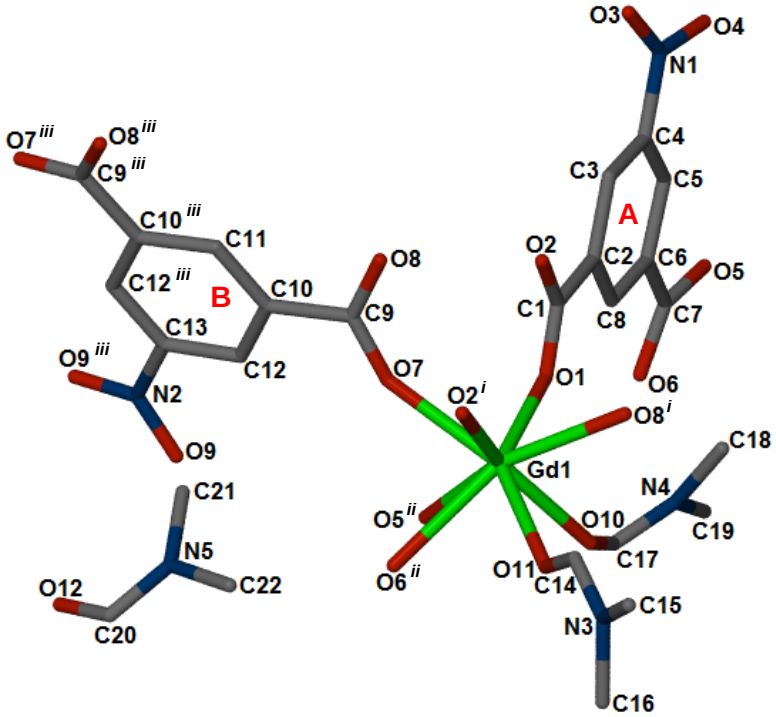

Figure 5.10: The asymmetric unit of **5** with hydrogen atoms omitted for clarity

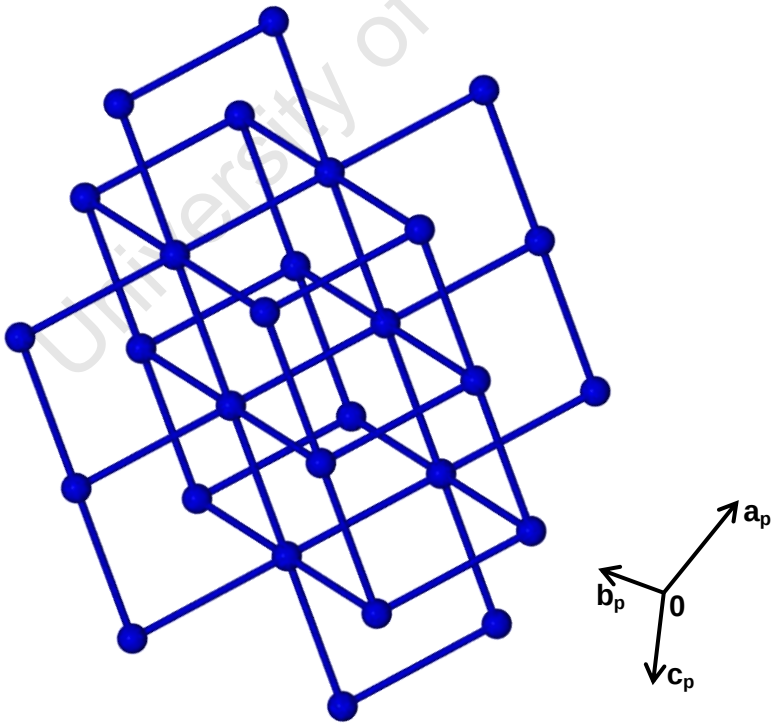

Figure 5.11: The **pcu**-net as seen in compound **5**

Related by symmetry: [i]1/2-x, 1/2-y, -z; [ii]x, 1-y, 1/2+z; [iii]1-x, y, 1/2-z

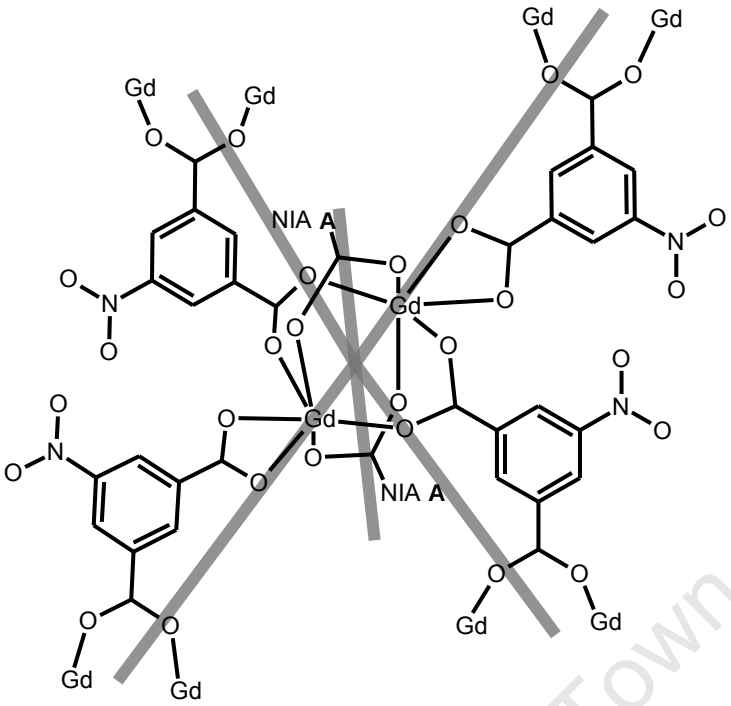

Figure 5.12: A schematic diagram of the six-connected, octahedral node found in **1**

The network is found to be the **pcu**-net (Figure 5.11). The complete short and long symbols for **5** are ($4^{12}.6^3$) and 4·4·4·4·4·4·4·4·4·4·4·4·*·*·* with a CD10 value of 1561.0000.

There are previously reported compounds that exhibit the **pcu** network. A paper by Eddaoudi *et al*[10] lists sixteen structures that all demonstrate **pcu** topology. **IRMOF1** – **IRMOF16** contain $Zn_4(\mu_4\text{-OH})$ clusters that coordinate to one another through a variety of 1,4-disubstituted carboxylate moieties. The $[V^{III}(H_2O)]_3O(O_2CC_6H_4CO_2)_3\cdot(Cl, 9H_2O)$ (**MIL-59**) compound of Barthelet *et al*[11] also demonstrates the **pcu** topology. The 1,3-benzenedicarboxylate ligand coordinates to two separate trimeric $V_3(\mu_3\text{-OH})$ clusters. In these examples the **pcu** net is formed because the ligand acts only as a bridge between metal-cluster SBUs. Also, no two ligands bridge the same two SBUs and each SBU contains six bridging ligands.

5.6 $[Gd_2(NIA)_3(DMF)_4]\cdot 1.8H_2O$ (6)

The asymmetric unit of **6** is given in Figure 5.13 with NIA units D, E and F labelled. Compound **6** also packs with the paddle-wheel motif as is described in Chapter 4.4.

In compound **6** these SBUs act as 4-connected nodes. Node 1 is placed between Gd1/Gd1* metal ion pairs and has square planar geometry. The schematic of node 1 is shown in Figure 5.14, left. Node 2 is placed between Gd2/Gd2* metal ion pairs and has a tetrahedral

* next to a metal denotes a generic symmetry generated atom

geometry. This is depicted in Figure 5.14, right. The C, D and E NIA units all bridge nodes 1 and 2 and neither node connects to another of the same type.

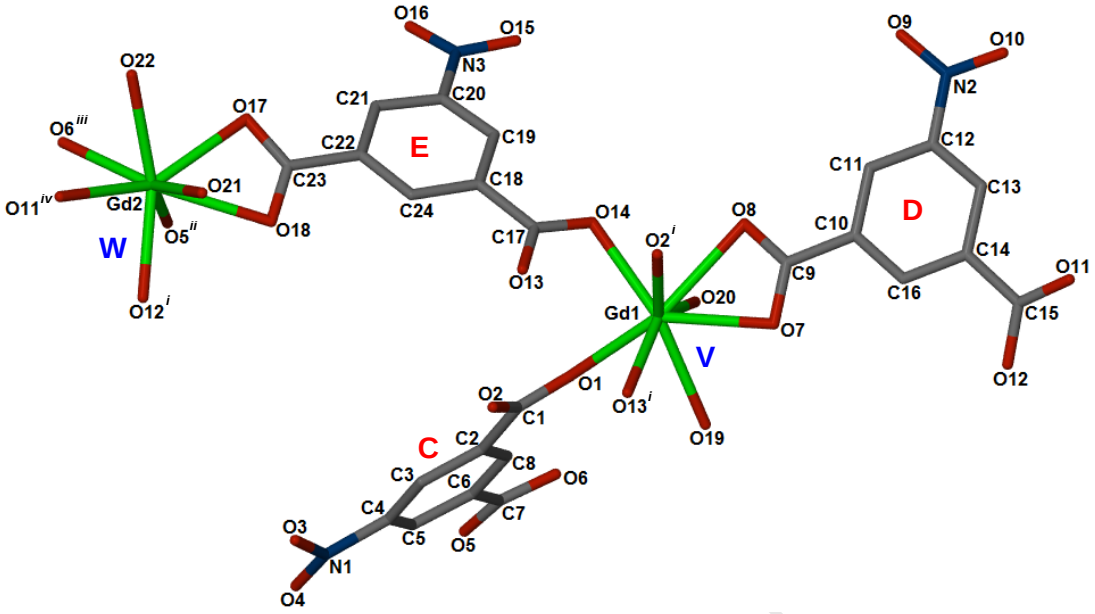

Figure 5.13: The asymmetric unit of **6** with hydrogen atoms and guest water molecules omitted

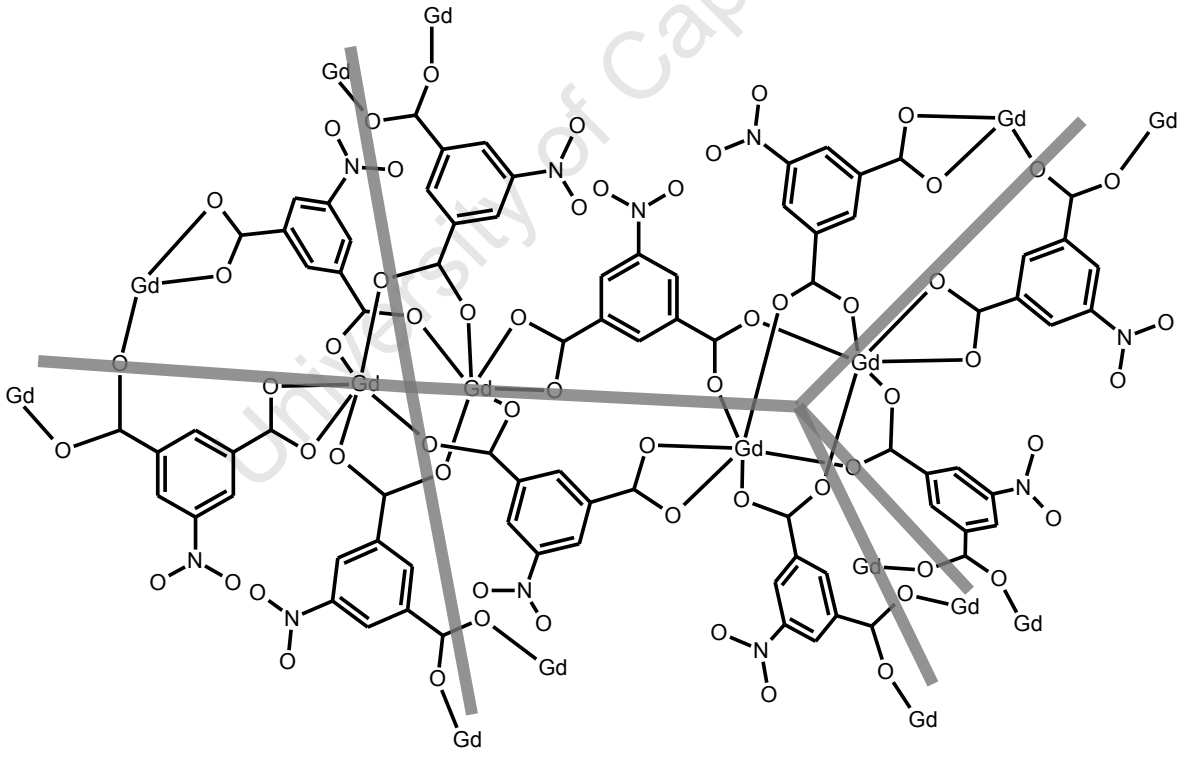

Figure 5.14: A schematic diagram of the square-planar and tetrahedral nodes found in compound **6**

NIA C coordinates in the same manner as NIA B of **5** with one carboxylate moiety bridging a Gd1/Gd1* metal ion pair and one bridging a Gd2/Gd2* metal ion pair. NIA D and E of **6** coordinate in an equivalent way to NIA A of **5**. One carboxylate of NIA D has bidentate

Related by symmetry: ^{i}1/2-x, 3/2-y, -z; ^{ii}1-x, 2-y, -z; ^{iii}x, 2-y, -1/2+z; ^{iv}1/2+x, 3/2-y, -1/2+z; * next to a metal denotes a generic symmetry generated atom

coordination on a Gd1 metal centre while the other bridges a Gd2/Gd2* metal ion pair. Similarly one carboxylate of NIA E is has bidentate coordination on a Gd2 metal centre and bridges a Gd1/Gd1* metal ion pair. In compound **5** each NIA A connects two different SBUs.

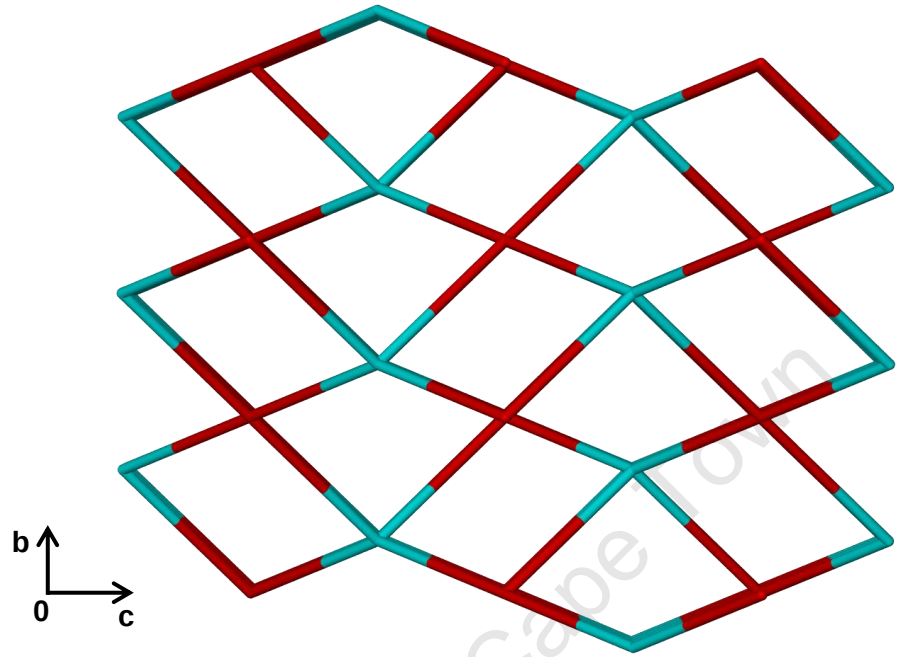

Figure 5.15: The **pts**-net as seen in compound **6**

The difference between compounds **5** and **6** is that in **6** for every NIA D that connects two SBUs there is a NIA E joining the same two SBUs. This results in four connected nodes. Two connections are from NIA C units and two are from combined NIA D and E units.

For node 1 two NIA C units are on opposite sides of the paddle-wheel SBU leading to a square planar geometry. This geometry is slightly distorted with angles of 82 and 98° where 90° is expected. For node 2 the two NIA C units are at right angles to one another with an angle of approximately 84° between the NIA C benzene rings. This leads to a tetrahedral geometry. This geometry is highly distorted with one angle of 152°. The other angles range from 98 - 104°.

The network is found to be the **pts** net as shown in Figure 5.15. The complete short and long symbols for **6** are $(4^2.8^4)(4^2.8^4)$ and $4{\cdot}4{\cdot}8_2{\cdot}8_2{\cdot}8_8{\cdot}8_8$, $4{\cdot}4{\cdot}8_7{\cdot}8_7{\cdot}8_7{\cdot}8_7$ with a CD10 value of 977.0000.

There are other compounds that exhibit the **pts** network. $[Cu(\mu_4\text{-TCNB})][PF_6]$ from Carlucci *et al*[12] (TCNB = 1,2,4,5-tetracyanobenzene) has the square planar node placed in the centre of

* next to a metal denotes a generic symmetry generated atom

the TCNB ligand and the Cu metal centre as the tetrahedral node. Another example is **MOF-36**[13] which contains zinc dimers in a paddle-wheel motif with methanetetrabenzoate (MTB). The square planar node is placed in the centre of the zinc dimer while the tetrahedral node is in the centre of the MTB ligand. In both these cases the metal cluster contains one node while the other node is the ligand itself. **6** is different because both nodes are placed in metal clusters while the ligand acts as a bridge between SBUs as seen for compound **5**.

5.7 RELATIONSHIP BETWEEN 5 AND 6

Rotation around the C6-C7 bond in the NIA A unit of compound **5** (see Figure 5.16a) would allow O1 of the O1-C1-O2 carboxylate to coordinate to the same metal centre as O5 and O6 of the O5-C7-O6 carboxylate moiety of the adjacent NIA A unit. The relevant NIA units are highlighted in blue in Figure 5.16a.

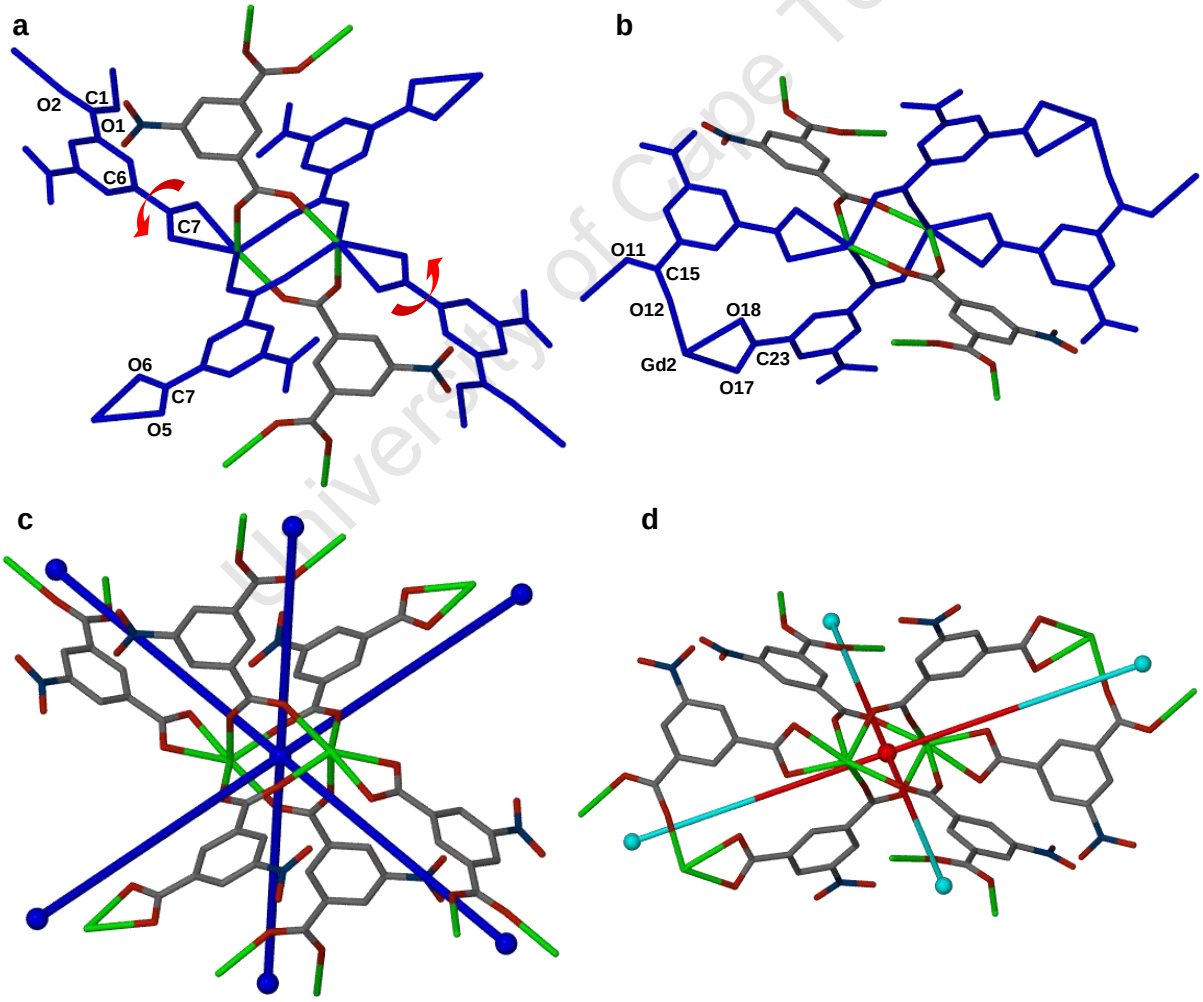

Figure 5.16: Paddle-wheel SBU of **a) 5** and **b) 6** with the relevant NIA units (NIA **A** for **5** and NIA **D** and **E** for **6**) given in blue. **c) 5** with the network shown in dark blue and **d) 6** with network shown in red and light blue

In compound **6** this rotation has occurred as shown in Figure 5.16b. Again the pertinent NIA units are highlighted in blue. O12 of the O11-C15-O12 carboxylate (NIA D) and both O17 and O18 of the O17-C23-O18 carboxylate (NIA E) are coordinated to the Gd2 metal centre in compound **6**. The result of this is that the six-connected node found in compound **5** is no longer present in compound **6**. Instead four-connected nodes are found in compound **6**. These nodes are shown in Figures 5.16c and 5.16d.

5.8 $[Gd_4(NIA)_6(DMF)_{5.5}(H_2O)_3]\cdot 4DMF\cdot H_2O$ (7)

The asymmetric unit of **7** is given in Figure 5.17 with the NIA units labelled in red. Compound **7** has a trinodal four-, five- and six- connected network as defined in Figure 5.18.

Node 1 is placed between a Gd1/Gd1* metal ion pair (see Figure 5.18, blue). This connects in the same way as the six-connected octahedral node found in compound **5**. Two NIA F units coordinate in a bidentate fashion to Gd1 metal centres with one carboxylate moiety while bridging Gd2/Gd3 metal dimers with the other. Similarly two NIA H units coordinate in a bidentate manner to Gd2 metal ions and bridge Gd1/Gd1* metal dimers. In this way the NIA F and H units act in the same manner as NIA A of compound **5**. Two NIA G units bridge a Gd1/Gd1* pair with one carboxylate and bridge a Gd2/Gd3 pair with the other. In this way NIA G acts in a similar manner to NIA B of **5**.

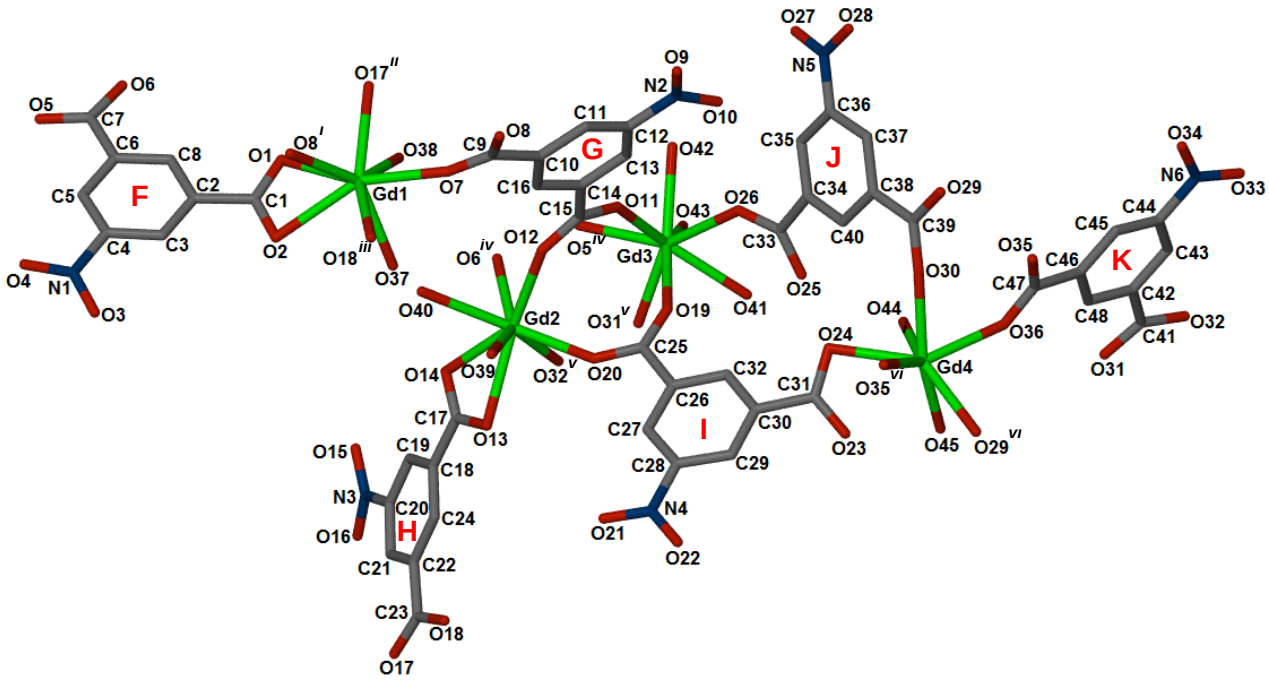

Figure 5.17: The asymmetric unit of **7** with the DMF and guest water molecules omitted for clarity. The oxygen atoms of the coordinated DMF molecules are shown

Related by symmetry: ^{i}-x, 1-y, -z; ^{ii}-1+x, 1+y, z; ^{iii}1-x, -y, -z; ^{iv}1-x, 1-y, -z; ^{v}1-x, -y, 1-z; ^{vi}-x,-y,1-z; * next to a metal denotes a generic symmetry generated atom

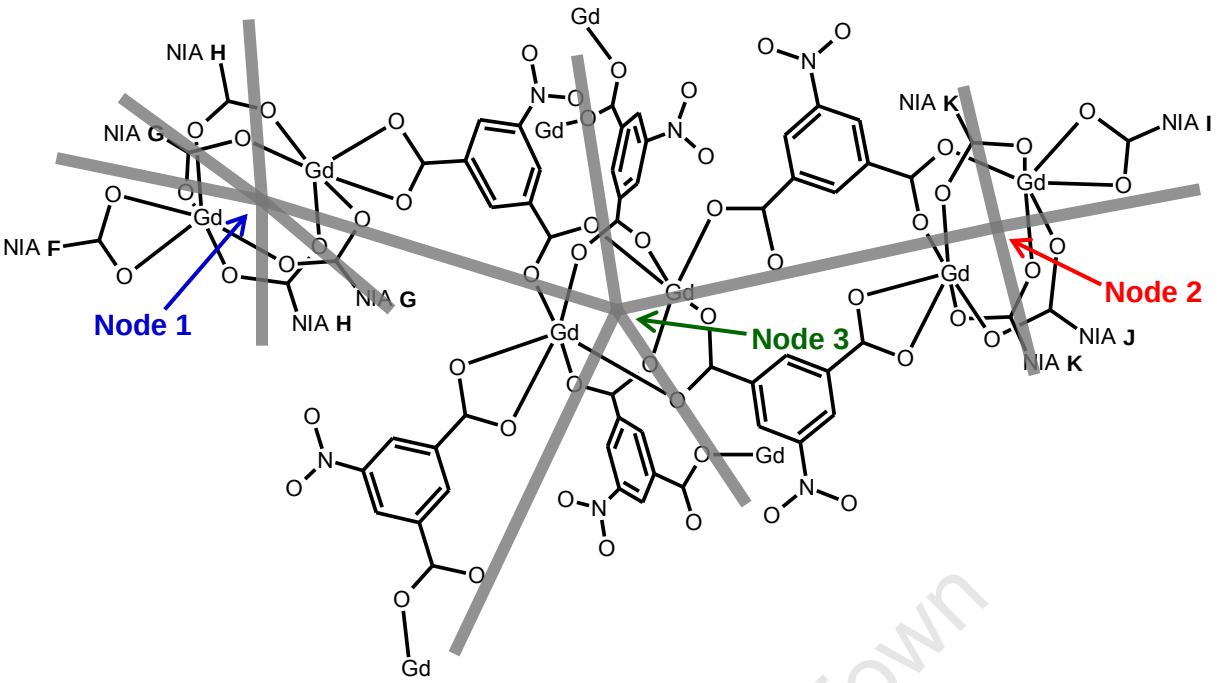

Figure 5.18: A schematic diagram of the octahedral six-connected node 1 (blue), square-planar four-connected node 2 (red), and five-connected node 3 (green) found in compound **7**

Node 2 is located between a Gd4/Gd4* pair (see Figure 5.18, red). This connects in the same way as the square planar four-connected node found in **6**. Two NIA I units coordinate in a bidentate manner to a Gd4 metal centre and bridge a Gd2/Gd3 metal ion pair. NIA J is similar with two units bridging a Gd4/Gd4* metal pair with one carboxylate and singly coordinating to a Gd3 metal centre with the other. For every NIA I that connects two SBUs there is a NIA **J** that connects the same two SBUs. In this way NIA I and J act in a comparable manner to NIA D and E in **6**. Two NIA K units bridge Gd4/Gd4* dimers with one carboxylate moiety and Gd2/Gd3 pairs with the other carboxylate. The NIA K unit acts like NIA **C** in compound **6** in that regard.

Node 3 is unique to compound **7** and is located between Gd2/Gd3 metal ion pairs. Node 3 acts as a linker between the four- and six-connected nodes and is shown in Figure 5.18 in green. NIA F bridges the Gd2/Gd3 pair with one carboxylate and doubly coordinates to a Gd1 metal centre with the other. Similarly NIA H is doubly coordinated to a Gd2 metal centre with one carboxylate and bridges a Gd1/Gd1* metal ion pair with the other. NIA F and H act in the same way as NIA A in compound **5**. Both NIA G and K bridge a Gd2/Gd3 pair with one carboxylate. NIA G bridges a Gd1/Gd1* metal pair while NIA K bridges a Gd4/Gd4* metal pair with the other carboxylate. NIA G and K act in the same way as NIA B in **5** and as NIA C in compound **6**. NIA I bridges a Gd2/Gd3 pair and coordinates in a bidentate fashion to a Gd4 metal centre. NIA J singly coordinates to the same Gd3 metal centre and bridges a Gd4/Gd4* pair containing the same Gd4 metal centre. NIA I and J perform the same function

* next to a metal denotes a generic symmetry generated atom

as NIA D and E in compound **6**. Figure 5.19 shows the topological net of **7** as it appears in this structure.

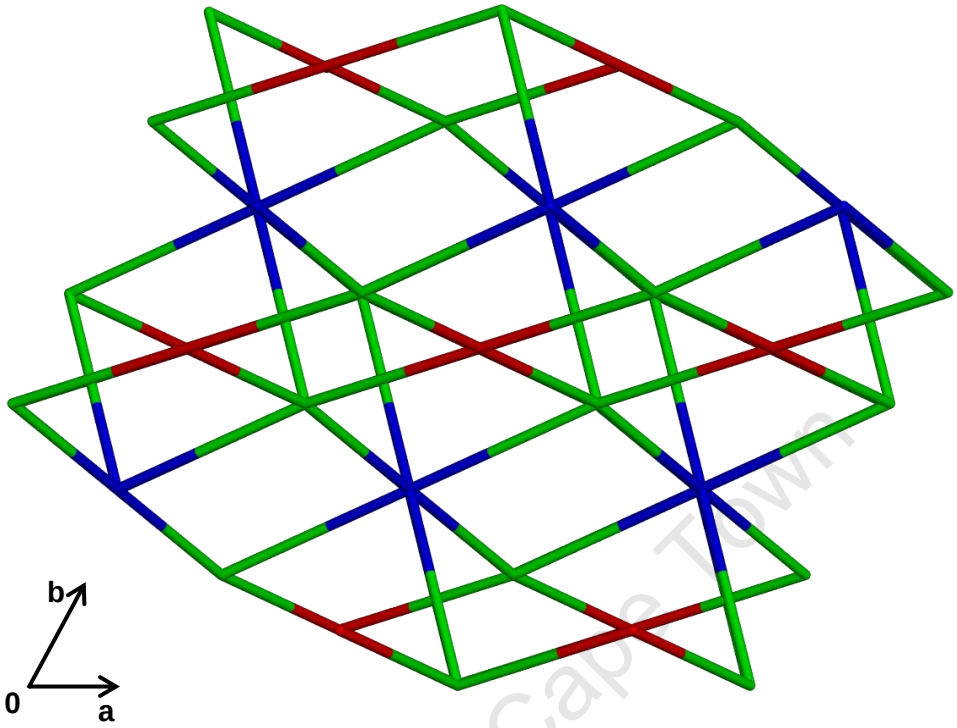

Figure 5.19: The topological net of **7** with node 1 in blue, node 2 in red and node 3 in green

The six-connected nodes (1) are shown in blue, the four-connected nodes (2) are shown in red and the five-connected nodes (3) are shown in green. Nodes 1 and 2 are joined exclusively to nodes of type 3. Node 3 is connected to three node 1 and two node 2 and thereby acts as a bridge between the other two types of node. Node 3 is located between the Gd2 and Gd3 metal ions and has full site occupancy, nodes 1 and 2 are located between the Gd1/Gd1* and Gd4/Gd4* metal ions respectively and possess half site occupancy. As a result there are two node 3 for every one of nodes 1 and 2.

Node 1 has a slightly distorted octahedral geometry with axial-axial angles of 180° but axial-equatorial angles ranging from 82.5 – 95.6°. Node 2 has almost perfect square-planar geometry with angles ranging from 88.7 – 90.5°. Node 3 has a distorted square pyramidal geometry. Four of the connections for node 3 (two node 1 and two node 2) are nearly square planar with angles of approximately 170° for the nodes directly opposite one another and angles of 88 - 94° for those next to each other. The fifth connection is roughly perpendicular to the plane with axial-equatorial angles ranging from 84 - 104°.

* next to a metal denotes a generic symmetry generated atom

This network is an unprecedented topology with no matches found in the RCSR or EPINET databases. The complete short and long symbols for **7** are $(4^4.6^2)(4^6.6^4)_2(4^8.6^6.8)$ and $4{\cdot}4{\cdot}4{\cdot}4{\cdot}{*}{\cdot}{*}$, $4{\cdot}4{\cdot}4{\cdot}4{\cdot}4{\cdot}4{\cdot}{\cdot}6_2{\cdot}6_2{\cdot}{*}{\cdot}{*}$, $4{\cdot}4{\cdot}4{\cdot}4{\cdot}4{\cdot}4{\cdot}4{\cdot}4{\cdot}6_2{\cdot}6_2{\cdot}6_2{\cdot}6_2{\cdot}8_8{\cdot}{*}{\cdot}{*}$ with a CD10 value of 1361.5000. This network will be submitted to the RCSR shortly.

5.9 SUMMARY

For compounds **1**, **2** and **3** fully deprotonated 1,3,5-benzenetricarboxylate (BTRI) units act as three-connecting nodes. In compound **3** the doubly deprotonated HBTRI unit acts as a bridge and is not a node. No matches were found in the databases for **1** and **3**, which were found to have new types of structures. These have been accepted by the RCSR as the **sab** and **kdd** nets respectively. Compound **2** forms the well-known 2-dimensional **kgd**-net. Compound **4** forms a three-dimensional network through strong hydrogen bonds and displays 9-connected nodes in this hydrogen-bonded net.

For compounds **5**, **6** and **7** coordination occurs through the carboxylate oxygen atoms but not the nitro moiety. A node placed within the NIA unit would be a two-connecting bridging node and can therefore be ignored. Compounds **5** and **6** display the common **pcu** and **pts**-nets respectively. Compound **7** has a new topological structure, which contains nodes seen in both **5** and **6**. It is probable that interpenetration does not occur for compounds **5**, **6** and **7** due to the small angle between coordinating moieties (*ca* 120°) and the shortness of the spacer.[14] The net for compound **7** will be submitted to the RCSR shortly.

The complete short and long symbols for **1**, **3** and **7** were calculated and confirmed with SYSTRE, TOPOS and OLEX.

5.10 REFERENCES

1. O. D. Friedrichs, Program SYSTRE 1.14 beta http://gavrog.sourceforge.net/, 2007.

2. M. O'Keeffe, M. A. Peskov, S. Ramsden and O. M. Yaghi, *Acc. Chem. Res.,* 2008, **41**, 1782.

3. M. O'Keeffe, O. M. Yaghi and S. Ramsden, Australian National University Supercomputer Facility, Reticular Chemistry Structure Resource, http://rcsr.anu.edu.ac/, 2009.

4. S. J. Ramsden, V. Robins, S. Hungerford and S. T. Hyde, EPINET, http://epinet.anu.adu.au, 2009.

5. V. A. Blatov, Program TOPOS 4.0, http://www.topos.ssu.samara.ru/, accessed May 2009.

6. V. A. Blatov and M. V. Peskov, *Acta Cryst.,* 2006, **62**, 457.

7. O. V. Dolomanov, A. J. Blake, N. R. Champness and M. Schröder, *J. Appl. Cryst.,* 2003, **36**, 1283.

8. L. Öhrström and K. Larsson, ***Molecule-based materials the structural network approach (1st ed.).***, Elsevier, Amsterdam, The Netherlands, 2005.

9. S. Xiang, J. Huang, L. Li, J. Zhang, L. Jiang, X. Kuang and C. -Y. Su, *Inorg. Chem.,* 2011, **50**, 1743.

10. M. Eddaoudi, J. Kim, N. Rosi, D. Vodak, J. Wachter, M. O'Keeffe and O. M. Yaghi, *Science,* 2002, **295**, 469.

11. K. Barthelet, D. Riou and G. Férey, *Chem. Commun.,* 2002, 1492.

12. L. Carlucci, G. Ciani, D. W. v. Gudenberg and D. M. Proserpio, *New J. Chem.,* 1999, **23**, 397.

13. J. Kim, B. Chen, T. M. Reineke, H. Li, M. Eddaoudi, D. B. Moler, M. O'Keeffe and O. M. Yaghi, *J. Am. Chem. Soc.,* 2001, **123**, 8239.

14. S. -P. Chen, Y. -X. Ren, W. -T. Wang and S. -L. Gao, *Dalton Trans.,* 2010, **39**, 1552.

Chapter 6

Conclusion

6.1 SUMMARY

The field of coordination polymers, and specifically metal-organic frameworks (MOFs), has developed significantly over the past decade. The design of these compounds has become an important area of research. The work discussed in this thesis pertains to the preparation and full characterisation of new MOFs and coordination polymers from the ligands 1,3,5-benzenetricarboxylic acid (H_3BTRI) and 5-nitroisophthalic acid (H_2NIA), and the metal salts zinc(II) sulphate heptahydrate and gadolinium(III) nitrate hexahydrate.

The thermal techniques used to study these structures include differential scanning calorimetry (DSC), thermogravimetric analysis (TG) and hot-stage microscopy (HSM). The X-ray diffraction techniques include powder X-ray diffraction (PXRD) and single crystal X-ray diffraction. Elemental analysis was also used to confirm the composition of the compounds. Where appropriate further experiments were performed including kinetic studies and scanning electron microscopy (SEM).

6.1.1 1,3,5-BENZENTRICARBOXYLATE COMPOUNDS

Three new compounds were prepared from 1,3,5-benzenetricarboxylic acid and zinc(II) sulphate heptahydrate: $[Zn_6(\mu_3\text{-}OH)_2(BTRI)_4(DMF)_{2.5}(H_2O)_2]\cdot[Zn(H_2O)_3(DMF)_3]\cdot 2.96H_2O$ (**1**), $[Zn(HCOO)(BTRI)_{0.3}(DMF)]$ (**2**) and $[Zn_2(\mu_2\text{-}OH_2)(HBTRI)(BTRI)(H_2O)_2]\cdot DMA\cdot 3H_2O$ (**3**). These compounds were all fully characterised using the thermal and X-ray diffraction techniques.

Compounds **1**, **2** and **3** were found to be heavily reliant on the concentration of the starting materials in the initial solution. The method used also played a role as the exact concentration range resulting in a specific compound was found to change with the method used. For all methods the metal salt was dissolved in H_2O at 60 °C while the ligand was dissolved in *N*,*N'*-dimethylformamide (DMF) also at 60 °C. The solutions were then filtered into the same vial. Methods 1 and 4 involved placing the sealed vial in an oil bath at 60 °C. The vial was then held at that temperature for 24 hours before being cooled to room temperature. For method 1 the cooling took place over 48 hours while for method 4 it was over 10 hours. For method 2 the vial was partially opened to the atmosphere immediately after the combination of the starting materials and placed in an oven held at 30 °C. For method 3 the vial was placed into a cool oil bath and then heated to 60 °C over 24 hours, held at that temperature for 24 hours and then cooled to room temperature over 48 hours.

Method 5 involved placing the sealed vial in a Dewar containing water at a temperature of 70 °C. The Dewar was sealed and allowed to cool slowly to room temperature. For methods 1, 3, 4 and 5 the vials were partially opened to the atmosphere after cooling if no crystals had formed.

Methods 1, 3 and 5 all showed a tendency to form compound **1** to form at low concentrations. This was lower than 0.2 mol.dm^{-3} for method 1, lower than 0.15 mol.dm^{-3} for method 3 and lower than 0.18 mol.dm^{-3} for method 4. Compound **2** was obtained at higher concentrations for all three methods with a crossover area where both compounds **1** and **3** were commonly obtained. For these methods compound **2** was formed sporadically over a large concentration range. The solvate **DMFBTRI** was obtained occasionally, and always at concentrations higher than 0.8 mol.dm^{-3}. Method 5 also showed a trend of forming compound **1** at lower concentrations and compound **3** at higher concentrations. However, compound **1** was formed in many more experiments and was the most probable product for concentrations below 0.4 mol.dm^{-3}. Compound **3** is only formed sporadically and no compound **2** was formed regardless of concentration. The **DMFBTRI** solvate was formed at much lower concentrations than for methods 1, 3 and 4. Method 2 was the best method to use when attempting to form compound **2** as many experiments resulted in **2**. However, there was no clear trend with concentration for compound formation. Compounds **1**, **2** and **3** formed at a range of concentrations between 0.03 and 0.45 mol.dm^{-3}. Above concentrations of 0.45 mol.dm^{-3} the **DMFBTRI** solvate was almost exclusively obtained. The solvate was especially prevalent in method 2 due to the lack of slow cooling with this method.

Compound **1** is an anionic MOF. It was found to be similar to a previously reported structure.[1] However, **1** has lower symmetry due to high disorder and a more complex and larger counter cation. Desolvation and resolvation experiments were performed on compound **1**. It was found to lose crystallinity with high temperature and guest removal. The desolvated sample regained crystallinity upon exposure to a mixture of water vapour and DMF, or to water vapour alone. The original structure was not regained. Compound **1** is one of only a few structures to contain zinc metal centres with more than two different coordination modes.[2]

Compound **2** is a neutral MOF. It was found to be isostructural with three compounds reported in the literature.[1, 3, 4]. Compound **2** undergoes a structural rearrangement between approximately 130 and 190 °C. It forms two-dimensional sheets with DMF molecules from each sheet interlocked with the sheet on either side.

Compound **3** is an anionic MOF. It loses crystallinity with the removal of guest water molecules. Dehydration and rehydration studies were performed on compound **3**. It lost crystallinity with dehydration but regained its original structure with rehydration. There are three guest water molecules in **3** and a further two terminally coordinated water molecules. All five of these water molecules are removed with heating. The rehydration studies showed that **3** can absorb a total of 6.5 water molecules, which is 1.5 molecules more than modelled in the single crystal structure. SEM studies were performed on crystals of **3** and cracks were observed on the surface of the sample with dehydration. The rehydrated sample was found to have scars on the surface indicating that it had "self-healed" with rehydration. Gas sorption studies were also performed on compound **3**, which absorbed CO_2 and N_2 gas to a low degree and showed some affinity for H_2 gas.

One new compound was prepared from 1,3,5-benzenetricarboxylic acid and gadolinium(III) nitrate hexahydrate: [Gd(BTRI)(H_2O)$_6$] (**4**). Regardless of the synthetic conditions used compound **4** was always obtained. A crystalline powder was formed more often than single crystals. The compound was characterised fully with the previously mentioned thermal and X-ray diffraction techniques. Compound **4** was found to undergo a structural rearrangement after the loss of 5 water molecules, which persisted with the removal of the final water molecule. Kinetic studies were performed on dehydrated samples of **4**. They showed that the dehydrated sample absorbs both water and ethanol in a high vapour pressure environment. The absorption of water at 30 °C resulted in a reversal of the structural rearrangement observed with water removal and the original compound **4** is obtained. Compound **4** was found to be stable up to 500 °C when heated directly after removal from the mother liquor. If the sample was left for exposed to air for an extended period of time however it became more susceptible to degradation and would decompose at temperatures just beyond 200 °C.

When crystals of **3** were submerged in a solution of gadolinium nitrate in DMF/H_2O they were found to transform into compound **4** in a partially solid-state process. The reverse process does not occur as shown by a sample of **4** submerged in a high concentration solution of zinc sulphate in DMF/H_2O, which retains the structure of **4**.

6.1.2 5-NITROISOPHTHALATE COMPOUNDS

Three new compounds were prepared from 5-nitroisophthalic acid and gadolinium(III) nitrate hexahydrate: $[Gd(NIA)_{1.5}(DMF)_2]\cdot DMF$ (**5**), $[Gd_2(NIA)_3(DMF)_4]\cdot 2.67H_2O$ (**6**) and $[Gd_4(NIA)_6(DMF)_{5.5}(H_2O)_3]\cdot 4DMF\cdot H_2O$ (**7**). Each of these compounds was fully characterised using the X-ray diffraction techniques as well as thermal methods.

Compounds **5**, **6** and **7** did not show strong trends with respect to concentration. The material obtained depended mostly on the method used. For all methods the metal salt was dissolved in either H_2O or DMF at 60 °C. The ligand was dissolved in DMF also at 60 °C. The two solutions were then filtered into the same vial. For method 1 the vial was sealed and placed in an oil bath at a temperature of 60 °C for 24 hours. The vial was then cooled to room temperature over 48 hours. Method 1a used a 1:1 metal to ligand ratio while method 1b used a 2:3 metal to ligand ratio. For method 2 the vial was sealed and placed in an oven at a temperature of 80 °C. The crystals were allowed to grow at high temperature. A metal to ligand ratio of 1:1 was used in method 2a, a ratio of 2:1 for 2b and a ratio of 1:2 for method 2c. A 1:1 metal to ligand ratio was used for method 3. The sealed vial was placed in a Dewar containing water at 70 °C. The Dewar was sealed and allowed to cool slowly to room temperature. For methods 1 and 3 the vials were partially opened to the atmosphere after cooling to allow for slow evaporation.

Method 1a produced compound **6** almost exclusively although some low concentration experiments resulted in compound **5** or compound **7**. In comparison compound **7** was only formed at high concentrations for method 1b. Compound **6** was still the majority product with method 1b but compound **5** was also formed sporadically across the entire concentration range. Method 2 involved growing crystals at 80 °C. Many of the results obtained were amorphous material or of poor diffraction quality. Method 2a resulted in compound **5** over most of the concentration range with a few amorphous results at high concentrations. Method 2b also had a majority product of compound **5** but compound **6** and **7** were formed occasionally. Method 2b resulted in amorphous material for a number of experiments. This was especially true at the lowest and highest concentrations. Method 2c produced compound **5** almost exclusively with only one experiment producing compound **6**. Method 3 also formed compound **5** in the majority of experiments. Only two experiments resulted in compound **6** and these were for experiments with very different concentrations of the starting materials. Compounds **5**, **6** and **7** all have a metal to ligand ratio of 2:3. It is therefore interesting to note that compound **5** is generally the only material produced when it forms, whereas compounds

6 and **7** were often obtained with a mixture of starting materials and other, almost amorphous material.

High quality single crystals of compound **5** were obtained through methods 1a, 1b and 3. Compound **5** is a neutral MOF and there are six compounds that are isostructural to **5** reported in the literature.[5, 6]. Three of these compounds used 4,4'-bipyridine and three used 2,2'-bipyridine to direct the final structure. This template was not necessary in the preparation of **5**. Compound **5** can be partially desolvated and resolvated with DMF vapour.

Compound **6** is a neutral MOF and contains large void spaces with a total of 683 $Å^3$ void space per unit cell. The void space is located in pockets in the framework that also contain guest water molecules. The amount of guest water trapped in those pockets is variable.

Compound **7** is a neutral MOF. It could not be analysed through PXRD due to the poor quality of the bulk material as well as the crystals of **7**. All three of compounds **5**, **6** and **7** did not diffract well in PXRD analysis resulting in poor quality PXRD diffraction patterns. Compound **7** can lose the guest water and one guest DMF molecule before any effect is seen in the crystal. True decomposition does not occur until after the removal of all guest DMF molecules.

Attempts were made to prepare compounds from 5-nitroisophthalic acid and zinc(II) sulphate. However, regardless of the method used no structure was obtained. Thin, plate-like crystals were observed in the reaction vessel but they dissolved when attempts were made to remove them from the mother liquor. There are reports in the literature of compounds prepared from zinc and 5-nitroisophthalic acid[7, 8] but in both those cases a different zinc metal salt was used indicating that the metal salt plays an important role, influencing the final structure.

Further evidence that the counter ion of the metal salt is important is shown by the fact that three novel compounds were prepared with H_3BTRI and zinc(II) sulphate in N,N'-dimethyl formamide (DMF). H_3BTRI and zinc are both common starting materials and DMF is often used as a solvent and yet three completely new complexes were obtained. The majority of previous studies in the literature appear to have used zinc(II) nitrate or zinc(II) chloride.

6.1.3 TOPOLOGICAL STUDIES

The topological networks of compounds **1**-**3** and **5**-**6** were determined and analysed. Compound **4** forms a 3-dimensional network through hydrogen-bonds between 1-dimensional chains, which was not fully characterised.

Compound **1** was found to form a new binodal network. This was submitted to and accepted by the Reticular Chemistry Structure Resource (RCSR) and is now known as the $(4.6^2)_2(4^2.6^{10}.8^3)$-**sab** net. The long symbol of this net is $4{\cdot}6_2{\cdot}6_2$, $4{\cdot}4{\cdot}6{\cdot}6{\cdot}6{\cdot}6{\cdot}6{\cdot}6{\cdot}6{\cdot}6{\cdot}6{\cdot}6_2{\cdot}6_2{\cdot}8_2{\cdot}8_2{\cdot}8_7$ and the network has a CD10 value of 1242.3333. The asymmetric unit of **1** has four BTRI units and three trimeric zinc clusters. Each BTRI unit is topologically equivalent and represents the same 3-connected node in the topological net. Each trimeric zinc cluster is also topologically equivalent and represents the same 6-connected node.

Compound **2** forms the well-known, two-dimensional $(4^3)(4^6)$-**kgd** topological net. The long symbol for this net is $4{\cdot}4{\cdot}4$, $\cdot4{\cdot}4{\cdot}4{\cdot}4{\cdot}4{\cdot}6{\cdot}6{\cdot}6{\cdot}6{\cdot}6{\cdot}6{\cdot}8_2{\cdot}8_2{\cdot}8_2$ and the network has a CD10 value of 251.0000.

Compound **3** was found to form a new, binodal network which was submitted to and accepted by the RCSR. This is now known as the $(6^3)(6^9.8)$-**kdd** net. This net has a long symbol of $6_3{\cdot}6_3{\cdot}6_3$, $6{\cdot}6{\cdot}6{\cdot}6_2{\cdot}6_2{\cdot}6_2{\cdot}6_2{\cdot}6_2{\cdot}6_2{\cdot}*$ and has a CD10 value of 1242.0000. The asymmetric unit of **2** has one fully deprotonated BTRI unit that acts as a three-connected node. The doubly deprotonated HBTRI unit acts only as a bridge, not a node. The metal dimer acts as a five-connected node. The common five- and three- connected **hms** and **bnn** nets have one link between five-connected nodes in the axial position and one in the equatorial position. The **kdd** net has both links between five-connected nodes in the axial position. Since submission of this net to the RCSR another compound has been reported that also possess the **kdd**-net topology.[9]

Compound **5** forms the well-known $(4^{12}.6^3)$-**pcu** network. This net has a long symbol of $4{\cdot}4{\cdot}4{\cdot}4{\cdot}4{\cdot}4{\cdot}4{\cdot}4{\cdot}4{\cdot}4{\cdot}4{\cdot}4{\cdot}*{\cdot}*{\cdot}*$ with a CD10 value of 1561.0000. This network is comprised of octahedral six-connected nodes, which in the case of compound **5** are located between the metal ions of each metal dimer. Compound **6** formed the well-known $(4^2.8^4)(4^2.8^4)$-**pts** network. This net has a long symbol of $4{\cdot}4{\cdot}8_2{\cdot}8_2{\cdot}8_8{\cdot}8_8$, $4{\cdot}4{\cdot}8_7{\cdot}8_7{\cdot}8_7{\cdot}8_7$ with a CD10 value of 977.0000. This network is comprised of two four-connected nodes. Both are located between

the metal ions of a metal dimer. One has square-planar geometry while the other possess tetrahedral geometry. Both compounds **5** and **6** consist of gadolinium metal ion dimers bridged by 5-nitroisophthalate anions (NIA) in a paddle-wheel fashion as well as two NIA units in axial positions. The analysis of the **pcu** and **pts** nets found in **5** and **6** respectively enabled a comparison of the two compounds. It was found that rotation around a C-C bond resulted in compound **5** or compound **6**. As a result of that rotation the six-connected node in **5** becomes the two four-connected nodes in **6**.

Compound **7** was found to form a new trinodal network, which will be submitted to the RCSR database shortly. This net consists of a four-, a five- and a six-connected node with the short symbol $(4^4.6^2)(4^6.6^4)(4^8.6^6.8)$. The net has a long symbol of $4\cdot4\cdot4\cdot4\cdot*\cdot*$, $4\cdot4\cdot4\cdot4\cdot4\cdot6_2\cdot6_2\cdot*\cdot*$, $4\cdot4\cdot4\cdot4\cdot4\cdot4\cdot4\cdot6_2\cdot6_2\cdot6_2\cdot8_8\cdot*\cdot*$ and a CD10 value of 1361.5000. Similarly to compounds **5** and **6**, compound **7** contains gadolinium metal ion dimers. Each node is located between two metal ions of a dimer. Compound **7** is particularly interesting as the four-connected node comprises similar connecting units to the square-planar node in compound **6**. The six-connected node connects in the same way as the octahedral node in compound **5**. The five-connected node possesses NIA units that have undergone the C-C bond rotation and NIA units that have not. This node joins the four- and six-connected nodes.

Topological analysis allowed the determination that compounds **5**, **6** and **7** are related by a simple rotation around a C-C bond allowing or preventing coordination to a specific metal centre.

Three of the structures reported in this thesis were found to display new topological nets. Compound **1** is interesting as there are 4 different BTRI units in the asymmetric unit and yet each of those are equivalent in terms of topology. The same is true of the three zinc metal ion clusters, which all form a six-connected node. Compound **2** has some similarities to the more common **hms** and **bnn** nets but has both links between the five-connected nodes in the axial position rather than one in the axial and one in the equatorial. The topology of compound **7** is particularly interesting has it combines nodes found in the common **pcu** and **pts** nets and joins them through a third, five-connected node. By analysing the topology of compounds **5**, **6** and **7** it was easier to discern the subtle alterations that make these compounds different.

6.2 FINAL REMARKS

There were five primary aims for this project (see Chapter 1.8.2 – Objectives). New metal-organic frameworks (MOFs) and coordination polymers were prepared from 1,3,5-benzenetricarboxylic (H_3BTRI) acid with both zinc(II) sulphate heptahydrate and gadolinium(III) nitrate hexahydrate. The majority of compounds in the literature with zinc and BTRI were prepared from zinc(II) nitrate or zinc(II) chloride. It would be possible to investigate other metal salts to explore the effect of the counter ion. It would also be interesting to investigate whether a significant change in the solvent and reaction conditions could produce a new gadolinium and BTRI structure. New MOFs and coordination polymers were also prepared from 5-nitroisophthalic acid (H_2NIA) and gadolinium(III) nitrate hexahydrate. These compounds were not stable with guest removal. Solvent exchange experiments could be performed to test whether stability increased. Unfortunately no compounds were obtained from H_2NIA and zinc(II) sulphate heptahydrate. The effect of a different metal salt as well as a complete change in the reaction conditions could be investigated further.

All the compounds that were prepared were fully characterised through single crystal X-ray diffraction and thermal analysis. Compounds **1**-**5** were also studied with powder X-ray diffraction. Compounds **6** and **7** diffracted poorly with PXRD and so full PXRD characterisation could not be completed with these compounds.

The topological nets of compounds **1**, **3** and **7** were found to be new and were therefore fully characterised. Compounds **1** and **3** were submitted to the RCSR and compound **7** will be submitted shortly. Topological analysis was also performed on compounds **2**, **5**, and **6**. Compounds **2**, **5**, and **6** were found to have well-known topologies. The topologies of **5**, **6**, and **7** were used to help fully understand the similarities and differences between the three compounds.

Dehydration and rehydration studies were performed on compounds **1**, **3** and **4**. Compound **1** became almost amorphous with dehydration but regained crystallinity with exposure to H_2O and DMF/H_2O vapour. Compound **3** was found to become almost amorphous upon dehydration but to rehydrate to its original structure. As a result it was studied using scanning electron microscopy. Regular cracks were present on the surface of the sample after dehydration. Scars formed on the surface of the crystal after rehydration showing that **3** "self-heals". A kinetics run was performed on compound **3** at 30 °C. It was found to absorb an

extra 1.5 guest water molecules in addition to the 3 guest water molecules modelled in the single crystal structure. Further kinetics runs on this material would be of interest as the absorption profile of **3** was found to have a high correlation coefficient of 0.9998 with the two-dimensional advancement of the phase boundary model. Compound **4** undergoes a structural rearrangement with dehydration. Kinetics experiments were performed on **4** with both water and ethanol. It would be interesting to do further kinetics tests at a variety of temperatures and with other hydrogen bonding potential guests.

Extensive studies were performed for all these compounds to determine which metal to ligand ratio, solvent system, cooling rate, and crystal growth environment results in which compound. Further studies could be performed to vary the solvent system to a greater extent and to test the effect of the metal to ligand ratio with the zinc complexes. As each experiment was necessarily done individually they were time-consuming. And due to the fact that a number of compounds can be prepared from the same starting materials with very similar reaction conditions it would be ideal to use high-throughput screening to determine the exact conditions that result in each compound.

6.3 REFERENCES

1. J. He, Y. Zhang, Q. Pan, J. Yu, H. Ding and R. Xu, *Microporous and Mesoporous Materials,* 2006, **90**, 145.

2. H. -Y. Liu, B. Zhao, W. Shi, Z. -J. Zhang, P. Cheng, D. -Z. Liao and S. -P. Yan, *Eur. J. Inorg. Chem.,* 2009, 2599.

3. J. Chen, M. Ohba and S. Kitagawa, *Chem. Lett.,* 2006, **35**, 526.

4. C. -T. Yeh, H. -K. Liu, C. -J. Lin and C. -H. Lin, *Acta Cryst. E,* 2010, **E66**, m1289.

5. G. Wang, T. Song, Y. Fan, W. Wan, J. Xu and L. Wang, *Inorg. Chem. Commun.,* 2010, **13**, 935.

6. S. -P. Chen, Y. -X. Ren, W. -T. Wang and S. -L. Gao, *Dalton Trans.,* 2010, **39**, 1552.

7. H. Xu and Y. Li, *J. Mol. Struct.,* 2004, **693**, 11.

8. J. Tao, X. Yin, Y. -B. Jiang, L. -F. Yang, R. -B. Huang and L. -S. Zheng, *Eur. J. Inorg. Chem.,* 2003, 2678.

9. S. Xiang, J. Huang, L. Li, J. Zhang, L. Jiang, X. Kuang and C. -Y. Su, *Inorg. Chem.,* 2011, **50**, 1743.

APPENDICES

Two appendix folders can be found on the disk attached.

Appendix A contains the supplementary crystallographic information for each fully solved structure presented in this thesis. The files have been saved in a subfolder with their complex number.

Appendix B contains the supplementary topological data including the full output data for each new network analysed. The files have been saved in a subfolder with their complex number